NASA
Technical
Paper
2334

November 1984

Experimental and Predicted Heating Distributions for Biconics at Incidence in Air at Mach 10

Charles G. Miller III

NASA

NASA Technical Paper 2334

1984

Experimental and Predicted Heating Distributions for Biconics at Incidence in Air at Mach 10

Charles G. Miller III

Langley Research Center
Hampton, Virginia

National Aeronautics and Space Administration

Scientific and Technical Information Branch

Introduction

Advances in navigation and knowledge of planetary atmospheres, along with the need for Earth orbital transfer vehicles (OTV's), have rekindled interest in aerobraking and aerocapture techniques for proposed Earth and planetary missions (refs. 1 to 3). A spherically blunted biconic with the fore-cone section bent upward relative to the aft-cone section to provide self-trim capability has been proposed as a generic vehicle for many planetary missions (refs. 2 and 3) and as a viable OTV candidate. This vehicle also offers advantages as a reentry vehicle. Because of the scarcity of experimental data for biconics, a study was initiated at the Langley Research Center (LaRC) to establish a comprehensive data base. Aerodynamic coefficients, pressure distributions, oil-flow patterns, and shock shapes have been measured on 2.9-percent-scale models of the proposed configuration and this configuration without a bent nose (straight biconic) (refs. 4 to 6). These measurements were made in three conventional (as opposed to impulse) hypersonic wind tunnels, namely, the Langley 20-Inch Mach 6 Tunnel, the Langley 31-Inch Mach 10 Tunnel (formerly known as the Langley Continuous-Flow Hypersonic Tunnel), and the Langley Hypersonic CF_4 Tunnel, to provide a range of Mach numbers, Reynolds numbers, and ratios of specific heats. More recently, heating distributions were measured on 1.9-percent-scale models in the Langley Expansion Tube at hypersonic-hypervelocity flow conditions for four test gases (ref. 7).

As part of the overall program to establish a data base for this generic aeroassisted vehicle, this paper presents heating distributions measured on a 1.9-percent-scale model of the generic vehicle in the Langley 31-Inch Mach 10 Tunnel. Also tested was a straight biconic with the same nose radius, base radius, and half-angles. The effects of nose bend, angle of attack, and Reynolds number on heating distributions are examined, and predictions from a three-dimensional "parabolized" Navier-Stokes (PNS) code (refs. 8 and 9) are compared with measurement. These comparisons are made over a range of angles of attack, referenced to the axis of the aft-cone, from 0° to 20°. The present results for ideal air are also compared with the results for real air of reference 7. These real-air data were obtained in the Langley Expansion Tube, an impulse-type facility with a run time of only 200 μsec, or approximately four orders of magnitude less than the present run time. The same models and instrumentation tested in the expansion tube were used in the present study. (It should be noted that the present study is the first at LaRC to use a model with a large number of thin-film resistance heat-transfer gages (ref. 10) in a conventional hypersonic wind tunnel.) The present measurements represent a significant step toward achieving the goal of a complete and accurate data base which provides an improved understanding of flow characteristics about biconics. They also provide the opportunity for comparison with and verification of flow-field computer codes.

Experimental Method

Facility

The Langley 31-Inch Mach 10 Tunnel, formerly known as the Langley Continuous-Flow Hypersonic Tunnel (ref. 11), uses a water-cooled, three-dimensional contoured nozzle to generate a nominal Mach number of 10 with dry air as the test gas. The test section is 78.7 cm square, the maximum operating reservoir pressure is 15.2 MPa, and the maximum reservoir temperature is 1060 K. This facility was operated in the blowdown mode for the present study and is referred to herein as the Mach 10 tunnel.

Models

A planform view and dimensions of the biconic models tested in the study of reference 7 and in the present study are shown in figure 1. The bent-nose biconic model represents a 1.9-percent-scale model of the proposed Mars sample-return single-mission vehicle (ref. 2). The models were fabricated from stainless steel, and five slots were machined in each model for instrumented inserts. (See fig. 2.) Two slots were machined along the most windward ray ($\phi = 180°$) (one on the fore-cone and one on the aft-cone), two along the most leeward ray ($\phi = 0°$), and one along the ray 90° from the most leeward ray on the aft-cone ($\phi = 90°$). The models were supported by a 1.9-cm diameter sting that was 35.6 cm long (fig. 3).

Instrumentation

The technology of thin-film resistance heat-transfer gages developed for the Langley Expansion Tube (refs. 7 and 10) was used without change in the present study. This use of the same gages in facilities with very different run times was possible because of the relatively large width (6.4 mm) and thickness (5.1 mm) of the substrates. The substrates were fabricated from MACOR[1] machinable glass-ceramic (ref. 12) and contoured to the conic section. Eight palladium gages, each approximately 100 nm thick, were deposited on the polished surface of each substrate (fig. 2(b)). The nose section was fabricated from MACOR with a single thin-film gage located at the spherical tip. All gages were in the

[1] MACOR glass-ceramic is a registered trademark of Corning Glass Works.

form of a serpentine pattern (as shown in fig. 2(b)) and provided nearly a point measurement since the sensing surface was 1.0 mm by 1.3 mm. Each gage was calibrated in a well-stirred oil bath for temperatures of 297 K to 380 K. This range covered the surface temperatures experienced during a test, with the exception of the gage at the tip of the spherical nose, where surface temperatures were much higher. Details of gage construction and calibration are discussed in reference 10. Each insert (i.e., substrate with thin-film gages) was sealed in place to provide a leak-free model surface.

A portable data-acquisition system consisting of 100 channels of constant-current circuits was used in this study. Each channel (circuit) had a differential amplifier allowing a gain selection of from 1 to 100 and a constant-current selection of either 1 mA or 4 mA. These circuits were wired to a 12-bit, 104-channel analog-to-digital (A/D) data-acquisition system which samples each channel at a rate of 50 samples per second; the extra 4 channels were used to monitor tunnel parameters. This A/D system was interfaced with a desktop computer. The 100-channel system was self-calibrating (100-Ω precision resistors were switched into each circuit, the voltage measured, and the current computed), and the initial voltage across each gage was recorded by the computer just minutes prior to the run.

Oil-flow tests were performed with larger models (2.9 percent scale) fabricated for force and moment tests (refs. 5 and 6). The models were painted black and sprayed with a mixture of white artist's oil pigment and silicon oils of various viscosities. The model was rapidly inserted into the test section and exposed to the free-stream flow for approximately 20 sec. Then, after a rapid retraction, the model was removed from the facility and the flow patterns were photographed. Separation lines are characterized by converging surface streamlines on both sides, indicated by an accumulation of white oil on the black model. Vortex reattachment is characterized by diverging surface streamlines on both sides providing a "feather-like" appearance. The oil-flow patterns presented herein were obtained by Vernon T. Helms III of LaRC.

Test Conditions

The pitot pressure in the test section could not be conveniently measured in the present study; hence, test-section flow conditions for measured reservoir pressures and temperatures were obtained from a previous calibration study (ref. 11). Test-section flow conditions were calculated by taking into account imperfect-gas (intermolecular-force) effects in the reservoir and by performing an isentropic nozzle expansion to the calibration value of free-stream Mach number. The post-normal-shock flow region is thermally perfect (the compressibility factor is equal to unity) but calorically imperfect ($\gamma_{t,2} \neq \gamma_\infty$). (A list of symbols used in this paper appears after the references.) Thus, the imperfect-air results of reference 13, which include vibrational excitation, were used in the present calculation of flow conditions.

Nominal reservoir stagnation conditions and corresponding free-stream flow parameters for the present study are as follows:

$p_{t,1}$, Pa	$T_{t,1}$, K	p_∞, Pa	T_∞, K	M_∞	$R_{\infty,L}$
2.4	980	61	49.8	9.9	2.2×10^5
10.9	1005	227	48.4	10.2	9.3

The value of L used to determine $R_{\infty,L}$ is 12.2 cm.

Both biconic models were tested over a range of angles of attack from 0° to 20° in 2° or 4° increments at each flow condition. The angle of attack is referenced to the axis of the aft-cone section.

Data Reduction

The numerical method used to compute values of the heat-transfer rate $\dot{q}$ from the output of the thin-film resistance gages is discussed in reference 10. As discussed in reference 7, the present values of $\dot{q}$ are based on a more accurate determination of the thermal properties of MACOR glass-ceramic than that presented in reference 10, and these values account for the variation of substrate thermal properties with temperature. Sample time histories of the heat-transfer rate and the heat-transfer coefficient C_h are shown in figure 4 for the gage at the nose tip and for the gages on the windward and leeward sides. Also shown in figure 4 are the changes in surface temperature ΔT_w at selected times. The heat-transfer coefficient is essentially constant for the time interval $0.5 < t < 1.4$ sec for all gages and all runs. ($t = 0$ is defined as the time the model first experiences an increase in surface temperature as it is inserted into the flow from a sheltered position.) Second-order least-square curve fits were applied to the time histories of $\dot{q}$ for $0.5 < t < 1.4$ sec, and values of $\dot{q}$ (or C_h) presented herein were obtained from these curve fits and correspond to $t = 1.0$ sec unless otherwise stated.

To eliminate time as a variable, the present heating data are plotted in terms of the heat-transfer coefficient $C_h = \dot{q}(t)/[h_{t,2} - h_w(t)]$. These values of C_h are nondimensionalized by the heat-transfer coefficient $C_{h,\mathrm{sph}}$ obtained from the stagnation-point heat-transfer rate of a sphere $\dot{q}_{\mathrm{sph}}$ with radius equal to the biconic nose radius. This value of $C_{h,\mathrm{sph}}$ is computed by using the theory of Fay and Riddell (ref. 14) with $T_w = 300$ K. Comparisons between prediction and measurement are made in terms of the heat-transfer rate for an isothermal model;

that is, because the measured heat-transfer coefficient is constant with time, values of $\dot{q}$ may be accurately determined as follows:

$$\dot{q}(t^*) = \dot{q}(t)\{[h_{t,2} - h_w(t^*)]/[h_{t,2} - h_w(t)]\}$$

where t^* is time at which $T_w = 300$ K.

Uncertainties

Probable sources of error for thin-film resistance heat-transfer gages are discussed in references 10 and 15. There are, however, other probable sources of error, unique to this study, which are discussed in the appendix. This study represents the first large-scale use of thin-film gages in a conventional hypersonic wind tunnel at LaRC. Lessons were learned with this "new" application of an "old" technique, and these too are discussed in the appendix. The heat-transfer rate inferred from the present thin-film gages is believed to be accurate to within 5 percent. Two tests were performed with the bent-nose biconic to examine run-to-run repeatability. As shown in figure 5, the agreement between $C_h/C_{h,\mathrm{sph}}$ values in these two tests is excellent (within 1 percent for all but two gages).

Prediction Method

Heating distributions were computed with a computer code that solves the steady, three-dimensional parabolized Navier-Stokes (PNS) equations (refs. 8 and 9). This code, obtained from the late John V. Rakich of the NASA Ames Research Center, requires supersonic flow in the downstream marching direction from the starting plane of data at or in front of the sphere-cone junction. The starting plane of data is determined from the Navier-Stokes solution over a sphere using the finite-volume, adaptive-grid algorithm described in reference 16. The PNS code of references 8 and 9 has been modified to include the straight biconic and bent-nose biconic geometries, and increased circumferential resolution was added (ref. 17); also added was the capability to compute real-gas effects of C, H, He, O, and N systems. The differences in predicted values of heat-transfer rate for ideal air and for real air in thermochemical equilibrium, which includes vibrational excitation, were insignificant for the present models and flow conditions.

Results and Discussion

Before presenting the data which illustrate the effects of nose bend, angle of attack, and free-stream Reynolds number on longitudinal heating distributions, a brief discussion of low Reynolds number effects on heating at the nose tip is presented. Next, oil-flow patterns illustrating the influence of Reynolds number and angle of attack on leeward surface flow characteristics are presented. These are presented prior to the measured longitudinal heating distributions to reveal certain aspects of the leeward flow that may not be inferred from the heating measurements alone. (The models used to measure heating rates provided relatively detailed longitudinal heating distributions on the most windward and leeward rays but did not provide circumferential heating distributions which would reveal information on leeward cross-flow separation phenomena.) The last two sections present comparisons of the data of this study with the real-air data obtained in the expansion tube (ref. 7) and with predictions from the PNS code (refs. 8 and 9). Tabulations of the measured heat-transfer rates for both biconics are presented in tables I to IV.

Low Reynolds Number Effects in Nose Region

As the Reynolds number is reduced, theories based on the assumption of a thin boundary layer, such as Fay and Riddell's (ref. 14), initially underestimate stagnation-point heating with decreasing Reynolds number and then progressively overestimate heating as slip effects become important. This trend is well documented in the literature (e.g., refs. 18 to 22) and is illustrated by the curves in figure 6, which were taken from reference 18. The experimental results in figure 6, shown by the symbols, were obtained with small quartz hemispheres (ref. 10) having a radius close to the nose radius r_n of the biconic models ($r_n = 4.1$ mm for the hemispheres and 3.8 mm for the biconics). A single thin-film gage was sputtered over the stagnation region of these hemispheres, which were tested in the Mach 10 tunnel and in the Langley Hypersonic CF_4 Tunnel (ref. 23). (These measured values of stagnation-region heating are expected to be 1 or 2 percent lower than the stagnation-point value since the thin-film element covers the stagnation region within 10° of the stagnation point.) The experimental results for air are nondimensionalized by the stagnation-point heating predicted with the theory of Fay and Riddell (ref. 14), where wall enthalpy h_w is determined from wall temperature T_w measured at $t = 0.6$ sec; the CF_4 results are nondimensionalized by values predicted by H. Harris Hamilton of LaRC using a boundary-layer code and the thermodynamic properties of reference 24 for CF_4. The experimental results in figure 6 show that low Reynolds number effects increase the stagnation-point heat-transfer rate by up to 10 percent over classic boundary-layer theory for the present model nose radius and flow conditions in air. These comparisons also illustrate the greater sensitivity of heating to viscous effects at larger values of the density ratio. (The curves of fig. 6 are shown to illustrate trends only. Because the calculated values of stagnation-point heat-transfer rate

used to nondimensionalize measured $\dot{q}$ in air and CF_4 were obtained from different sources than those used in reference 18, the good agreement between the curves and symbols may be fortuitous.)

Values of the stagnation-point heat-transfer rate measured on the quartz hemispheres in air are also compared with values predicted with the flow-field code of reference 16; this code solves the Navier-Stokes equations. These results are summarized in table V. The agreement between measurement and prediction with the Navier-Stokes code is quite good (within the experimental accuracy of 5 percent) over the present range of Reynolds numbers.

Leeward Surface Oil-Flow Patterns

Surface oil-flow patterns provide information on surface streamlines and thus reveal the complexity of the leeward flow of these biconics at incidence. The effect of Reynolds number at Mach 10 on leeward oil-flow patterns for the straight and bent-nose biconics at various angles of attack are shown in figures 7 and 8, respectively. These patterns were obtained with the larger biconic models used in references 5 and 6, and the values of $R_{\infty,L}$ were different than those for the heating measurements. Also, the larger models had an open base whereas the heat-transfer models had a solid, flat base. Although the ratio of sting radius to base radius was about the same for the two different-size models, the models used for oil-flow patterns had a smaller ratio of sting length to base diameter. These differences are mentioned since support interference effects may exist which influence the base flow and possibly the low-pressure leeward flow. (See the appendix and ref. 6.) Thus, comparisons between leeward flow characteristics inferred from the oil-flow patterns and from the heating distributions may be qualitative.

Typical of blunt cones at incidence (e.g., ref. 25), a large, favorable pressure gradient exists on the leeward side just downstream of the nose, causing the boundary layer to remain attached. In this region close to the nose (denoted as region A in fig. 8(c) which is a good example to illustrate this effect), the lateral component of skin friction is in the direction of the most leeward ray (plane of symmetry); however, at larger distances downstream of the nose (region B, fig. 8(c)), the lateral component changes direction and is now away from the most leeward ray. When this change in direction occurs, two symmetrical separation lines develop just downstream of the region where the lateral component of skin friction passes through zero (region C, fig. 8(c)). The longitudinal component of skin friction in the vicinity of the most leeward ray is finite, as revealed by oil which flowed from the attached region just downstream of the nose, through the region of zero lateral skin friction, and into the vortex region.

The photographs in figures 7 and 8 illustrate a strong influence of Reynolds number on leeward surface flow characteristics. For the straight biconic at $\alpha = 10°$, corresponding to $\alpha_f/\theta_f = 0.78$, the leeward flow remains attached over all or most of the surface at the lower Reynolds number (fig. 7(a)); however, an increase in Reynolds number (fig. 7(b)) promotes separation and the flow over the leeward side becomes quite complex. The intriguing, asymmetric oil-flow pattern observed in figure 7(b) is repeatable and appears to indicate the beginning of a secondary vortex near the base. These oil-flow patterns near the base resemble bubble-type flow separation patterns (ref. 25) and may be due to the influence of the base-region flow. The tendency of the separated leeward flow at $\alpha = 20°$ to become more complex (i.e., to establish primary and secondary vortices) with increasing Reynolds number is illustrated in figures 7(c) and 7(d). This trend of the primary vortex splitting to form a secondary vortex with increasing Reynolds number is also observed on the bent-nose biconic (fig. 8).

Oil-flow patterns photographed on the leeward side of the bent-nose biconic model at various angles of attack are shown in figure 9 for $R_{\infty,L} = 1.3 \times 10^6$. At $\alpha = 0°$ (fig. 9(a)), the flow is attached on the leeward side but separates as the angle of attack is increased to 5° (fig. 9(b)), that is, as the fore-cone angle of attack approaches the fore-cone half-angle. The separation region moves upstream with increasing angle of attack and is near the nose tip at $\alpha = 20°$. Primary and secondary vortices are observed for $\alpha \geq 10°$, again illustrating the complexity of the flow in this region with increasing angle of attack.

Effect of Nose Bend

Longitudinal heating distributions for the bent-nose biconic are compared with those for the straight biconic in figure 10 for various angles of attack at the lower value of Reynolds number. As mentioned previously, the angle of attack is referenced to the aft-cone section of both models; that is, the effect of nose bend is examined by holding the aft section fixed at a given angle of attack and bending the fore-cone upward 7°. Naturally, at $\alpha = 0°$ (fig. 10(a)), higher heating along the most windward ray ($\phi = 180°$) and lower heating along the most leeward ray ($\phi = 0°$) of the fore-cone occur for the bent-nose biconic; however, because of the larger expansion at the fore-cone–aft-cone junction, a decrease in the windward aft-cone heating occurs. Heating along the most windward ray of the aft-cone is actually less than that along the midmeridian ray ($\phi = 90°$) for the bent-nose biconic at $\alpha = 0°$ (fig. 10(a)). This trend is in qualitative agreement with the results of reference 4, in which the surface pressure

along the midmeridian ray of the bent-nose biconic aft-cone at $\alpha = 0°$ exceeded the pressure along the most windward ray by 5 to 10 percent at Mach 6 in air. (The relatively large difference in heating along the leeward ray and the windward ray of the straight biconic fore-cone is attributed primarily to misalignment of the insert on the leeward ray, as discussed in the appendix.) As the angle of attack is increased to 4° (fig. 10(b)), aft-cone heating levels along the windward and midmeridian rays of the bent-nose biconic are essentially the same; it is not until $\alpha \geq 8°$ (figs. 10(c) to 10(f)) that the heating along the windward ray exceeds that along the midmeridian ray.

Another interesting trend observed in figure 10 is the crossing of the leeward heating distributions for the two biconics as the angle of attack is increased. The nose bend results in a lower leeward heating at the lower angles of attack but a higher heating at the higher angles of attack. This crossing and trend reversal may be attributed possibly to the nose bend causing an earlier circumferential separation of the flow on the leeward side for a given angle of attack or possibly to an earlier transition from laminar to turbulent flow. Now, the oil-flow patterns shown in figure 7 reveal the leeward flow for the straight biconic remains attached for $0° \leq \alpha \leq 8°$, whereas circumferential flow separation is expected for the bent-nose biconic for $\alpha > 4°$ (fig. 9). Thus, the lower leeward heating for the bent-nose biconic at $\alpha = 0°$ and 4° (figs. 10(a) and 10(b)) is expected. At $\alpha = 8°$, the circumferential flow separation that occurs for the bent-nose biconic results in the formation of longitudinal, counterrotating primary vortices that reattach along the most leeward ray, thereby forming a "stagnation line" and augmenting the heating along this ray. From the oil-flow patterns, the flow separation originates just upstream of the base and moves upstream with increasing angle of attack, which is expected to cause a forward movement of the augmented leeward heating. Hence, the leeward heating distributions of figure 10 are consistent with the oil-flow patterns of figures 7 to 9. The fact that circumferential flow separation occurred is known; what is unknown is whether the separated flow remained laminar or became transitional. There is general agreement in the literature that transition location for blunt cones moves forward on the leeward ray with increasing angle of attack (e.g., see ref. 26); that is, the transition Reynolds number for leeward flow decreases with increasing angle of attack. Because both circumferential flow separation and transition cause an increase in leeward heating and produce the same trends with angle of attack (forward movement with increasing α), there is a problem distinguishing the effects of these two phenomena. The primary contributor to the trends in leeward heating observed in figure 10 is believed to be flow separation for the following two reasons: (1) the consistency between the oil-flow patterns and heating distributions, and (2) the qualitative agreement between measurement and laminar flow predictions, to be discussed subsequently in the section entitled "Comparison of Prediction With Measurement." This is not to imply that transition did not occur in the separated flow region (vortex system); however, whether or not transition occurred for the conditions of this study is unknown.

The windward heating for the bent-nose biconic at a given angle of attack is nondimensionalized by the windward heating for the straight biconic at the same angle of attack and is presented in figure 11 for the higher value of Reynolds number. The increase in windward fore-cone heating because of nose bend diminishes rapidly with increasing angle of attack (as expected) and is only about 20 percent at $\alpha = 20°$ (design trim angle of attack for bent-nose biconic configuration (ref. 2)). The decrease in windward aft-cone heating caused by nose bend is clearly illustrated in figure 11 and should also be of interest to the designer sizing the thermal protection system for such a biconic vehicle because the aft-cone surface area represents roughly 60 percent of the total surface area. Contrary to the fore-cone heating, this ratio (bent nose to straight) on the aft cone is not strongly influenced by the angle of attack. The windward aft-cone heating levels for the two biconics approach one another with distance downstream from the fore-cone–aft-cone junction; that is, the effect of nose bend on windward aft-cone heating diminishes with distance downstream from the junction and is less than 10 percent just ahead of the base for these biconics.

Effect of Reynolds Number

The effect of Reynolds number on heating distributions for the straight and bent-nose biconics are shown in figures 12 and 13 for various angles of attack. No effect of Reynolds number on windward fore-cone heating is observed on either biconic over the present range of angles of attack; this was also the case for a 15.1°/11.3° straight biconic tested at these same conditions in the Mach 10 tunnel (ref. 27). A small but distinguishable effect of Reynolds number on windward aft-cone heating is observed. However, the variation in heating between the two values of Reynolds number is generally within the experimental uncertainty, thereby precluding a definite conclusion that the aft-cone windward heating is dependent on the Reynolds number for $\alpha \leq 16°$ and independent of Reynolds number at $\alpha = 20°$. In general, heating along the midmeridian ray increases slightly with decreasing $R_{\infty,L}$ over the present range of α for both biconics.

Unlike the windward side, a large effect of Reynolds number is observed on the leeward heating. For the

straight biconic at $\alpha = 4°$ and 8° (figs. 12(b) and 12(c)) and for the bent-nose biconic at $\alpha = 0°$ (fig. 13(a)), a significant increase in leeward heating occurs as the Reynolds number is decreased. This increase in leeward heating with decreasing Reynolds number for attached flow may be primarily due to a significant increase in the boundary-layer displacement thickness with decreasing $R_{\infty,L}$. The larger displacement thickness causes a larger induced surface pressure and heating level. Another possible contributor to this difference in leeward heating is vorticity interaction resulting from the boundary-layer thickening and interacting with the inviscid flow. As the angle of attack is increased, the leeward heating distributions for the two values of $R_{\infty,L}$ cross one another (figs. 12 and 13). This crossing is the result of an increase in leeward heating (at the higher Reynolds number) that first occurs on the aft-cone near the base and moves upstream with increasing angle of attack. For $\alpha_f > 16°$, an opposite variation in leeward heating with $R_{\infty,L}$ is observed for x/L or $z/L > 0.2$; the leeward heating now increases with increasing $R_{\infty,L}$, as was also observed in reference 27. The trends of leeward heating in figures 12 and 13 are consistent with the oil-flow patterns, which show that for a given α an increase in Reynolds number will cause the flow to separate, thereby augmenting the leeward heating. The longitudinal leeward heating distributions at the highest value of $R_{\infty,L}$ also resemble those expected for transition from laminar to turbulent flow. Again, this is not to imply that transitional or turbulent flow on the leeward side necessarily occurred. Based on the present longitudinal heating distributions along the most windward ray ($\phi = 180°$) and along the midmeridian ray ($\phi = 90°$), which give no indication of transitional flow, and on previous studies in the Mach 10 tunnel, transition on these relatively small, smooth models is not expected for attached flow; however, as discussed in the previous section, the possibility that transition occurs on the leeward side at angles of attack sufficiently large to cause circumferential flow separation may exist.

Effect of Angle of Attack

Heating to the most windward ray increases orderly with angle of attack for both biconics, as expected (fig. 14). The sensitivity of windward heating to angle of attack is shown in figure 15 for both biconics and the lower Reynolds number in terms of the fore-cone angle of attack α_f and the aft-cone angle of attack α_a. ($\alpha_f = \alpha$ for the straight biconic, and $\alpha_f = \alpha + \eta$ for the bent-nose biconic, where η is the nose bend angle.) Although not readily apparent from the semilog plots of figure 15, the aft-cone windward heating for the biconics varies linearly with angle of attack, as does the fore-cone windward heating for the bent-nose biconic at $\alpha \geq 0°$ and for the straight biconic at $\alpha \geq 4°$. Good agreement in the windward heating is observed for the fore-cones of the two biconics, as expected. The trends are the same for the aft-cones, but the heating is less for the bent-nose biconic because of the larger flow expansion at the junction. Heating along the midmeridian ray of the aft-cone of both biconics is nearly independent of angle of attack over the present range (fig. 16), this heating being typical of cones (e.g., see ref. 28).

The variation of leeward heating with angle of attack (fig. 17) is not as orderly (i.e., increase only or decrease only with α) as that for the most windward and midmeridian rays. The influence of Reynolds number on leeward heating adds to this disorder. Leeward heating initially decreases with increasing angle of attack but reaches a point where it then increases with further increases in angle of attack, which is indicative of flow separation and possibly transition. The results of figure 17 also imply that flow separation on the leeward side first occurs just upstream of the base and moves upstream as the angle of attack increases, as observed in the oil-flow tests. Leeward cross-flow separation occurs for the straight biconic at the lower Reynolds number (fig. 17(a)) when the fore-cone angle of attack exceeds 0.8 times the fore-cone half-angle θ_f ($\alpha \geq 10°$ for this model) and at the higher Reynolds number (fig. 17(b)) when $\alpha > 0.6\theta_f$. The sensitivity of leeward heating to angle of attack at a given value of x/L or z/L on the fore-cone and aft-cone sections is shown in figure 18 for both biconics and for both values of Reynolds number. When presented in this manner, the angle of attack at which separation occurs on the aft-cone at $x/L = 0.78$ becomes more apparent. For example, for the straight biconic (fig. 18(a)), the minimum in aft-cone heating at $x/L = 0.78$ occurs at $\alpha = 12°$ for the lowest Reynolds number and at $\alpha = 8°$ for the highest Reynolds number. Thus, an increase in Reynolds number causes separation to occur at a lower angle of attack. It is interesting to note that leeward flow separation on the aft-cone of the bent-nose biconic appears to occur around $\alpha = 0°$ for the higher Reynolds number but does not occur on the fore-cone until $\alpha \geq 4°$ (fig. 18 (b)). For convenience, a comparison of heating levels on the most windward ray with those on the most leeward ray is presented in figure 19 for both biconics. For the present range of angles of attack and Reynolds numbers, the windward heating for these biconics is up to 20 times the leeward heating.

Comparison of Ideal-Air and Real-Air Heating

The ideal-air flow environment about the biconic models in the Mach 10 tunnel is quite different from the environment experienced by the full-scale vehicle during reentry. Generally, the "extrapolation" of heating data obtained in conventional hypersonic wind tunnels to flight conditions is implicit; that is, wind tunnel

data are used to verify a computer code which in turn is used, with the appropriate gas chemistry, to predict the flow environment in flight. This approach (verification of a computer code) is the subject of the next section of this report. Another method of extrapolation is to compare conventional hypersonic wind tunnel results with flight data for the same configuration or similar configurations. Unfortunately, flight data are generally scarce. Although not as desirable as comparison with flight data, a rough deduction of real-gas effects on heating may be made by comparing conventional hypersonic wind tunnel data with heating rates measured in hypervelocity-hypersonic impulse facilities. Such a comparison (i.e., heating distributions measured in a conventional hypersonic tunnel with those measured in an impulse facility) is the subject of this section.

The present results provide the opportunity to compare heating distributions measured in two distinctly different facilities—a hypervelocity-hypersonic impulse facility (the Langley Expansion Tube) and a conventional hypersonic wind tunnel (the Langley 31-Inch Mach 10 Tunnel)—containing the same models and model instrumentation. The flow conditions for the present tests in the Mach 10 tunnel and those in the expansion tube for real (i.e., dissociated) air in thermochemical equilibrium (ref. 7) are compared in table VI to illustrate the differences in free-stream flow conditions, ratio of specific heats behind the normal shock, density ratio, and ratio of wall to total temperature.

Heating distributions on the biconics (in terms of $C_h/C_{h,\mathrm{sph}}$) measured in the expansion tube exceed those measured in the Mach 10 tunnel at the lower Reynolds number over the present range of angles of attack (figs. 20 and 21). This is true for both the windward and leeward rays. For the windward ray at the higher Reynolds number, this trend also holds true; however, leeward heating at this higher Reynolds number in the Mach 10 tunnel often exceeds the results obtained in the expansion tube, particularly at the higher angles of attack. Higher windward heating is expected for a real gas; however, the differences in figures 20 and 21, which are typically 20 to 50 percent, are significantly higher than those usually associated with real-air effects alone (e.g., see refs. 29 and 30).

Several factors are expected to contribute to the differences observed between the ideal-air Mach 10 tunnel results and the real-air expansion tube results (figs. 20 and 21). One is the ratio of wall to total temperature. Although the substrate surface temperature at 200 μsec in the expansion tube and at 1 sec in the Mach 10 tunnel are nearly the same, the expansion tube data correspond to a relatively low value of $T_w/T_{t,2}$ (from table VI), a fact which is expected to increase the heat-transfer rate. A second factor is viscous effects. Where the flow is attached, the boundary-layer displacement thickness increases with decreasing Reynolds number, resulting in a larger effective cone angle and hence a larger induced surface pressure and higher heat-transfer rate. At high values of Reynolds number, the increase in displacement thickness may not be significant enough to cause a measurable effect on heating; however, for the relatively low Reynolds number of the expansion tube tests in air, the effect on heating may be significant. In the Reynolds number regime where vorticity interaction between the boundary layer and the outer inviscid layer are significant, where viscous effects are no longer confined to a thin boundary layer but exist throughout the shock layer, and where there is an absence of significant slip effects, an increase in relative heating (i.e., $C_h/C_{h,\mathrm{sph}}$) is expected over that at a higher Reynolds number. Also, viscous effects on heating are expected to be more significant for the expansion tube results (compared with the Mach 10 tunnel results) because of the higher density ratio and thus the smaller shock detachment distance. Now, the lower value of $T_w/T_{t,2}$ for the expansion tube data is expected to thin the boundary layer and diminish the effect of vorticity interaction; nevertheless, the larger viscous effects expected in the expansion tube tests are believed to contribute to the increase in windward heating over that measured in the Mach 10 tunnel. As illustrated in the section "Effect of Reynolds Number," there is a strong influence of Reynolds number on leeward heating for a given Mach number, $T_w/T_{t,2}$, and γ. Thus, the difference in Reynolds numbers for the two facilities is expected to contribute to the differences observed in the leeward heating. A third factor is entropy swallowing. The higher density ratio of the expansion tube causes a decrease in the shock detachment distance as compared with that in the Mach 10 tunnel. Thus, the entropy layer is expected to be swallowed much quicker in the expansion tube tests, and the lower Reynolds number of the expansion tube flow accelerates this swallowing.

Because of combined real-gas effects, which result in high density ratios and may include nonequilibrium (or frozen) flow effects, viscous effects, and high wall cooling for the expansion tube results, it is difficult to determine the major contributor(s) to the differences observed in figures 21 and 22. It should be noted, however, that the windward heating on these biconics in the hypervelocity helium flow, which behaves ideally, and in the hypervelocity air and nitrogen flows of the expansion tube (ref. 7) are correlated to within 10 percent for $\alpha > 4°$ with an expression in the form

$$N_{St,\infty}\alpha\frac{\bar{v}^*\ sin\theta_e}{(\rho_2/\rho_\infty)^{1/4}}$$

This proportionality shows that the windward heating for the conditions of the expansion tube tests is ex-

pected to be 30 percent higher than for the Mach 10 tunnel tests at the lower Reynolds number, this difference being close to the differences observed in figures 20 and 21. This closeness is shown in figure 22, where the quantity $N_{St,\infty}(\rho_2/\rho_\infty)^{1/4}/\bar{v}^*$ provides a reasonable correlation of the ideal-air and the real-air windward heating for the straight biconic. Thus, this proportionality may provide an approximate determination of real-air effects on windward heating for biconics from data obtained in hypersonic ideal-air wind tunnels.

Comparison of Prediction With Measurement

Heating distributions predicted with the PNS code (refs. 8 and 9) are compared with measurements for the most windward ray and the most leeward ray of the bent-nose biconic in figure 23 for both Reynolds numbers. Both the measured and the predicted results correspond to a model surface temperature of 300 K. In general, the PNS code slightly underpredicts heating on the fore-cone but is within 10 percent. This code overpredicts the heating just downstream of the fore-cone–aft-cone junction at the lower angles of attack but underpredicts the heating in this region at the higher angles of attack. On the leeward side, the agreement between prediction and measurement is poorer. The PNS code underpredicts heating by up to 25 percent at the lower angles of attack, and the agreement improves at $\alpha \geq 16°$. The different trends in measured leeward heating distributions due to the Reynolds number are qualitatively predicted by the PNS code. Since this code was exercised only for laminar flow, this qualitative agreement implies the leeward flow prior to separation is laminar for both values of Reynolds number. One possible explanation for the differences between measurement and prediction may be, naturally, errors in the measurement as discussed in the appendix. Another possible reason for the PNS code tending to underpredict measured heating is this code does not account for downstream influences propagating upstream through the subsonic portion of the boundary layer. There is evidence (ref. 31) that failure to include this effect will yield values of heating that are too low. Another possible contributor to the differences observed in leeward heating is the separated leeward flow may be subjected to transitional flow effects at or prior to flow reattachment. All things considered, the PNS code provides a reasonably accurate prediction of the heating distributions on the present biconics in Mach 10 air for $0° < \alpha < 20°$.

Concluding Remarks

Laminar heating distributions were measured on a 1.9-percent-scale model of a generic aeroassisted vehicle represented by a spherically blunted, 12.84/7° biconic with the fore-cone section bent upward 7°; also tested was a straight biconic. Heating distributions were measured along the most windward, the most leeward, and the midmeridian rays of the biconic models in the Langley 31-Inch Mach 10 Tunnel (formerly known as the Langley Continuous-Flow Hypersonic Tunnel) at values of the free-stream Reynolds number based on model length of about 2×10^5 and 9×10^5. The angle of attack, referenced to the aft-cone, was varied from 0° to 20°.

With the aft-cone section as the reference for angle of attack, the penalty (increase) in windward fore-cone heating because of the nose bend decreased with increasing angle of attack (as expected) and was only 20 percent at an angle of attack of 20°. This nose bend caused a decrease in windward aft-cone heating which is significant since the aft-cone represents approximately 60 percent of the vehicle surface. No effect of Reynolds number on heating was observed on the windward side of the fore-cone (although a small effect may have occurred on the aft-cone), but a large effect of Reynolds number on heating occurred on the leeward side. Two phenomena may have caused the observed trends in heating along the most leeward ray. One is circumferential flow separation and the formation of primary vortices that impinge on the leeward ray. The other is transition in the separated flow region. Comparisons between the oil-flow patterns and measured heating distributions and between measured and predicted heating distributions imply flow separation was the primary contributor to these trends. An increase in Reynolds number caused the flow on the leeward side to separate at a lower angle of attack. For the case of attached flow (i.e., at low angles of attack), leeward heating increased with decreasing Reynolds number; the opposite was true for separated flow, which occurred when the fore-cone angle of attack exceeded about 0.6 to 0.8 times the fore-cone half-angle. Leeward cross-flow separation first occurred just ahead of the base and moved upstream with increasing angle of attack. The influence of Reynolds number on the leeward flow was illustrated by leeward surface oil-flow patterns as well, which clearly revealed the complexity of the separated flow in this region. In general, windward heating was predicted to within 10 percent with a computer code that solves the steady, three-dimensional parabolized Navier-Stokes (PNS) equations. Although leeward heating distributions were predicted qualitatively by the PNS code for both values of Reynolds number, quantitative agreement was somewhat poorer than on the windward side.

Langley Research Center
National Aeronautics and Space Administration
Hampton, VA 23665
August 17, 1984

Appendix

Uncertainties in Measured Heating Rates

Because the use of thin-film gages to measure heating distributions on models in wind tunnels is expected to grow at the Langley Research Center and at other research centers in the future, a fairly detailed discussion of some of the lessons learned is presented in this appendix. The inserts (i.e., MACOR glass-ceramic substrates with palladium thin-film gages sputtered onto the surface) used in the present study were from the same batch fabricated for the study of reference 7. That is, the thin-film technology developed for the Langley Expansion Tube was used without change in the Langley 31-Inch Mach 10 Tunnel. This usage in two very different facilities with run times that differ by four orders of magnitude was possible because of the relatively large width and thickness of the MACOR substrates. The large size of these substrates allowed the substrate to behave as an infinite slab for several seconds. Even though the gage fabrication process, circuitry, and data-acquisition system had been developed to a high level for the expansion tube, the use of these gages in a conventional hypersonic wind tunnel ushered in other concerns regarding accuracy.

A number of inserts for the aft-cone from the batch of inserts fabricated for the study of reference 7 were available for the present study, but only a few were available for the forecone. Thus, the aft-cone of each biconic was fitted with inserts of very good quality, whereas the fore-cone inserts had several gages open, a wider range of gage resistance for a given substrate, and generally provided a poorer fit to the steel models.

Calibrations before and immediately after the present tests revealed that all but a few gages on the aft-cone ($\phi = 0°, 90°$, and $180°$) for both biconics were stable to within 0.2 percent. That is, the temperature coefficient of resistance remained constant to within 0.2 percent for the 12 to 15 runs made with each insert, and the resistance at $T = 297$ K remained constant to within 1.0 percent. Agreement between the two calibrations was poorer for the fore-cone substrates, but the coefficient of resistance was within 1.2 percent. The post-run calibration revealed that only 3 of the 48 gages on the aft-cones of the biconic models were damaged (but not destroyed) during this test series, and 1 of the 16 leeward fore-cone gages was damaged. Of the 11 working gages on the windward fore-cone of the 2 models at the beginning of the test series, 2 were destroyed and all but 1 were damaged. This account of gage damage is presented because, as discussed in reference 10, the delicate nature of these gages was considered a major disadvantage for their use in such tunnels. The present results demonstrate this was a valid concern but also demonstrate the feasibility of such usage.

Until recently, probably the major uncertainties associated with the use of MACOR substrates were the uncertainty in the thermal properties of MACOR and the variation of these properties with temperature. A study (ref. 7) was performed in the Mach 10 tunnel in which the stagnation-point heat-transfer rate was measured simultaneously on five small hemispheres. Two hemispheres were made of MACOR glass-ceramic, two were made of quartz, and one was made of Pyrex 7740 glass. Each hemisphere contained a thin-film gage (with the same serpentine pattern as on the substrates for the biconic models) at the stagnation region. This study, reported in appendix B of reference 7, was designed so that the substrate material was the only intended variable for a given run. Because the thermal properties for quartz and for Pyrex glass are believed to be accurately known, direct comparison of the stagnation-point heat-transfer rates of the five hemispheres over a range of flow conditions allowed a determination of the thermal properties of MACOR glass-ceramic. The thermal properties of MACOR glass-ceramic were also determined in three other independent studies (ref. 7). All four of these sources, each using a different technique, provided thermal properties for MACOR to within ± 2 percent of one another.

Based on uncertainties associated with gage characteristics, circuitry, data-acquisition system, calibration, and data-reduction procedure, measured values of the heat-transfer rate are believed to be accurate to within ± 5 percent (refs. 7 and 10). However, other phenomena may have led to errors in the present measured heating distributions. These were (1) uncertainty in angle of attack ($\pm 0.20°$), (2) possible source flow effects (maximum flow angularity of $\pm 0.25°$), (3) misalignment of the inserts, (4) discontinuity in substrate and model surface properties, (5) departure of the substrate from one-dimensional behavior, (6) sting interference effects, (7) sting deflection, and (8) disturbances resulting from the model injection procedure.

The substrates were 6.35 mm wide and 5.10 mm thick, thereby assuring one-dimensional behavior for $t \leq 1.0$ sec, as discussed in reference 10 and verified by the fact that C_h remained constant for $0.5 \leq t \leq 1.5$ sec. All inserts except the leeward fore-cone fit nicely in the straight biconic model. This one insert was inclined into the flow, and the effect of this inclination was apparent at $\alpha = 0$. (The decision was made to test this model with the misaligned insert because of tunnel scheduling considerations and because only two inserts for the fore-cone of each model were left over from the study of ref. 7 and a considerable amount of time is required to machine and polish the substrate, install gages and leads, and calibrate.)

Whether or not there was a significant effect on heating because of the mismatch in substrate and model materials (ref. 15) is unknown. Ideally, the entire model should be MACOR glass-ceramic, but this was not structurally or economically feasible for tests in the expansion tube. The effect of different materials on heating distributions increases with the difference in surface temperature between the materials (ref. 15). As a worst case example, if the steel surface temperature is assumed to remain near ambient for $t \leq 1.0$ sec, the difference in T_w on the leeward side is relatively small (typically less than 5 K); hence, any effect on leeward heating because of a material mismatch is expected to be essentially negligible (less than 1 percent or so (ref. 15)). The effect on the windward side will naturally be larger, but whether it is of significant magnitude is unknown. This effect diminishes with distance from the discontinuity, and C_h measured on the MACOR glass-ceramic surface is less than C_h measured for an all steel model with a lower surface temperature (ref. 15).

Other phenomena of concern were sting deflection during a run and the possible existence of support interference effects. As shown in figure 3, a relatively long sting was used ($L_s/d_b = 7$ and $d_s/d_b = 0.38$); in fact, this sting was about the maximum length permissible to ensure the shock layer about the model remained fully within the inviscid test core for the present range of angles of attack. The sting deflection was predicted by using the aerodynamic coefficients tabulated in reference 6 to obtain the force acting at the center of gravity of the model. For the bent-nose biconic at $\alpha = 20°$ and $R_{\infty,L} = 2.2 \times 10^5$ (lower value of free-stream dynamic pressure), the sting deflection was only 0.05°; hence, the sting deflection was negligible at the lower Reynolds number for both biconic models and the present range of angles of attack. At the higher Reynolds number, the predicted sting deflection for the bent-nose biconic was 0.1° at $\alpha = 10°$ and 0.2° at $\alpha = 20°$; this deflection had a relatively small effect (less than 1 percent) on the windward heating (fig. 15). To illustrate support interference effects, the pressure distribution measured on the 2.9-percent-scale straight biconic model in the Mach 10 tunnel at $\alpha = 0°$ and $R_{\infty,L} = 0.3 \times 10^6$ is shown in figure 24. The maximum possible sting length for this model and sting adapter was only 9.9 cm ($L_s/d_b = 1.3$). Tests were performed with this sting length and with $L_s/d_b = 0.8$. From figure 24, the measured base pressures (at $x/L = 1.0$) for both sting lengths exceed the aft-cone surface pressure. This resulted in the base region influencing the flow over the aft-cone, as indicated by the increase in the longitudinal pressure distribution in the direction of the base. (The influence of the base region on the aft-cone pressure distribution diminished with increasing angle of attack.) In general, laminar heating distributions for blunt cones essentially follow the trend in the corresponding pressure distributions (e.g., see refs. 28, 32, and 33). No increase in heating on the aft-cone in the direction of the base was observed for the present tests at $\alpha = 0°$ (figs. 10(a) and 12(a)). Thus, it is assumed that the present results are free of support interference effects.

The last uncertainty for the present heating measurements discussed was due to the model injection procedure. This potential problem was not detected until after completion of the present tests when a Space Shuttle orbiter model having a number of thin-film gages on the leeward fuselage and wing was tested in the Mach 10 tunnel. At the time of the present tests, the controller for the 100-channel data-acquisition system was capable of acquiring data for a 6-sec period. Approximately 1 to 2 sec of this period was used for establishing a baseline, which was always quite steady with time. At the time of the orbiter tests, data could be acquired over a 12-sec period. This increased capability was used to examine the baseline for a longer period, typically 8 to 9 sec. As shown in figure 25, the model was subjected to a transient prior to its being inserted into the flow. Once steady flow was established in the tunnel, a door (section of the nozzle wall) was opened and the model was inserted into the flow. Upon this opening, the conditions in the large model-support-system housing, and thus ambient conditions for the model, changed somewhat. Because of their high sensitivity and fast response, the thin-film gages immediately detected this change, as shown in figure 25.

The sequence of events that occurred for a thin-film gage in the Mach 10 tunnel is depicted in the following sketch:

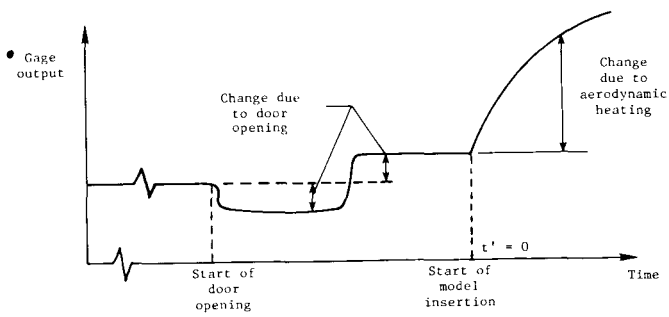

Naturally, the subject of interest was the aerodynamic heating (i.e., the heating that occurred for $t' > 0$), and the concern was with the possible effect of the transient resulting from the door opening on the determination of this aerodynamic heating. Now, the basic equation relating the substrate surface temperature change to the voltage change in the thin-film element is

$$\Delta T(t) = \frac{\Delta E(t)}{E_i \alpha_R}[1 + \alpha_R(T_i - T_r)] \qquad \text{(A1)}$$

where E_i is the initial gage voltage and T_i is the initial gage temperature. These values are measured several minutes prior to the run (and thus prior to the door opening). The initial substrate temperature is assumed to be the room temperature, and the thermal coefficient of resistance α_R is obtained from the gage calibration, where T_r is the reference temperature (297 K) used to determine α_R. Thus, α_R and T_r are constants. The term in brackets accounts for $T_i \neq T_r$. This equation was used to infer the substrate surface temperature change from the measured voltage change for $t' > 0$; however, the initial gage voltage and the initial gage temperature at t' are unknown for the present tests with the biconic models because of the transient. For this reason, results from the previously mentioned tests with a Space Shuttle orbiter model were analyzed to estimate the effect of this transient.

At $t' = 0, \Delta E$ is known for the Space Shuttle orbiter tests, and

$$E_i \equiv E_i' = E_i + \Delta E_{t'=0} \quad (t' = 0)$$

and

$$T_i \equiv T_i' = T_i + \Delta T_{t'=0} \quad (t' = 0)$$

where $\Delta T_{t'=0}$ is obtained from equation (A1) with $\Delta E = \Delta E_{t'=0}$. The heat-transfer rate is obtained from the expression (ref. 34)

$$\dot{q}(t) = \frac{2\beta_{s,i}}{\pi^{1/2}} \sum_{j=1}^{n} \frac{\Delta T_j - \Delta T_{j-1}}{(t_n - t_j)^{1/2} + (t_n - t_{j-1})^{1/2}} \qquad \text{(A2)}$$

where the change in temperature because of aerodynamic heating ($t' > 0$) is given by

$$\Delta T(t') = \frac{\Delta E(t')}{E_i' \alpha_R}[1 + \alpha_R(T_i' - T_r)] \qquad \text{(A3)}$$

Substrate thermal properties (i.e., β_s) vary with temperature. For MACOR glass-ceramic

$$\beta_{s,i} = 1816.6 + 0.6303 T_i \quad (294 \text{ K} < T_i < 312 \text{ K}) \qquad \text{(A4)}$$

Thus, the ratio of $\dot{q}(t)$ based on corrected values of the initial voltage and temperature (i.e., E_i' and T_i') to $\dot{q}(t)$ based on values of E_i and T_i measured prior to the door opening is

$$\frac{\dot{q}(E_i', T_i')_{t'>0}}{\dot{q}(E_i, T_i)_{t>0}} = \frac{\beta_{s,i}(T_i')E_i[1 + \alpha_R(T_i' - T_r)]}{\beta_{s,i}(T_i)E_i'[1 + \alpha_R(T_i - T_r)]} \qquad \text{(A5)}$$

The baselines for three thin-film gages installed along the leeward centerline of the Space Shuttle model fuselage were used to estimate the effect of the door opening. Results were examined at the lowest and the highest Reynolds numbers (reservoir pressures) of the Mach 10 tunnel and with different orientations of the model with respect to the door (i.e., wing into the flow first and leeward side into the flow first). A typical value of α_R for the Pyrex glass substrates was 2.3×10^{-3} K^{-1}, T_i prior to the door opening was 299 K, and E_i was 0.4 V. For all the runs examined, the maximum change in gage output between $t' = 0$ and prior to the door opening was 1.45 mV. Even for this worst case, the effect on $\dot{q}$ was negligible (less than 0.1 percent). Thus, the effects of this transient on the present results, which had similar values of α_R, T_i, and E_i, are believed to have been negligible.

During the evacuation of the model support housing in preparation for a tunnel run, the temperature decreases appreciably inside this housing. For this reason, a thermocouple was attached to the sting of the Space Shuttle orbiter model to monitor the model temperature. This measurement revealed that the model temperature was not significantly affected by the evacuation and was generally within a few degrees Fahrenheit of the room temperature a few minutes prior to a run. Thus, the assumption that T_i was equal to the room temperature appears to have been valid for the present tests.

References

1. Walberg, Gerald D.: A Review of Aeroassisted Orbit Transfer. AIAA-82-1378, Aug. 1982.
2. Florence, Dwight E.: Aerothermodynamic Design Feasibility of a Generic Planetary Aerocapture/ Aeromaneuver Vehicle. *Thermophysics of Atmospheric Entry*, T. E. Horton, ed., AIAA, 1982, pp. 477–519.
3. Florence, Dwight E.: Aerothermodynamic Design Feasibility of a Generic Planetary Aerocapture/ Aeromaneuver Vehicle. AIAA-81-1127, June 1981.
4. Miller, Charles G., III; and Gnoffo, Peter A.: *Pressure Distributions and Shock Shapes for* 12.84°/7° *On-Axis and Bent-Nose Biconics in Air at Mach 6.* NASA TM-83222, 1981.
5. Miller, C. G.; and Gnoffo, P. A.: An Experimental Investigation of Hypersonic Flow Over Biconics at Incidence and Comparison to Prediction. AIAA-82-1382, Aug. 1982.
6. Miller, C. G.; Blackstock, T. A.; Helms, V. T.; and Midden, R. E.: An Experimental Investigation of Control Surface Effectiveness and Real-Gas Simulation for Biconics. AIAA-83-0213, Jan. 1983.
7. Miller, Charles G., III; Micol, John R.; and Gnoffo, Peter A.: *Laminar Heat-Transfer Distributions on Biconics at Incidence in Hypersonic-Hypervelocity Flows.* NASA TP-2213, 1984.
8. Vigneron, Y. C.: Calculation of Supersonic Viscous Flow Over Delta Wings With Sharp Subsonic Leading Edges. AIAA Paper 78-1137, July 1978.
9. Agarwal, R.; and Rakich, J. V.: Supersonic Laminar Viscous Flow Past a Cone at Angle of Attack in Spinning and Coning Motion. *AIAA J.*, vol. 20, no. 6, June 1982, pp. 761–768.
10. Miller, Charles G., III: *Comparison of Thin-Film Resistance Heat-Transfer Gages With Thin-Skin Transient Calorimeter Gages in Conventional-Hypersonic Wind Tunnels.* NASA TM-83197, 1981.
11. Miller, Charles G., III: *Measured Pressure Distributions, Aerodynamic Coefficients, and Shock Shapes on Blunt Bodies at Incidence in Hypersonic Air and* CF_4. NASA TM-84489, 1982.
12. Grossman, David G.: Machining a Machinable Glass-Ceramic. *Vacuum*, vol. 28, no. 2, Feb. 1978, pp. 55–61.
13. Brahinsky, Herbert S.; and Neel, Charles A.: *Tables of Equilibrium Thermodynamic Properties of Air. Volume III. Constant Entropy.* AEDC-TR-69-89, Vol. III, U.S. Air Force, Apr. 1969. (Available from DTIC as AD 687 092.)
14. Fay, J. A.; and Riddell, F. R.: Theory of Stagnation Point Heat Transfer in Dissociated Air. *J. Aeronaut. Sci.*, vol. 25, no. 2, Feb. 1958, pp. 73–85, 121.
15. Schultz, D. L.; and Jones, T. V.: Heat-Transfer Measurements in Short-Duration Hypersonic Facilities. AGARD-AG-165, Feb. 1973.
16. Gnoffo, P. A.: A Vectorized, Finite-Volume, Adaptive Grid Algorithm Applied to Planetary Entry Problems. AIAA-82-1018, June 1982.
17. Gnoffo, Peter A.: Hypersonic Flows Over Biconics Using a Variable-Effective Gamma, Parabolized-Navier-Stokes Code. AIAA-83-1666, July 1983.
18. Gilbert, Leon M.; and Goldberg, Leon: A Reynolds Number Scaling Theory for Hypersonic Ablation. AIAA Paper 67-155, Jan. 1967.
19. Cheng, H. K.: The Blunt-Body Problem in Hypersonic Flow at Low Reynolds Number. IAS Paper 63-92, Jan. 1963.
20. Ferri, Antonio; Zakkay, Victor; and Ting, Lu: On Blunt-Body Heat Transfer at Hypersonic Speed and Low Reynolds Numbers. *J. Aerosp. Sci.*, vol. 29, no. 7, July 1962, pp. 882–883.
21. Ferri, Antonio; and Zakkay, Victor: Measurements of Stagnation Point Heat Transfer at Low Reynolds Numbers. *J. Aerosp. Sci.*, vol. 29, no. 7, July 1962, pp. 847–850.
22. Kao, Hsiao C.: Hypersonic Viscous Flow Near the Stagnation Streamline of a Blunt Body: II. Third-Order Boundary-Layer Theory and Comparison With Other Methods. *AIAA J.*, vol. 2, no. 11, Nov. 1964, pp. 1898–1906.
23. Midden, R. E.; and Miller, C. G.: *Description and Preliminary Calibration Results for the Langley Hypersonic* CF_4 *Tunnel.* NASA TM-78800, 1978.
24. Sutton, Kenneth: *Relations for the Thermodynamic and Transport Properties in the Testing Environment of the Langley Hypersonic* CF_4 *Tunnel.* NASA TM-83220, 1981.
25. Stetson, Kenneth F.: Boundary-Layer Separation on Slender Cones at Angle of Attack. *AIAA J.*, vol. 10, no. 5, May 1972, pp. 642–648.
26. Stetson, Kenneth F.: Effect of Bluntness and Angle of Attack on Boundary Layer Transition on Cones and Biconic Configurations. AIAA Paper 79-0269, Jan. 1979.
27. Dearing, J. David: *Laminar Heat-Transfer Distributions for a Blunted-Cone, Cone-Frustum Reentry Configuration at Mach 10.* NASA TN D-5146, 1969.
28. Widhopf, George F.: Turbulent Heat-Transfer Measurements on a Blunt Cone at Angle of Attack. *AIAA J.*, vol. 9, no. 8, Aug. 1971, pp. 1574–1580.
29. Swaminathan, S.; Kim, M. D.; and Lewis, Clark H.: Real Gas Flows Over Complex Geometries at Moderate Angles of Attack. AIAA-82-0392, Jan. 1982.
30. Griffith, B. J.; Adams, J. C., Jr.; and Majors, B. M.: Hypersonic Turbulent Boundary-Layer Parameters on Spherically Blunted Cones, Including Entropy-Layer Swallowing and Real-Gas Effects. AIAA-81-1089, June 1981.
31. Rakich, John V.: Iterative PNS Method for Attached Flows With Upstream Influence. *AIAA 6th Computational Fluid Dynamics Conference—A Collection of Technical Papers*, July 1983, pp. 473–482. (Available as AIAA-83-1955.)
32. Widhopf, George F.: Heat-Transfer Correlations for Blunt Cones at Angle of Attack. *J. Spacecr. & Rockets*, vol. 8, no. 9, Sept. 1971, pp. 1002–1004.

33. Griffith, B. J.; and Lewis, Clark H.: Laminar Heat Transfer to Spherically Blunted Cones at Hypersonic Conditions. *AIAA J.*, vol. 2, no. 3, Mar. 1964, pp. 438–444.

34. Cook, William J.: Unsteady Heat Transfer to a Semi-Infinite Solid With Arbitrary Surface Temperature History and Variable Thermal Properties. ISU-ERI-AMES-67500, Iowa State Univ., Feb. 1970. (Available from NTIS as PB 190 040.)

Symbols

C^*	$= \mu^* T_\infty / \mu_\infty T^*$
C_h	heat-transfer coefficient, $\dot{q}/(h_{t,2} - h_w)$, J-sec/m^4
C_p	pressure coefficient, $(p - p_\infty)/q_\infty$
c	specific heat, J/kg-K
d	diameter, m
E	voltage, V
h	enthalpy, J/kg
k	thermal conductivity, W/m-K
L	length, m
M	Mach number
N_{St}	Stanton number, $C_h/\rho_\infty U_\infty$
p	pressure, Pa
q	dynamic pressure, Pa
$\dot{q}$	heat-transfer rate, W/m^2
R	unit Reynolds number, m^{-1}
r	radius, m
T	temperature, K
T^*	reference temperature, $(T_{t,2}/6)$ $[1 + (3T_w/T_{t,2})]$, K
t	time, sec
t^*	time at which $T_w = 300$ K
U	velocity, m/sec
$\bar{v}^*$	viscous interaction parameter, $M_\infty (C^*/R_{\infty,L})^{1/2}$
x, y, z	model coordinates (see fig. 1), m
α	angle of attack, deg
α_R	temperature coefficient of resistance, K^{-1}
β	$(\rho c k)^{1/2}$, W-sec$^{1/2}$/m^2-K
γ	ratio of specific heats
η	nose bend angle, deg
θ	cone half-angle, deg
μ	viscosity, N-sec/m^2
μ^*	viscosity evaluated at T^*, N-sec/m^2
ρ	density, kg/m^3
ϕ	circumferential angle measured from the most leeward ray, deg

Subscripts:

a	aft-cone section
b	base
BL	thin-boundary-layer theory
e	effective
f	fore-cone section
i	initial
iso	isothermal ($T_w = 300$ K)
L	length
m	measured
n	nose
r	reference
s	sting
sph	stagnation-point value for a sphere
$t, 1$	reservoir stagnation conditions
$t, 2$	stagnation conditions behind normal shock
w	model surface; wall surface
2	static conditions immediately behind normal shock
∞	free-stream conditions

The following symbols are used in computer-generated tables:

Ch/Chsph	ratio of heat-transfer coefficient to stagnation-point heat- transfer coefficient of a sphere
Ht,2	stagnation enthalpy behind normal shock, J/kg
Minf	free-stream Mach number
phi	circumferential angle, deg ($\phi = 180°$ on most windward ray; $\phi = 0°$ on most leeward ray)
pt,1	reservoir stagnation pressure, N/m^2 (1 N/m^2 = 1 Pa)
pt,2	stagnation pressure behind normal shock, N/m^2
pinf	free-stream pressure, N/m^2
p2	static pressure immediately behind normal shock, N/m^2

Q/Qsph	ratio of heat-transfer rate to stagnation-point heat-transfer rate of a sphere
Qdot	heat-transfer rate, W/m^2
Qsph,FR	stagnation-point heat-transfer rate predicted with theory of Fay and Riddell, W/m^2
Q(Tw=300K)	heat-transfer rate evaluated at a wall temperature of 300 K, W/m^2
Rhoinf	free-stream density, kg/m^3
Rho2	static density immediately behind normal shock, kg/m^3
Rho2/Rhoinf	ratio of static density immediately behind normal shock to free-stream density
Rinf,L	free-stream unit Reynolds number based on model length
R2,L	static unit Reynolds number, based on model length, immediately behind normal shock
St_inf	free-stream Stanton number
Tinf	free-stream temperature, K
Tt,1	reservoir stagnation temperature
Twall	wall temperature, K
T2	static temperature immediately behind normal shock, K
Uinf	free-stream velocity, m/sec
x/L	ratio of model station in x-direction to model length
z/L	ratio of model station in z-direction to model length

TABLE I. MEASURED HEAT-TRANSFER DATA FOR STRAIGHT BICONIC AT LOW REYNOLDS NUMBER

(a) $\alpha = 0°$

FLOW CONDITIONS

Pt,1 N/m^2	Tt,1 K	Minf	pinf N/m^2	Tinf K	Rhoinf kg/m^3	Uinf m/s	Rinf,L
2.384E+06	9.636E+02	9.860E+00	5.992E+01	4.888E+01	4.271E-03	1.382E+03	2.318E+05

p2 N/m^2	T2 K	Rho2 kg/m^3	R2,L	Rho2/ Rhoinf	Pt,2 N/m^2	Ht,2 J/kg	Qsph,FR W/m^2
6.857E+03	9.424E+02	2.535E-02	1.794E+04	5.935E+00	7.557E+03	1.005E+06	3.171E+05

MEASURED HEAT TRANSFER DATA

x/L or z/L	Phi, deg	Twall, K	Qdot, W/m^2	Q(Tw=300K) W/m^2	St_inf	Q/Qsph	Ch/Chsph
.000	180	458.7	3.372E+05	4.432E+05	1.050E-01	1.063E+00	1.378E+00
.247	180	307.3	1.956E+04	1.978E+04	4.753E-03	6.169E-02	6.234E-02
.287	180	307.0	1.893E+04	1.913E+04	4.597E-03	5.969E-02	6.029E-02
.328	180	306.7	1.839E+04	1.858E+04	4.464E-03	5.799E-02	5.855E-02
.368	180	306.5	1.789E+04	1.807E+04	4.343E-03	5.643E-02	5.696E-02
.408	180	305.3	1.561E+04	1.573E+04	3.781E-03	4.922E-02	4.959E-02
.449	180	305.4	1.551E+04	1.563E+04	3.757E-03	4.890E-02	4.928E-02
.489	180	306.1	1.716E+04	1.732E+04	4.162E-03	5.411E-02	5.459E-02
.530	180	305.8	1.649E+04	1.663E+04	3.998E-03	5.200E-02	5.243E-02
.613	180	303.8	1.249E+04	1.256E+04	3.020E-03	3.940E-02	3.961E-02
.654	180	303.5	1.179E+04	1.185E+04	2.849E-03	3.718E-02	3.737E-02
.695	180	302.4	9.524E+03	9.559E+03	2.298E-03	3.004E-02	3.014E-02
.737	180	302.1	8.994E+03	9.022E+03	2.169E-03	2.837E-02	2.845E-02
.778	180	301.8	8.456E+03	8.479E+03	2.039E-03	2.667E-02	2.674E-02
.819	180	301.6	8.079E+03	8.098E+03	1.947E-03	2.548E-02	2.554E-02
.860	180	301.4	7.645E+03	7.661E+03	1.842E-03	2.411E-02	2.416E-02
.901	180	301.3	7.333E+03	7.347E+03	1.766E-03	2.313E-02	2.317E-02
.247	0	308.3	2.170E+04	2.197E+04	5.280E-03	6.843E-02	6.925E-02
.287	0	308.1	2.127E+04	2.153E+04	5.175E-03	6.709E-02	6.787E-02
.328	0	307.9	2.086E+04	2.111E+04	5.073E-03	6.579E-02	6.653E-02
.368	0	307.7	2.054E+04	2.078E+04	4.994E-03	6.479E-02	6.550E-02
.408	0	307.7	2.002E+04	2.025E+04	4.867E-03	6.313E-02	6.383E-02
.449	0	307.4	2.008E+04	2.031E+04	4.880E-03	6.332E-02	6.400E-02
.489	0	307.4	1.987E+04	2.010E+04	4.830E-03	6.268E-02	6.334E-02
.530	0	307.2	1.948E+04	1.969E+04	4.732E-03	6.142E-02	6.206E-02
.613	0	304.2	1.343E+04	1.352E+04	3.249E-03	4.236E-02	4.262E-02
.654	0	303.3	1.160E+04	1.166E+04	2.802E-03	3.658E-02	3.675E-02
.695	0	302.7	1.028E+04	1.032E+04	2.482E-03	3.242E-02	3.255E-02
.737	0	302.3	9.487E+03	9.520E+03	2.289E-03	2.992E-02	3.002E-02
.778	0	302.1	8.909E+03	8.937E+03	2.149E-03	2.810E-02	2.818E-02
.819	0	301.8	8.491E+03	8.515E+03	2.047E-03	2.678E-02	2.685E-02
.860	0	301.7	8.166E+03	8.186E+03	1.968E-03	2.575E-02	2.581E-02
.901	0	301.5	7.908E+03	7.927E+03	1.906E-03	2.494E-02	2.500E-02
.613	90	304.9	1.446E+04	1.457E+04	3.502E-03	4.562E-02	4.594E-02
.654	90	303.1	1.123E+04	1.128E+04	2.712E-03	3.541E-02	3.557E-02
.695	90	303.1	1.094E+04	1.099E+04	2.642E-03	3.450E-02	3.465E-02
.737	90	302.6	9.913E+03	9.952E+03	2.393E-03	3.126E-02	3.138E-02
.778	90	302.3	9.318E+03	9.351E+03	2.248E-03	2.939E-02	2.949E-02
.819	90	302.1	8.847E+03	8.875E+03	2.134E-03	2.790E-02	2.798E-02
.860	90	301.9	8.531E+03	8.556E+03	2.057E-03	2.690E-02	2.698E-02
.901	90	301.8	8.260E+03	8.282E+03	1.991E-03	2.605E-02	2.612E-02

TABLE I. Continued

(b) $\alpha = 4°$

FLOW CONDITIONS

Pt,1 N/m^2	Tt,1 K	Minf	pinf N/m^2	Tinf K	Rhoinf kg/m^3	Uinf m/s	Rinf,L
2.402E+06	9.656E+02	9.860E+00	6.039E+01	4.899E+01	4.295E-03	1.383E+03	2.327E+05

p2 N/m^2	T2 K	Rho2 kg/m^3	R2,L	Rho2/ Rhoinf	Pt,2 N/m^2	Ht,2 J/kg	Qsph,FR W/m^2
6.910E+03	9.444E+02	2.549E-02	1.804E+04	5.935E+00	7.616E+03	1.007E+06	3.193E+05

MEASURED HEAT TRANSFER DATA

x/L or z/L	Phi, deg	Twall, K	Qdot, W/m^2	Q(Tw=300K) W/m^2	St_inf	Q/Qsph	Ch/Chsph
.000	180	459.9	3.480E+05	4.581E+05	1.075E-01	1.090E+00	1.414E+00
.247	180	313.0	3.188E+04	3.251E+04	7.732E-03	9.984E-02	1.017E-01
.287	180	313.0	3.202E+04	3.265E+04	7.766E-03	1.003E-01	1.021E-01
.328	180	312.8	3.165E+04	3.227E+04	7.673E-03	9.910E-02	1.009E-01
.368	180	312.5	3.102E+04	3.161E+04	7.517E-03	9.713E-02	9.888E-02
.408	180	311.1	2.815E+04	2.863E+04	6.809E-03	8.815E-02	8.957E-02
.449	180	310.4	2.647E+04	2.689E+04	6.396E-03	8.289E-02	8.413E-02
.489	180	311.5	2.885E+04	2.935E+04	6.982E-03	9.034E-02	9.184E-02
.530	180	310.8	2.733E+04	2.778E+04	6.607E-03	8.558E-02	8.691E-02
.613	180	306.6	1.856E+04	1.874E+04	4.459E-03	5.811E-02	5.866E-02
.654	180	305.3	1.615E+04	1.628E+04	3.873E-03	5.056E-02	5.095E-02
.695	180	304.5	1.428E+04	1.438E+04	3.422E-03	4.472E-02	4.501E-02
.737	180	304.0	1.319E+04	1.327E+04	3.158E-03	4.130E-02	4.154E-02
.778	180	303.8	1.259E+04	1.266E+04	3.012E-03	3.941E-02	3.962E-02
.819	180	303.7	1.245E+04	1.251E+04	2.978E-03	3.898E-02	3.918E-02
.860	180	303.5	1.216E+04	1.223E+04	2.910E-03	3.809E-02	3.828E-02
.901	180	303.4	1.198E+04	1.204E+04	2.865E-03	3.750E-02	3.768E-02
.247	0	304.2	1.366E+04	1.375E+04	3.272E-03	4.278E-02	4.304E-02
.287	0	303.8	1.270E+04	1.277E+04	3.040E-03	3.977E-02	3.999E-02
.328	0	303.4	1.185E+04	1.191E+04	2.834E-03	3.710E-02	3.728E-02
.368	0	303.1	1.119E+04	1.124E+04	2.675E-03	3.503E-02	3.519E-02
.408	0	302.7	1.093E+04	1.097E+04	2.611E-03	3.422E-02	3.435E-02
.449	0	302.5	1.008E+04	1.012E+04	2.409E-03	3.158E-02	3.169E-02
.489	0	302.3	9.630E+03	9.663E+03	2.300E-03	3.016E-02	3.026E-02
.530	0	302.2	9.282E+03	9.312E+03	2.217E-03	2.907E-02	2.916E-02
.613	0	301.0	6.854E+03	6.864E+03	1.634E-03	2.146E-02	2.149E-02
.654	0	300.6	6.103E+03	6.109E+03	1.454E-03	1.911E-02	1.913E-02
.695	0	300.3	5.479E+03	5.482E+03	1.305E-03	1.716E-02	1.717E-02
.737	0	300.1	5.041E+03	5.042E+03	1.200E-03	1.579E-02	1.579E-02
.778	0	299.9	4.621E+03	4.620E+03	1.100E-03	1.447E-02	1.447E-02
.819	0	298.0	1.551E+03	1.547E+03	3.683E-04	4.858E-03	4.844E-03
.860	0	299.6	4.084E+03	4.082E+03	9.718E-04	1.279E-02	1.278E-02
.901	0	299.5	3.897E+03	3.895E+03	9.272E-04	1.220E-02	1.220E-02
.613	90	305.2	1.545E+04	1.557E+04	3.706E-03	4.839E-02	4.875E-02
.654	90	303.3	1.152E+04	1.158E+04	2.756E-03	3.609E-02	3.626E-02
.695	90	303.4	1.164E+04	1.170E+04	2.784E-03	3.644E-02	3.662E-02
.737	90	302.9	1.062E+04	1.067E+04	2.539E-03	3.326E-02	3.340E-02
.778	90	302.7	1.019E+04	1.023E+04	2.435E-03	3.190E-02	3.203E-02
.819	90	302.4	9.597E+03	9.631E+03	2.292E-03	3.005E-02	3.015E-02
.860	90	302.2	9.255E+03	9.286E+03	2.210E-03	2.898E-02	2.908E-02
.901	90	302.1	8.973E+03	9.001E+03	2.143E-03	2.810E-02	2.818E-02

TABLE I. Continued

(c) $\alpha = 6°$

FLOW CONDITIONS

Pt,1 N/m^2	Tt,1 K	Minf	pinf N/m^2	Tinf K	Rhoinf kg/m^3	Uinf m/s	Rinf,L
2.387E+06	9.887E+02	9.860E+00	6.001E+01	5.016E+01	4.168E-03	1.400E+03	2.222E+05

p2 N/m^2	T2 K	Rho2 kg/m^3	R2,L	Rho2/ Rhoinf	Pt,2 N/m^2	Ht,2 J/kg	Qsph,FR W/m^2
6.867E+03	9.670E+02	2.474E-02	1.747E+04	5.935E+00	7.568E+03	1.033E+06	3.300E+05

MEASURED HEAT TRANSFER DATA

x/L or z/L	Phi, deg	Twall, K	Qdot, W/m^2	Q(Tw=300K) W/m^2	St_inf	Q/Qsph	Ch/Chsph
.000	180	467.9	3.598E+05	4.758E+05	1.095E-01	1.090E+00	1.420E+00
.247	180	318.1	4.100E+04	4.211E+04	9.827E-03	1.242E-01	1.274E-01
.287	180	318.2	4.125E+04	4.237E+04	9.888E-03	1.250E-01	1.282E-01
.328	180	317.6	4.013E+04	4.118E+04	9.612E-03	1.216E-01	1.246E-01
.368	180	317.0	3.882E+04	3.980E+04	9.290E-03	1.176E-01	1.204E-01
.408	180	314.9	3.464E+04	3.541E+04	8.266E-03	1.050E-01	1.071E-01
.449	180	313.9	3.222E+04	3.288E+04	7.677E-03	9.761E-02	9.951E-02
.489	180	314.8	3.427E+04	3.502E+04	8.177E-03	1.038E-01	1.060E-01
.530	180	314.0	3.240E+04	3.307E+04	7.721E-03	9.816E-02	1.001E-01
.613	180	308.7	2.147E+04	2.174E+04	5.078E-03	6.504E-02	6.582E-02
.654	180	307.6	1.918E+04	1.940E+04	4.531E-03	5.813E-02	5.874E-02
.695	180	306.7	1.726E+04	1.743E+04	4.071E-03	5.229E-02	5.277E-02
.737	180	306.0	1.602E+04	1.616E+04	3.775E-03	4.853E-02	4.893E-02
.778	180	305.8	1.551E+04	1.565E+04	3.655E-03	4.701E-02	4.738E-02
.819	180	305.8	1.546E+04	1.559E+04	3.643E-03	4.685E-02	4.723E-02
.860	180	305.7	1.527E+04	1.540E+04	3.598E-03	4.627E-02	4.663E-02
.901	180	305.6	1.512E+04	1.525E+04	3.563E-03	4.583E-02	4.618E-02
.247	0	303.7	1.131E+04	1.137E+04	2.657E-03	3.427E-02	3.445E-02
.287	0	303.2	1.018E+04	1.023E+04	2.390E-03	3.084E-02	3.098E-02
.328	0	302.7	9.266E+03	9.303E+03	2.174E-03	2.808E-02	2.818E-02
.368	0	302.4	8.504E+03	8.533E+03	1.994E-03	2.577E-02	2.585E-02
.408	0	301.6	7.913E+03	7.932E+03	1.854E-03	2.398E-02	2.403E-02
.449	0	301.8	7.240E+03	7.258E+03	1.696E-03	2.194E-02	2.199E-02
.489	0	301.6	6.811E+03	6.826E+03	1.595E-03	2.064E-02	2.068E-02
.530	0	301.4	6.494E+03	6.507E+03	1.521E-03	1.968E-02	1.971E-02
.613	0	300.6	4.847E+03	4.851E+03	1.134E-03	1.469E-02	1.470E-02
.654	0	300.3	4.327E+03	4.329E+03	1.012E-03	1.311E-02	1.312E-02
.695	0	300.1	3.911E+03	3.911E+03	9.143E-04	1.185E-02	1.185E-02
.737	0	300.0	3.650E+03	3.650E+03	8.532E-04	1.106E-02	1.106E-02
.778	0	299.9	3.353E+03	3.352E+03	7.835E-04	1.016E-02	1.016E-02
.819	0	299.8	3.145E+03	3.144E+03	7.349E-04	9.528E-03	9.526E-03
.860	0	299.7	2.943E+03	2.941E+03	6.876E-04	8.917E-03	8.913E-03
.901	0	299.6	2.860E+03	2.859E+03	6.682E-04	8.666E-03	8.662E-03
.613	90	306.4	1.658E+04	1.673E+04	3.909E-03	5.023E-02	5.067E-02
.654	90	305.1	1.298E+04	1.308E+04	3.056E-03	3.934E-02	3.961E-02
.695	90	304.3	1.237E+04	1.245E+04	2.910E-03	3.749E-02	3.772E-02
.737	90	303.8	1.133E+04	1.139E+04	2.662E-03	3.433E-02	3.451E-02
.778	90	303.6	1.087E+04	1.093E+04	2.554E-03	3.294E-02	3.310E-02
.819	90	303.3	1.018E+04	1.023E+04	2.390E-03	3.084E-02	3.098E-02
.860	90	303.1	9.854E+03	9.898E+03	2.313E-03	2.986E-02	2.998E-02
.901	90	303.0	9.552E+03	9.594E+03	2.242E-03	2.894E-02	2.906E-02

TABLE I. Continued

(d) $\alpha = 8°$

FLOW CONDITIONS

Pt,1 N/m^2	Tt,1 K	Minf	pinf N/m^2	Tinf K	Rhoinf kg/m^3	Uinf m/s	Rinf,L
2.376E+06	9.977E+02	9.860E+00	5.973E+01	5.061E+01	4.112E-03	1.406E+03	2.178E+05

p2 N/m^2	T2 K	Rho2 kg/m^3	R2,L	Rho2/ Rhoinf	Pt,2 N/m^2	Ht,2 J/kg	Qsph,FR W/m^2
6.835E+03	9.758E+02	2.440E-02	1.721E+04	5.935E+00	7.533E+03	1.044E+06	3.339E+05

MEASURED HEAT TRANSFER DATA

x/L or z/L	Phi, deg	Twall, K	Qdot, W/m^2	Q(Tw=300K) W/m^2	St_inf	Q/Qsph	Ch/Chsph
.000	180	472.7	3.619E+05	4.809E+05	1.101E-01	1.084E+00	1.418E+00
.247	180	322.7	4.947E+04	5.114E+04	1.187E-02	1.482E-01	1.529E-01
.287	180	322.4	4.896E+04	5.059E+04	1.175E-02	1.467E-01	1.512E-01
.328	180	321.3	4.683E+04	4.831E+04	1.122E-02	1.403E-01	1.444E-01
.368	180	320.2	4.465E+04	4.598E+04	1.068E-02	1.337E-01	1.375E-01
.408	180	317.9	3.977E+04	4.081E+04	9.479E-03	1.191E-01	1.220E-01
.449	180	316.6	3.693E+04	3.783E+04	8.788E-03	1.106E-01	1.131E-01
.489	180	317.5	3.888E+04	3.987E+04	9.262E-03	1.164E-01	1.192E-01
.530	180	316.4	3.663E+04	3.751E+04	8.713E-03	1.097E-01	1.122E-01
.613	180	310.2	2.400E+04	2.435E+04	5.660E-03	7.187E-02	7.287E-02
.654	180	308.8	2.152E+04	2.180E+04	5.066E-03	6.445E-02	6.523E-02
.695	180	308.0	1.982E+04	2.005E+04	4.660E-03	5.935E-02	6.000E-02
.737	180	307.7	1.909E+04	1.930E+04	4.487E-03	5.717E-02	5.777E-02
.778	180	307.6	1.872E+04	1.892E+04	4.400E-03	5.607E-02	5.665E-02
.819	180	307.5	1.859E+04	1.879E+04	4.369E-03	5.568E-02	5.625E-02
.860	180	307.4	1.840E+04	1.860E+04	4.324E-03	5.512E-02	5.568E-02
.901	180	307.3	1.825E+04	1.845E+04	4.288E-03	5.467E-02	5.521E-02
.247	0	302.8	9.191E+03	9.227E+03	2.146E-03	2.753E-02	2.763E-02
.287	0	302.3	8.094E+03	8.120E+03	1.889E-03	2.424E-02	2.432E-02
.328	0	301.8	7.154E+03	7.173E+03	1.668E-03	2.143E-02	2.148E-02
.368	0	301.4	6.408E+03	6.421E+03	1.493E-03	1.919E-02	1.923E-02
.408	0	301.0	6.072E+03	6.081E+03	1.415E-03	1.819E-02	1.821E-02
.449	0	300.9	5.287E+03	5.294E+03	1.231E-03	1.584E-02	1.585E-02
.489	0	300.7	4.874E+03	4.879E+03	1.135E-03	1.460E-02	1.461E-02
.530	0	300.6	4.642E+03	4.646E+03	1.081E-03	1.390E-02	1.391E-02
.613	0	300.0	3.545E+03	3.545E+03	8.247E-04	1.062E-02	1.062E-02
.654	0	299.8	3.219E+03	3.218E+03	7.486E-04	9.640E-03	9.638E-03
.695	0	299.7	2.946E+03	2.945E+03	6.851E-04	8.824E-03	8.820E-03
.737	0	299.6	2.799E+03	2.798E+03	6.509E-04	8.385E-03	8.380E-03
.778	0	299.6	2.648E+03	2.646E+03	6.157E-04	7.931E-03	7.927E-03
.819	0	299.5	2.468E+03	2.466E+03	5.736E-04	7.391E-03	7.386E-03
.860	0	299.4	2.410E+03	2.408E+03	5.602E-04	7.218E-03	7.213E-03
.901	0	299.4	2.371E+03	2.369E+03	5.512E-04	7.102E-03	7.097E-03
.613	90	306.8	1.711E+04	1.728E+04	4.017E-03	5.124E-02	5.172E-02
.654	90	305.4	1.347E+04	1.358E+04	3.158E-03	4.036E-02	4.066E-02
.695	90	304.6	1.259E+04	1.267E+04	2.947E-03	3.771E-02	3.794E-02
.737	90	304.0	1.144E+04	1.151E+04	2.676E-03	3.427E-02	3.446E-02
.778	90	303.8	1.091E+04	1.097E+04	2.551E-03	3.268E-02	3.285E-02
.819	90	303.4	1.022E+04	1.027E+04	2.389E-03	3.062E-02	3.076E-02
.860	90	303.2	9.861E+03	9.907E+03	2.304E-03	2.954E-02	2.967E-02
.901	90	303.1	9.590E+03	9.633E+03	2.240E-03	2.872E-02	2.884E-02

TABLE I. Continued

(e) $\alpha = 10°$

FLOW CONDITIONS

Pt,1 N/m^2	Tt,1 K	Minf	pinf N/m^2	Tinf K	Rhoinf kg/m^3	Uinf m/s	Rinf,L
2.388E+06	1.018E+03	9.860E+00	6.004E+01	5.166E+01	4.049E-03	1.421E+03	2.115E+05

p2 N/m^2	T2 K	Rho2 kg/m^3	R2,L	Rho2/ Rhoinf	Pt,2 N/m^2	Ht,2 J/kg	Qsph,FR W/m^2
6.871E+03	9.960E+02	2.403E-02	1.691E+04	5.935E+00	7.573E+03	1.067E+06	3.452E+05

MEASURED HEAT TRANSFER DATA

x/L or z/L	Phi, deg	Twall, K	Qdot, W/m^2	Q(Tw=300K) W/m^2	St_inf	Q/Qsph	Ch/Chsph
.000	180	474.5	3.695E+05	4.880E+05	1.088E-01	1.070E+00	1.391E+00
.247	180	326.5	5.761E+04	5.981E+04	1.352E-02	1.669E-01	1.729E-01
.287	180	311.9	1.823E+04	1.854E+04	4.197E-03	5.282E-02	5.365E-02
.328	180	324.2	5.317E+04	5.503E+04	1.244E-02	1.540E-01	1.591E-01
.368	180	322.9	5.062E+04	5.229E+04	1.183E-02	1.466E-01	1.512E-01
.408	180	320.1	4.473E+04	4.602E+04	1.041E-02	1.296E-01	1.331E-01
.449	180	318.6	4.162E+04	4.273E+04	9.667E-03	1.206E-01	1.236E-01
.489	180	319.7	4.392E+04	4.516E+04	1.022E-02	1.272E-01	1.306E-01
.530	180	318.6	4.157E+04	4.268E+04	9.655E-03	1.204E-01	1.234E-01
.613	180	311.6	2.726E+04	2.771E+04	6.273E-03	7.896E-02	8.019E-02
.654	180	310.4	2.478E+04	2.514E+04	5.692E-03	7.177E-02	7.276E-02
.695	180	309.7	2.323E+04	2.355E+04	5.331E-03	6.729E-02	6.815E-02
.737	180	309.5	2.277E+04	2.307E+04	5.224E-03	6.596E-02	6.678E-02
.778	180	309.3	2.241E+04	2.270E+04	5.140E-03	6.490E-02	6.570E-02
.819	180	309.2	2.226E+04	2.255E+04	5.105E-03	6.447E-02	6.526E-02
.860	180	309.1	2.203E+04	2.231E+04	5.051E-03	6.380E-02	6.457E-02
.901	180	309.0	2.181E+04	2.209E+04	5.002E-03	6.318E-02	6.394E-02
.247	0	302.0	7.679E+03	7.701E+03	1.745E-03	2.224E-02	2.230E-02
.287	0	301.5	6.643E+03	6.657E+03	1.508E-03	1.924E-02	1.928E-02
.328	0	301.1	5.779E+03	5.787E+03	1.311E-03	1.674E-02	1.676E-02
.368	0	300.8	5.160E+03	5.166E+03	1.170E-03	1.495E-02	1.496E-02
.408	0	300.5	4.508E+03	4.511E+03	1.022E-03	1.306E-02	1.307E-02
.449	0	300.3	4.200E+03	4.201E+03	9.520E-04	1.216E-02	1.217E-02
.489	0	300.2	3.891E+03	3.892E+03	8.819E-04	1.127E-02	1.127E-02
.530	0	300.1	3.730E+03	3.730E+03	8.452E-04	1.080E-02	1.080E-02
.613	0	299.7	2.903E+03	2.901E+03	6.575E-04	8.408E-03	8.404E-03
.654	0	299.6	2.776E+03	2.774E+03	6.287E-04	8.041E-03	8.037E-03
.695	0	299.5	2.547E+03	2.546E+03	5.769E-04	7.379E-03	7.374E-03
.737	0	299.5	2.463E+03	2.461E+03	5.578E-04	7.135E-03	7.130E-03
.778	0	299.4	2.335E+03	2.333E+03	5.288E-04	6.765E-03	6.759E-03
.819	0	299.4	2.306E+03	2.304E+03	5.220E-04	6.679E-03	6.673E-03
.860	0	299.4	2.277E+03	2.275E+03	5.156E-04	6.596E-03	6.591E-03
.901	0	299.4	2.299E+03	2.297E+03	5.204E-04	6.658E-03	6.653E-03
.613	90	306.8	1.728E+04	1.745E+04	3.951E-03	5.006E-02	5.051E-02
.654	90	305.2	1.316E+04	1.326E+04	3.003E-03	3.813E-02	3.839E-02
.695	90	304.5	1.248E+04	1.256E+04	2.844E-03	3.615E-02	3.636E-02
.737	90	303.9	1.137E+04	1.143E+04	2.589E-03	3.292E-02	3.309E-02
.778	90	303.6	1.069E+04	1.074E+04	2.434E-03	3.096E-02	3.111E-02
.819	90	303.4	1.021E+04	1.026E+04	2.324E-03	2.957E-02	2.970E-02
.860	90	303.2	9.891E+03	9.935E+03	2.251E-03	2.865E-02	2.877E-02
.901	90	303.1	9.735E+03	9.778E+03	2.215E-03	2.820E-02	2.832E-02

TABLE I. Continued

(f) $\alpha = 12°$

FLOW CONDITIONS

Pt,1 N/m^2	Tt,1 K	Minf	pinf N/m^2	Tinf K	Rhoinf kg/m^3	Uinf m/s	Rinf,L
2.372E+06	9.839E+02	9.860E+00	5.963E+01	4.992E+01	4.162E-03	1.396E+03	2.226E+05

p2 N/m^2	T2 K	Rho2 kg/m^3	R2,L	Rho2/ Rhoinf	Pt,2 N/m^2	Ht,2 J/kg	Qsph,FR W/m^2
6.823E+03	9.623E+02	2.470E-02	1.745E+04	5.935E+00	7.520E+03	1.028E+06	3.266E+05

MEASURED HEAT TRANSFER DATA

x/L or z/L	Phi, deg	Twall, K	Qdot, W/m^2	Q(Tw=300K) W/m^2	St_inf	Q/Qsph	Ch/Chsph
.000	180	460.5	3.404E+05	4.448E+05	1.036E-01	1.042E+00	1.342E+00
.247	180	325.2	5.813E+04	6.036E+04	1.424E-02	1.780E-01	1.844E-01
.287	180	0.0	0.000E+00	0.000E+00	0.000E+00	0.000E+00	0.000E+00
.328	180	322.6	5.328E+04	5.510E+04	1.300E-02	1.631E-01	1.684E-01
.368	180	321.6	5.126E+04	5.294E+04	1.249E-02	1.570E-01	1.618E-01
.408	180	318.7	4.534E+04	4.662E+04	1.100E-02	1.388E-01	1.425E-01
.449	180	317.3	4.232E+04	4.342E+04	1.025E-02	1.296E-01	1.327E-01
.489	180	318.5	4.482E+04	4.606E+04	1.087E-02	1.372E-01	1.408E-01
.530	180	317.4	4.247E+04	4.358E+04	1.029E-02	1.300E-01	1.332E-01
.613	180	310.4	2.810E+04	2.854E+04	6.741E-03	8.605E-02	8.730E-02
.654	180	309.4	2.659E+04	2.696E+04	6.369E-03	8.141E-02	8.248E-02
.695	180	308.8	2.514E+04	2.546E+04	6.015E-03	7.696E-02	7.790E-02
.737	180	308.5	2.438E+04	2.468E+04	5.831E-03	7.463E-02	7.552E-02
.778	180	308.3	2.399E+04	2.429E+04	5.738E-03	7.345E-02	7.430E-02
.819	180	308.2	2.389E+04	2.418E+04	5.712E-03	7.313E-02	7.397E-02
.860	180	308.1	2.356E+04	2.384E+04	5.633E-03	7.214E-02	7.295E-02
.901	180	308.0	2.330E+04	2.357E+04	5.569E-03	7.133E-02	7.212E-02
.247	0	299.5	5.917E+03	5.913E+03	1.398E-03	1.812E-02	1.810E-02
.287	0	299.1	5.071E+03	5.064E+03	1.197E-03	1.553E-02	1.551E-02
.328	0	298.7	4.399E+03	4.391E+03	1.038E-03	1.347E-02	1.344E-02
.368	0	298.5	3.953E+03	3.944E+03	9.326E-04	1.210E-02	1.208E-02
.408	0	298.4	3.510E+03	3.501E+03	8.279E-04	1.075E-02	1.072E-02
.449	0	298.2	3.291E+03	3.282E+03	7.761E-04	1.008E-02	1.005E-02
.489	0	298.1	3.124E+03	3.115E+03	7.365E-04	9.563E-03	9.538E-03
.530	0	298.1	3.036E+03	3.028E+03	7.159E-04	9.296E-03	9.271E-03
.613	0	297.8	2.448E+03	2.440E+03	5.769E-04	7.494E-03	7.471E-03
.654	0	297.7	2.288E+03	2.280E+03	5.392E-04	7.005E-03	6.983E-03
.695	0	297.6	2.222E+03	2.214E+03	5.236E-04	6.802E-03	6.780E-03
.737	0	297.7	2.244E+03	2.236E+03	5.288E-04	6.870E-03	6.848E-03
.778	0	297.6	2.098E+03	2.090E+03	4.943E-04	6.422E-03	6.401E-03
.819	0	0.0	0.000E+00	0.000E+00	0.000E+00	0.000E+00	0.000E+00
.860	0	297.6	2.196E+03	2.188E+03	5.175E-04	6.723E-03	6.701E-03
.901	0	297.6	2.206E+03	2.198E+03	5.197E-04	6.753E-03	6.731E-03
.613	90	304.2	1.514E+04	1.523E+04	3.600E-03	4.635E-02	4.662E-02
.654	90	0.0	0.000E+00	0.000E+00	0.000E+00	0.000E+00	0.000E+00
.695	90	302.1	1.090E+04	1.094E+04	2.585E-03	3.338E-02	3.348E-02
.737	90	301.7	1.005E+04	1.007E+04	2.381E-03	3.076E-02	3.083E-02
.778	90	301.4	9.487E+03	9.506E+03	2.247E-03	2.905E-02	2.910E-02
.819	90	301.3	9.255E+03	9.272E+03	2.192E-03	2.834E-02	2.839E-02
.860	90	301.2	9.129E+03	9.145E+03	2.162E-03	2.795E-02	2.800E-02
.901	90	301.2	9.071E+03	9.087E+03	2.148E-03	2.777E-02	2.782E-02

TABLE I. Continued

(g) $\alpha = 16°$

FLOW CONDITIONS

Pt,1 N/m^2	Tt,1 K	Minf	pinf N/m^2	Tinf K	Rhoinf kg/m^3	Uinf m/s	Rinf,L
2.378E+06	9.951E+02	9.860E+00	5.978E+01	5.048E+01	4.126E-03	1.404E+03	2.190E+05

p2 N/m^2	T2 K	Rho2 kg/m^3	R2,L	Rho2/ Rhoinf	Pt,2 N/m^2	Ht,2 J/kg	Qsph,FR W/m^2
6.841E+03	9.732E+02	2.449E-02	1.728E+04	5.935E+00	7.540E+03	1.041E+06	3.326E+05

MEASURED HEAT TRANSFER DATA

x/L or z/L	Phi, deg	Twall, K	Qdot, W/m^2	Q(Tw=300K) W/m^2	St_inf	Q/Qsph	Ch/Chsph
.000	180	462.8	3.404E+05	4.445E+05	1.021E-01	1.023E+00	1.317E+00
.247	180	331.1	6.793E+04	7.111E+04	1.653E-02	2.042E-01	2.132E-01
.287	180	0.0	0.000E+00	0.000E+00	0.000E+00	0.000E+00	0.000E+00
.328	180	328.1	6.242E+04	6.505E+04	1.512E-02	1.876E-01	1.951E-01
.368	180	326.7	5.971E+04	6.210E+04	1.444E-02	1.795E-01	1.863E-01
.408	180	323.6	5.327E+04	5.514E+04	1.283E-02	1.601E-01	1.654E-01
.449	180	321.9	4.985E+04	5.147E+04	1.197E-02	1.498E-01	1.544E-01
.489	180	323.2	5.269E+04	5.451E+04	1.268E-02	1.584E-01	1.636E-01
.530	180	322.0	5.011E+04	5.175E+04	1.204E-02	1.506E-01	1.553E-01
.613	180	314.3	3.452E+04	3.524E+04	8.204E-03	1.038E-01	1.058E-01
.654	180	313.3	3.316E+04	3.381E+04	7.872E-03	9.969E-02	1.015E-01
.695	180	312.7	3.191E+04	3.250E+04	7.568E-03	9.592E-02	9.761E-02
.737	180	312.6	3.132E+04	3.190E+04	7.427E-03	9.417E-02	9.580E-02
.778	180	312.4	3.107E+04	3.164E+04	7.366E-03	9.340E-02	9.500E-02
.819	180	312.2	3.081E+04	3.137E+04	7.303E-03	9.263E-02	9.420E-02
.860	180	312.1	3.052E+04	3.106E+04	7.233E-03	9.176E-02	9.329E-02
.901	180	312.2	3.072E+04	3.127E+04	7.282E-03	9.236E-02	9.392E-02
.247	0	299.5	4.710E+03	4.706E+03	1.097E-03	1.416E-02	1.415E-02
.287	0	299.2	4.171E+03	4.166E+03	9.710E-04	1.254E-02	1.252E-02
.328	0	299.0	3.801E+03	3.796E+03	8.847E-04	1.143E-02	1.141E-02
.368	0	298.9	3.521E+03	3.516E+03	8.195E-04	1.059E-02	1.057E-02
.408	0	298.6	2.010E+03	2.006E+03	4.676E-04	6.042E-03	6.031E-03
.449	0	298.7	3.258E+03	3.253E+03	7.581E-04	9.795E-03	9.779E-03
.489	0	298.7	3.216E+03	3.210E+03	7.482E-04	9.667E-03	9.650E-03
.530	0	298.7	3.225E+03	3.219E+03	7.504E-04	9.695E-03	9.678E-03
.613	0	298.4	2.671E+03	2.665E+03	6.211E-04	8.028E-03	8.011E-03
.654	0	298.3	2.517E+03	2.511E+03	5.852E-04	7.565E-03	7.548E-03
.695	0	298.3	2.451E+03	2.445E+03	5.700E-04	7.369E-03	7.352E-03
.737	0	298.3	2.469E+03	2.463E+03	5.742E-04	7.423E-03	7.406E-03
.778	0	298.3	2.388E+03	2.382E+03	5.552E-04	7.177E-03	7.161E-03
.819	0	0.0	0.000E+00	0.000E+00	0.000E+00	0.000E+00	0.000E+00
.860	0	298.3	2.466E+03	2.460E+03	5.734E-04	7.413E-03	7.396E-03
.901	0	298.3	2.450E+03	2.444E+03	5.697E-04	7.365E-03	7.348E-03
.613	90	304.4	1.430E+04	1.439E+04	3.353E-03	4.299E-02	4.324E-02
.654	90	0.0	0.000E+00	0.000E+00	0.000E+00	0.000E+00	0.000E+00
.695	90	302.7	1.081E+04	1.085E+04	2.529E-03	3.250E-02	3.262E-02
.737	90	302.4	1.024E+04	1.027E+04	2.394E-03	3.078E-02	3.088E-02
.778	90	302.4	1.022E+04	1.025E+04	2.388E-03	3.071E-02	3.081E-02
.819	90	302.1	9.744E+03	9.774E+03	2.278E-03	2.929E-02	2.938E-02
.860	90	302.0	9.610E+03	9.638E+03	2.246E-03	2.889E-02	2.897E-02
.901	90	302.0	9.536E+03	9.563E+03	2.229E-03	2.867E-02	2.874E-02

TABLE I. Concluded

(h) $\alpha = 20°$

FLOW CONDITIONS

Pt,1 N/m^2	Tt,1 K	Minf	pinf N/m^2	Tinf K	Rhoinf kg/m^3	Uinf m/s	Rinf,L
2.366E+06	9.864E+02	9.860E+00	5.949E+01	5.004E+01	4.142E-03	1.398E+03	2.211E+05

p2 N/m^2	T2 K	Rho2 kg/m^3	R2,L	Rho2/ Rhoinf	Pt,2 N/m^2	Ht,2 J/kg	Qsph,FR W/m^2
6.807E+03	9.648E+02	2.458E-02	1.736E+04	5.935E+00	7.503E+03	1.031E+06	3.275E+05

MEASURED HEAT TRANSFER DATA

x/L or z/L	Phi, deg	Twall, K	Qdot, W/m^2	Q(Tw=300K) W/m^2	St_inf	Q/Qsph	Ch/Chsph
.000	180	456.2	3.255E+05	4.213E+05	9.818E-02	9.938E-01	1.268E+00
.247	180	334.8	7.491E+04	7.891E+04	1.860E-02	2.287E-01	2.402E-01
.287	180	0.0	0.000E+00	0.000E+00	0.000E+00	0.000E+00	0.000E+00
.328	180	331.8	6.934E+04	7.270E+04	1.714E-02	2.117E-01	2.214E-01
.368	180	329.7	6.549E+04	6.845E+04	1.614E-02	2.000E-01	2.085E-01
.408	180	326.3	5.857E+04	6.090E+04	1.436E-02	1.788E-01	1.855E-01
.449	180	324.4	5.452E+04	5.653E+04	1.333E-02	1.665E-01	1.723E-01
.489	180	326.0	5.799E+04	6.027E+04	1.421E-02	1.771E-01	1.836E-01
.530	180	324.7	5.528E+04	5.734E+04	1.352E-02	1.688E-01	1.747E-01
.613	180	316.7	3.920E+04	4.017E+04	9.481E-03	1.197E-01	1.225E-01
.654	180	316.2	3.837E+04	3.930E+04	9.275E-03	1.172E-01	1.198E-01
.695	180	315.4	3.688E+04	3.773E+04	8.905E-03	1.126E-01	1.151E-01
.737	180	315.2	3.637E+04	3.719E+04	8.779E-03	1.110E-01	1.134E-01
.778	180	315.0	3.592E+04	3.672E+04	8.668E-03	1.097E-01	1.120E-01
.819	180	314.7	3.557E+04	3.635E+04	8.581E-03	1.086E-01	1.109E-01
.860	180	314.8	3.575E+04	3.654E+04	8.624E-03	1.092E-01	1.114E-01
.901	180	315.0	3.611E+04	3.692E+04	8.715E-03	1.103E-01	1.126E-01
.247	0	299.2	4.264E+03	4.260E+03	1.007E-03	1.302E-02	1.301E-02
.287	0	299.1	4.062E+03	4.057E+03	9.588E-04	1.240E-02	1.239E-02
.328	0	299.0	3.896E+03	3.891E+03	9.196E-04	1.190E-02	1.188E-02
.368	0	299.0	3.840E+03	3.834E+03	9.063E-04	1.173E-02	1.171E-02
.408	0	299.0	3.944E+03	3.938E+03	9.307E-04	1.204E-02	1.202E-02
.449	0	299.0	3.822E+03	3.816E+03	9.020E-04	1.167E-02	1.165E-02
.489	0	299.0	3.833E+03	3.827E+03	9.046E-04	1.170E-02	1.169E-02
.530	0	299.0	3.838E+03	3.833E+03	9.059E-04	1.172E-02	1.170E-02
.613	0	298.6	3.034E+03	3.028E+03	7.157E-04	9.264E-03	9.246E-03
.654	0	298.5	2.786E+03	2.780E+03	6.571E-04	8.507E-03	8.489E-03
.695	0	298.4	2.656E+03	2.650E+03	6.263E-04	8.109E-03	8.092E-03
.737	0	298.4	2.582E+03	2.576E+03	6.089E-04	7.885E-03	7.867E-03
.778	0	298.3	2.412E+03	2.406E+03	5.688E-04	7.365E-03	7.348E-03
.819	0	0.0	0.000E+00	0.000E+00	0.000E+00	0.000E+00	0.000E+00
.860	0	298.3	2.375E+03	2.369E+03	5.600E-04	7.252E-03	7.235E-03
.901	0	298.2	2.285E+03	2.279E+03	5.388E-04	6.978E-03	6.961E-03
.613	90	304.1	1.366E+04	1.374E+04	3.247E-03	4.171E-02	4.195E-02
.654	90	0.0	0.000E+00	0.000E+00	0.000E+00	0.000E+00	0.000E+00
.695	90	302.6	1.063E+04	1.067E+04	2.522E-03	3.247E-02	3.259E-02
.737	90	302.3	1.007E+04	1.010E+04	2.387E-03	3.074E-02	3.084E-02
.778	90	302.2	9.893E+03	9.925E+03	2.345E-03	3.021E-02	3.030E-02
.819	90	302.1	9.639E+03	9.668E+03	2.285E-03	2.943E-02	2.952E-02
.860	90	302.0	9.539E+03	9.568E+03	2.261E-03	2.913E-02	2.921E-02
.901	90	302.0	9.514E+03	9.542E+03	2.255E-03	2.905E-02	2.913E-02

TABLE II. MEASURED HEAT-TRANSFER DATA FOR STRAIGHT BICONIC AT HIGH REYNOLDS NUMBER

(a) $\alpha = 0°$

FLOW CONDITIONS

Pt,1 N/m^2	Tt,1 K	Minf	pinf N/m^2	Tinf K	Rhoinf kg/m^3	Uinf m/s	Rinf,L
1.086E+07	1.019E+03	1.016E+01	2.293E+02	4.920E+01	1.624E-02	1.429E+03	9.037E+05

p2 N/m^2	T2 K	Rho2 kg/m^3	R2,L	Rho2/ Rhoinf	Pt,2 N/m^2	Ht,2 J/kg	Qsph,FR W/m^2
2.787E+04	1.001E+03	9.703E-02	6.802E+04	5.977E+00	3.070E+04	1.068E+06	6.932E+05

MEASURED HEAT TRANSFER DATA

x/L or z/L	Phi, deg	Twall, K	Qdot, W/m^2	Q(Tw=300K) W/m^2	St_inf	Q/Qsph	Ch/Chsph
.000	180	583.5	6.083E+05	1.004E+06	5.492E-02	8.775E-01	1.410E+00
.247	180	315.4	4.052E+04	4.141E+04	2.323E-03	5.845E-02	5.966E-02
.287	180	315.3	4.047E+04	4.135E+04	2.320E-03	5.839E-02	5.958E-02
.328	180	314.5	3.879E+04	3.959E+04	2.221E-03	5.595E-02	5.704E-02
.368	180	314.2	3.807E+04	3.883E+04	2.179E-03	5.491E-02	5.595E-02
.408	180	312.6	3.491E+04	3.554E+04	1.994E-03	5.036E-02	5.121E-02
.449	180	311.9	3.332E+04	3.388E+04	1.901E-03	4.806E-02	4.882E-02
.489	180	313.1	3.577E+04	3.643E+04	2.044E-03	5.160E-02	5.250E-02
.530	180	312.9	3.537E+04	3.601E+04	2.021E-03	5.102E-02	5.189E-02
.613	180	308.2	2.594E+04	2.624E+04	1.473E-03	3.742E-02	3.783E-02
.654	180	306.6	2.267E+04	2.288E+04	1.284E-03	3.270E-02	3.299E-02
.695	180	305.2	1.993E+04	2.008E+04	1.127E-03	2.875E-02	2.895E-02
.737	180	304.5	1.837E+04	1.848E+04	1.038E-03	2.650E-02	2.665E-02
.778	180	303.9	1.717E+04	1.727E+04	9.696E-04	2.477E-02	2.490E-02
.819	180	303.5	1.641E+04	1.649E+04	9.259E-04	2.367E-02	2.378E-02
.860	180	303.2	1.567E+04	1.574E+04	8.838E-04	2.260E-02	2.270E-02
.901	180	302.9	1.512E+04	1.518E+04	8.524E-04	2.181E-02	2.189E-02
.247	0	317.9	4.571E+04	4.687E+04	2.629E-03	6.593E-02	6.751E-02
.287	0	317.5	4.502E+04	4.615E+04	2.588E-03	6.494E-02	6.647E-02
.328	0	317.2	4.428E+04	4.537E+04	2.544E-03	6.388E-02	6.535E-02
.368	0	316.8	4.367E+04	4.471E+04	2.508E-03	6.299E-02	6.441E-02
.408	0	316.5	4.497E+04	4.603E+04	2.582E-03	6.488E-02	6.631E-02
.449	0	316.4	4.271E+04	4.370E+04	2.451E-03	6.161E-02	6.296E-02
.489	0	316.2	4.215E+04	4.312E+04	2.419E-03	6.080E-02	6.212E-02
.530	0	315.6	4.077E+04	4.167E+04	2.338E-03	5.881E-02	6.004E-02
.613	0	308.4	2.638E+04	2.669E+04	1.498E-03	3.806E-02	3.848E-02
.654	0	306.4	2.227E+04	2.247E+04	1.262E-03	3.213E-02	3.240E-02
.695	0	305.1	1.966E+04	1.980E+04	1.112E-03	2.836E-02	2.855E-02
.737	0	304.5	1.830E+04	1.841E+04	1.034E-03	2.639E-02	2.655E-02
.778	0	304.0	1.721E+04	1.731E+04	9.719E-04	2.483E-02	2.496E-02
.819	0	303.6	1.632E+04	1.640E+04	9.210E-04	2.354E-02	2.365E-02
.860	0	303.2	1.566E+04	1.573E+04	8.831E-04	2.258E-02	2.268E-02
.901	0	303.0	1.512E+04	1.519E+04	8.528E-04	2.182E-02	2.190E-02
.613	90	310.2	2.893E+04	2.935E+04	1.647E-03	4.174E-02	4.230E-02
.654	90	305.6	2.053E+04	2.069E+04	1.162E-03	2.962E-02	2.984E-02
.695	90	306.4	2.152E+04	2.172E+04	1.219E-03	3.105E-02	3.131E-02
.737	90	305.4	1.970E+04	1.985E+04	1.114E-03	2.842E-02	2.862E-02
.778	90	304.8	1.833E+04	1.845E+04	1.036E-03	2.644E-02	2.661E-02
.819	90	304.3	1.740E+04	1.751E+04	9.832E-04	2.511E-02	2.525E-02
.860	90	304.0	1.661E+04	1.670E+04	9.380E-04	2.396E-02	2.409E-02
.901	90	303.7	1.591E+04	1.599E+04	8.977E-04	2.294E-02	2.306E-02

TABLE II. Continued

(b) $\alpha = 4°$

FLOW CONDITIONS

Pt,1 N/m^2	Tt,1 K	Minf	pinf N/m^2	Tinf K	Rhoinf kg/m^3	Uinf m/s	Rinf,L
1.089E+07	1.012E+03	1.016E+01	2.299E+02	4.887E+01	1.639E-02	1.424E+03	9.168E+05

p2 N/m^2	T2 K	Rho2 kg/m^3	R2,L	Rho2/ Rhoinf	Pt,2 N/m^2	Ht,2 J/kg	Qsph,FR W/m^2
2.794E+04	9.937E+02	9.796E-02	6.872E+04	5.977E+00	3.078E+04	1.060E+06	6.870E+05

MEASURED HEAT TRANSFER DATA

x/L or z/L	Phi, deg	Twall, K	Qdot, W/m^2	Q(Tw=300K) W/m^2	St_inf	Q/Qsph	Ch/Chsph
.000	180	581.8	5.988E+05	9.913E+05	5.444E-02	8.715E-01	1.405E+00
.247	180	328.6	6.748E+04	7.030E+04	3.957E-03	9.822E-02	1.021E-01
.287	180	329.5	6.941E+04	7.241E+04	4.075E-03	1.010E-01	1.051E-01
.328	180	328.7	6.794E+04	7.080E+04	3.984E-03	9.889E-02	1.028E-01
.368	180	328.2	6.683E+04	6.959E+04	3.917E-03	9.728E-02	1.011E-01
.408	180	325.3	6.069E+04	6.293E+04	3.543E-03	8.834E-02	9.140E-02
.449	180	323.7	5.717E+04	5.914E+04	3.330E-03	8.322E-02	8.591E-02
.489	180	325.3	6.036E+04	6.258E+04	3.523E-03	8.786E-02	9.090E-02
.530	180	324.1	5.771E+04	5.973E+04	3.363E-03	8.400E-02	8.676E-02
.613	180	313.7	3.680E+04	3.753E+04	2.115E-03	5.357E-02	5.456E-02
.654	180	311.0	3.134E+04	3.183E+04	1.794E-03	4.562E-02	4.629E-02
.695	180	309.4	2.809E+04	2.846E+04	1.604E-03	4.088E-02	4.139E-02
.737	180	308.8	2.680E+04	2.713E+04	1.530E-03	3.901E-02	3.947E-02
.778	180	308.4	2.599E+04	2.630E+04	1.483E-03	3.783E-02	3.825E-02
.819	180	308.2	2.562E+04	2.591E+04	1.461E-03	3.728E-02	3.769E-02
.860	180	308.1	2.533E+04	2.562E+04	1.444E-03	3.686E-02	3.726E-02
.901	180	308.1	2.531E+04	2.561E+04	1.444E-03	3.685E-02	3.724E-02
.247	0	308.1	2.524E+04	2.553E+04	1.439E-03	3.674E-02	3.714E-02
.287	0	307.0	2.305E+04	2.327E+04	1.312E-03	3.354E-02	3.386E-02
.328	0	306.1	2.117E+04	2.135E+04	1.204E-03	3.081E-02	3.106E-02
.368	0	305.3	1.958E+04	1.973E+04	1.112E-03	2.850E-02	2.870E-02
.408	0	305.6	1.997E+04	2.012E+04	1.135E-03	2.906E-02	2.928E-02
.449	0	304.0	1.693E+04	1.702E+04	9.601E-04	2.464E-02	2.477E-02
.489	0	303.6	1.586E+04	1.594E+04	8.988E-04	2.308E-02	2.319E-02
.530	0	303.2	1.529E+04	1.536E+04	8.664E-04	2.226E-02	2.235E-02
.613	0	300.8	1.057E+04	1.058E+04	5.968E-04	1.538E-02	1.540E-02
.654	0	300.1	9.080E+03	9.081E+03	5.123E-04	1.322E-02	1.322E-02
.695	0	299.5	8.069E+03	8.064E+03	4.550E-04	1.174E-02	1.174E-02
.737	0	299.3	7.498E+03	7.491E+03	4.226E-04	1.091E-02	1.090E-02
.778	0	299.0	6.920E+03	6.910E+03	3.899E-04	1.007E-02	1.006E-02
.819	0	298.7	6.265E+03	6.253E+03	3.528E-04	9.119E-03	9.103E-03
.860	0	298.5	5.890E+03	5.878E+03	3.316E-04	8.573E-03	8.556E-03
.901	0	298.3	5.596E+03	5.582E+03	3.150E-04	8.145E-03	8.127E-03
.613	90	310.7	2.972E+04	3.018E+04	1.701E-03	4.326E-02	4.388E-02
.654	90	307.2	1.758E+04	1.776E+04	1.002E-03	2.559E-02	2.584E-02
.695	90	306.9	2.222E+04	2.244E+04	1.265E-03	3.234E-02	3.264E-02
.737	90	305.9	2.045E+04	2.063E+04	1.163E-03	2.977E-02	3.001E-02
.778	90	305.8	2.005E+04	2.021E+04	1.140E-03	2.918E-02	2.940E-02
.819	90	304.8	1.810E+04	1.823E+04	1.028E-03	2.635E-02	2.652E-02
.860	90	304.4	1.733E+04	1.744E+04	9.835E-04	2.523E-02	2.538E-02
.901	90	304.1	1.666E+04	1.676E+04	9.450E-04	2.425E-02	2.438E-02

TABLE II. Continued

(c) $\alpha = 8°$

FLOW CONDITIONS

Pt,1 N/m^2	Tt,1 K	Minf	pinf N/m^2	Tinf K	Rhoinf kg/m^3	Uinf m/s	Rinf,L
1.088E+07	1.009E+03	1.016E+01	2.297E+02	4.872E+01	1.642E-02	1.422E+03	9.204E+05

p2 N/m^2	T2 K	Rho2 kg/m^3	R2,L	Rho2/ Rhoinf	Pt,2 N/m^2	Ht,2 J/kg	Qsph,FR W/m^2
2.791E+04	9.908E+02	9.815E-02	6.887E+04	5.977E+00	3.075E+04	1.056E+06	6.837E+05

MEASURED HEAT TRANSFER DATA

x/L or z/L	Phi, deg	Twall, K	Qdot, W/m^2	Q(Tw=300K) W/m^2	St_inf	Q/Qsph	Ch/Chsph
.000	180	573.7	5.868E+05	9.559E+05	5.275E-02	8.582E-01	1.362E+00
.247	180	343.7	9.452E+04	1.007E+05	5.685E-03	1.383E-01	1.468E-01
.287	180	343.9	9.553E+04	1.018E+05	5.746E-03	1.397E-01	1.484E-01
.328	180	341.2	9.050E+04	9.609E+04	5.424E-03	1.324E-01	1.401E-01
.368	180	339.3	8.676E+04	9.185E+04	5.186E-03	1.269E-01	1.339E-01
.408	180	335.7	7.971E+04	8.394E+04	4.740E-03	1.166E-01	1.224E-01
.449	180	332.8	7.293E+04	7.647E+04	4.319E-03	1.067E-01	1.115E-01
.489	180	334.5	7.671E+04	8.063E+04	4.554E-03	1.122E-01	1.176E-01
.530	180	332.7	7.264E+04	7.615E+04	4.301E-03	1.063E-01	1.111E-01
.613	180	319.5	4.511E+04	4.639E+04	2.623E-03	6.599E-02	6.774E-02
.654	180	317.5	4.100E+04	4.203E+04	2.377E-03	5.997E-02	6.139E-02
.695	180	316.5	3.905E+04	3.998E+04	2.262E-03	5.712E-02	5.840E-02
.737	180	316.5	3.907E+04	4.000E+04	2.263E-03	5.715E-02	5.843E-02
.778	180	316.4	3.885E+04	3.977E+04	2.250E-03	5.683E-02	5.809E-02
.819	180	316.3	3.855E+04	3.945E+04	2.232E-03	5.638E-02	5.763E-02
.860	180	316.1	3.819E+04	3.908E+04	2.210E-03	5.586E-02	5.708E-02
.901	180	316.1	3.795E+04	3.883E+04	2.197E-03	5.551E-02	5.672E-02
.247	0	304.9	1.479E+04	1.489E+04	8.431E-04	2.163E-02	2.177E-02
.287	0	303.7	1.239E+04	1.246E+04	7.053E-04	1.812E-02	1.821E-02
.328	0	302.7	1.042E+04	1.046E+04	5.921E-04	1.523E-02	1.529E-02
.368	0	302.1	9.088E+03	9.115E+03	5.162E-04	1.329E-02	1.333E-02
.408	0	301.7	7.815E+03	7.833E+03	4.436E-04	1.143E-02	1.146E-02
.449	0	301.2	6.920E+03	6.931E+03	3.926E-04	1.012E-02	1.014E-02
.489	0	300.9	6.312E+03	6.319E+03	3.579E-04	9.232E-03	9.243E-03
.530	0	300.7	6.116E+03	6.122E+03	3.468E-04	8.945E-03	8.954E-03
.613	0	300.1	4.722E+03	4.723E+03	2.675E-04	6.907E-03	6.908E-03
.654	0	299.8	4.218E+03	4.217E+03	2.389E-04	6.170E-03	6.168E-03
.695	0	299.8	4.095E+03	4.094E+03	2.319E-04	5.990E-03	5.988E-03
.737	0	299.8	4.191E+03	4.190E+03	2.373E-04	6.130E-03	6.128E-03
.778	0	299.8	4.212E+03	4.211E+03	2.386E-04	6.161E-03	6.160E-03
.819	0	299.8	4.157E+03	4.156E+03	2.354E-04	6.080E-03	6.078E-03
.860	0	299.9	4.317E+03	4.316E+03	2.445E-04	6.314E-03	6.313E-03
.901	0	299.9	4.375E+03	4.374E+03	2.478E-04	6.399E-03	6.398E-03
.613	90	312.8	3.046E+04	3.102E+04	1.755E-03	4.455E-02	4.532E-02
.654	90	310.3	1.567E+04	1.590E+04	9.001E-04	2.292E-02	2.324E-02
.695	90	308.5	2.165E+04	2.192E+04	1.241E-03	3.167E-02	3.204E-02
.737	90	307.6	1.996E+04	2.017E+04	1.142E-03	2.919E-02	2.949E-02
.778	90	308.0	2.060E+04	2.083E+04	1.179E-03	3.013E-02	3.045E-02
.819	90	306.6	1.763E+04	1.780E+04	1.008E-03	2.579E-02	2.602E-02
.860	90	306.2	1.690E+04	1.705E+04	9.652E-04	2.472E-02	2.492E-02
.901	90	306.0	1.636E+04	1.649E+04	9.339E-04	2.392E-02	2.411E-02

TABLE II. Continued

(d) $\alpha = 12°$

FLOW CONDITIONS

Pt,1 N/m^2	Tt,1 K	Minf	pinf N/m^2	Tinf K	Rhoinf kg/m^3	Uinf m/s	Rinf,L
1.093E+07	1.003E+03	1.016E+01	2.308E+02	4.846E+01	1.659E-02	1.418E+03	9.334E+05

p2 N/m^2	T2 K	Rho2 kg/m^3	R2,L	Rho2/ Rhoinf	Pt,2 N/m^2	Ht,2 J/kg	Qsph,FR W/m^2
2.805E+04	9.854E+02	9.916E-02	6.962E+04	5.977E+00	3.090E+04	1.050E+06	6.798E+05

MEASURED HEAT TRANSFER DATA

x/L or z/L	Phi, deg	Twall, K	Qdot, W/m^2	Q(Tw=300K) W/m^2	St_inf	Q/Qsph	Ch/Chsph
.000	180	569.8	5.725E+05	9.287E+05	5.131E-02	8.422E-01	1.332E+00
.247	180	353.4	1.143E+05	1.236E+05	6.976E-03	1.681E-01	1.810E-01
.287	180	352.0	1.119E+05	1.208E+05	6.819E-03	1.646E-01	1.770E-01
.328	180	348.5	1.051E+05	1.128E+05	6.369E-03	1.545E-01	1.653E-01
.368	180	346.7	1.012E+05	1.084E+05	6.121E-03	1.489E-01	1.588E-01
.408	180	341.2	8.997E+04	9.557E+04	5.398E-03	1.323E-01	1.401E-01
.449	180	338.3	8.478E+04	8.967E+04	5.066E-03	1.247E-01	1.315E-01
.489	180	340.2	8.743E+04	9.273E+04	5.238E-03	1.286E-01	1.359E-01
.530	180	338.2	8.308E+04	8.786E+04	4.964E-03	1.222E-01	1.288E-01
.613	180	323.3	5.249E+04	5.429E+04	3.071E-03	7.721E-02	7.970E-02
.654	180	322.3	5.060E+04	5.225E+04	2.956E-03	7.443E-02	7.672E-02
.695	180	321.6	4.919E+04	5.075E+04	2.871E-03	7.236E-02	7.452E-02
.737	180	321.6	4.935E+04	5.091E+04	2.881E-03	7.260E-02	7.476E-02
.778	180	321.4	4.900E+04	5.054E+04	2.859E-03	7.208E-02	7.421E-02
.819	180	321.2	4.876E+04	5.027E+04	2.845E-03	7.172E-02	7.382E-02
.860	180	321.2	4.860E+04	5.011E+04	2.835E-03	7.149E-02	7.358E-02
.901	180	320.8	4.781E+04	4.926E+04	2.788E-03	7.033E-02	7.234E-02
.247	0	302.1	9.112E+03	9.139E+03	5.179E-04	1.340E-02	1.344E-02
.287	0	301.5	7.683E+03	7.699E+03	4.363E-04	1.130E-02	1.132E-02
.328	0	301.0	6.677E+03	6.687E+03	3.790E-04	9.823E-03	9.836E-03
.368	0	300.7	6.203E+03	6.209E+03	3.519E-04	9.125E-03	9.133E-03
.408	0	299.8	5.436E+03	5.434E+03	3.080E-04	7.996E-03	7.993E-03
.449	0	300.7	6.032E+03	6.038E+03	3.422E-04	8.874E-03	8.882E-03
.489	0	300.8	6.400E+03	6.407E+03	3.632E-04	9.414E-03	9.425E-03
.530	0	301.1	7.120E+03	7.131E+03	4.042E-04	1.047E-02	1.049E-02
.613	0	300.9	6.770E+03	6.779E+03	3.842E-04	9.959E-03	9.971E-03
.654	0	301.0	6.884E+03	6.893E+03	3.907E-04	1.013E-02	1.014E-02
.695	0	301.3	7.449E+03	7.462E+03	4.229E-04	1.096E-02	1.098E-02
.737	0	301.5	8.143E+03	8.161E+03	4.625E-04	1.198E-02	1.200E-02
.778	0	301.8	8.632E+03	8.655E+03	4.905E-04	1.270E-02	1.273E-02
.819	0	302.2	9.266E+03	9.295E+03	5.268E-04	1.363E-02	1.367E-02
.860	0	302.4	9.799E+03	9.833E+03	5.572E-04	1.442E-02	1.446E-02
.901	0	302.5	1.015E+04	1.019E+04	5.775E-04	1.494E-02	1.499E-02
.613	90	311.2	2.712E+04	2.756E+04	1.561E-03	3.989E-02	4.050E-02
.654	90	305.1	1.675E+04	1.687E+04	9.558E-04	2.464E-02	2.481E-02
.695	90	307.4	1.912E+04	1.932E+04	1.095E-03	2.813E-02	2.841E-02
.737	90	306.7	1.795E+04	1.812E+04	1.027E-03	2.641E-02	2.665E-02
.778	90	306.9	1.828E+04	1.846E+04	1.046E-03	2.688E-02	2.713E-02
.819	90	306.4	1.727E+04	1.743E+04	9.873E-04	2.540E-02	2.562E-02
.860	90	306.5	1.732E+04	1.748E+04	9.904E-04	2.548E-02	2.570E-02
.901	90	306.5	1.732E+04	1.749E+04	9.906E-04	2.548E-02	2.571E-02

TABLE II. Continued

(e) $\alpha = 16°$

FLOW CONDITIONS

Pt,1 N/m^2	Tt,1 K	Minf	pinf N/m^2	Tinf K	Rhoinf kg/m^3	Uinf m/s	Rinf,L
1.088E+07	1.003E+03	1.016E+01	2.297E+02	4.844E+01	1.652E-02	1.418E+03	9.297E+05

p2 N/m^2	T2 K	Rho2 kg/m^3	R2,L	Rho2/ Rhoinf	Pt,2 N/m^2	Ht,2 J/kg	Qsph,FR W/m^2
2.792E+04	9.851E+02	9.875E-02	6.933E+04	5.977E+00	3.076E+04	1.050E+06	6.779E+05

MEASURED HEAT TRANSFER DATA

x/L or z/L	Phi, deg	Twall, K	Qdot, W/m^2	Q(Tw=300K) W/m^2	St_inf	Q/Qsph	Ch/Chsph
.000	180	567.3	5.555E+05	8.962E+05	4.977E-02	8.195E-01	1.289E+00
.247	180	362.0	1.286E+05	1.411E+05	7.993E-03	1.898E-01	2.070E-01
.287	180	360.7	1.267E+05	1.386E+05	7.855E-03	1.869E-01	2.034E-01
.328	180	356.8	1.196E+05	1.301E+05	7.377E-03	1.765E-01	1.910E-01
.368	180	354.0	1.141E+05	1.236E+05	7.006E-03	1.683E-01	1.814E-01
.408	180	348.4	1.027E+05	1.103E+05	6.257E-03	1.515E-01	1.620E-01
.449	180	345.4	9.649E+04	1.031E+05	5.853E-03	1.423E-01	1.516E-01
.489	180	347.5	1.012E+05	1.086E+05	6.158E-03	1.493E-01	1.595E-01
.530	180	345.3	9.631E+04	1.029E+05	5.841E-03	1.421E-01	1.513E-01
.613	180	329.7	6.482E+04	6.768E+04	3.846E-03	9.562E-02	9.959E-02
.654	180	328.9	6.349E+04	6.622E+04	3.763E-03	9.366E-02	9.744E-02
.695	180	328.0	6.162E+04	6.417E+04	3.646E-03	9.089E-02	9.443E-02
.737	180	327.8	6.106E+04	6.357E+04	3.612E-03	9.007E-02	9.355E-02
.778	180	327.5	6.057E+04	6.303E+04	3.582E-03	8.934E-02	9.277E-02
.819	180	327.0	5.931E+04	6.167E+04	3.505E-03	8.748E-02	9.077E-02
.860	180	326.6	5.859E+04	6.090E+04	3.461E-03	8.643E-02	8.963E-02
.901	180	326.8	5.875E+04	6.107E+04	3.471E-03	8.666E-02	8.989E-02
.247	0	301.9	8.614E+03	8.637E+03	4.919E-04	1.271E-02	1.274E-02
.287	0	302.1	8.832E+03	8.858E+03	5.045E-04	1.303E-02	1.306E-02
.328	0	302.4	9.549E+03	9.582E+03	5.457E-04	1.409E-02	1.413E-02
.368	0	303.1	1.101E+04	1.105E+04	6.295E-04	1.624E-02	1.630E-02
.408	0	303.5	1.212E+04	1.218E+04	6.934E-04	1.787E-02	1.796E-02
.449	0	304.5	1.391E+04	1.400E+04	7.971E-04	2.052E-02	2.064E-02
.489	0	305.0	1.506E+04	1.517E+04	8.635E-04	2.221E-02	2.236E-02
.530	0	305.4	1.584E+04	1.596E+04	9.088E-04	2.337E-02	2.353E-02
.613	0	303.8	1.270E+04	1.277E+04	7.274E-04	1.874E-02	1.884E-02
.654	0	303.5	1.201E+04	1.207E+04	6.875E-04	1.772E-02	1.780E-02
.695	0	303.2	1.148E+04	1.154E+04	6.569E-04	1.694E-02	1.701E-02
.737	0	303.3	1.161E+04	1.167E+04	6.644E-04	1.713E-02	1.721E-02
.778	0	303.3	1.151E+04	1.156E+04	6.584E-04	1.698E-02	1.705E-02
.819	0	303.2	1.140E+04	1.145E+04	6.521E-04	1.682E-02	1.689E-02
.860	0	303.2	1.142E+04	1.147E+04	6.534E-04	1.685E-02	1.692E-02
.901	0	303.2	1.139E+04	1.144E+04	6.515E-04	1.680E-02	1.687E-02
.613	90	310.6	2.518E+04	2.556E+04	1.455E-03	3.714E-02	3.767E-02
.654	90	306.0	1.376E+04	1.387E+04	7.899E-04	2.029E-02	2.046E-02
.695	90	307.5	1.898E+04	1.919E+04	1.092E-03	2.800E-02	2.829E-02
.737	90	307.3	1.854E+04	1.873E+04	1.066E-03	2.734E-02	2.761E-02
.778	90	307.5	1.899E+04	1.920E+04	1.093E-03	2.802E-02	2.830E-02
.819	90	307.0	1.796E+04	1.814E+04	1.033E-03	2.650E-02	2.675E-02
.860	90	306.8	1.766E+04	1.783E+04	1.015E-03	2.605E-02	2.629E-02
.901	90	306.7	1.739E+04	1.756E+04	9.995E-04	2.565E-02	2.588E-02

TABLE II. Concluded

(f) $\alpha = 20°$

FLOW CONDITIONS

Pt,1 N/m^2	Tt,1 K	Minf	pinf N/m^2	Tinf K	Rhoinf kg/m^3	Uinf m/s	Rinf,L
1.092E+07	9.964E+02	1.016E+01	2.306E+02	4.813E+01	1.669E-02	1.413E+03	9.436E+05

p2 N/m^2	T2 K	Rho2 kg/m^3	R2,L	Rho2/ Rhoinf	Pt,2 N/m^2	Ht,2 J/kg	Qsph,FR W/m^2
2.802E+04	9.786E+02	9.976E-02	7.009E+04	5.977E+00	3.087E+04	1.042E+06	6.732E+05

MEASURED HEAT TRANSFER DATA

x/L or z/L	Phi, deg	Twall, K	Qdot, W/m^2	Q(Tw=300K) W/m^2	St_inf	Q/Qsph	Ch/Chsph
.000	180	565.4	5.461E+05	8.824E+05	4.917E-02	8.112E-01	1.278E+00
.247	180	369.4	1.455E+05	1.616E+05	9.177E-03	2.161E-01	2.385E-01
.287	180	367.6	1.429E+05	1.582E+05	8.988E-03	2.122E-01	2.336E-01
.328	180	363.8	1.359E+05	1.496E+05	8.504E-03	2.019E-01	2.211E-01
.368	180	360.1	1.287E+05	1.408E+05	8.005E-03	1.911E-01	2.081E-01
.408	180	353.8	1.165E+05	1.262E+05	7.179E-03	1.730E-01	1.866E-01
.449	180	350.7	1.112E+05	1.199E+05	6.824E-03	1.652E-01	1.774E-01
.489	180	350.2	1.078E+05	1.161E+05	6.609E-03	1.601E-01	1.718E-01
.530	180	350.1	1.094E+05	1.179E+05	6.708E-03	1.625E-01	1.744E-01
.613	180	333.9	7.736E+04	8.132E+04	4.634E-03	1.149E-01	1.205E-01
.654	180	333.4	7.677E+04	8.064E+04	4.595E-03	1.140E-01	1.194E-01
.695	180	332.1	7.417E+04	7.775E+04	4.431E-03	1.102E-01	1.152E-01
.737	180	332.0	7.399E+04	7.755E+04	4.420E-03	1.099E-01	1.149E-01
.778	180	331.4	7.304E+04	7.648E+04	4.359E-03	1.085E-01	1.133E-01
.819	180	330.8	7.188E+04	7.520E+04	4.286E-03	1.068E-01	1.114E-01
.860	180	331.1	7.261E+04	7.599E+04	4.331E-03	1.079E-01	1.126E-01
.901	180	331.4	7.265E+04	7.607E+04	4.336E-03	1.079E-01	1.127E-01
.247	0	302.2	1.481E+04	1.486E+04	8.490E-04	2.200E-02	2.207E-02
.287	0	303.6	1.747E+04	1.756E+04	1.003E-03	2.595E-02	2.608E-02
.328	0	304.4	1.926E+04	1.938E+04	1.107E-03	2.861E-02	2.878E-02
.368	0	304.8	2.016E+04	2.030E+04	1.159E-03	2.994E-02	3.014E-02
.408	0	305.5	2.211E+04	2.229E+04	1.273E-03	3.285E-02	3.310E-02
.449	0	305.0	2.045E+04	2.059E+04	1.176E-03	3.037E-02	3.058E-02
.489	0	304.9	2.039E+04	2.054E+04	1.173E-03	3.029E-02	3.049E-02
.530	0	304.7	1.979E+04	1.993E+04	1.138E-03	2.940E-02	2.959E-02
.613	0	301.9	1.412E+04	1.415E+04	8.087E-04	2.097E-02	2.102E-02
.654	0	301.3	1.302E+04	1.305E+04	7.454E-04	1.934E-02	1.938E-02
.695	0	300.8	1.194E+04	1.195E+04	6.828E-04	1.773E-02	1.775E-02
.737	0	300.4	1.109E+04	1.110E+04	6.340E-04	1.647E-02	1.648E-02
.778	0	300.2	1.079E+04	1.079E+04	6.165E-04	1.602E-02	1.603E-02
.819	0	300.1	1.047E+04	1.047E+04	5.983E-04	1.555E-02	1.555E-02
.860	0	299.9	1.015E+04	1.014E+04	5.797E-04	1.507E-02	1.507E-02
.901	0	299.8	9.918E+03	9.915E+03	5.666E-04	1.473E-02	1.473E-02
.613	90	308.2	2.542E+04	2.572E+04	1.469E-03	3.776E-02	3.819E-02
.654	90	307.3	1.988E+04	2.009E+04	1.147E-03	2.953E-02	2.982E-02
.695	90	305.6	2.034E+04	2.050E+04	1.171E-03	3.022E-02	3.045E-02
.737	90	305.1	1.941E+04	1.956E+04	1.117E-03	2.884E-02	2.904E-02
.778	90	304.8	1.883E+04	1.896E+04	1.083E-03	2.798E-02	2.816E-02
.819	90	304.8	1.875E+04	1.888E+04	1.079E-03	2.786E-02	2.804E-02
.860	90	304.7	1.842E+04	1.855E+04	1.059E-03	2.737E-02	2.754E-02
.901	90	304.6	1.823E+04	1.835E+04	1.048E-03	2.708E-02	2.725E-02

TABLE III. MEASURED HEAT-TRANSFER DATA FOR BENT-NOSE BICONIC AT LOW REYNOLDS NUMBER

(a) $\alpha = 0°$

FLOW CONDITIONS

Pt,1 N/m^2	Tt,1 K	Minf	pinf N/m^2	Tinf K	Rhoinf kg/m^3	Uinf m/s	Rinf,L
2.375E+06	9.806E+02	9.860E+00	5.970E+01	4.975E+01	4.181E-03	1.394E+03	2.241E+05

p2 N/m^2	T2 K	Rho2 kg/m^3	R2,L	Rho2/ Rhoinf	Pt,2 N/m^2	Ht,2 J/kg	Qsph,FR W/m^2
6.831E+03	9.591E+02	2.481E-02	1.753E+04	5.935E+00	7.529E+03	1.024E+06	3.251E+05

MEASURED HEAT TRANSFER DATA

x/L or z/L	Phi, deg	Twall, K	Qdot, W/m^2	Q(Tw=300K) W/m^2	St_inf	Q/Qsph	Ch/Chsph
.000	180	457.9	3.413E+05	4.444E+05	1.038E-01	1.050E+00	1.347E+00
.256	180	316.6	4.117E+04	4.220E+04	9.986E-03	1.266E-01	1.296E-01
.296	180	316.7	4.175E+04	4.280E+04	1.013E-02	1.284E-01	1.315E-01
.337	180	316.4	4.108E+04	4.209E+04	9.962E-03	1.264E-01	1.293E-01
.377	180	315.6	3.954E+04	4.046E+04	9.577E-03	1.216E-01	1.243E-01
.418	180	0.0	0.000E+00	0.000E+00	0.000E+00	0.000E+00	0.000E+00
.459	180	314.2	3.661E+04	3.739E+04	8.850E-03	1.126E-01	1.149E-01
.499	180	0.0	0.000E+00	0.000E+00	0.000E+00	0.000E+00	0.000E+00
.540	180	0.0	0.000E+00	0.000E+00	0.000E+00	0.000E+00	0.000E+00
.634	180	302.2	1.156E+04	1.160E+04	2.748E-03	3.556E-02	3.567E-02
.676	180	301.1	9.324E+03	9.339E+03	2.213E-03	2.868E-02	2.872E-02
.717	180	300.6	8.208E+03	8.215E+03	1.947E-03	2.525E-02	2.527E-02
.759	180	300.3	7.616E+03	7.619E+03	1.805E-03	2.342E-02	2.343E-02
.800	180	300.1	7.224E+03	7.225E+03	1.712E-03	2.222E-02	2.222E-02
.842	180	300.0	7.000E+03	6.999E+03	1.659E-03	2.153E-02	2.153E-02
.884	180	299.9	6.831E+03	6.830E+03	1.619E-03	2.101E-02	2.101E-02
.925	180	299.8	6.718E+03	6.716E+03	1.592E-03	2.066E-02	2.066E-02
.256	0	301.4	9.883E+03	9.903E+03	2.346E-03	3.040E-02	3.046E-02
.296	0	300.9	8.887E+03	8.898E+03	2.109E-03	2.733E-02	2.737E-02
.337	0	300.5	8.044E+03	8.050E+03	1.908E-03	2.474E-02	2.476E-02
.377	0	300.1	7.273E+03	7.274E+03	1.724E-03	2.237E-02	2.237E-02
.418	0	0.0	0.000E+00	0.000E+00	0.000E+00	0.000E+00	0.000E+00
.459	0	0.0	0.000E+00	0.000E+00	0.000E+00	0.000E+00	0.000E+00
.499	0	299.4	5.731E+03	5.726E+03	1.357E-03	1.763E-02	1.761E-02
.540	0	0.0	0.000E+00	0.000E+00	0.000E+00	0.000E+00	0.000E+00
.636	0	299.2	5.356E+03	5.350E+03	1.268E-03	1.647E-02	1.646E-02
.679	0	299.2	5.261E+03	5.254E+03	1.245E-03	1.618E-02	1.616E-02
.721	0	299.1	5.236E+03	5.229E+03	1.239E-03	1.610E-02	1.609E-02
.764	0	299.1	5.159E+03	5.152E+03	1.221E-03	1.587E-02	1.585E-02
.806	0	299.1	5.177E+03	5.170E+03	1.225E-03	1.592E-02	1.590E-02
.849	0	0.0	0.000E+00	0.000E+00	0.000E+00	0.000E+00	0.000E+00
.892	0	299.1	5.177E+03	5.170E+03	1.225E-03	1.592E-02	1.590E-02
.935	0	299.2	5.257E+03	5.250E+03	1.244E-03	1.617E-02	1.615E-02
.635	90	303.4	1.378E+04	1.385E+04	3.281E-03	4.239E-02	4.259E-02
.678	90	302.8	1.263E+04	1.268E+04	3.005E-03	3.885E-02	3.900E-02
.719	90	302.4	1.175E+04	1.179E+04	2.793E-03	3.613E-02	3.625E-02
.763	90	302.1	1.134E+04	1.137E+04	2.694E-03	3.486E-02	3.497E-02
.803	90	302.0	1.102E+04	1.105E+04	2.618E-03	3.388E-02	3.398E-02
.846	90	301.9	1.076E+04	1.079E+04	2.556E-03	3.309E-02	3.317E-02
.888	90	301.8	1.069E+04	1.072E+04	2.539E-03	3.288E-02	3.296E-02
.930	90	301.8	1.055E+04	1.057E+04	2.505E-03	3.243E-02	3.251E-02

TABLE III. Continued

(b) $\alpha = 4°$

FLOW CONDITIONS

Pt,1 N/m^2	Tt,1 K	Minf	pinf N/m^2	Tinf K	Rhoinf kg/m^3	Uinf m/s	Rinf,L
2.410E+06	9.704E+02	9.860E+00	6.058E+01	4.923E+01	4.287E-03	1.387E+03	2.315E+05

p2 N/m^2	T2 K	Rho2 kg/m^3	R2,L	Rho2/ Rhoinf	Pt,2 N/m^2	Ht,2 J/kg	Qsph,FR W/m^2
6.932E+03	9.491E+02	2.545E-02	1.800E+04	5.935E+00	7.640E+03	1.013E+06	3.223E+05

MEASURED HEAT TRANSFER DATA

x/L or z/L	Phi, deg	Twall, K	Qdot, W/m^2	Q(Tw=300K) W/m^2	St_inf	Q/Qsph	Ch/Chsph
.000	180	454.7	3.375E+05	4.387E+05	1.021E-01	1.047E+00	1.342E+00
.256	180	322.3	5.363E+04	5.547E+04	1.307E-02	1.664E-01	1.718E-01
.296	180	321.7	5.270E+04	5.447E+04	1.284E-02	1.635E-01	1.687E-01
.337	180	320.4	4.974E+04	5.130E+04	1.209E-02	1.543E-01	1.589E-01
.377	180	319.2	4.734E+04	4.874E+04	1.149E-02	1.469E-01	1.510E-01
.418	180	0.0	0.000E+00	0.000E+00	0.000E+00	0.000E+00	0.000E+00
.459	180	316.9	4.258E+04	4.368E+04	1.030E-02	1.321E-01	1.353E-01
.499	180	0.0	0.000E+00	0.000E+00	0.000E+00	0.000E+00	0.000E+00
.540	180	0.0	0.000E+00	0.000E+00	0.000E+00	0.000E+00	0.000E+00
.634	180	303.1	1.331E+04	1.337E+04	3.156E-03	4.130E-02	4.148E-02
.676	180	302.1	1.146E+04	1.149E+04	2.713E-03	3.555E-02	3.566E-02
.717	180	301.8	1.078E+04	1.081E+04	2.551E-03	3.344E-02	3.352E-02
.759	180	301.7	1.051E+04	1.054E+04	2.487E-03	3.261E-02	3.268E-02
.800	180	301.6	1.033E+04	1.035E+04	2.444E-03	3.205E-02	3.212E-02
.842	180	301.5	1.027E+04	1.029E+04	2.430E-03	3.187E-02	3.194E-02
.884	180	301.6	1.022E+04	1.024E+04	2.418E-03	3.171E-02	3.178E-02
.925	180	301.5	1.028E+04	1.030E+04	2.431E-03	3.189E-02	3.195E-02
.256	0	0.0	0.000E+00	0.000E+00	0.000E+00	0.000E+00	0.000E+00
.296	0	299.2	5.479E+03	5.472E+03	1.292E-03	1.700E-02	1.698E-02
.337	0	298.9	4.790E+03	4.782E+03	1.129E-03	1.486E-02	1.484E-02
.377	0	298.6	4.238E+03	4.229E+03	9.985E-04	1.315E-02	1.312E-02
.418	0	0.0	0.000E+00	0.000E+00	0.000E+00	0.000E+00	0.000E+00
.459	0	0.0	0.000E+00	0.000E+00	0.000E+00	0.000E+00	0.000E+00
.499	0	298.2	3.293E+03	3.284E+03	7.753E-04	1.022E-02	1.019E-02
.540	0	0.0	0.000E+00	0.000E+00	0.000E+00	0.000E+00	0.000E+00
.636	0	298.1	3.102E+03	3.093E+03	7.303E-04	9.624E-03	9.598E-03
.679	0	298.1	3.081E+03	3.072E+03	7.253E-04	9.559E-03	9.533E-03
.721	0	298.0	3.040E+03	3.031E+03	7.156E-04	9.431E-03	9.405E-03
.764	0	298.0	2.984E+03	2.975E+03	7.025E-04	9.260E-03	9.234E-03
.806	0	298.0	2.985E+03	2.977E+03	7.028E-04	9.263E-03	9.238E-03
.849	0	0.0	0.000E+00	0.000E+00	0.000E+00	0.000E+00	0.000E+00
.892	0	298.0	2.950E+03	2.941E+03	6.944E-04	9.152E-03	9.126E-03
.935	0	298.0	2.997E+03	2.988E+03	7.056E-04	9.300E-03	9.274E-03
.635	90	303.2	1.350E+04	1.356E+04	3.201E-03	4.189E-02	4.207E-02
.678	90	302.5	1.225E+04	1.229E+04	2.901E-03	3.800E-02	3.813E-02
.719	90	302.1	1.136E+04	1.140E+04	2.691E-03	3.526E-02	3.536E-02
.763	90	301.9	1.098E+04	1.101E+04	2.599E-03	3.407E-02	3.416E-02
.803	90	0.0	0.000E+00	0.000E+00	0.000E+00	0.000E+00	0.000E+00
.846	90	301.6	1.033E+04	1.035E+04	2.443E-03	3.204E-02	3.211E-02
.888	90	301.5	1.019E+04	1.021E+04	2.411E-03	3.162E-02	3.169E-02
.930	90	301.5	1.003E+04	1.006E+04	2.374E-03	3.113E-02	3.120E-02

TABLE III. Continued

(c) $\alpha = 8°$

FLOW CONDITIONS

Pt,1 N/m^2	Tt,1 K	Minf	pinf N/m^2	Tinf K	Rhoinf kg/m^3	Uinf m/s	Rinf,L
2.395E+06	9.901E+02	9.860E+00	6.020E+01	5.023E+01	4.176E-03	1.401E+03	2.224E+05

p2 N/m^2	T2 K	Rho2 kg/m^3	R2,L	Rho2/ Rhoinf	Pt,2 N/m^2	Ht,2 J/kg	Qsph,FR W/m^2
6.889E+03	9.684E+02	2.478E-02	1.749E+04	5.935E+00	7.592E+03	1.035E+06	3.313E+05

MEASURED HEAT TRANSFER DATA

x/L or z/L	Phi, deg	Twall, K	Qdot, W/m^2	Q(Tw=300K) W/m^2	St_inf	Q/Qsph	Ch/Chsph
.000	180	459.1	3.645E+05	4.738E+05	1.086E-01	1.100E+00	1.410E+00
.256	180	328.8	6.492E+04	6.774E+04	1.572E-02	1.960E-01	2.040E-01
.296	180	327.7	6.321E+04	6.585E+04	1.529E-02	1.908E-01	1.983E-01
.337	180	326.4	6.037E+04	6.277E+04	1.457E-02	1.822E-01	1.890E-01
.377	180	325.5	5.856E+04	6.081E+04	1.412E-02	1.768E-01	1.832E-01
.418	180	0.0	0.000E+00	0.000E+00	0.000E+00	0.000E+00	0.000E+00
.459	180	322.5	5.236E+04	5.413E+04	1.257E-02	1.581E-01	1.631E-01
.499	180	0.0	0.000E+00	0.000E+00	0.000E+00	0.000E+00	0.000E+00
.540	180	0.0	0.000E+00	0.000E+00	0.000E+00	0.000E+00	0.000E+00
.634	180	305.6	1.723E+04	1.737E+04	4.040E-03	5.201E-02	5.241E-02
.676	180	305.0	1.605E+04	1.616E+04	3.759E-03	4.843E-02	4.877E-02
.717	180	304.7	1.551E+04	1.561E+04	3.631E-03	4.681E-02	4.711E-02
.759	180	304.7	1.542E+04	1.552E+04	3.610E-03	4.654E-02	4.684E-02
.800	180	304.7	1.537E+04	1.548E+04	3.599E-03	4.640E-02	4.670E-02
.842	180	304.6	1.534E+04	1.545E+04	3.592E-03	4.631E-02	4.661E-02
.884	180	304.6	1.526E+04	1.536E+04	3.572E-03	4.606E-02	4.635E-02
.925	180	304.6	1.531E+04	1.541E+04	3.584E-03	4.620E-02	4.650E-02
.256	0	0.0	0.000E+00	0.000E+00	0.000E+00	0.000E+00	0.000E+00
.296	0	299.2	4.257E+03	4.252E+03	9.894E-04	1.285E-02	1.284E-02
.337	0	299.0	3.840E+03	3.834E+03	8.921E-04	1.159E-02	1.157E-02
.377	0	298.8	3.538E+03	3.532E+03	8.217E-04	1.068E-02	1.066E-02
.418	0	0.0	0.000E+00	0.000E+00	0.000E+00	0.000E+00	0.000E+00
.459	0	0.0	0.000E+00	0.000E+00	0.000E+00	0.000E+00	0.000E+00
.499	0	298.7	3.147E+03	3.141E+03	7.309E-04	9.501E-03	9.483E-03
.540	0	0.0	0.000E+00	0.000E+00	0.000E+00	0.000E+00	0.000E+00
.636	0	298.7	3.333E+03	3.327E+03	7.742E-04	1.006E-02	1.005E-02
.679	0	298.8	3.450E+03	3.444E+03	8.014E-04	1.041E-02	1.040E-02
.721	0	298.8	3.497E+03	3.491E+03	8.123E-04	1.056E-02	1.054E-02
.764	0	298.8	3.563E+03	3.557E+03	8.277E-04	1.076E-02	1.074E-02
.806	0	298.9	3.612E+03	3.606E+03	8.390E-04	1.090E-02	1.089E-02
.849	0	0.0	0.000E+00	0.000E+00	0.000E+00	0.000E+00	0.000E+00
.892	0	298.9	3.736E+03	3.730E+03	8.679E-04	1.128E-02	1.126E-02
.935	0	298.9	3.778E+03	3.772E+03	8.776E-04	1.140E-02	1.139E-02
.635	90	303.6	1.301E+04	1.308E+04	3.042E-03	3.927E-02	3.946E-02
.678	90	303.0	1.188E+04	1.193E+04	2.775E-03	3.585E-02	3.600E-02
.719	90	302.7	1.114E+04	1.119E+04	2.602E-03	3.364E-02	3.376E-02
.763	90	302.5	1.082E+04	1.086E+04	2.526E-03	3.267E-02	3.278E-02
.803	90	0.0	0.000E+00	0.000E+00	0.000E+00	0.000E+00	0.000E+00
.846	90	302.2	1.020E+04	1.023E+04	2.380E-03	3.079E-02	3.088E-02
.888	90	302.1	1.001E+04	1.004E+04	2.335E-03	3.021E-02	3.030E-02
.930	90	302.1	9.870E+03	9.899E+03	2.303E-03	2.979E-02	2.988E-02

TABLE III. Continued

(d) $\alpha = 12°$

FLOW CONDITIONS

Pt,1 N/m^2	Tt,1 K	Minf	pinf N/m^2	Tinf K	Rhoinf kg/m^3	Uinf m/s	Rinf,L
2.395E+06	9.872E+02	9.860E+00	6.020E+01	5.008E+01	4.188E-03	1.399E+03	2.235E+05

p2 N/m^2	T2 K	Rho2 kg/m^3	R2,L	Rho2/ Rhoinf	Pt,2 N/m^2	Ht,2 J/kg	Qsph,FR W/m^2
6.889E+03	9.656E+02	2.486E-02	1.755E+04	5.935E+00	7.592E+03	1.032E+06	3.298E+05

MEASURED HEAT TRANSFER DATA

x/L or z/L	Phi, deg	Twall, K	Qdot, W/m^2	Q(Tw=300K) W/m^2	St_inf	Q/Qsph	Ch/Chsph
.000	180	0.0	0.000E+00	0.000E+00	0.000E+00	0.000E+00	0.000E+00
.256	180	333.5	7.402E+04	7.780E+04	1.811E-02	2.244E-01	2.352E-01
.296	180	332.3	7.239E+04	7.596E+04	1.768E-02	2.195E-01	2.297E-01
.337	180	331.0	6.982E+04	7.312E+04	1.702E-02	2.117E-01	2.211E-01
.377	180	329.7	6.715E+04	7.019E+04	1.634E-02	2.036E-01	2.123E-01
.418	180	0.0	0.000E+00	0.000E+00	0.000E+00	0.000E+00	0.000E+00
.459	180	326.7	6.098E+04	6.344E+04	1.477E-02	1.849E-01	1.919E-01
.499	180	0.0	0.000E+00	0.000E+00	0.000E+00	0.000E+00	0.000E+00
.540	180	0.0	0.000E+00	0.000E+00	0.000E+00	0.000E+00	0.000E+00
.634	180	307.9	2.201E+04	2.227E+04	5.194E-03	6.675E-02	6.748E-02
.676	180	307.6	2.151E+04	2.175E+04	5.073E-03	6.522E-02	6.591E-02
.717	180	307.5	2.120E+04	2.144E+04	4.999E-03	6.429E-02	6.496E-02
.759	180	307.4	2.118E+04	2.141E+04	4.994E-03	6.423E-02	6.489E-02
.800	180	307.4	2.111E+04	2.134E+04	4.976E-03	6.399E-02	6.465E-02
.842	180	307.4	2.110E+04	2.133E+04	4.975E-03	6.398E-02	6.463E-02
.884	180	307.4	2.101E+04	2.124E+04	4.954E-03	6.371E-02	6.436E-02
.925	180	307.5	2.119E+04	2.142E+04	4.996E-03	6.425E-02	6.491E-02
.256	0	0.0	0.000E+00	0.000E+00	0.000E+00	0.000E+00	0.000E+00
.296	0	299.1	4.030E+03	4.025E+03	9.393E-04	1.222E-02	1.220E-02
.337	0	299.0	3.848E+03	3.842E+03	8.967E-04	1.167E-02	1.165E-02
.377	0	299.0	3.779E+03	3.774E+03	8.807E-04	1.146E-02	1.144E-02
.418	0	0.0	0.000E+00	0.000E+00	0.000E+00	0.000E+00	0.000E+00
.459	0	0.0	0.000E+00	0.000E+00	0.000E+00	0.000E+00	0.000E+00
.499	0	299.0	3.807E+03	3.801E+03	8.872E-04	1.154E-02	1.153E-02
.540	0	0.0	0.000E+00	0.000E+00	0.000E+00	0.000E+00	0.000E+00
.636	0	299.1	4.173E+03	4.168E+03	9.727E-04	1.265E-02	1.264E-02
.679	0	299.2	4.284E+03	4.279E+03	9.985E-04	1.299E-02	1.297E-02
.721	0	299.2	4.358E+03	4.353E+03	1.016E-03	1.321E-02	1.320E-02
.764	0	299.2	4.402E+03	4.397E+03	1.026E-03	1.335E-02	1.333E-02
.806	0	299.2	4.414E+03	4.409E+03	1.029E-03	1.338E-02	1.337E-02
.849	0	298.7	2.399E+03	2.395E+03	5.589E-04	7.274E-03	7.261E-03
.892	0	299.2	4.396E+03	4.391E+03	1.025E-03	1.333E-02	1.331E-02
.935	0	299.2	4.334E+03	4.329E+03	1.010E-03	1.314E-02	1.313E-02
.635	90	303.5	1.279E+04	1.285E+04	2.999E-03	3.877E-02	3.896E-02
.678	90	303.1	1.199E+04	1.204E+04	2.809E-03	3.634E-02	3.650E-02
.719	90	302.8	1.138E+04	1.143E+04	2.666E-03	3.451E-02	3.464E-02
.763	90	302.6	1.104E+04	1.108E+04	2.585E-03	3.346E-02	3.358E-02
.803	90	302.5	1.073E+04	1.077E+04	2.513E-03	3.254E-02	3.265E-02
.846	90	302.3	1.034E+04	1.038E+04	2.421E-03	3.136E-02	3.146E-02
.888	90	302.1	1.007E+04	1.011E+04	2.358E-03	3.054E-02	3.063E-02
.930	90	302.1	9.871E+03	9.901E+03	2.310E-03	2.993E-02	3.001E-02

TABLE III. Continued

(e) $\alpha = 16°$

FLOW CONDITIONS

Pt,1 N/m^2	Tt,1 K	Minf	pinf N/m^2	Tinf K	Rhoinf kg/m^3	Uinf m/s	Rinf,L
2.549E+06	9.651E+02	9.860E+00	6.408E+01	4.896E+01	4.560E-03	1.383E+03	2.472E+05

p2 N/m^2	T2 K	Rho2 kg/m^3	R2,L	Rho2/ Rhoinf	Pt,2 N/m^2	Ht,2 J/kg	Qsph,FR W/m^2
7.333E+03	9.439E+02	2.707E-02	1.916E+04	5.935E+00	8.082E+03	1.007E+06	3.284E+05

MEASURED HEAT TRANSFER DATA

x/L or z/L	Phi, deg	Twall, K	Qdot, W/m^2	Q(Tw=300K) W/m^2	St_inf	Q/Qsph	Ch/Chsph
.000	180	0.0	0.000E+00	0.000E+00	0.000E+00	0.000E+00	0.000E+00
.256	180	335.4	7.913E+04	8.358E+04	1.871E-02	2.410E-01	2.538E-01
.296	180	334.1	7.720E+04	8.138E+04	1.821E-02	2.351E-01	2.471E-01
.337	180	333.1	7.523E+04	7.917E+04	1.772E-02	2.291E-01	2.404E-01
.377	180	0.0	0.000E+00	0.000E+00	0.000E+00	0.000E+00	0.000E+00
.418	180	0.0	0.000E+00	0.000E+00	0.000E+00	0.000E+00	0.000E+00
.459	180	328.0	6.480E+04	6.765E+04	1.515E-02	1.973E-01	2.055E-01
.499	180	0.0	0.000E+00	0.000E+00	0.000E+00	0.000E+00	0.000E+00
.540	180	0.0	0.000E+00	0.000E+00	0.000E+00	0.000E+00	0.000E+00
.634	180	309.5	2.564E+04	2.601E+04	5.834E-03	7.808E-02	7.914E-02
.676	180	309.5	2.600E+04	2.638E+04	5.916E-03	7.918E-02	8.026E-02
.717	180	309.5	2.605E+04	2.643E+04	5.927E-03	7.933E-02	8.041E-02
.759	180	309.5	2.611E+04	2.649E+04	5.941E-03	7.951E-02	8.059E-02
.800	180	309.5	2.617E+04	2.655E+04	5.956E-03	7.970E-02	8.079E-02
.842	180	309.5	2.625E+04	2.663E+04	5.974E-03	7.994E-02	8.104E-02
.884	180	309.7	2.664E+04	2.703E+04	6.063E-03	8.111E-02	8.225E-02
.925	180	310.0	2.714E+04	2.756E+04	6.180E-03	8.265E-02	8.384E-02
.256	0	0.0	0.000E+00	0.000E+00	0.000E+00	0.000E+00	0.000E+00
.296	0	299.2	4.377E+03	4.372E+03	9.814E-04	1.333E-02	1.331E-02
.337	0	299.3	4.514E+03	4.509E+03	1.012E-03	1.375E-02	1.373E-02
.377	0	299.3	4.506E+04	4.501E+04	1.010E-02	1.372E-01	1.371E-01
.418	0	0.0	0.000E+00	0.000E+00	0.000E+00	0.000E+00	0.000E+00
.459	0	0.0	0.000E+00	0.000E+00	0.000E+00	0.000E+00	0.000E+00
.499	0	299.2	4.469E+03	4.464E+03	1.002E-03	1.361E-02	1.359E-02
.540	0	299.2	4.378E+03	4.372E+03	9.816E-04	1.333E-02	1.332E-02
.636	0	299.3	4.613E+03	4.608E+03	1.034E-03	1.405E-02	1.403E-02
.679	0	299.3	4.654E+03	4.649E+03	1.044E-03	1.417E-02	1.416E-02
.721	0	299.3	4.609E+03	4.604E+03	1.034E-03	1.404E-02	1.402E-02
.764	0	299.3	4.577E+03	4.572E+03	1.026E-03	1.394E-02	1.392E-02
.806	0	299.2	4.456E+03	4.451E+03	9.991E-04	1.357E-02	1.355E-02
.849	0	0.0	0.000E+00	0.000E+00	0.000E+00	0.000E+00	0.000E+00
.892	0	299.1	4.285E+03	4.279E+03	9.607E-04	1.305E-02	1.303E-02
.935	0	299.1	4.172E+03	4.167E+03	9.353E-04	1.271E-02	1.269E-02
.635	90	303.1	1.214E+04	1.220E+04	2.738E-03	3.698E-02	3.714E-02
.678	90	302.9	1.162E+04	1.167E+04	2.619E-03	3.538E-02	3.553E-02
.719	90	302.5	1.096E+04	1.101E+04	2.470E-03	3.339E-02	3.351E-02
.763	90	302.3	1.054E+04	1.057E+04	2.373E-03	3.208E-02	3.219E-02
.803	90	302.2	1.022E+04	1.025E+04	2.300E-03	3.111E-02	3.121E-02
.846	90	302.0	9.833E+03	9.862E+03	2.213E-03	2.994E-02	3.003E-02
.888	90	301.9	9.662E+03	9.689E+03	2.175E-03	2.942E-02	2.950E-02
.930	90	301.8	9.518E+03	9.544E+03	2.142E-03	2.898E-02	2.906E-02

TABLE III. Concluded

(f) $\alpha = 20°$

FLOW CONDITIONS

Pt,1 N/m^2	Tt,1 K	Minf	pinf N/m^2	Tinf K	Rhoinf kg/m^3	Uinf m/s	Rinf,L
2.352E+06	9.860E+02	9.860E+00	5.912E+01	5.002E+01	4.118E-03	1.398E+03	2.199E+05

p2 N/m^2	T2 K	Rho2 kg/m^3	R2,L	Rho2/ Rhoinf	Pt,2 N/m^2	Ht,2 J/kg	Qsph,FR W/m^2
6.766E+03	9.644E+02	2.444E-02	1.726E+04	5.935E+00	7.457E+03	1.030E+06	3.263E+05

MEASURED HEAT TRANSFER DATA

x/L or z/L	Phi, deg	Twall, K	Qdot, W/m^2	Q(Tw=300K) W/m^2	St_inf	Q/Qsph	Ch/Chsph
.000	180	0.0	0.000E+00	0.000E+00	0.000E+00	0.000E+00	0.000E+00
.256	180	340.4	8.747E+04	9.294E+04	2.203E-02	2.680E-01	2.838E-01
.296	180	338.8	8.536E+04	9.048E+04	2.145E-02	2.616E-01	2.764E-01
.337	180	337.7	8.309E+04	8.792E+04	2.085E-02	2.546E-01	2.686E-01
.377	180	0.0	0.000E+00	0.000E+00	0.000E+00	0.000E+00	0.000E+00
.418	180	0.0	0.000E+00	0.000E+00	0.000E+00	0.000E+00	0.000E+00
.459	180	332.1	7.196E+04	7.550E+04	1.791E-02	2.205E-01	2.307E-01
.499	180	0.0	0.000E+00	0.000E+00	0.000E+00	0.000E+00	0.000E+00
.540	180	0.0	0.000E+00	0.000E+00	0.000E+00	0.000E+00	0.000E+00
.634	180	312.4	3.102E+04	3.159E+04	7.507E-03	9.505E-02	9.670E-02
.676	180	312.6	3.181E+04	3.241E+04	7.702E-03	9.750E-02	9.921E-02
.717	180	312.5	3.167E+04	3.225E+04	7.666E-03	9.704E-02	9.874E-02
.759	180	312.6	3.187E+04	3.247E+04	7.716E-03	9.767E-02	9.939E-02
.800	180	312.6	3.191E+04	3.251E+04	7.726E-03	9.779E-02	9.952E-02
.842	180	312.8	3.245E+04	3.306E+04	7.857E-03	9.943E-02	1.012E-01
.884	180	313.0	3.289E+04	3.353E+04	7.967E-03	1.008E-01	1.026E-01
.925	180	313.1	3.312E+04	3.377E+04	8.025E-03	1.015E-01	1.034E-01
.256	0	0.0	0.000E+00	0.000E+00	0.000E+00	0.000E+00	0.000E+00
.296	0	299.4	4.697E+03	4.693E+03	1.116E-03	1.439E-02	1.438E-02
.337	0	299.4	4.693E+03	4.688E+03	1.115E-03	1.438E-02	1.437E-02
.377	0	299.3	4.555E+03	4.550E+03	1.083E-03	1.396E-02	1.394E-02
.418	0	0.0	0.000E+00	0.000E+00	0.000E+00	0.000E+00	0.000E+00
.459	0	0.0	0.000E+00	0.000E+00	0.000E+00	0.000E+00	0.000E+00
.499	0	299.1	4.127E+03	4.121E+03	9.805E-04	1.265E-02	1.263E-02
.540	0	299.0	3.956E+03	3.950E+03	9.398E-04	1.212E-02	1.211E-02
.636	0	299.1	4.072E+03	4.066E+03	9.674E-04	1.248E-02	1.246E-02
.679	0	299.0	4.026E+03	4.021E+03	9.567E-04	1.234E-02	1.232E-02
.721	0	299.0	3.977E+03	3.971E+03	9.449E-04	1.219E-02	1.217E-02
.764	0	299.0	3.908E+03	3.902E+03	9.285E-04	1.198E-02	1.196E-02
.806	0	298.9	3.784E+03	3.778E+03	8.988E-04	1.159E-02	1.158E-02
.849	0	298.9	3.688E+03	3.682E+03	8.760E-04	1.130E-02	1.128E-02
.892	0	298.8	3.612E+03	3.606E+03	8.580E-04	1.107E-02	1.105E-02
.935	0	298.8	3.493E+03	3.487E+03	8.297E-04	1.070E-02	1.069E-02
.635	90	303.4	1.254E+04	1.260E+04	2.997E-03	3.842E-02	3.861E-02
.678	90	303.2	1.208E+04	1.214E+04	2.887E-03	3.702E-02	3.718E-02
.719	90	302.8	1.136E+04	1.141E+04	2.714E-03	3.482E-02	3.495E-02
.763	90	302.6	1.087E+04	1.091E+04	2.596E-03	3.332E-02	3.344E-02
.803	90	302.4	1.056E+04	1.060E+04	2.521E-03	3.236E-02	3.247E-02
.846	90	302.3	1.024E+04	1.028E+04	2.445E-03	3.139E-02	3.149E-02
.888	90	302.2	1.010E+04	1.013E+04	2.410E-03	3.095E-02	3.104E-02
.930	90	302.2	1.001E+04	1.004E+04	2.389E-03	3.068E-02	3.077E-02

TABLE IV. MEASURED HEAT-TRANSFER DATA FOR BENT-NOSE BICONIC AT HIGH REYNOLDS NUMBER

(a) $\alpha = 0°$

FLOW CONDITIONS

Pt,1 N/m^2	Tt,1 K	Minf	pinf N/m^2	Tinf K	Rhoinf kg/m^3	Uinf m/s	Rinf,L
1.084E+07	9.968E+02	1.016E+01	2.289E+02	4.815E+01	1.656E-02	1.413E+03	9.360E+05

p2 N/m^2	T2 K	Rho2 kg/m^3	R2,L	Rho2/ Rhoinf	Pt,2 N/m^2	Ht,2 J/kg	Qsph,FR W/m^2
2.782E+04	9.791E+02	9.899E-02	6.954E+04	5.977E+00	3.065E+04	1.043E+06	6.713E+05

MEASURED HEAT TRANSFER DATA

x/L or z/L	Phi, deg	Twall, K	Qdot, W/m^2	Q(Tw=300K) W/m^2	St_inf	Q/Qsph	Ch/Chsph
.000	180	0.0	0.000E+00	0.000E+00	0.000E+00	0.000E+00	0.000E+00
.256	180	337.7	8.263E+04	8.735E+04	5.010E-03	1.231E-01	1.297E-01
.296	180	338.2	8.454E+04	8.944E+04	5.129E-03	1.259E-01	1.328E-01
.337	180	337.5	8.306E+04	8.778E+04	5.035E-03	1.237E-01	1.304E-01
.377	180	0.0	0.000E+00	0.000E+00	0.000E+00	0.000E+00	0.000E+00
.418	180	0.0	0.000E+00	0.000E+00	0.000E+00	0.000E+00	0.000E+00
.459	180	332.9	7.348E+04	7.711E+04	4.424E-03	1.095E-01	1.146E-01
.499	180	0.0	0.000E+00	0.000E+00	0.000E+00	0.000E+00	0.000E+00
.540	180	0.0	0.000E+00	0.000E+00	0.000E+00	0.000E+00	0.000E+00
.634	180	306.6	1.917E+04	1.935E+04	1.113E-03	2.855E-02	2.881E-02
.676	180	304.9	1.559E+04	1.570E+04	9.030E-04	2.323E-02	2.338E-02
.717	180	304.1	1.414E+04	1.422E+04	8.178E-04	2.106E-02	2.118E-02
.759	180	303.8	1.350E+04	1.358E+04	7.809E-04	2.011E-02	2.022E-02
.800	180	303.7	1.317E+04	1.324E+04	7.613E-04	1.961E-02	1.971E-02
.842	180	303.5	1.301E+04	1.307E+04	7.519E-04	1.937E-02	1.947E-02
.884	180	303.5	1.287E+04	1.294E+04	7.440E-04	1.917E-02	1.926E-02
.925	180	303.5	1.297E+04	1.303E+04	7.496E-04	1.932E-02	1.941E-02
.256	0	0.0	0.000E+00	0.000E+00	0.000E+00	0.000E+00	0.000E+00
.296	0	303.8	1.347E+04	1.354E+04	7.787E-04	2.006E-02	2.016E-02
.337	0	302.9	1.168E+04	1.173E+04	6.747E-04	1.740E-02	1.747E-02
.377	0	302.2	1.012E+04	1.015E+04	5.842E-04	1.508E-02	1.512E-02
.418	0	0.0	0.000E+00	0.000E+00	0.000E+00	0.000E+00	0.000E+00
.459	0	0.0	0.000E+00	0.000E+00	0.000E+00	0.000E+00	0.000E+00
.499	0	300.7	7.105E+03	7.113E+03	4.092E-04	1.058E-02	1.060E-02
.540	0	300.4	6.354E+03	6.357E+03	3.658E-04	9.465E-03	9.470E-03
.636	0	300.5	6.401E+03	6.405E+03	3.685E-04	9.536E-03	9.542E-03
.679	0	300.5	6.405E+03	6.409E+03	3.687E-04	9.541E-03	9.547E-03
.721	0	300.5	6.513E+03	6.517E+03	3.750E-04	9.702E-03	9.709E-03
.764	0	300.5	6.317E+03	6.322E+03	3.637E-04	9.411E-03	9.417E-03
.806	0	300.5	6.374E+03	6.378E+03	3.670E-04	9.495E-03	9.501E-03
.849	0	0.0	0.000E+00	0.000E+00	0.000E+00	0.000E+00	0.000E+00
.892	0	300.6	6.483E+03	6.488E+03	3.733E-04	9.658E-03	9.665E-03
.935	0	300.7	6.744E+03	6.751E+03	3.884E-04	1.005E-02	1.006E-02
.635	90	310.2	2.554E+04	2.592E+04	1.490E-03	3.804E-02	3.858E-02
.678	90	308.9	2.347E+04	2.377E+04	1.367E-03	3.496E-02	3.538E-02
.719	90	308.2	2.209E+04	2.235E+04	1.285E-03	3.290E-02	3.327E-02
.763	90	307.9	2.150E+04	2.175E+04	1.250E-03	3.203E-02	3.238E-02
.803	90	307.8	2.120E+04	2.144E+04	1.233E-03	3.159E-02	3.192E-02
.846	90	307.7	2.101E+04	2.125E+04	1.222E-03	3.131E-02	3.163E-02
.888	90	307.7	2.097E+04	2.121E+04	1.219E-03	3.124E-02	3.157E-02
.930	90	307.7	2.084E+04	2.107E+04	1.212E-03	3.105E-02	3.137E-02

TABLE IV. Continued

(b) $\alpha = 4°$

FLOW CONDITIONS

Pt,1 N/m^2	Tt,1 K	Minf	pinf N/m^2	Tinf K	Rhoinf kg/m^3	Uinf m/s	Rinf,L
1.085E+07	1.005E+03	1.016E+01	2.291E+02	4.856E+01	1.644E-02	1.419E+03	9.235E+05

p2 N/m^2	T2 K	Rho2 kg/m^3	R2,L	Rho2/ Rhoinf	Pt,2 N/m^2	Ht,2 J/kg	Qsph,FR W/m^2
2.784E+04	9.874E+02	9.825E-02	6.896E+04	5.977E+00	3.068E+04	1.052E+06	6.793E+05

MEASURED HEAT TRANSFER DATA

x/L or z/L	Phi, deg	Twall, K	Qdot, W/m^2	Q(Tw=300K) W/m^2	St_inf	Q/Qsph	Ch/Chsph
.000	180	0.0	0.000E+00	0.000E+00	0.000E+00	0.000E+00	0.000E+00
.256	180	352.3	1.094E+05	1.181E+05	6.700E-03	1.610E-01	1.731E-01
.296	180	351.6	1.091E+05	1.177E+05	6.678E-03	1.606E-01	1.725E-01
.337	180	348.8	1.033E+05	1.109E+05	6.295E-03	1.520E-01	1.626E-01
.377	180	344.8	9.472E+04	1.011E+05	5.741E-03	1.394E-01	1.483E-01
.418	180	343.2	9.167E+04	9.764E+04	5.543E-03	1.349E-01	1.432E-01
.459	180	341.9	8.839E+04	9.396E+04	5.335E-03	1.301E-01	1.378E-01
.499	180	337.3	7.971E+04	8.416E+04	4.780E-03	1.173E-01	1.235E-01
.540	180	0.0	0.000E+00	0.000E+00	0.000E+00	0.000E+00	0.000E+00
.634	180	310.4	2.323E+04	2.357E+04	1.342E-03	3.419E-02	3.467E-02
.676	180	309.3	2.152E+04	2.180E+04	1.241E-03	3.167E-02	3.207E-02
.717	180	309.3	2.143E+04	2.171E+04	1.236E-03	3.154E-02	3.194E-02
.759	180	309.4	2.142E+04	2.171E+04	1.236E-03	3.154E-02	3.194E-02
.800	180	309.4	2.151E+04	2.180E+04	1.241E-03	3.166E-02	3.207E-02
.842	180	309.5	2.177E+04	2.206E+04	1.256E-03	3.204E-02	3.245E-02
.884	180	309.7	2.202E+04	2.233E+04	1.271E-03	3.241E-02	3.284E-02
.925	180	309.8	2.231E+04	2.263E+04	1.288E-03	3.285E-02	3.328E-02
.256	0	0.0	0.000E+00	0.000E+00	0.000E+00	0.000E+00	0.000E+00
.296	0	302.8	8.081E+03	8.113E+03	4.622E-04	1.190E-02	1.194E-02
.337	0	302.3	7.010E+03	7.033E+03	4.007E-04	1.032E-02	1.035E-02
.377	0	301.9	6.279E+03	6.296E+03	3.587E-04	9.243E-03	9.267E-03
.418	0	301.7	5.949E+03	5.963E+03	3.398E-04	8.757E-03	8.777E-03
.459	0	0.0	0.000E+00	0.000E+00	0.000E+00	0.000E+00	0.000E+00
.499	0	301.7	5.814E+03	5.827E+03	3.320E-04	8.558E-03	8.577E-03
.540	0	301.8	6.018E+03	6.033E+03	3.437E-04	8.859E-03	8.880E-03
.636	0	302.5	7.510E+03	7.536E+03	4.293E-04	1.106E-02	1.109E-02
.679	0	302.8	8.288E+03	8.322E+03	4.741E-04	1.220E-02	1.225E-02
.721	0	303.2	9.164E+03	9.206E+03	5.244E-04	1.349E-02	1.355E-02
.764	0	303.6	9.878E+03	9.928E+03	5.655E-04	1.454E-02	1.461E-02
.806	0	303.8	1.049E+04	1.055E+04	6.008E-04	1.544E-02	1.552E-02
.849	0	304.1	1.108E+04	1.114E+04	6.348E-04	1.631E-02	1.640E-02
.892	0	304.3	1.158E+04	1.165E+04	6.638E-04	1.705E-02	1.715E-02
.935	0	304.5	1.203E+04	1.211E+04	6.899E-04	1.772E-02	1.782E-02
.635	90	311.0	2.400E+04	2.438E+04	1.388E-03	3.534E-02	3.586E-02
.678	90	310.1	2.236E+04	2.268E+04	1.291E-03	3.291E-02	3.336E-02
.719	90	309.5	2.110E+04	2.139E+04	1.218E-03	3.106E-02	3.146E-02
.763	90	309.2	2.054E+04	2.081E+04	1.185E-03	3.023E-02	3.061E-02
.803	90	309.0	2.012E+04	2.038E+04	1.160E-03	2.961E-02	2.997E-02
.846	90	308.5	1.904E+04	1.927E+04	1.097E-03	2.803E-02	2.835E-02
.888	90	308.7	1.931E+04	1.954E+04	1.113E-03	2.842E-02	2.875E-02
.930	90	308.5	1.899E+04	1.922E+04	1.095E-03	2.796E-02	2.828E-02

TABLE IV. Continued

(c) $\alpha = 8°$

FLOW CONDITIONS

Pt,1 N/m^2	Tt,1 K	Minf	pinf N/m^2	Tinf K	Rhoinf kg/m^3	Uinf m/s	Rinf,L
1.093E+07	1.011E+03	1.016E+01	2.308E+02	4.882E+01	1.647E-02	1.423E+03	9.217E+05

p2 N/m^2	T2 K	Rho2 kg/m^3	R2,L	Rho2/ Rhoinf	Pt,2 N/m^2	Ht,2 J/kg	Qsph,FR W/m^2
2.805E+04	9.928E+02	9.843E-02	6.905E+04	5.977E+00	3.090E+04	1.059E+06	6.875E+05

MEASURED HEAT TRANSFER DATA

x/L or z/L	Phi, deg	Twall, K	Qdot, W/m^2	Q(Tw=300K) W/m^2	St_inf	Q/Qsph	Ch/Chsph
.000	180	562.1	5.665E+05	8.973E+05	4.924E-02	8.240E-01	1.273E+00
.256	180	358.4	1.256E+05	1.368E+05	7.657E-03	1.827E-01	1.980E-01
.296	180	357.2	1.248E+05	1.357E+05	7.597E-03	1.816E-01	1.965E-01
.337	180	355.1	1.207E+05	1.309E+05	7.326E-03	1.756E-01	1.894E-01
.377	180	352.1	1.145E+05	1.236E+05	6.921E-03	1.666E-01	1.790E-01
.418	180	318.2	2.741E+04	2.813E+04	1.580E-03	3.987E-02	4.085E-02
.459	180	348.6	1.073E+05	1.152E+05	6.451E-03	1.561E-01	1.668E-01
.499	180	343.6	9.707E+04	1.034E+05	5.795E-03	1.412E-01	1.499E-01
.540	180	0.0	0.000E+00	0.000E+00	0.000E+00	0.000E+00	0.000E+00
.634	180	313.2	3.214E+04	3.274E+04	1.840E-03	4.674E-02	4.758E-02
.676	180	313.3	3.273E+04	3.336E+04	1.874E-03	4.761E-02	4.846E-02
.717	180	313.1	3.250E+04	3.311E+04	1.860E-03	4.727E-02	4.811E-02
.759	180	313.2	3.255E+04	3.317E+04	1.863E-03	4.734E-02	4.819E-02
.800	180	313.4	3.293E+04	3.356E+04	1.886E-03	4.790E-02	4.876E-02
.842	180	313.6	3.339E+04	3.404E+04	1.912E-03	4.856E-02	4.945E-02
.884	180	313.6	3.330E+04	3.395E+04	1.907E-03	4.843E-02	4.932E-02
.925	180	313.7	3.339E+04	3.405E+04	1.913E-03	4.857E-02	4.947E-02
.256	0	0.0	0.000E+00	0.000E+00	0.000E+00	0.000E+00	0.000E+00
.296	0	301.4	7.714E+03	7.729E+03	4.347E-04	1.122E-02	1.124E-02
.337	0	301.5	7.885E+03	7.902E+03	4.444E-04	1.147E-02	1.149E-02
.377	0	301.8	8.586E+03	8.608E+03	4.841E-04	1.249E-02	1.252E-02
.418	0	302.4	1.012E+04	1.016E+04	5.712E-04	1.473E-02	1.477E-02
.459	0	0.0	0.000E+00	0.000E+00	0.000E+00	0.000E+00	0.000E+00
.499	0	303.5	1.225E+04	1.231E+04	6.923E-04	1.782E-02	1.790E-02
.540	0	304.0	1.336E+04	1.343E+04	7.553E-04	1.943E-02	1.953E-02
.636	0	305.5	1.664E+04	1.677E+04	9.428E-04	2.420E-02	2.438E-02
.679	0	305.9	1.749E+04	1.764E+04	9.916E-04	2.544E-02	2.564E-02
.721	0	306.1	1.800E+04	1.816E+04	1.021E-03	2.619E-02	2.640E-02
.764	0	306.3	1.843E+04	1.860E+04	1.046E-03	2.681E-02	2.704E-02
.806	0	306.4	1.861E+04	1.878E+04	1.056E-03	2.707E-02	2.730E-02
.849	0	303.7	1.385E+04	1.392E+04	7.827E-04	2.014E-02	2.024E-02
.892	0	306.6	1.913E+04	1.931E+04	1.086E-03	2.783E-02	2.808E-02
.935	0	306.7	1.920E+04	1.939E+04	1.090E-03	2.793E-02	2.818E-02
.635	90	308.9	2.264E+04	2.293E+04	1.289E-03	3.293E-02	3.333E-02
.678	90	308.4	2.155E+04	2.180E+04	1.226E-03	3.134E-02	3.169E-02
.719	90	308.1	2.085E+04	2.109E+04	1.186E-03	3.033E-02	3.066E-02
.763	90	307.9	2.048E+04	2.071E+04	1.164E-03	2.979E-02	3.011E-02
.803	90	307.8	2.038E+04	2.061E+04	1.159E-03	2.965E-02	2.996E-02
.846	90	307.4	1.954E+04	1.975E+04	1.110E-03	2.842E-02	2.870E-02
.888	90	307.5	1.975E+04	1.996E+04	1.122E-03	2.872E-02	2.901E-02
.930	90	307.3	1.934E+04	1.954E+04	1.098E-03	2.813E-02	2.840E-02

TABLE IV. Continued

(d) $\alpha = 12°$

FLOW CONDITIONS

Pt,1 N/m^2	Tt,1 K	Minf	pinf N/m^2	Tinf K	Rhoinf kg/m^3	Uinf m/s	Rinf,L
1.093E+07	9.901E+02	1.016E+01	2.309E+02	4.782E+01	1.682E-02	1.408E+03	9.549E+05

p2 N/m^2	T2 K	Rho2 kg/m^3	R2,L	Rho2/ Rhoinf	Pt,2 N/m^2	Ht,2 J/kg	Qsph,FR W/m^2
2.806E+04	9.725E+02	1.005E-01	7.066E+04	5.977E+00	3.091E+04	1.035E+06	6.673E+05

MEASURED HEAT TRANSFER DATA

x/L or z/L	Phi, deg	Twall, K	Qdot, W/m^2	Q(Tw=300K) W/m^2	St_inf	Q/Qsph	Ch/Chsph
.000	180	558.0	5.832E+05	9.315E+05	5.223E-02	8.740E-01	1.362E+00
.256	180	366.2	1.380E+05	1.526E+05	8.717E-03	2.068E-01	2.274E-01
.296	180	364.6	1.368E+05	1.509E+05	8.620E-03	2.049E-01	2.248E-01
.337	180	362.2	1.318E+05	1.448E+05	8.277E-03	1.975E-01	2.159E-01
.377	180	357.5	1.221E+05	1.332E+05	7.612E-03	1.829E-01	1.986E-01
.418	180	0.0	0.000E+00	0.000E+00	0.000E+00	0.000E+00	0.000E+00
.459	180	354.6	1.158E+05	1.258E+05	7.193E-03	1.736E-01	1.876E-01
.499	180	347.8	1.021E+05	1.097E+05	6.274E-03	1.530E-01	1.637E-01
.540	180	0.0	0.000E+00	0.000E+00	0.000E+00	0.000E+00	0.000E+00
.634	180	317.7	3.888E+04	3.991E+04	2.289E-03	5.827E-02	5.972E-02
.676	180	318.3	4.048E+04	4.159E+04	2.386E-03	6.067E-02	6.223E-02
.717	180	318.6	4.116E+04	4.229E+04	2.426E-03	6.168E-02	6.328E-02
.759	180	318.7	4.155E+04	4.270E+04	2.450E-03	6.226E-02	6.389E-02
.800	180	319.0	4.208E+04	4.327E+04	2.482E-03	6.306E-02	6.474E-02
.842	180	319.3	4.262E+04	4.384E+04	2.515E-03	6.386E-02	6.560E-02
.884	180	319.1	4.235E+04	4.355E+04	2.498E-03	6.346E-02	6.517E-02
.925	180	319.6	4.317E+04	4.443E+04	2.549E-03	6.470E-02	6.648E-02
.256	0	0.0	0.000E+00	0.000E+00	0.000E+00	0.000E+00	0.000E+00
.296	0	305.0	1.287E+04	1.296E+04	7.443E-04	1.928E-02	1.941E-02
.337	0	306.2	1.532E+04	1.546E+04	8.876E-04	2.296E-02	2.315E-02
.377	0	307.0	1.712E+04	1.730E+04	9.931E-04	2.566E-02	2.591E-02
.418	0	308.1	1.956E+04	1.979E+04	1.136E-03	2.931E-02	2.963E-02
.459	0	0.0	0.000E+00	0.000E+00	0.000E+00	0.000E+00	0.000E+00
.499	0	307.8	1.887E+04	1.909E+04	1.096E-03	2.828E-02	2.858E-02
.540	0	307.8	1.884E+04	1.905E+04	1.094E-03	2.823E-02	2.853E-02
.636	0	308.8	2.120E+04	2.147E+04	1.233E-03	3.177E-02	3.216E-02
.679	0	308.8	2.116E+04	2.144E+04	1.231E-03	3.171E-02	3.210E-02
.721	0	308.9	2.124E+04	2.151E+04	1.235E-03	3.183E-02	3.222E-02
.764	0	308.7	2.084E+04	2.111E+04	1.212E-03	3.123E-02	3.161E-02
.806	0	308.6	2.057E+04	2.083E+04	1.196E-03	3.083E-02	3.119E-02
.849	0	305.9	1.090E+04	1.099E+04	6.311E-04	1.633E-02	1.646E-02
.892	0	308.3	2.020E+04	2.044E+04	1.174E-03	3.026E-02	3.061E-02
.935	0	308.2	1.975E+04	1.999E+04	1.148E-03	2.960E-02	2.993E-02
.635	90	309.6	2.160E+04	2.191E+04	1.258E-03	3.237E-02	3.281E-02
.678	90	309.6	2.152E+04	2.182E+04	1.253E-03	3.225E-02	3.268E-02
.719	90	309.3	2.106E+04	2.135E+04	1.226E-03	3.156E-02	3.197E-02
.763	90	309.1	2.061E+04	2.089E+04	1.199E-03	3.089E-02	3.128E-02
.803	90	308.8	2.007E+04	2.033E+04	1.167E-03	3.008E-02	3.045E-02
.846	90	0.0	0.000E+00	0.000E+00	0.000E+00	0.000E+00	0.000E+00
.888	90	307.9	1.818E+04	1.839E+04	1.056E-03	2.724E-02	2.754E-02
.930	90	307.7	1.772E+04	1.792E+04	1.029E-03	2.656E-02	2.684E-02

TABLE IV. Continued

(e) $\alpha = 16°$

FLOW CONDITIONS

Pt,1 N/m^2	Tt,1 K	Minf	pinf N/m^2	Tinf K	Rhoinf kg/m^3	Uinf m/s	Rinf,L
1.093E+07	1.002E+03	1.016E+01	2.309E+02	4.839E+01	1.662E-02	1.417E+03	9.361E+05

p2 N/m^2	T2 K	Rho2 kg/m^3	R2,L	Rho2/ Rhoinf	Pt,2 N/m^2	Ht,2 J/kg	Qsph,FR W/m^2
2.806E+04	9.840E+02	9.934E-02	6.976E+04	5.977E+00	3.091E+04	1.048E+06	6.784E+05

MEASURED HEAT TRANSFER DATA

x/L or z/L	Phi, deg	Twall, K	Qdot, W/m^2	Q(Tw=300K) W/m^2	St_inf	Q/Qsph	Ch/Chsph
.000	180	522.0	4.379E+05	6.405E+05	3.561E-02	6.455E-01	9.248E-01
.256	180	376.3	1.561E+05	1.751E+05	9.873E-03	2.301E-01	2.564E-01
.296	180	374.1	1.543E+05	1.725E+05	9.728E-03	2.275E-01	2.527E-01
.337	180	0.0	0.000E+00	0.000E+00	0.000E+00	0.000E+00	0.000E+00
.377	180	366.3	1.382E+05	1.526E+05	8.609E-03	2.037E-01	2.236E-01
.418	180	0.0	0.000E+00	0.000E+00	0.000E+00	0.000E+00	0.000E+00
.459	180	362.8	1.319E+05	1.448E+05	8.174E-03	1.944E-01	2.123E-01
.499	180	355.8	1.184E+05	1.286E+05	7.264E-03	1.745E-01	1.887E-01
.540	180	0.0	0.000E+00	0.000E+00	0.000E+00	0.000E+00	0.000E+00
.634	180	324.1	5.135E+04	5.318E+04	3.012E-03	7.570E-02	7.822E-02
.676	180	324.8	5.349E+04	5.546E+04	3.141E-03	7.885E-02	8.157E-02
.717	180	324.8	5.346E+04	5.542E+04	3.139E-03	7.881E-02	8.152E-02
.759	180	324.8	5.345E+04	5.542E+04	3.138E-03	7.879E-02	8.151E-02
.800	180	325.1	5.407E+04	5.608E+04	3.176E-03	7.970E-02	8.248E-02
.842	180	325.1	5.402E+04	5.603E+04	3.173E-03	7.963E-02	8.241E-02
.884	180	325.5	5.493E+04	5.700E+04	3.228E-03	8.097E-02	8.384E-02
.925	180	326.0	5.596E+04	5.811E+04	3.291E-03	8.249E-02	8.547E-02
.256	0	0.0	0.000E+00	0.000E+00	0.000E+00	0.000E+00	0.000E+00
.296	0	309.1	2.124E+04	2.152E+04	1.220E-03	3.131E-02	3.170E-02
.337	0	309.3	2.161E+04	2.190E+04	1.242E-03	3.185E-02	3.225E-02
.377	0	309.1	2.131E+04	2.159E+04	1.225E-03	3.142E-02	3.180E-02
.418	0	309.0	2.125E+04	2.152E+04	1.221E-03	3.132E-02	3.170E-02
.459	0	0.0	0.000E+00	0.000E+00	0.000E+00	0.000E+00	0.000E+00
.499	0	308.2	1.944E+04	1.967E+04	1.116E-03	2.866E-02	2.898E-02
.540	0	307.8	1.865E+04	1.886E+04	1.069E-03	2.748E-02	2.778E-02
.636	0	308.6	2.042E+04	2.067E+04	1.172E-03	3.010E-02	3.045E-02
.679	0	308.5	2.004E+04	2.029E+04	1.150E-03	2.954E-02	2.988E-02
.721	0	308.5	2.021E+04	2.046E+04	1.160E-03	2.979E-02	3.014E-02
.764	0	308.4	1.979E+04	2.003E+04	1.136E-03	2.917E-02	2.951E-02
.806	0	308.0	1.913E+04	1.935E+04	1.097E-03	2.819E-02	2.850E-02
.849	0	307.4	1.568E+04	1.585E+04	8.989E-04	2.311E-02	2.335E-02
.892	0	307.8	1.861E+04	1.882E+04	1.067E-03	2.743E-02	2.772E-02
.935	0	307.6	1.825E+04	1.845E+04	1.047E-03	2.691E-02	2.718E-02
.635	90	310.1	2.230E+04	2.263E+04	1.283E-03	3.287E-02	3.332E-02
.678	90	310.4	2.279E+04	2.313E+04	1.312E-03	3.359E-02	3.407E-02
.719	90	309.9	2.179E+04	2.210E+04	1.253E-03	3.212E-02	3.255E-02
.763	90	309.3	2.078E+04	2.106E+04	1.194E-03	3.063E-02	3.102E-02
.803	90	308.9	1.983E+04	2.008E+04	1.139E-03	2.923E-02	2.958E-02
.846	90	0.0	0.000E+00	0.000E+00	0.000E+00	0.000E+00	0.000E+00
.888	90	308.3	1.864E+04	1.886E+04	1.070E-03	2.748E-02	2.779E-02
.930	90	308.3	1.865E+04	1.887E+04	1.070E-03	2.749E-02	2.780E-02

TABLE IV. Concluded

(f) $\alpha = 20°$

FLOW CONDITIONS

Pt,1 N/m^2	Tt,1 K	Minf	pinf N/m^2	Tinf K	Rhoinf kg/m^3	Uinf m/s	Rinf,L
1.096E+07	1.005E+03	1.016E+01	2.315E+02	4.855E+01	1.661E-02	1.419E+03	9.334E+05

p2 N/m^2	T2 K	Rho2 kg/m^3	R2,L	Rho2/ Rhoinf	Pt,2 N/m^2	Ht,2 J/kg	Qsph,FR W/m^2
2.813E+04	9.872E+02	9.929E-02	6.969E+04	5.977E+00	3.099E+04	1.052E+06	6.827E+05

MEASURED HEAT TRANSFER DATA

x/L or z/L	Phi, deg	Twall, K	Qdot, W/m^2	Q(Tw=300K) W/m^2	St_inf	Q/Qsph	Ch/Chsph
.000	180	0.0	0.000E+00	0.000E+00	0.000E+00	0.000E+00	0.000E+00
.256	180	383.5	1.709E+05	1.938E+05	1.085E-02	2.503E-01	2.818E-01
.296	180	381.0	1.683E+05	1.901E+05	1.065E-02	2.465E-01	2.765E-01
.337	180	0.0	0.000E+00	0.000E+00	0.000E+00	0.000E+00	0.000E+00
.377	180	372.9	1.513E+05	1.687E+05	9.456E-03	2.216E-01	2.456E-01
.418	180	361.1	1.259E+05	1.379E+05	7.735E-03	1.844E-01	2.009E-01
.459	180	369.0	1.448E+05	1.605E+05	8.999E-03	2.121E-01	2.337E-01
.499	180	360.0	1.271E+05	1.390E+05	7.798E-03	1.862E-01	2.025E-01
.540	180	0.0	0.000E+00	0.000E+00	0.000E+00	0.000E+00	0.000E+00
.634	180	330.0	6.402E+04	6.686E+04	3.762E-03	9.378E-02	9.770E-02
.676	180	330.8	6.666E+04	6.970E+04	3.922E-03	9.764E-02	1.018E-01
.717	180	330.4	6.589E+04	6.886E+04	3.874E-03	9.652E-02	1.006E-01
.759	180	331.0	6.678E+04	6.984E+04	3.930E-03	9.782E-02	1.020E-01
.800	180	331.0	6.709E+04	7.018E+04	3.948E-03	9.827E-02	1.025E-01
.842	180	331.5	6.807E+04	7.126E+04	4.009E-03	9.972E-02	1.041E-01
.884	180	331.9	6.880E+04	7.206E+04	4.054E-03	1.008E-01	1.053E-01
.925	180	331.9	6.869E+04	7.195E+04	4.048E-03	1.006E-01	1.051E-01
.256	0	0.0	0.000E+00	0.000E+00	0.000E+00	0.000E+00	0.000E+00
.296	0	309.6	2.254E+04	2.285E+04	1.288E-03	3.301E-02	3.344E-02
.337	0	309.2	2.158E+04	2.187E+04	1.232E-03	3.161E-02	3.201E-02
.377	0	308.5	2.034E+04	2.059E+04	1.161E-03	2.980E-02	3.014E-02
.418	0	308.4	1.995E+04	2.019E+04	1.138E-03	2.922E-02	2.955E-02
.459	0	0.0	0.000E+00	0.000E+00	0.000E+00	0.000E+00	0.000E+00
.499	0	307.3	1.781E+04	1.799E+04	1.014E-03	2.608E-02	2.634E-02
.540	0	307.1	1.717E+04	1.735E+04	9.779E-04	2.515E-02	2.540E-02
.636	0	307.8	1.894E+04	1.915E+04	1.080E-03	2.775E-02	2.804E-02
.679	0	307.8	1.876E+04	1.896E+04	1.069E-03	2.747E-02	2.776E-02
.721	0	307.8	1.894E+04	1.915E+04	1.079E-03	2.774E-02	2.803E-02
.764	0	307.7	1.854E+04	1.875E+04	1.057E-03	2.716E-02	2.744E-02
.806	0	307.3	1.782E+04	1.801E+04	1.015E-03	2.611E-02	2.637E-02
.849	0	307.1	1.741E+04	1.758E+04	9.912E-04	2.550E-02	2.574E-02
.892	0	307.0	1.716E+04	1.733E+04	9.772E-04	2.514E-02	2.538E-02
.935	0	306.8	1.675E+04	1.691E+04	9.533E-04	2.453E-02	2.476E-02
.635	90	0.0	0.000E+00	0.000E+00	0.000E+00	0.000E+00	0.000E+00
.678	90	311.1	2.438E+04	2.477E+04	1.396E-03	3.572E-02	3.625E-02
.719	90	310.4	2.303E+04	2.338E+04	1.318E-03	3.374E-02	3.422E-02
.763	90	309.6	2.133E+04	2.163E+04	1.219E-03	3.125E-02	3.165E-02
.803	90	309.3	2.065E+04	2.092E+04	1.179E-03	3.025E-02	3.063E-02
.846	90	308.6	1.941E+04	1.965E+04	1.108E-03	2.843E-02	2.876E-02
.888	90	308.9	1.995E+04	2.021E+04	1.139E-03	2.923E-02	2.958E-02
.930	90	308.8	1.970E+04	1.995E+04	1.125E-03	2.886E-02	2.921E-02

TABLE V. SUMMARY OF MEASURED AND PREDICTED HEAT-TRANSFER RATES FOR 8.1-mm-DIAMETER HEMISPHERE

p_∞, Pa	T_∞, K	M_∞	R_{2,r_n}	T_w, K	$\dot{q}_{t,2,m}$, MW/m^2	$\dot{q}_{t,2}$, MW/m^2 (a)	$\dot{q}_{t,2}$, MW/m^2 (b)
59.6	47.9	9.86	608	417	0.268	0.244	0.256
115.5	48.0	10.03	1172	456	.370	.343	.356
230.2	47.3	10.16	2379	482	.482	.475	.488

[a]From reference 14.
[b]From reference 16.

TABLE VI. FLOW CONDITIONS FOR TEST FACILITIES

Facility	M_∞	$R_{\infty,L}$	γ_∞	ρ_2/ρ_∞	γ_2	$\bar{v}^*_\infty$	$T_w/T_{t,2}$
Expansion tube	6.9	0.5×10^5	1.3	11.10	1.14	0.03	0.05
Mach 10 tunnel	9.9	2.2×10^5	1.4	5.94	1.34	0.02	0.30
	10.2	9.3×10^5	1.4	5.94	1.34	.01	.30

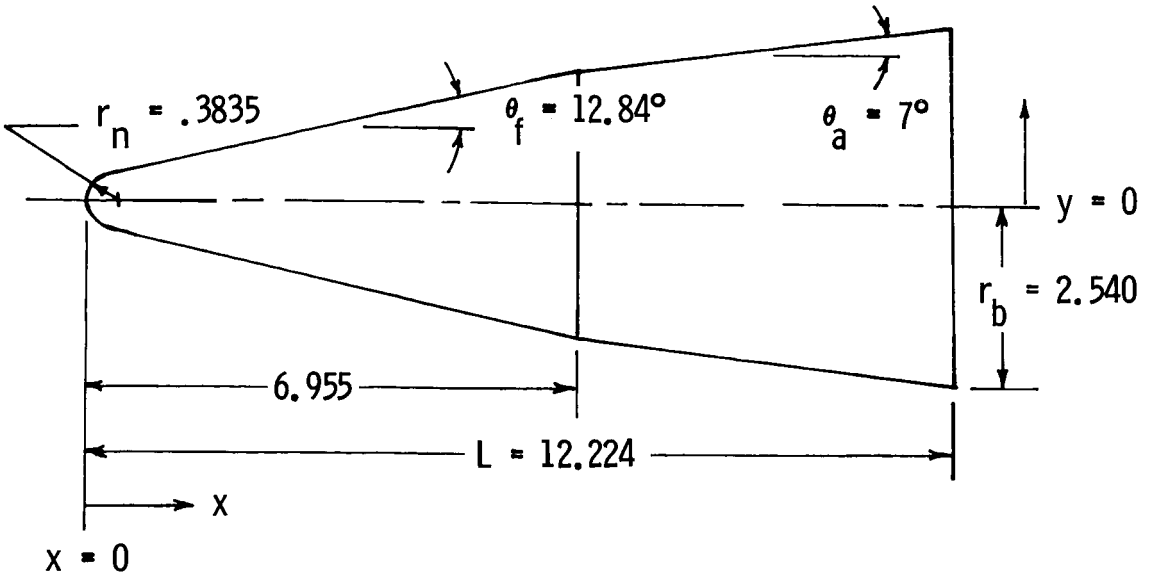

(a) Straight biconic.

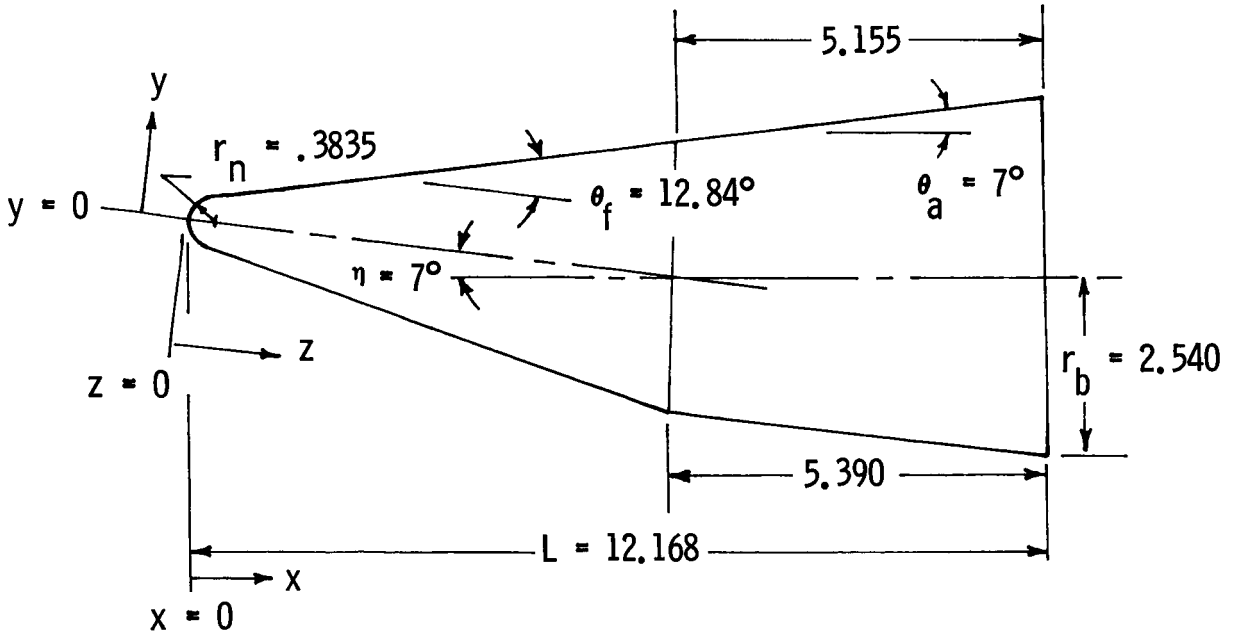

(b) Bent-nose biconic.

Figure 1. Sketch of biconic models. All dimensions in centimeters unlesss otherwise noted.

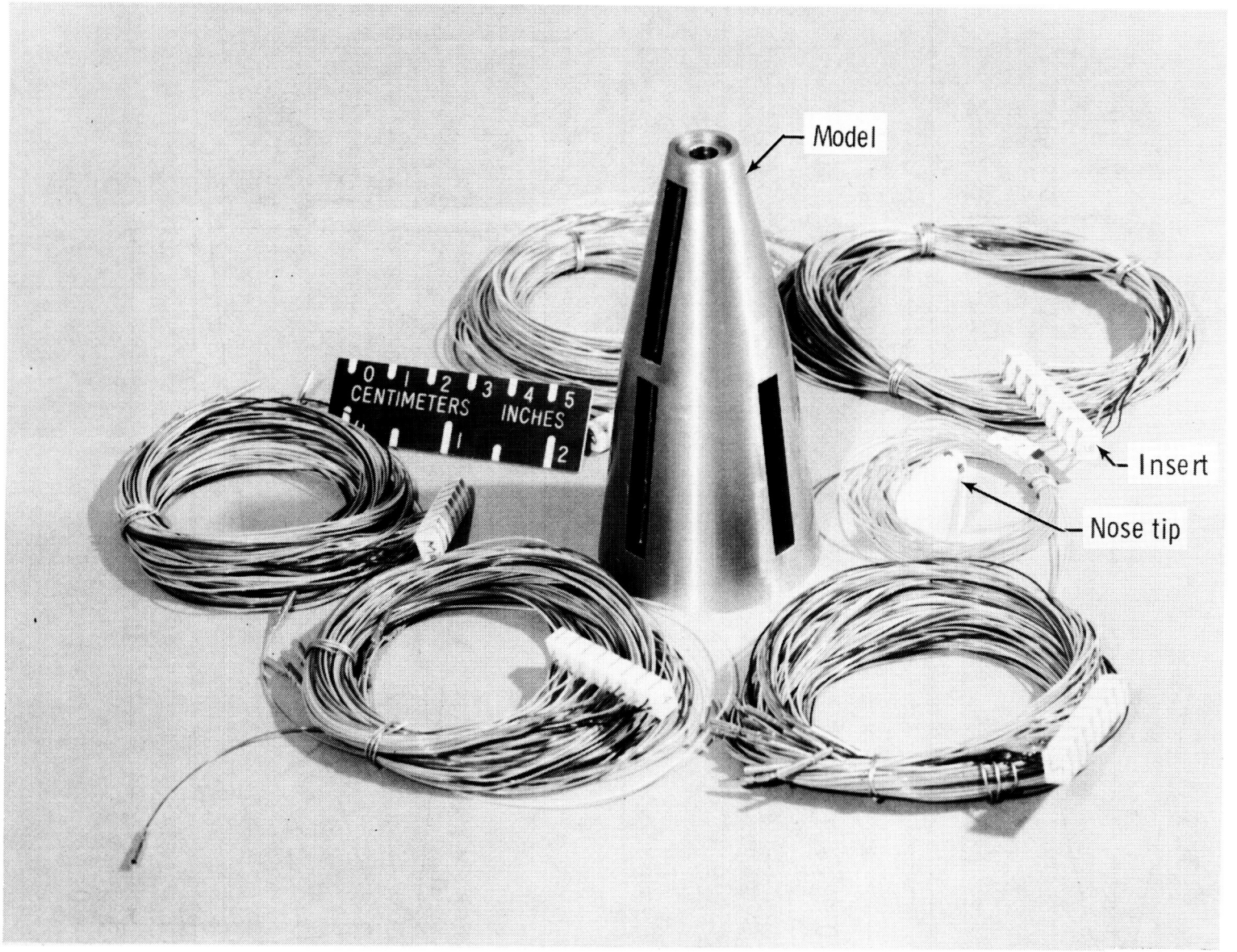

(a) Unassembled.

Figure 2. Unassembled model and instrumented inserts.

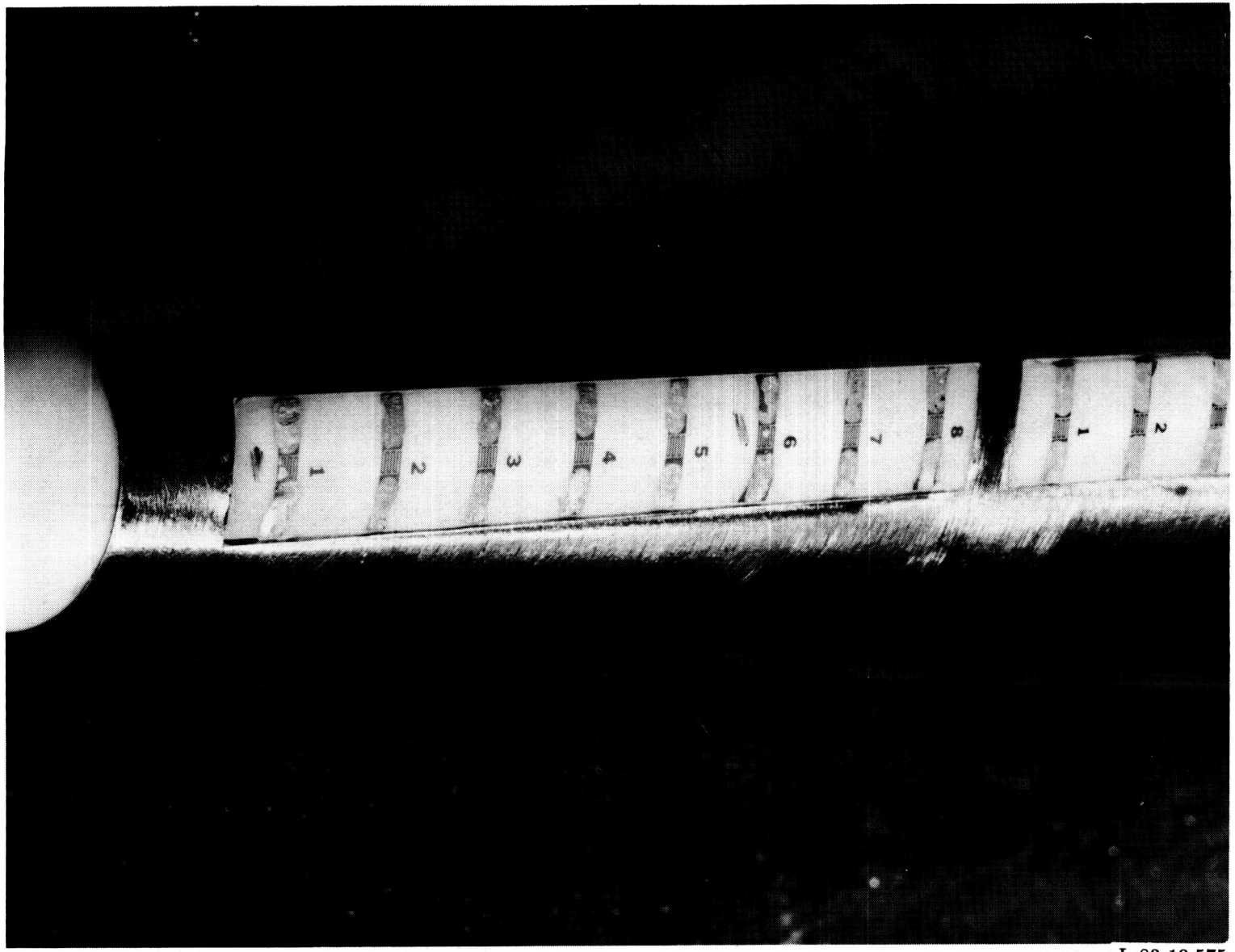

L-83-10,575

(b) Close-up of insert.

Figure 2. Concluded.

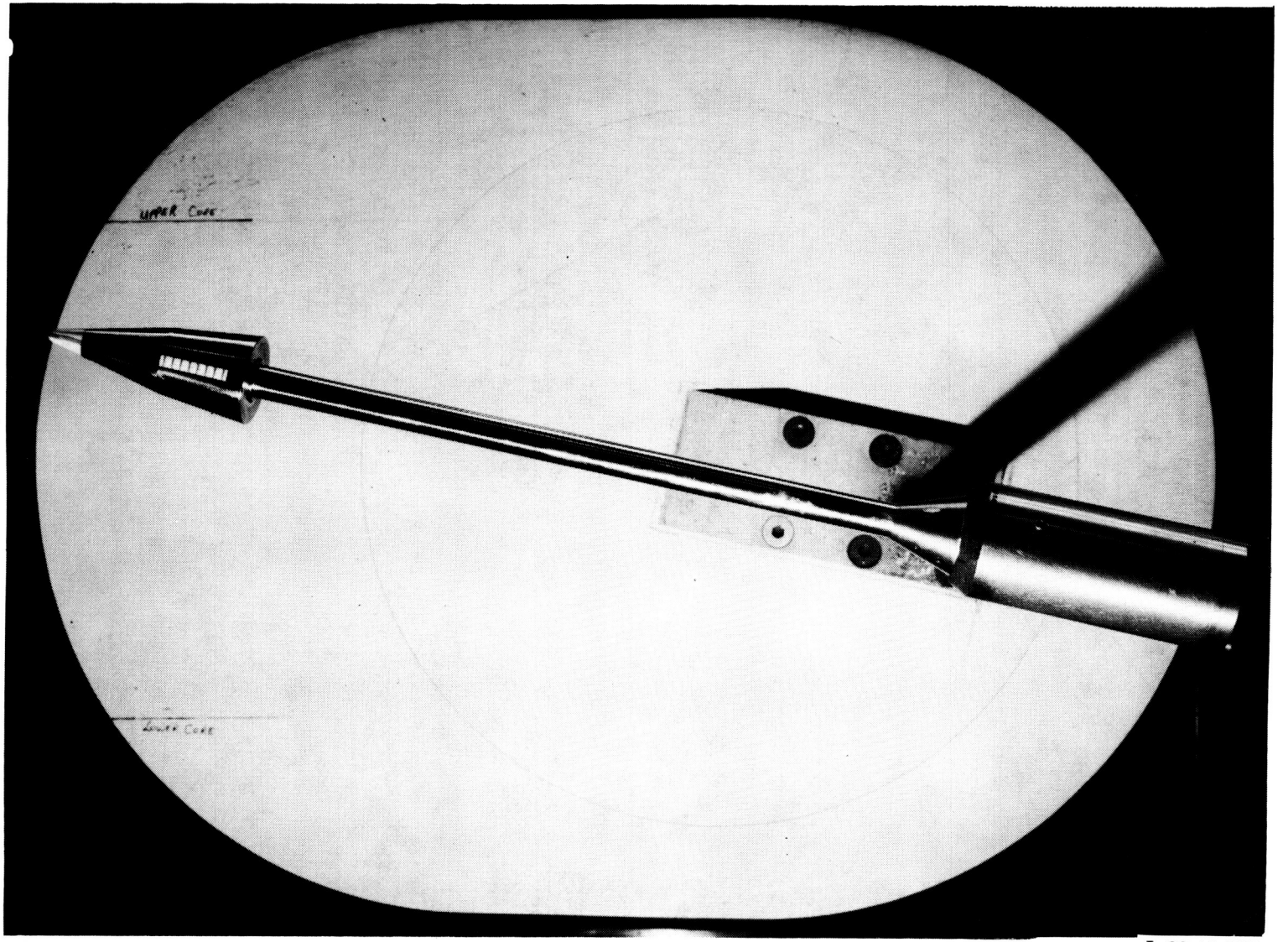

L-83-10,577

Figure 3. Straight biconic model mounted on injection mechanism.

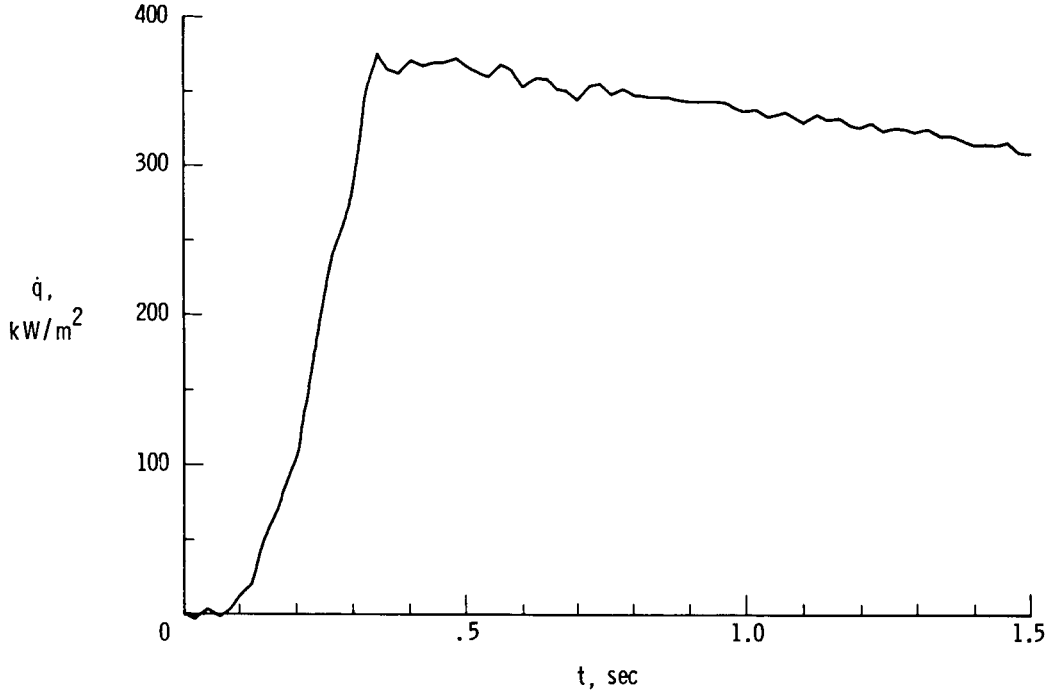

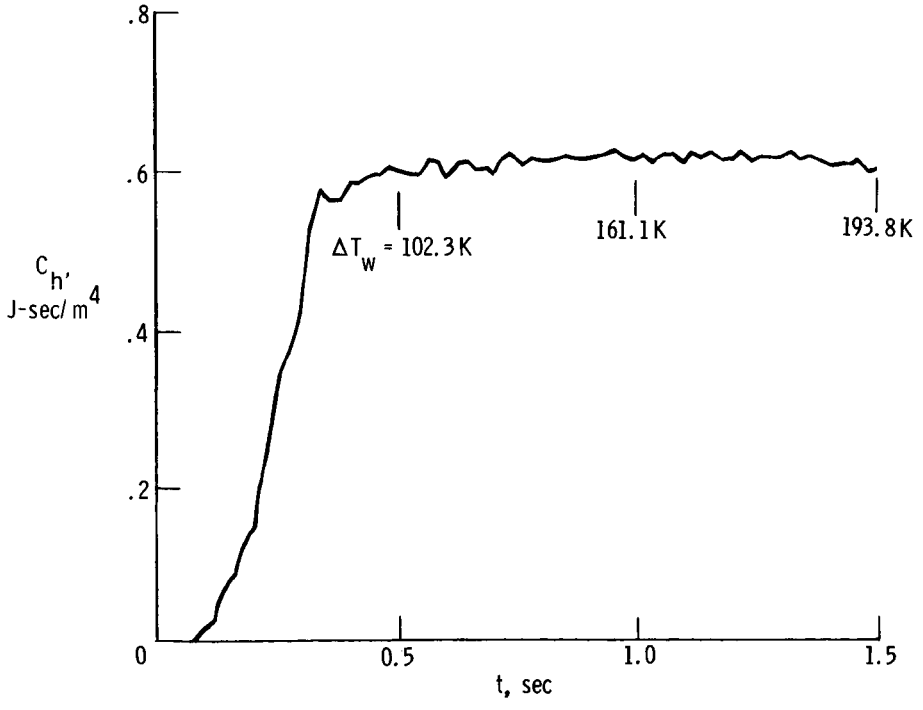

(a) Gage at nose tip; straight biconic; $\alpha = 0°$; $M_\infty = 9.86$.

Figure 4. Time histories of heat-transfer rate and heat-transfer coefficient.

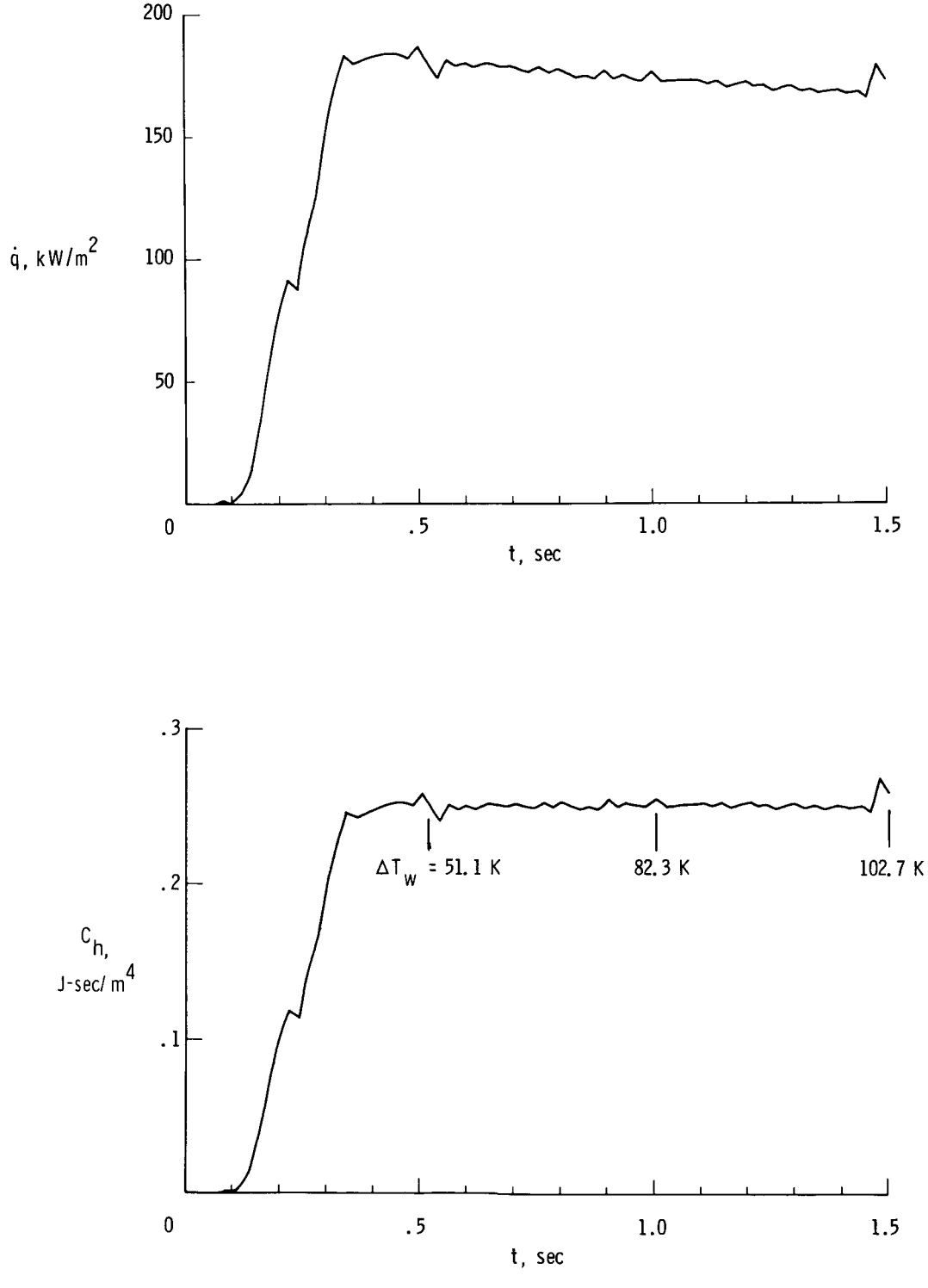

(b) Gage at windward ray of fore-cone ($z/L = 0.296$); bent-nose biconic; $\alpha = 20°$; $M_\infty = 10.16$.

Figure 4. Continued.

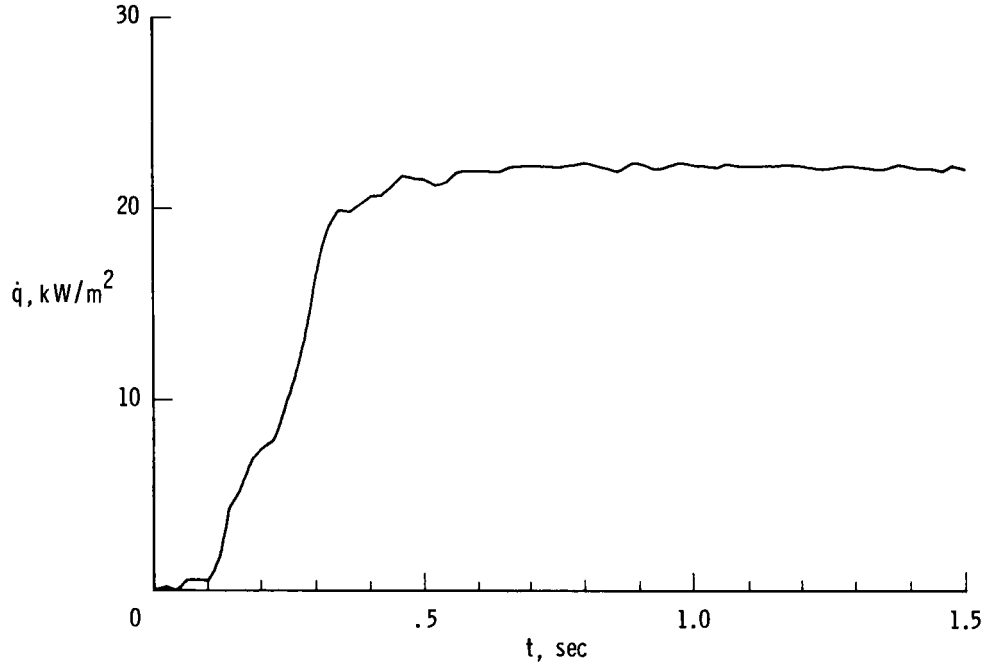

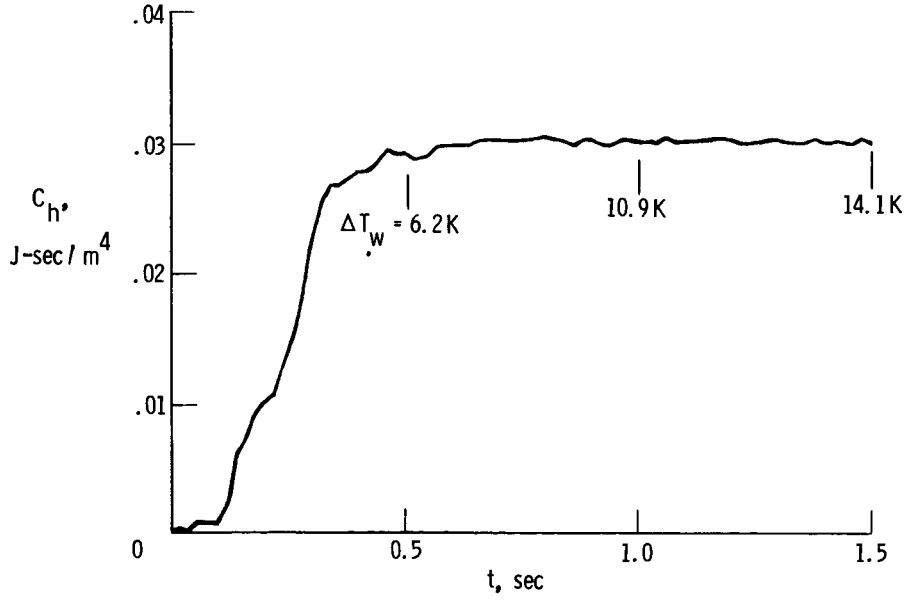

(c) Gage at leeward ray of fore-cone ($z/L = 0.296$); bent-nose biconic; $\alpha = 20°$; $M_\infty = 10.16$.

Figure 4. Concluded.

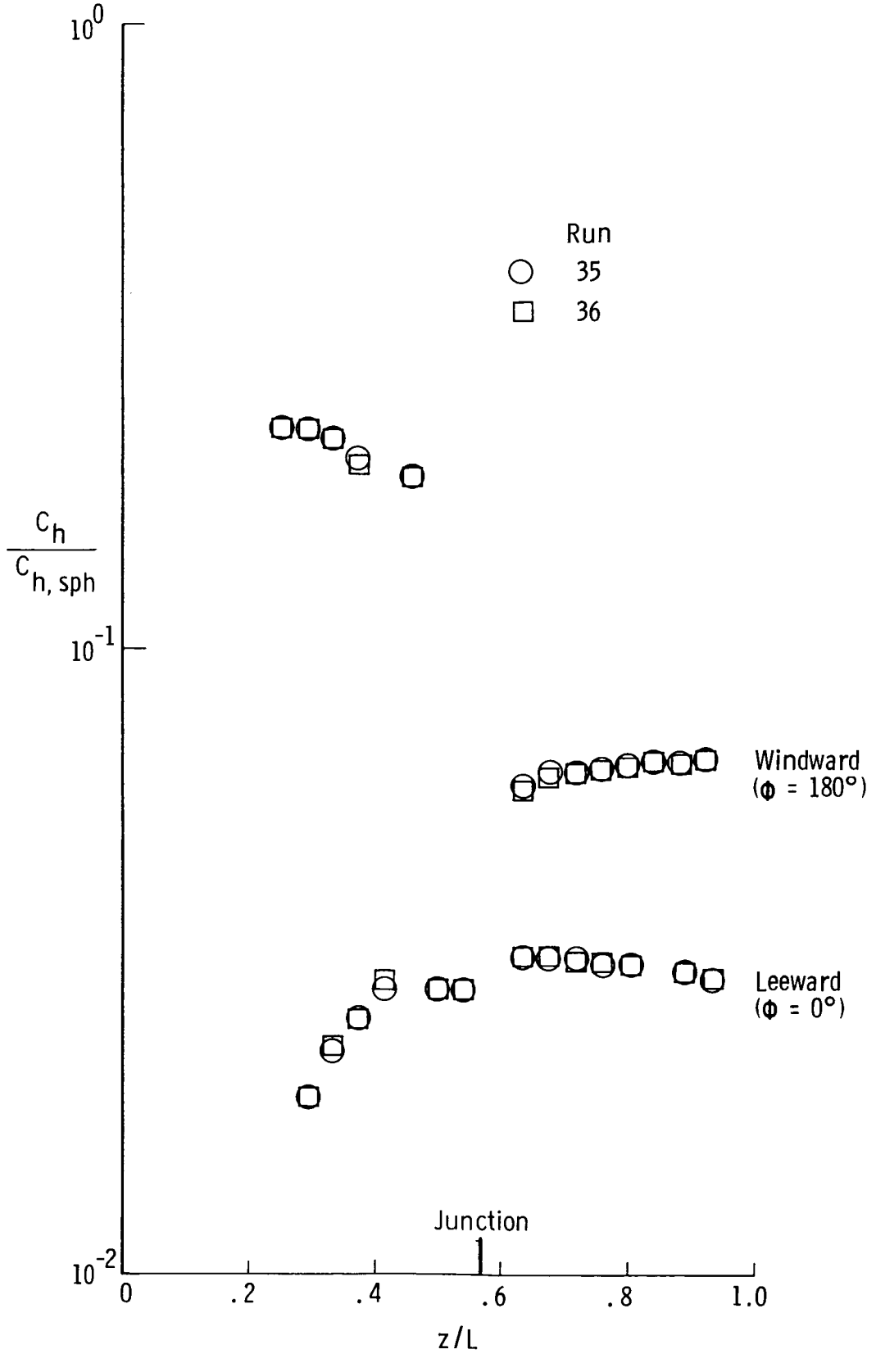

Figure 5. Example of run-to-run repeatability for bent-nose biconic. $\alpha = 12°$; $R_{\infty,L} \approx 9.3 \times 10^5$.

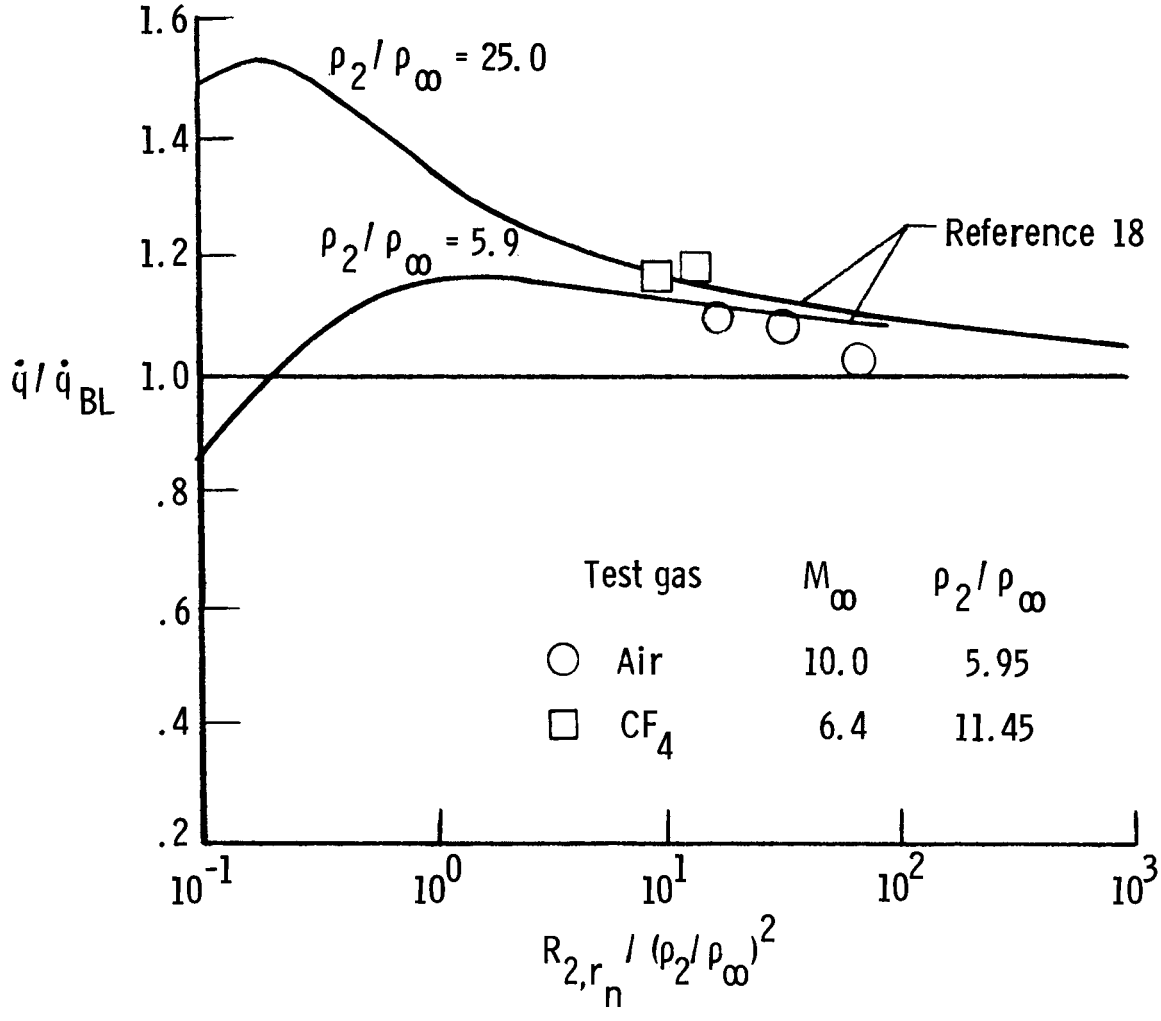

Figure 6. Ratio of measured to predicted stagnation-point heat-transfer rate to a hemisphere as a function of post-normal-shock Reynolds number and density ratio.

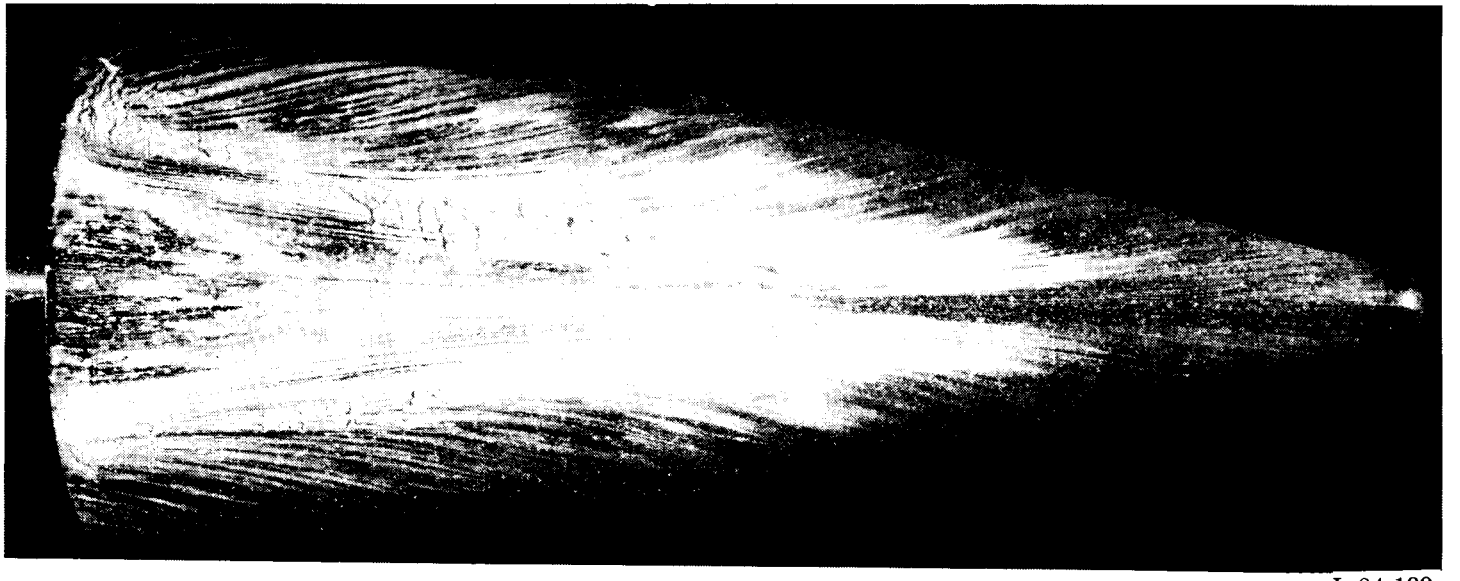

(a) $\alpha = 10°$; $R_{\infty,L} \approx 0.3 \times 10^6$. L-84-109

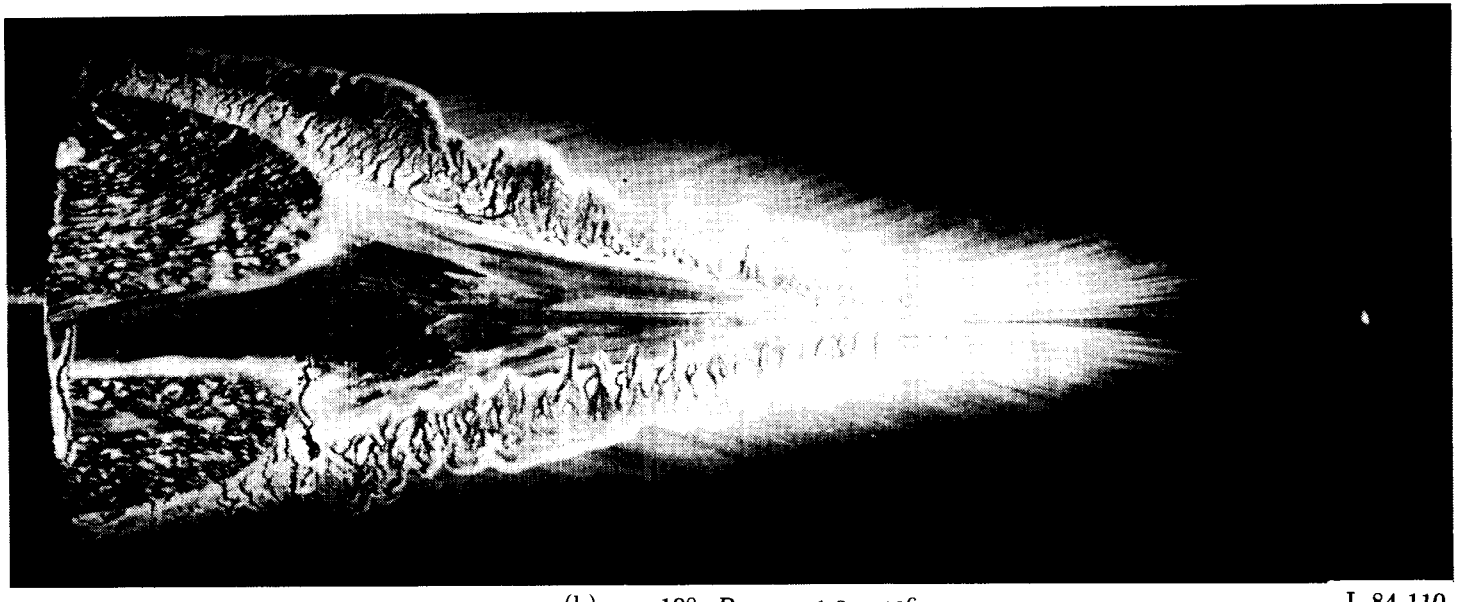

(b) $\alpha = 10°$; $R_{\infty,L} \approx 1.3 \times 10^6$. L-84-110

Figure 7. Effect of Reynolds number on leeward-surface oil-flow patterns for straight biconic.

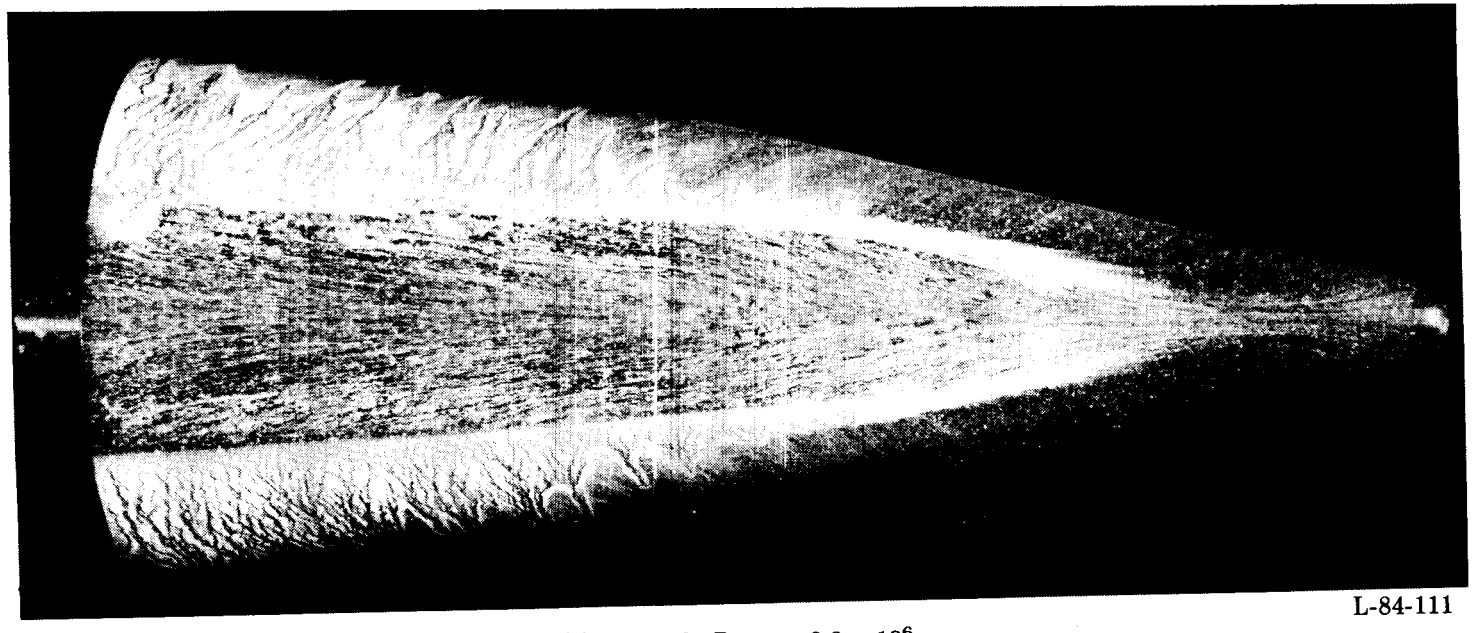

L-84-111

(c) $\alpha = 20°$; $R_{\infty,L} \approx 0.3 \times 10^6$.

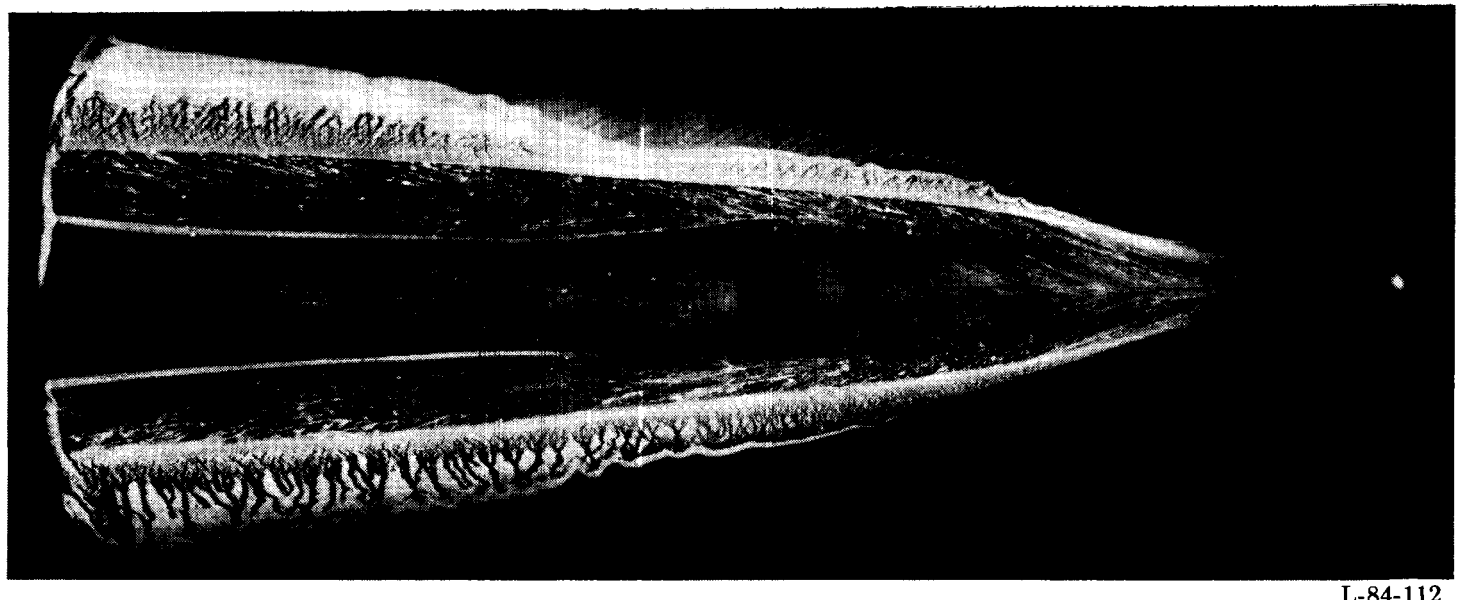

L-84-112

(d) $\alpha = 20°$; $R_{\infty,L} \approx 1.3 \times 10^6$.

Figure 7. Concluded.

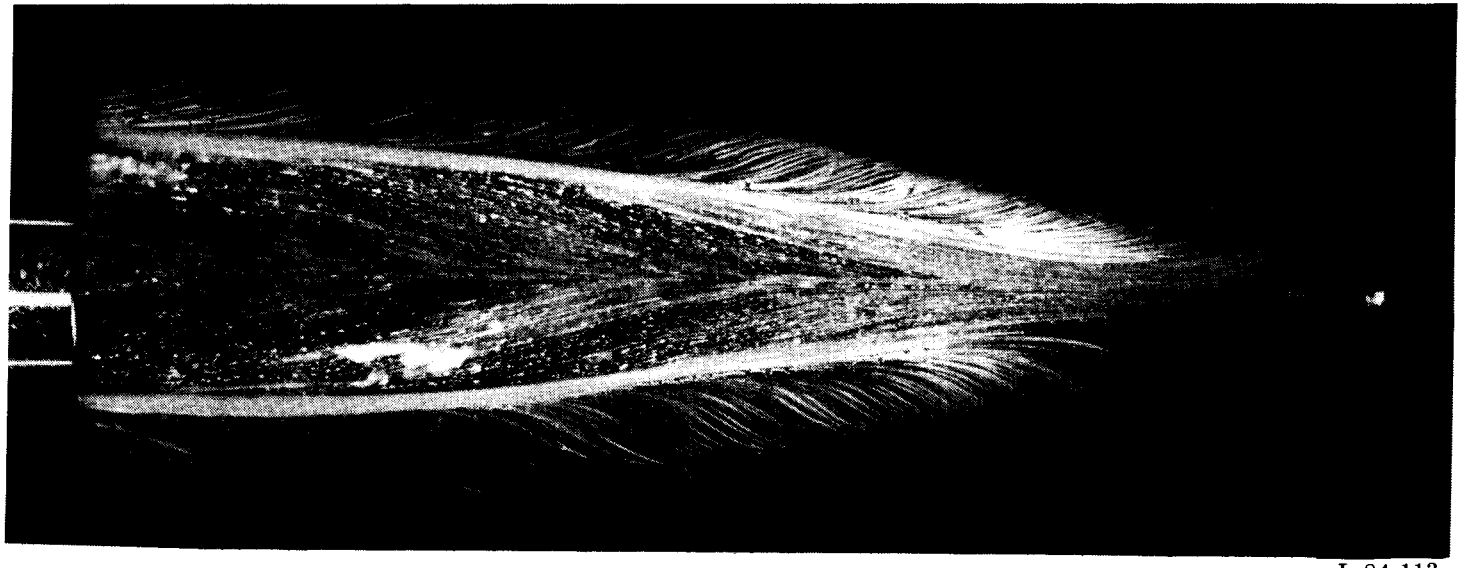

(a) $\alpha = 10°$; $R_{\infty,L} \approx 0.3 \times 10^6$. L-84-113

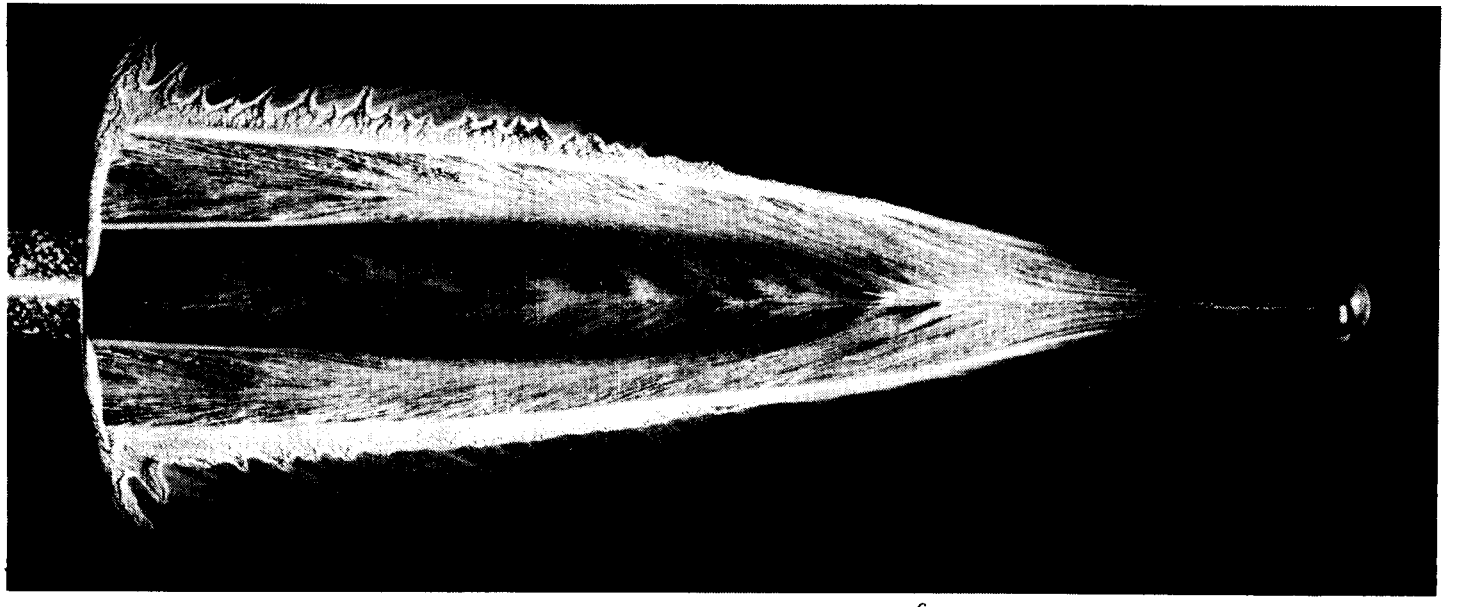

(b) $\alpha = 10°$; $R_{\infty,L} \approx 1.3 \times 10^6$. L-84-114

Figure 8. Effect of Reynolds number on leeward-surface oil-flow patterns for bent-nose biconic.

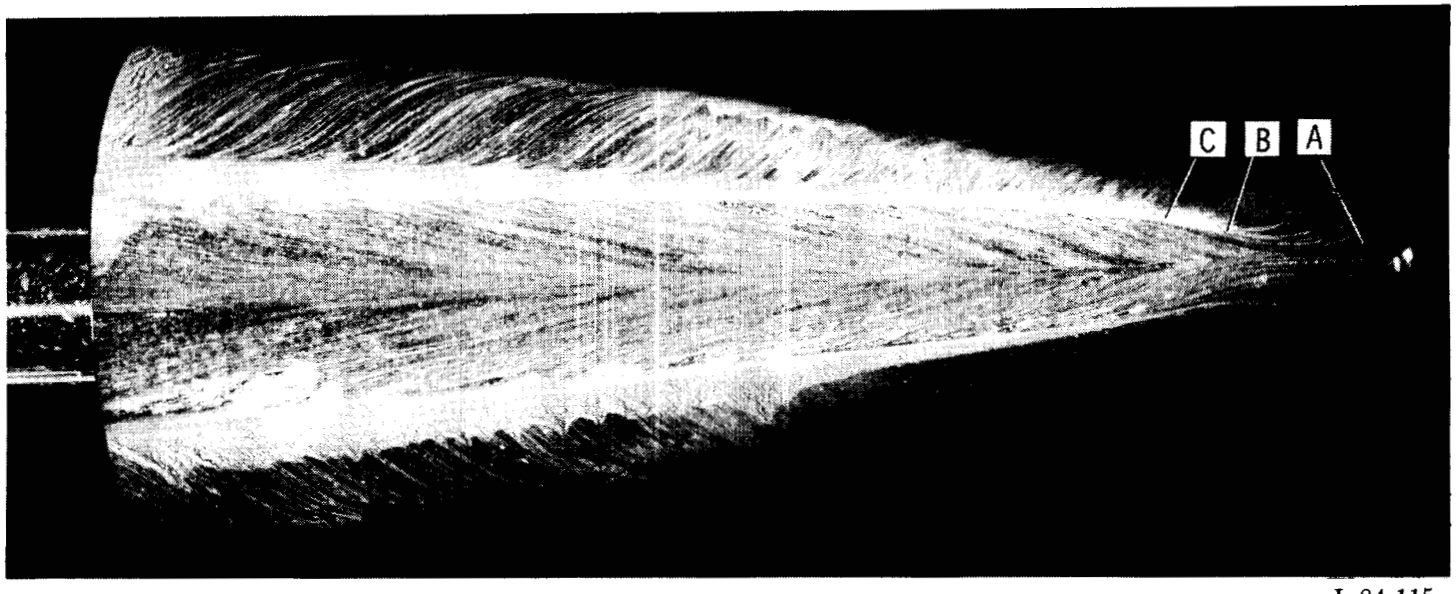

L-84-115

(c) $\alpha = 20°$; $R_{\infty,L} \approx 0.3 \times 10^6$.

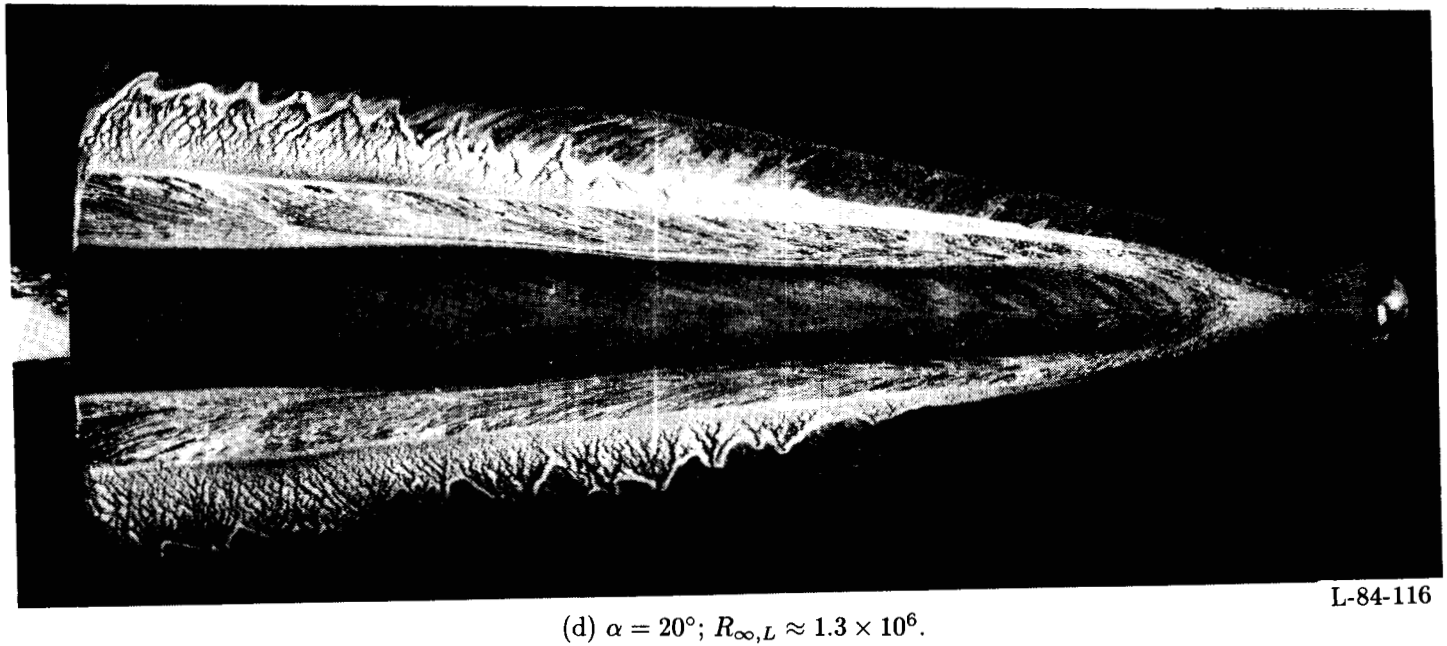

L-84-116

(d) $\alpha = 20°$; $R_{\infty,L} \approx 1.3 \times 10^6$.

Figure 8. Concluded.

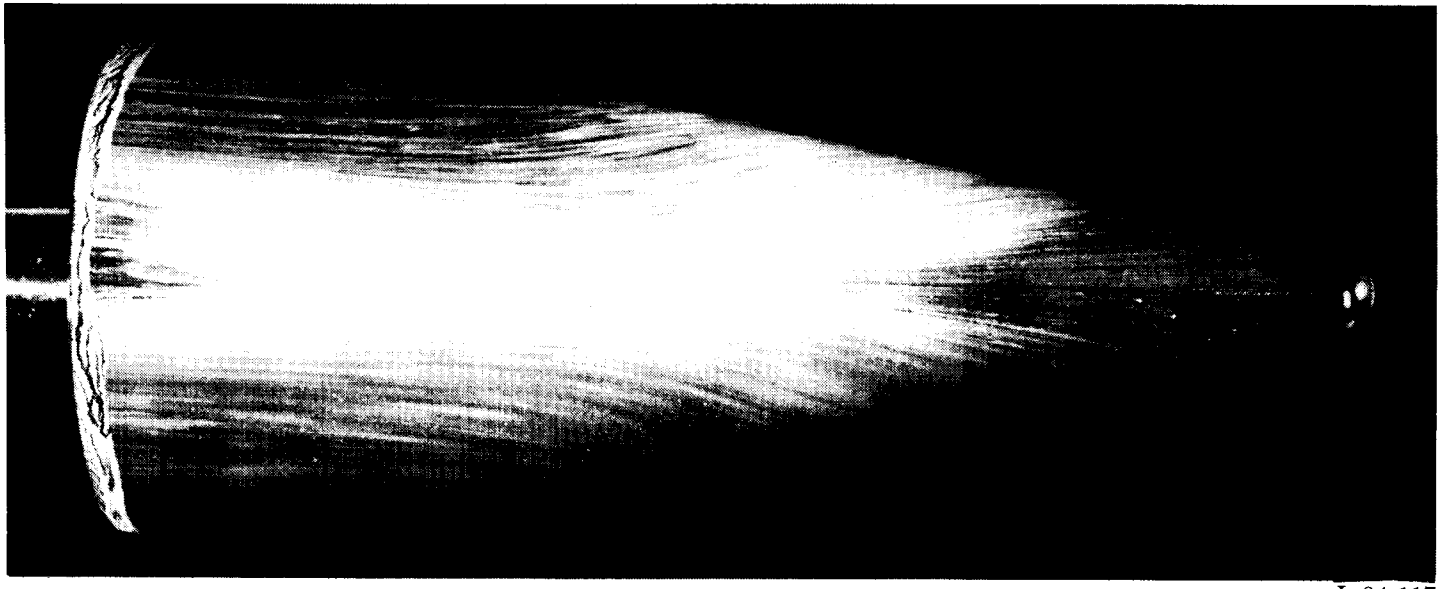

(a) $\alpha = 0°$. L-84-117

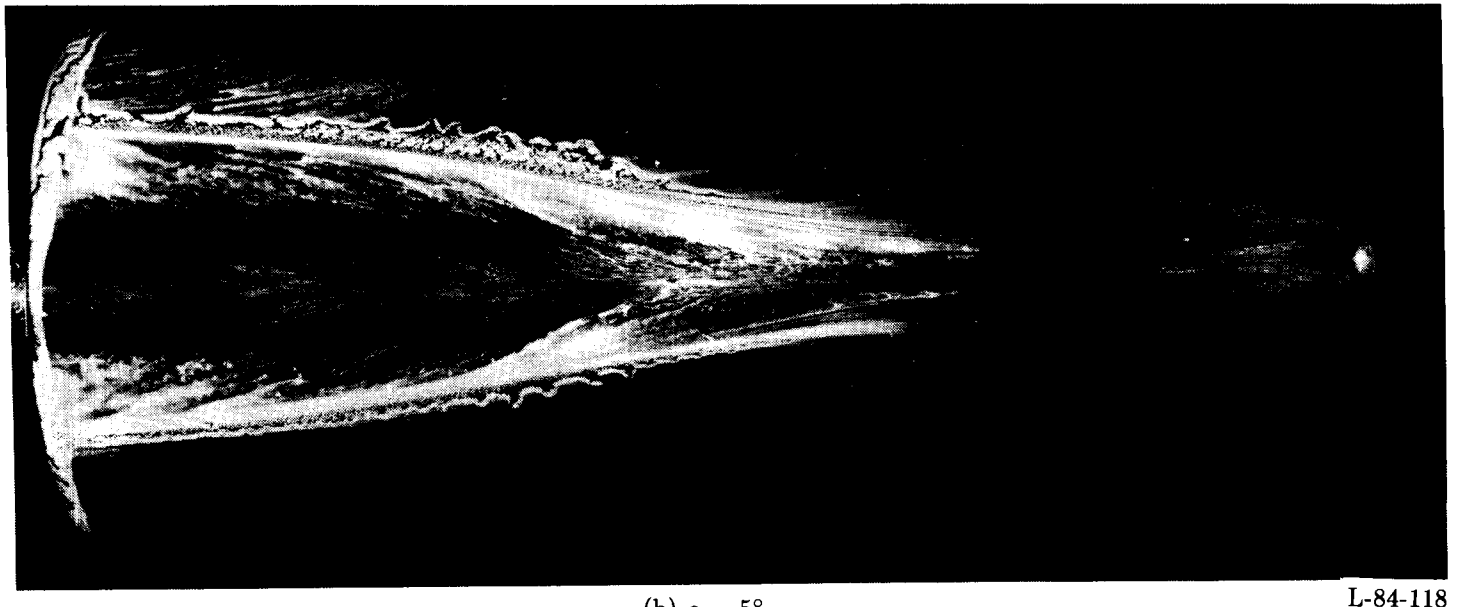

(b) $\alpha = 5°$. L-84-118

Figure 9. Effect of angle of attack on leeward-surface oil-flow patterns for bent-nose biconic. $R_{\infty,L} \approx 1.3 \times 10^6$.

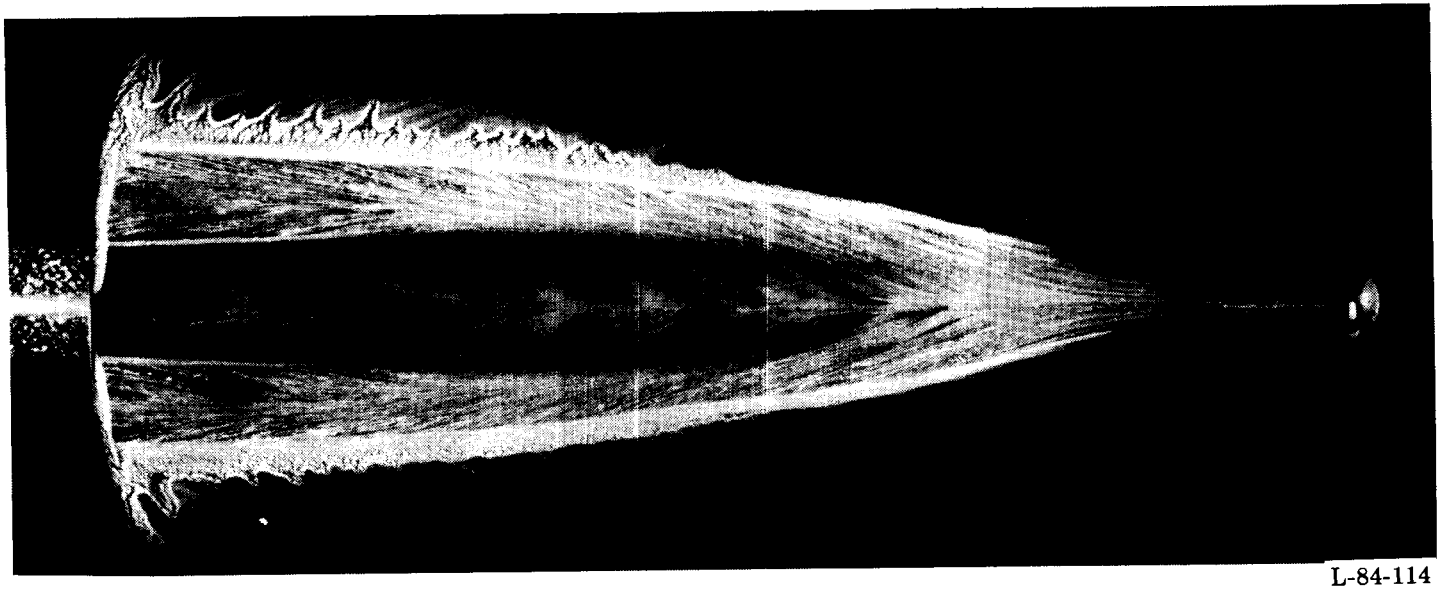

L-84-114

(c) $\alpha = 10°$.

Figure 9. Continued.

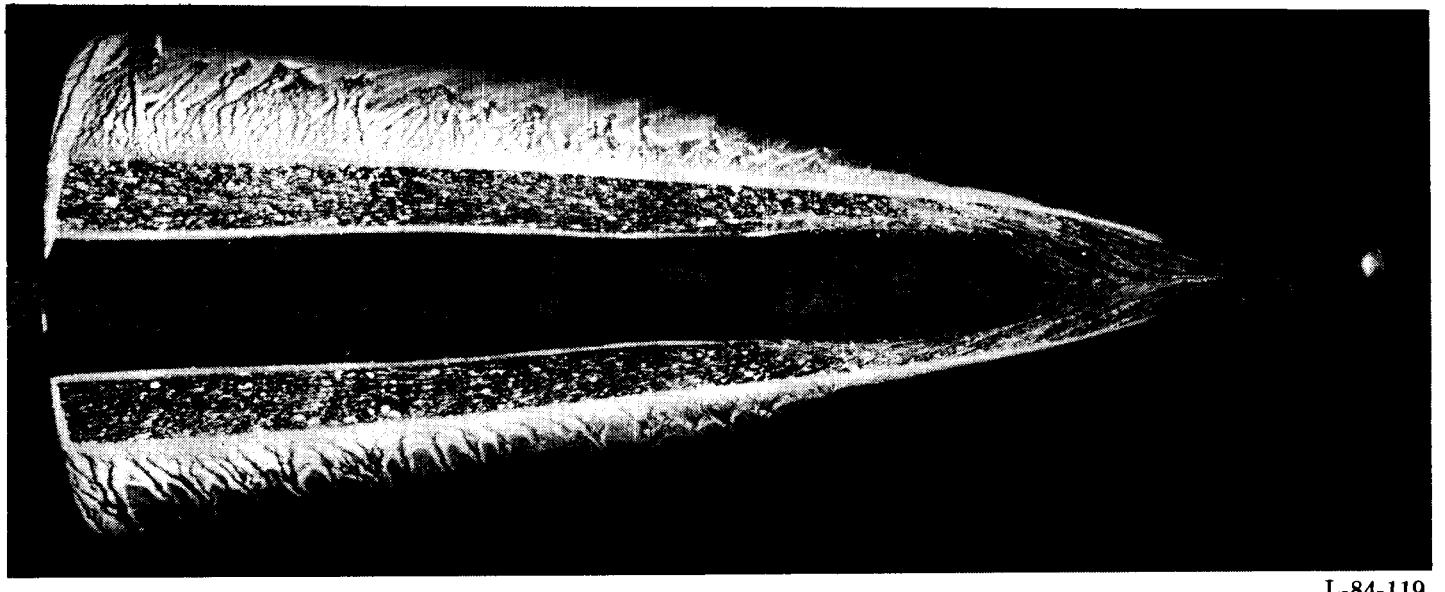

L-84-119

(d) $\alpha = 15°$.

Figure 9. Continued.

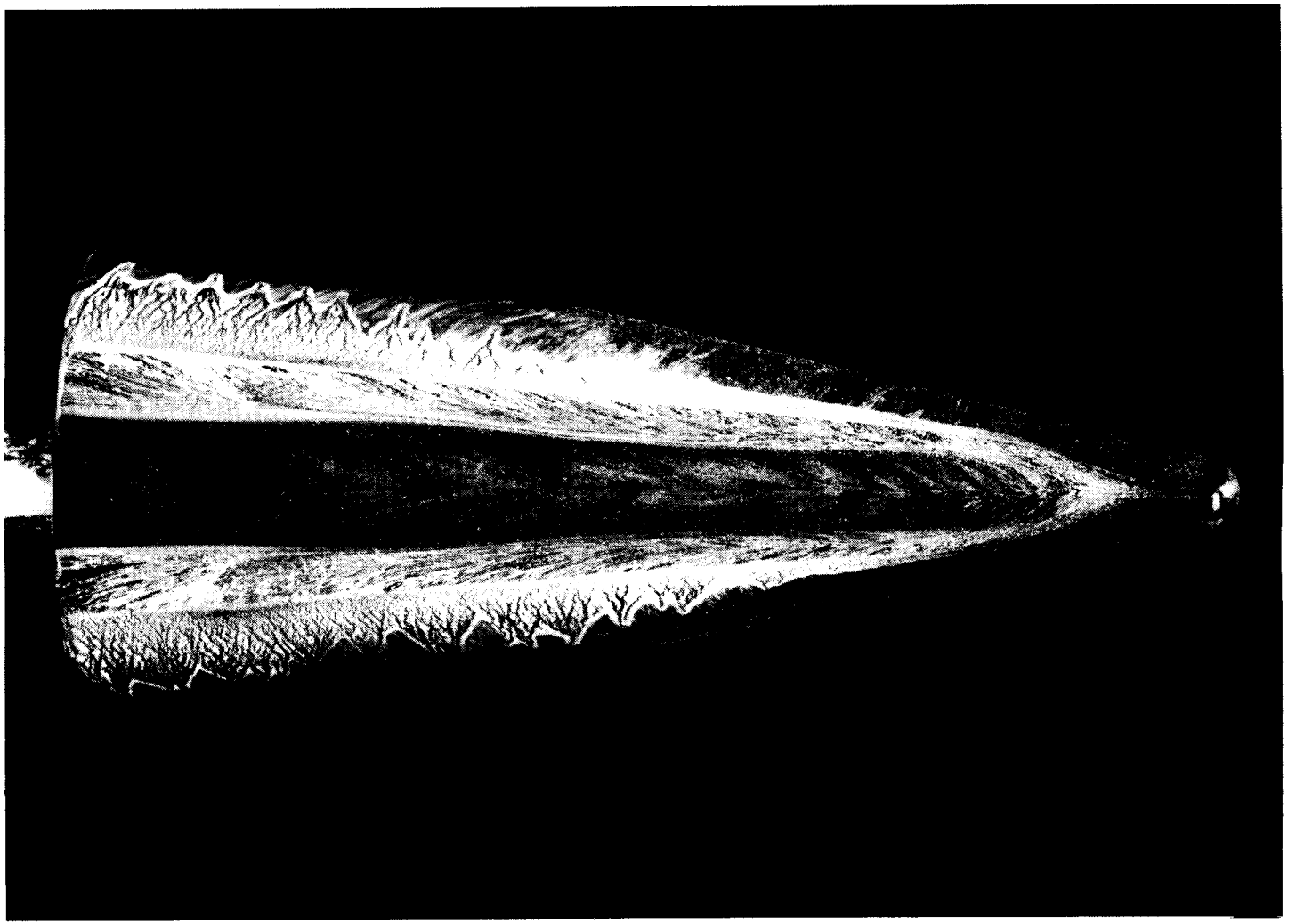

L-84-116

(e) $\alpha = 20°$.

Figure 9. Concluded.

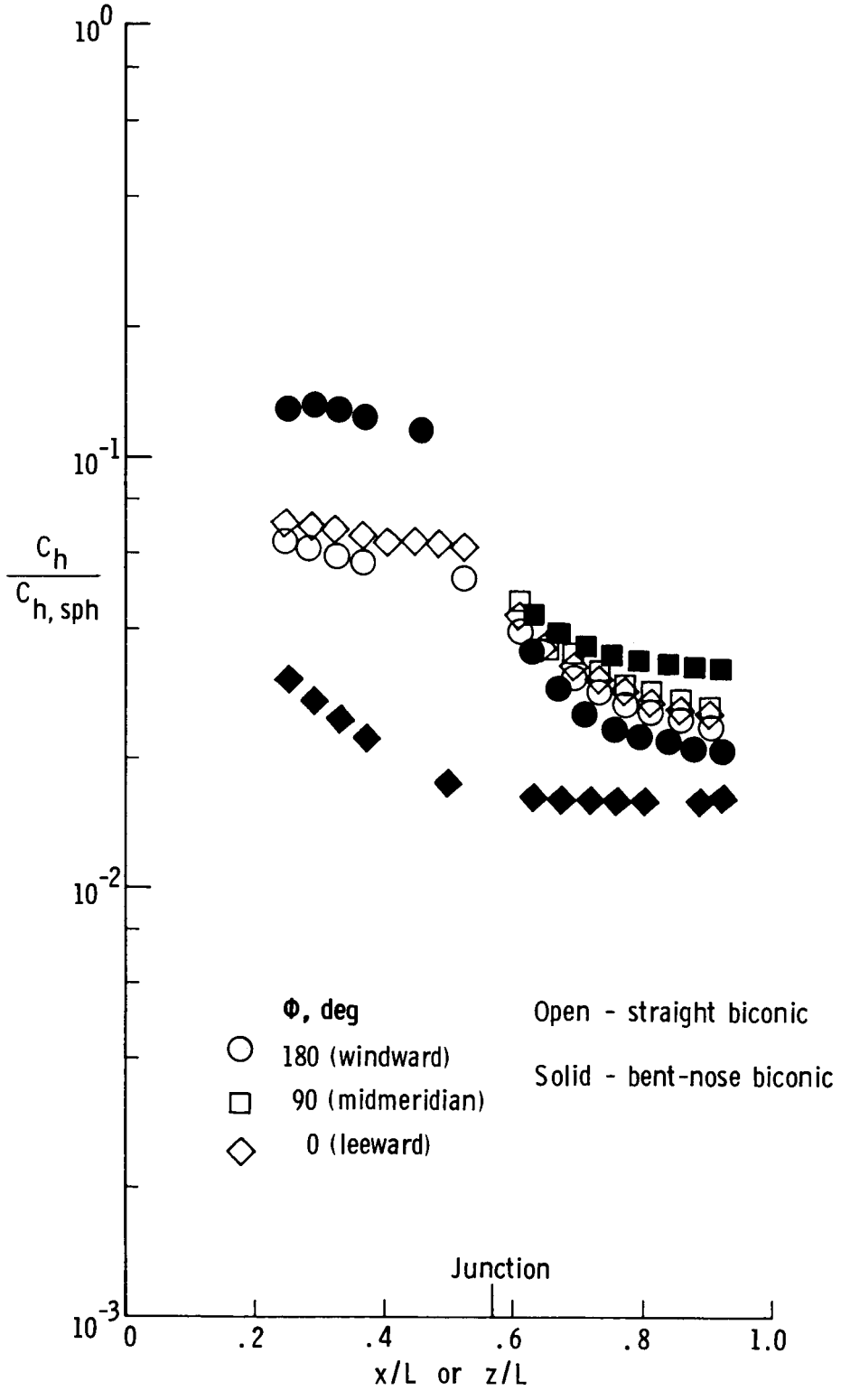

(a) $\alpha = 0°$.

Figure 10. Effect of nose bend on heating distribution for $R_{\infty,L} \approx 2.2 \times 10^5$.

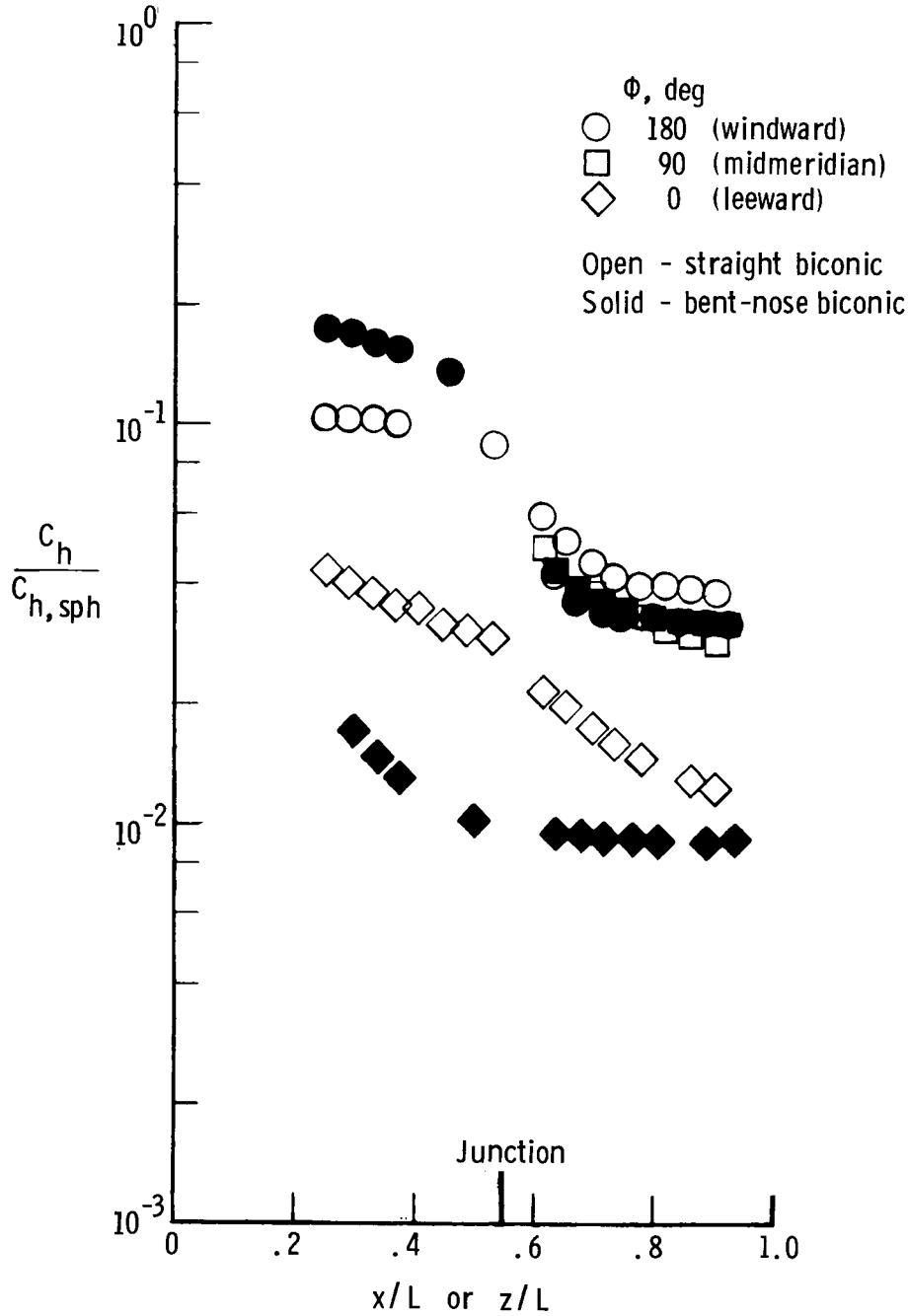

(b) $\alpha = 4°$.

Figure 10. Continued.

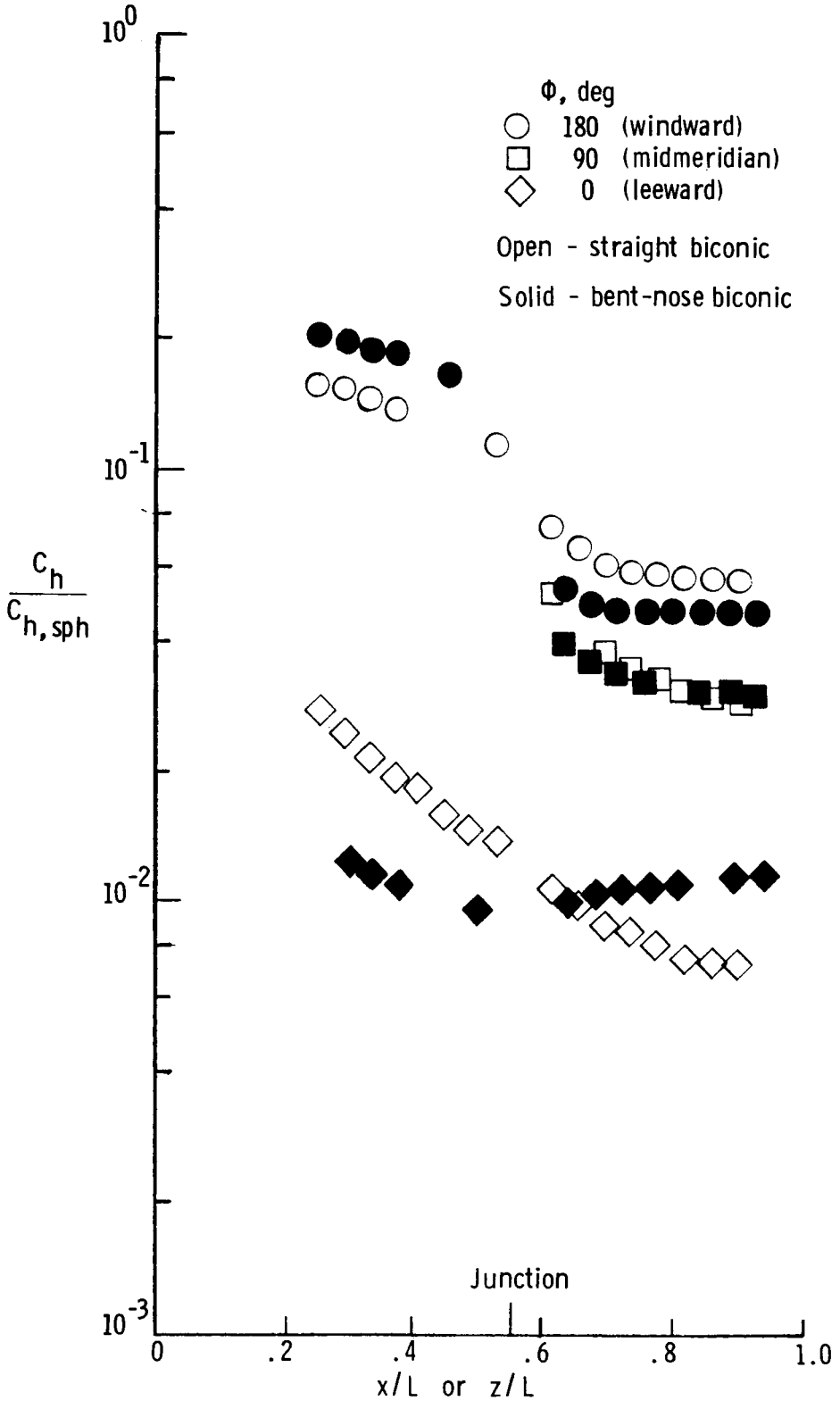

(c) $\alpha = 8°$.

Figure 10. Continued.

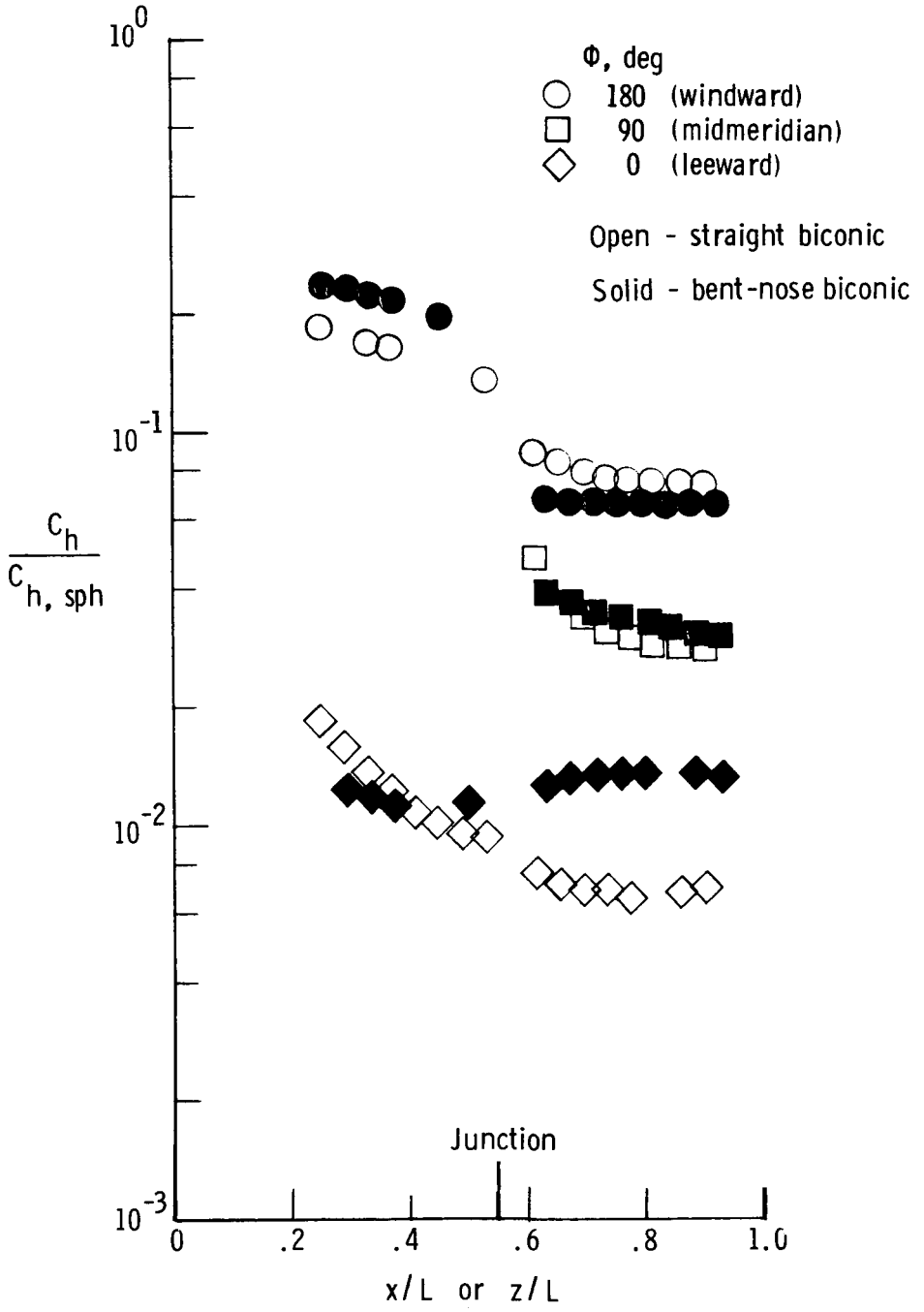

(d) $\alpha = 12°$.

Figure 10. Continued.

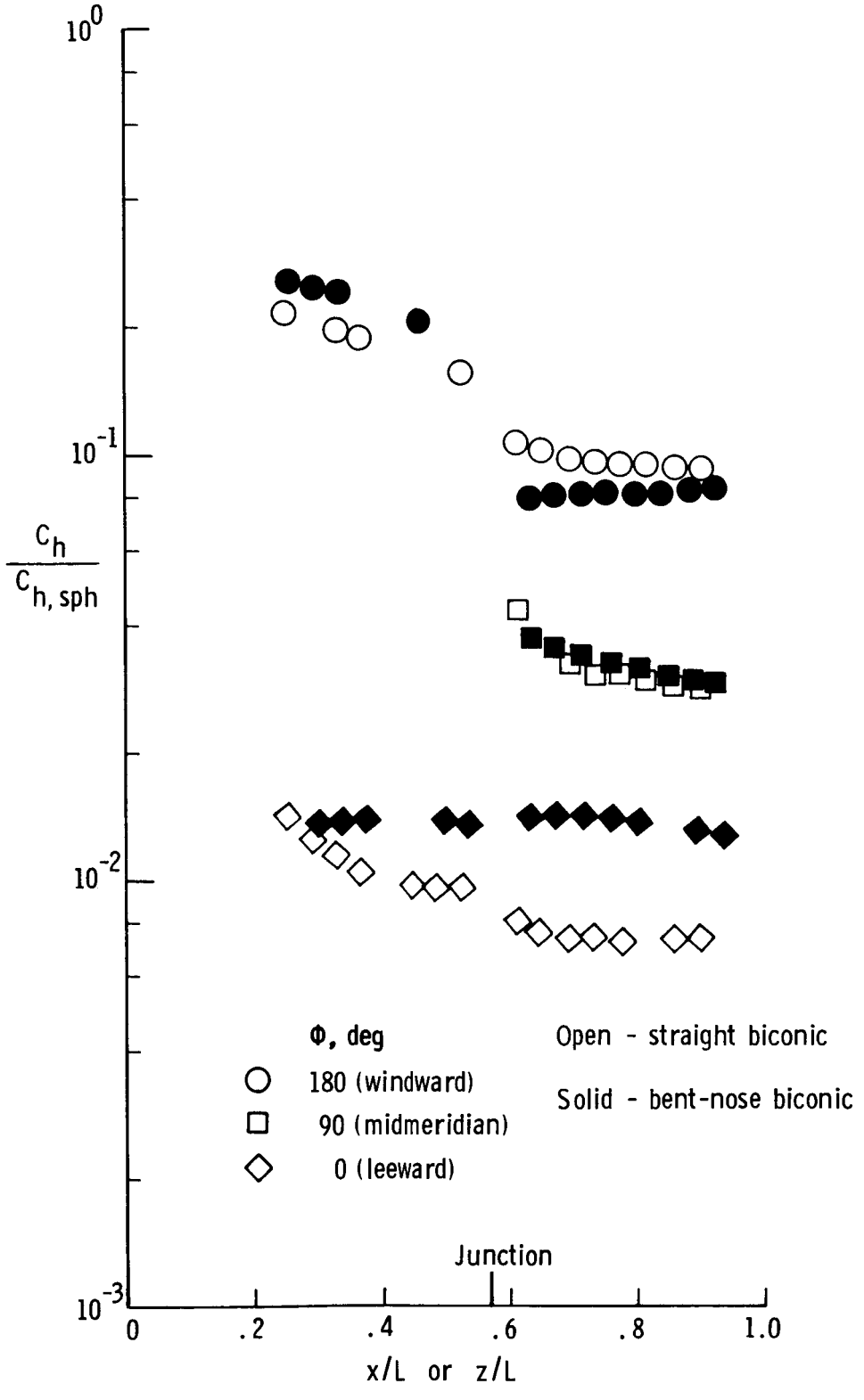

(e) $\alpha = 16°$.

Figure 10. Continued.

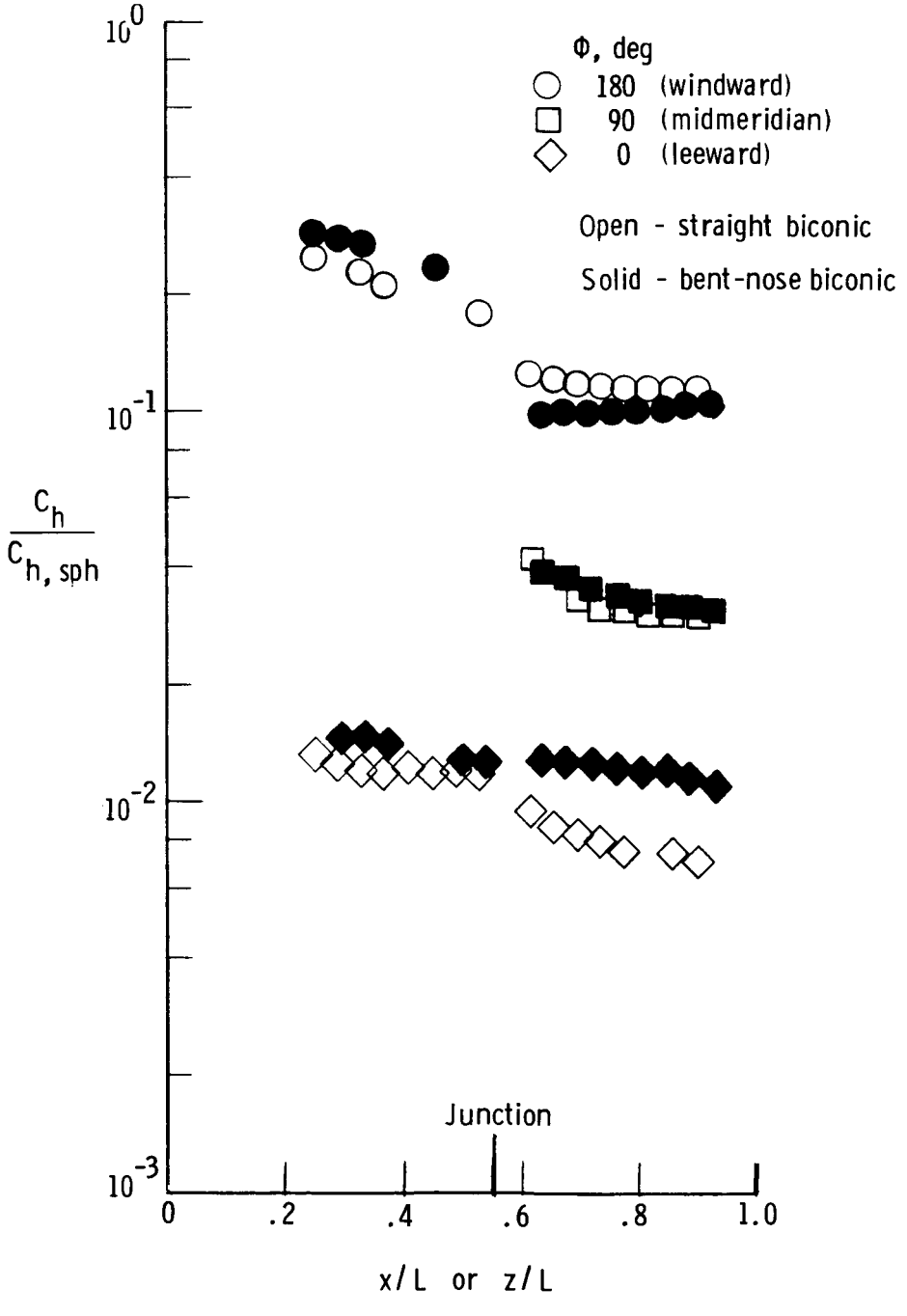

(f) $\alpha = 20°$.

Figure 10. Concluded.

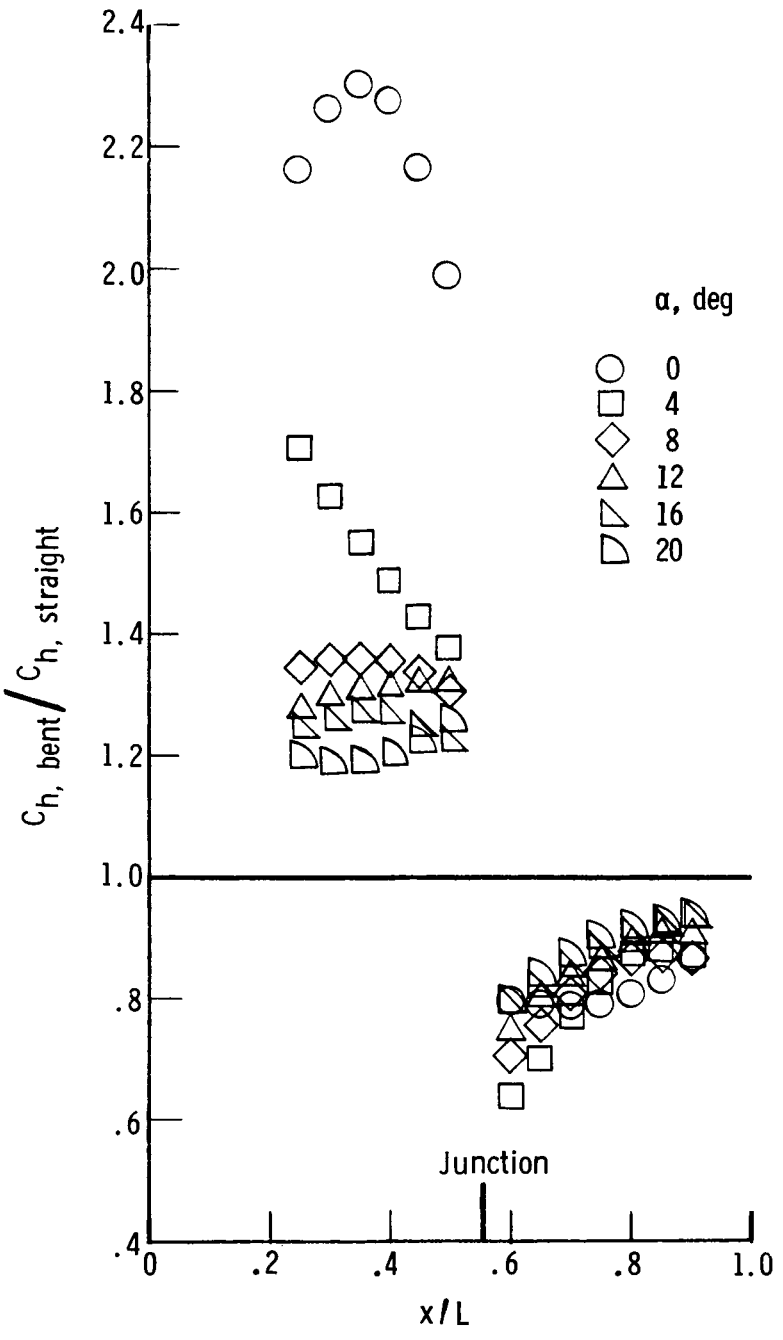

Figure 11. Ratio of bent-nose biconic to straight biconic windward heating ($\phi = 180°$) for various angles of attack. $R_{\infty,L} \approx 9.3 \times 10^5$; $M_\infty = 10.16$.

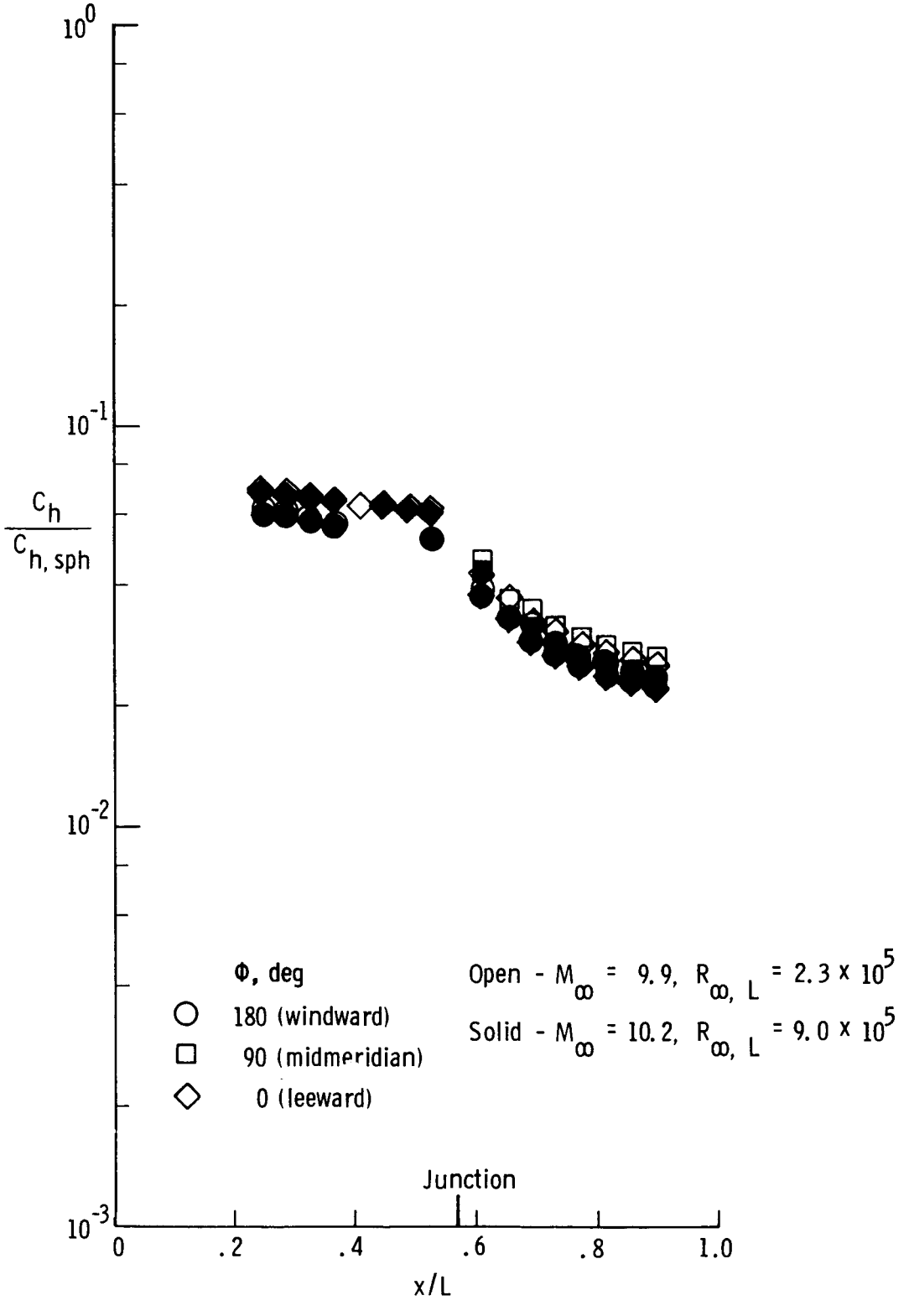

(a) $\alpha = 0°$.

Figure 12. Effect of Reynolds number on heating distribution for straight biconic.

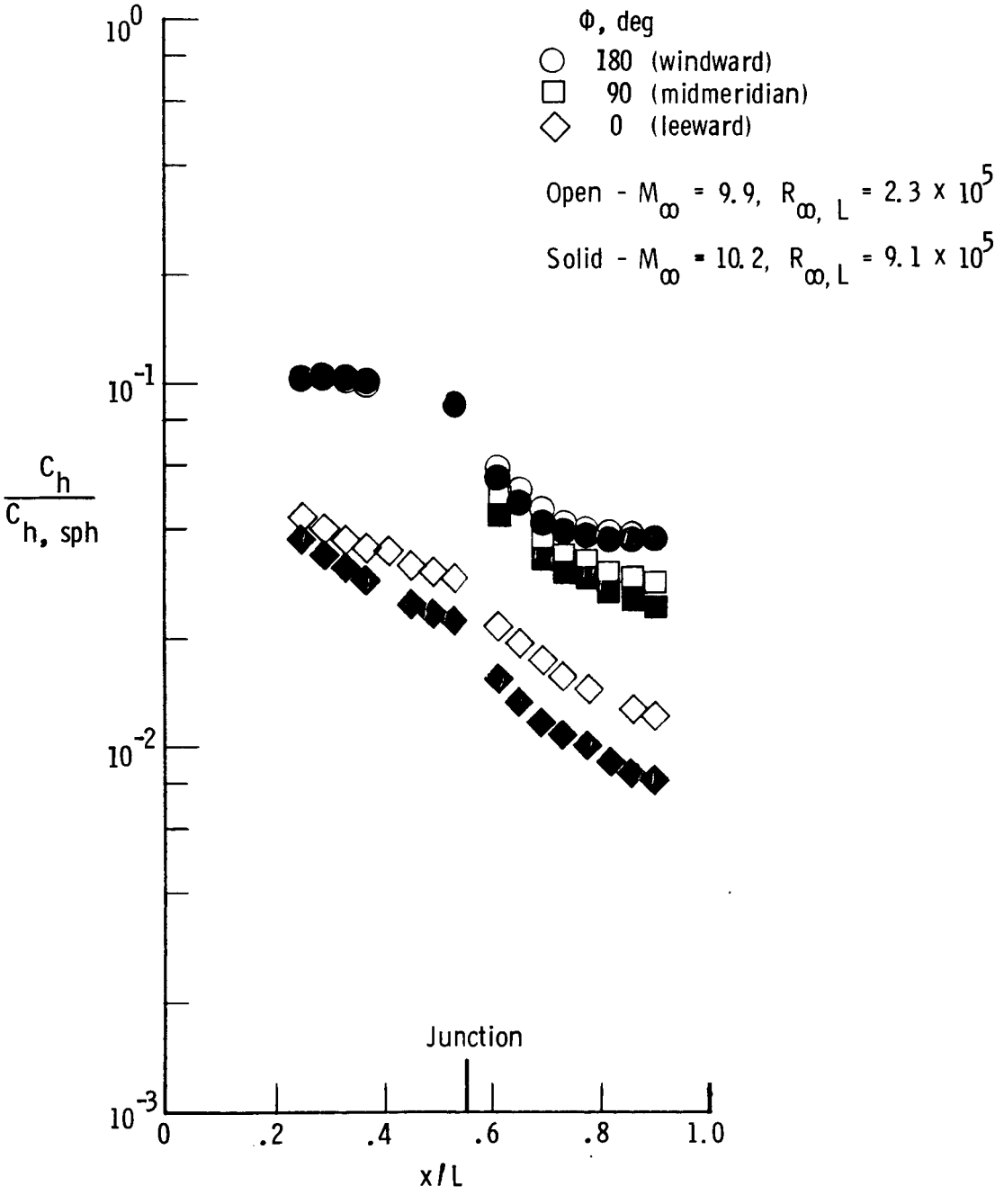

(b) $\alpha = 4°$.

Figure 12. Continued.

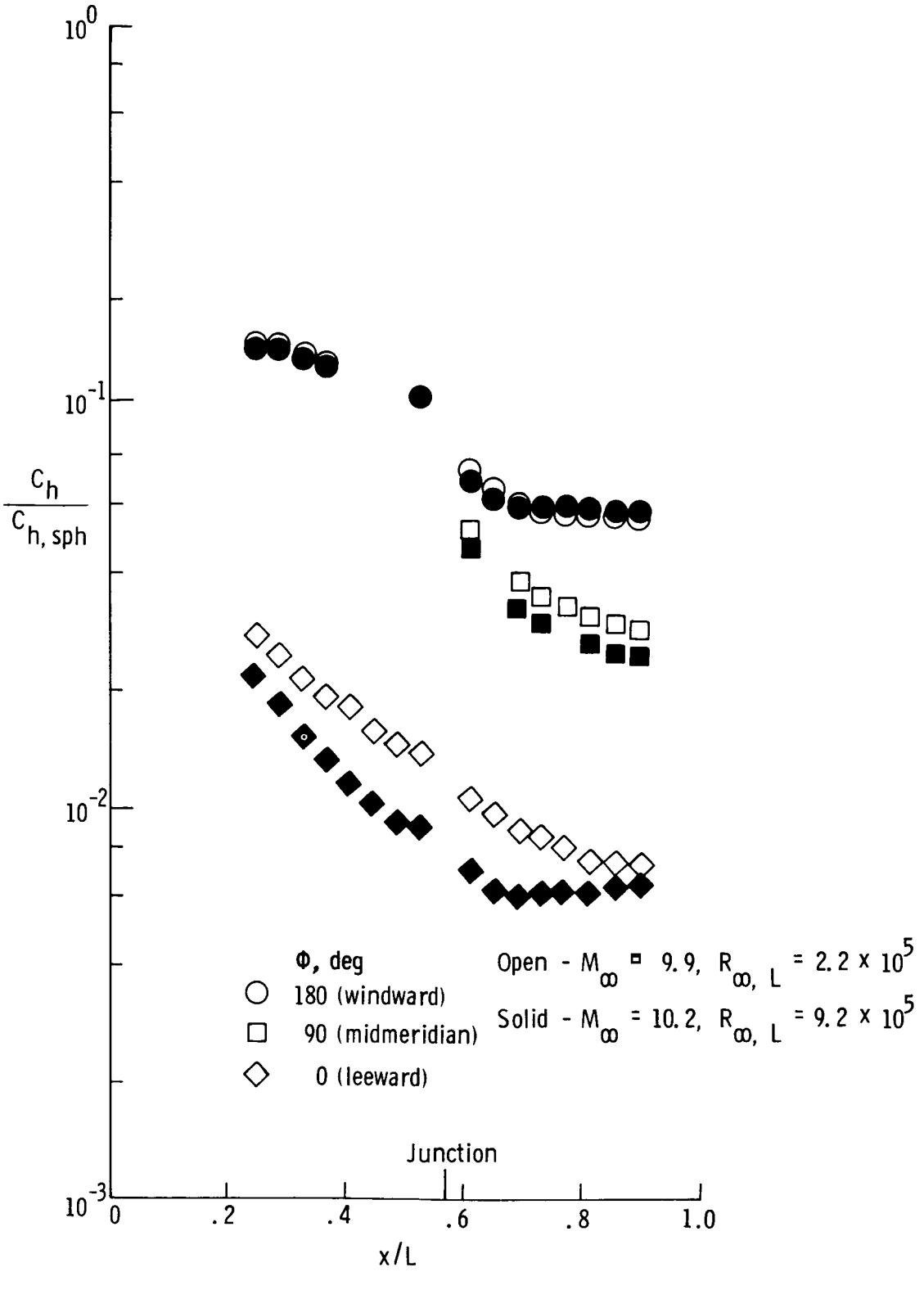

(c) $\alpha = 8°$.

Figure 12. Continued.

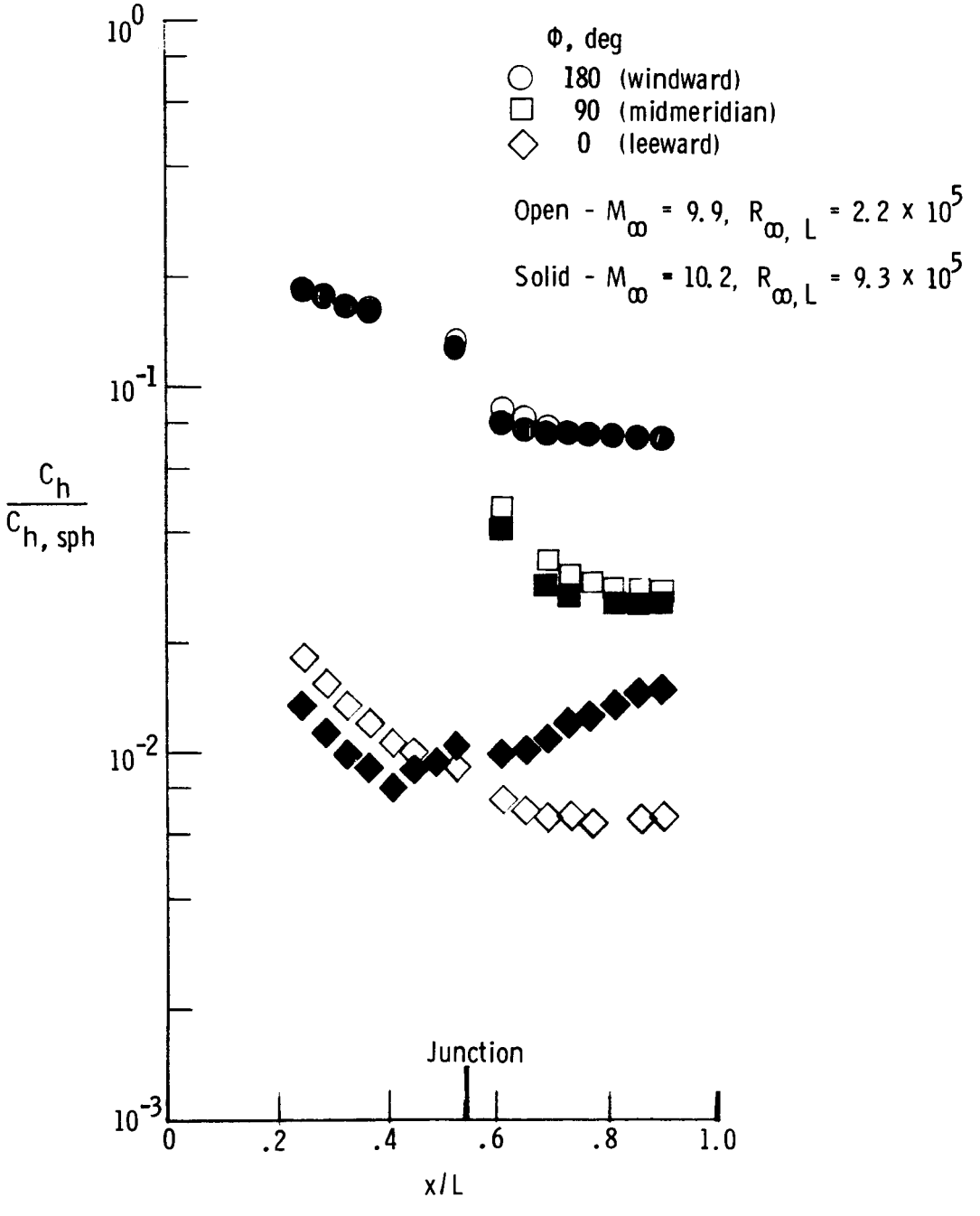

(d) $\alpha = 12°$.

Figure 12. Continued.

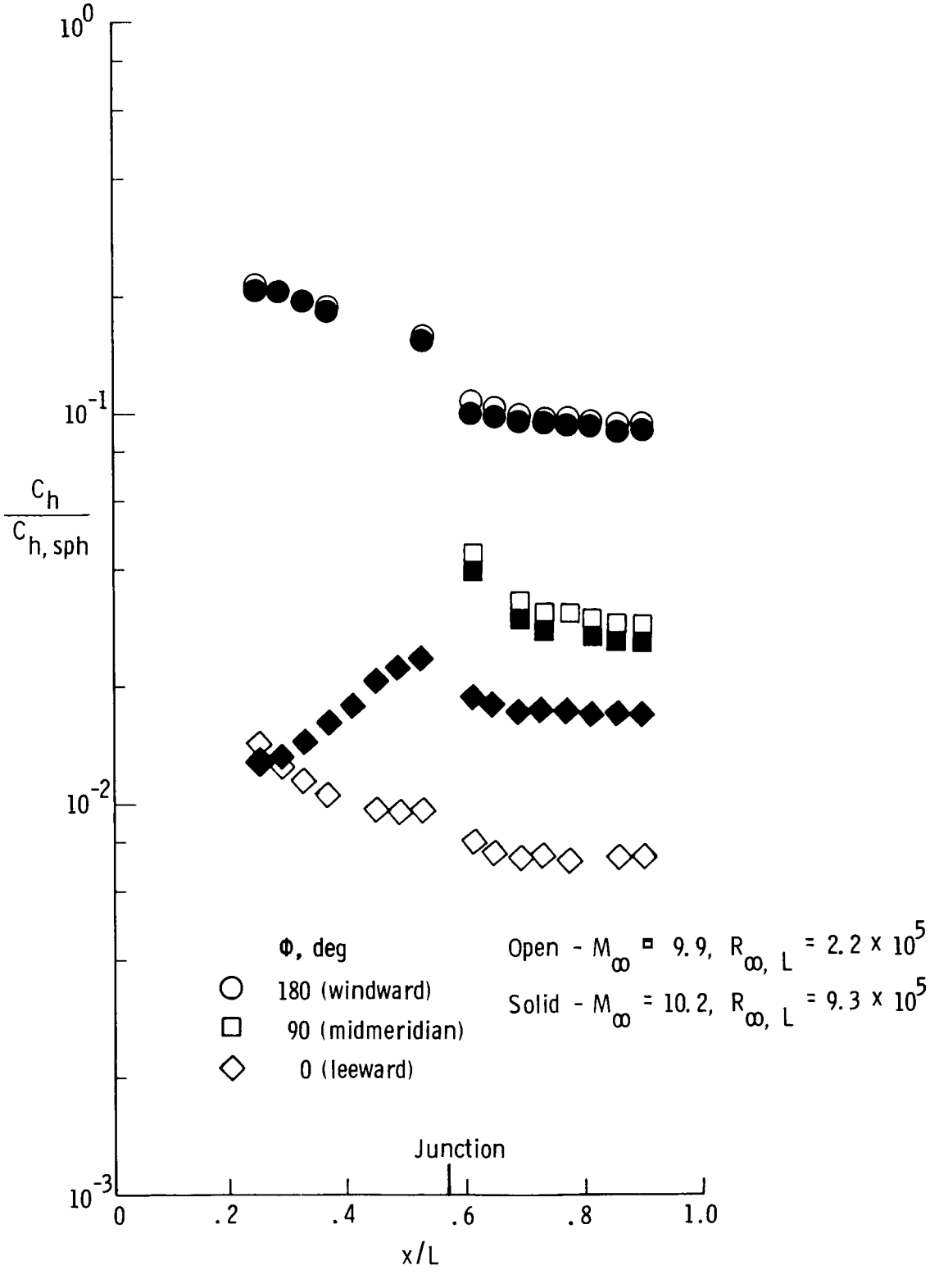

(e) $\alpha = 16°$.

Figure 12. Continued.

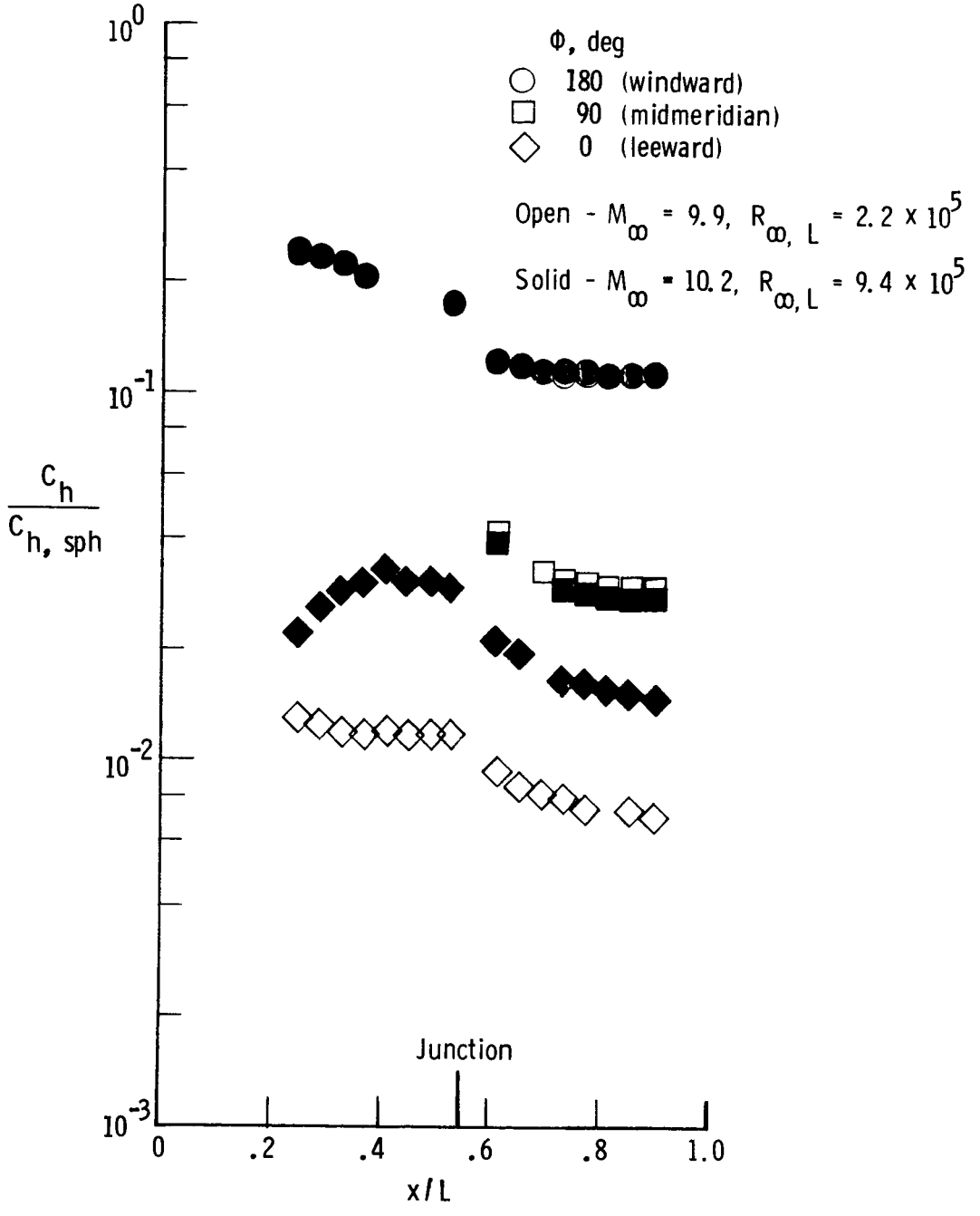

(f) $\alpha = 20°$.

Figure 12. Concluded.

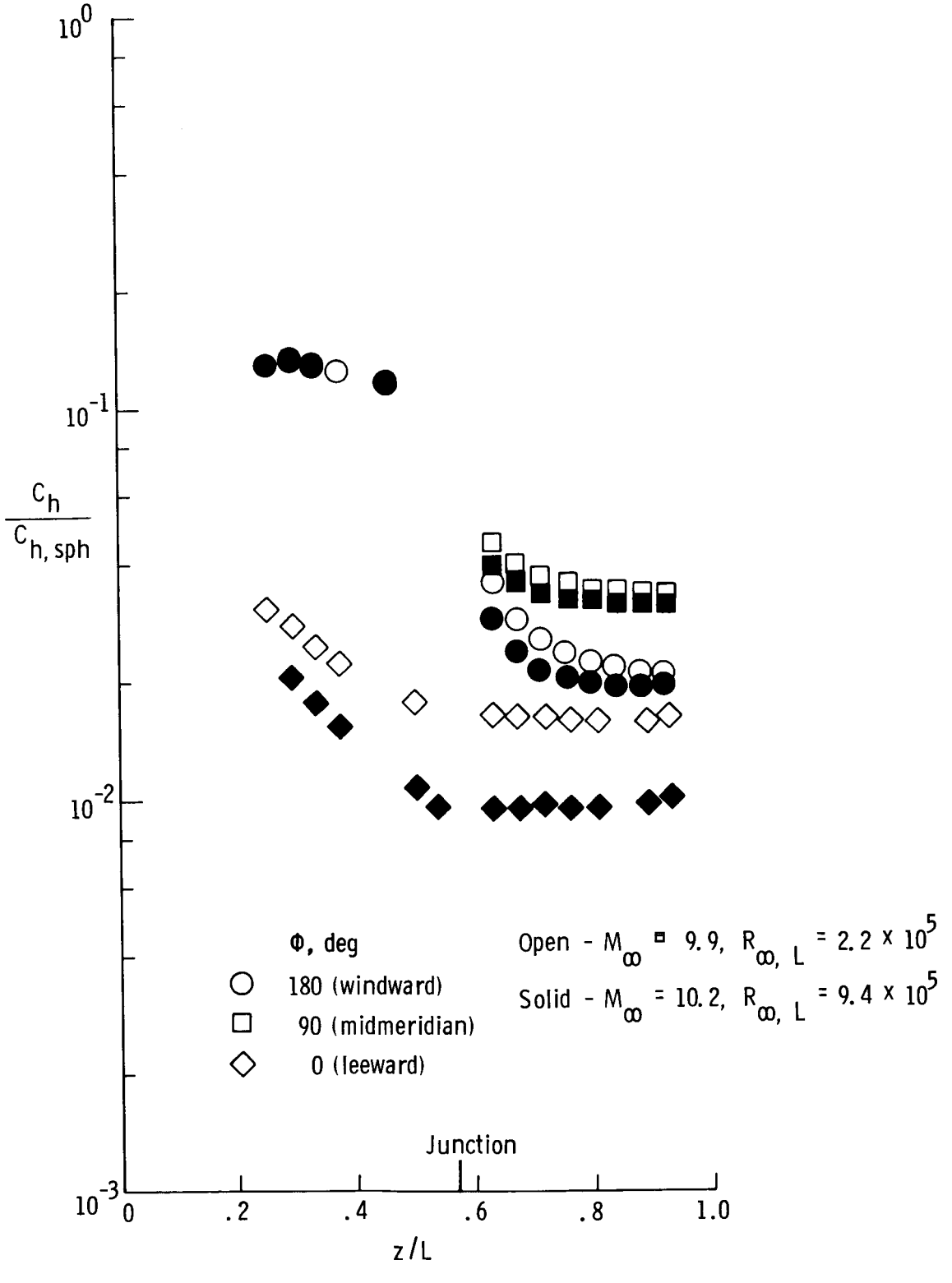

(a) $\alpha = 0°$.

Figure 13. Effect of Reynolds number on heating distribution for bent-nose biconic.

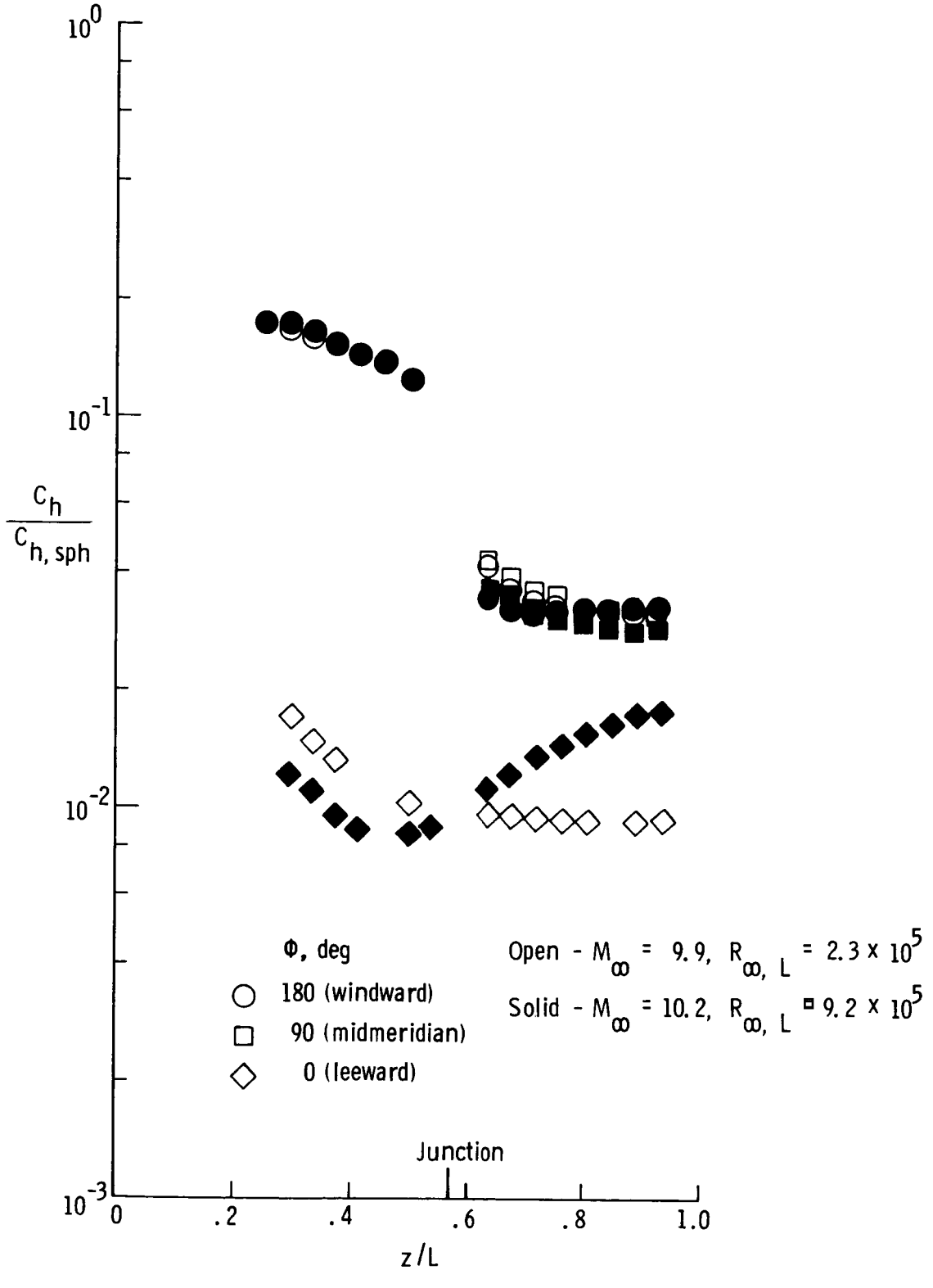

(b) $\alpha = 4°$.

Figure 13. Continued.

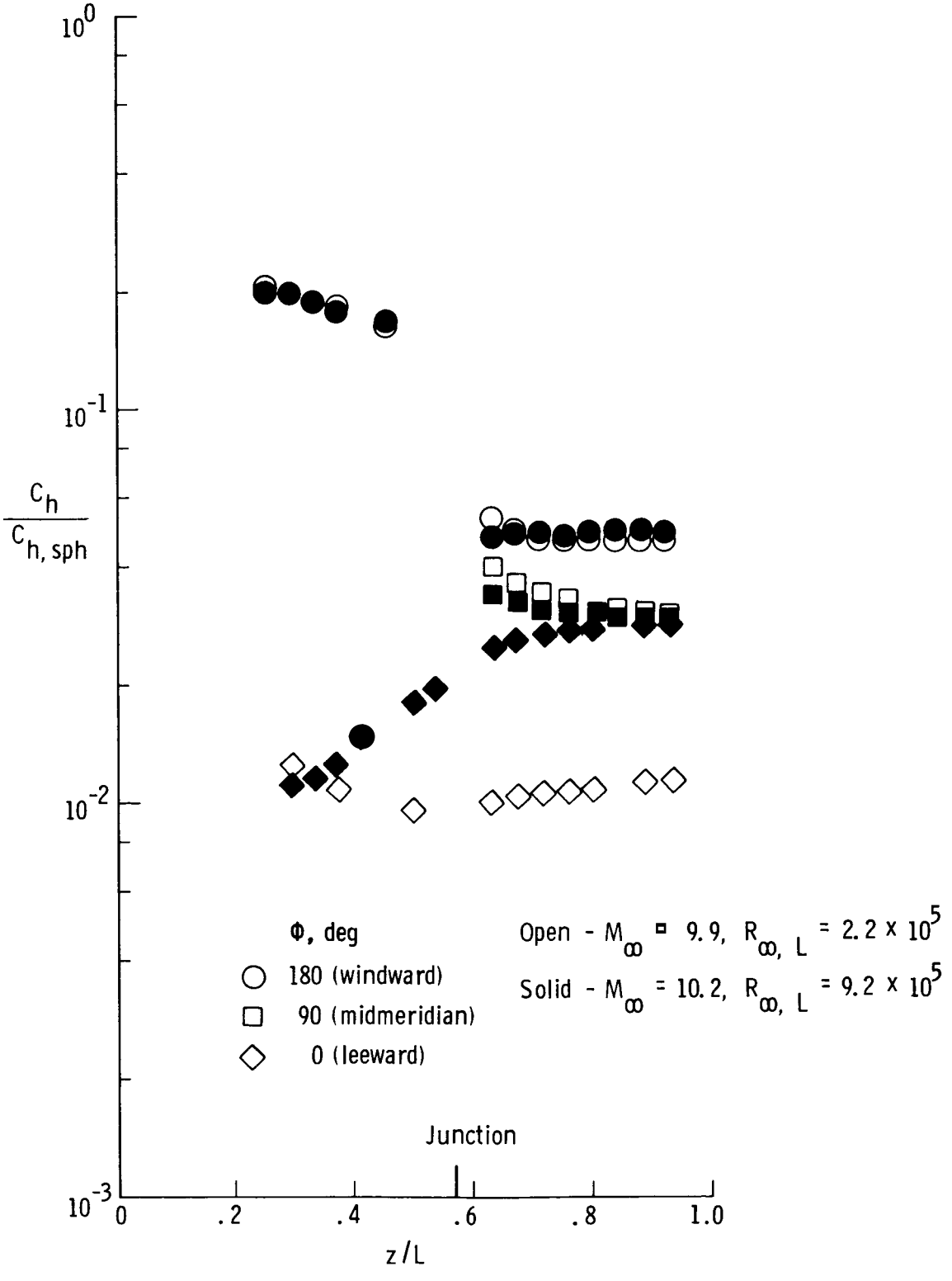

(c) $\alpha = 8°$.

Figure 13. Continued.

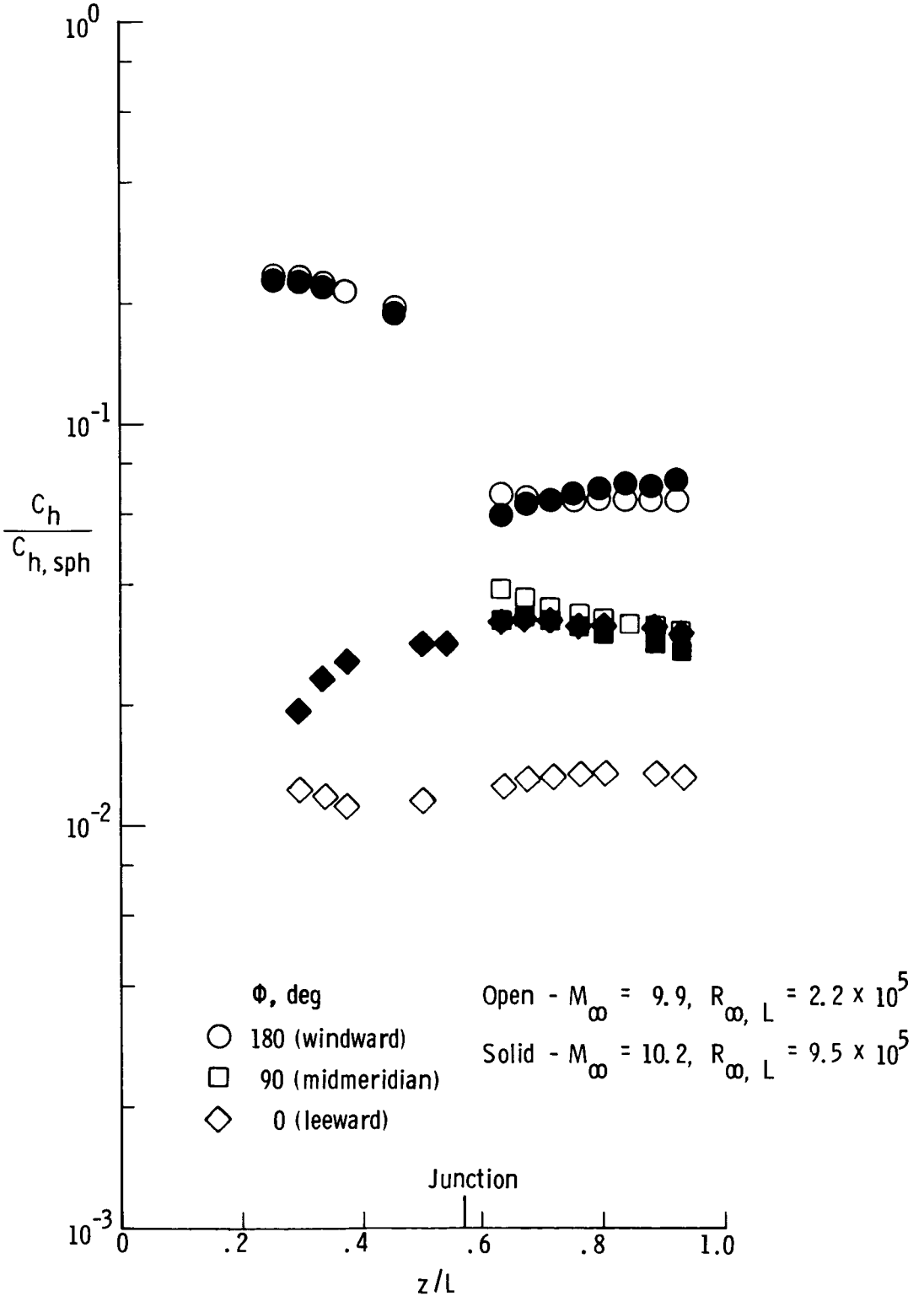

(d) $\alpha = 12°$.

Figure 13. Continued.

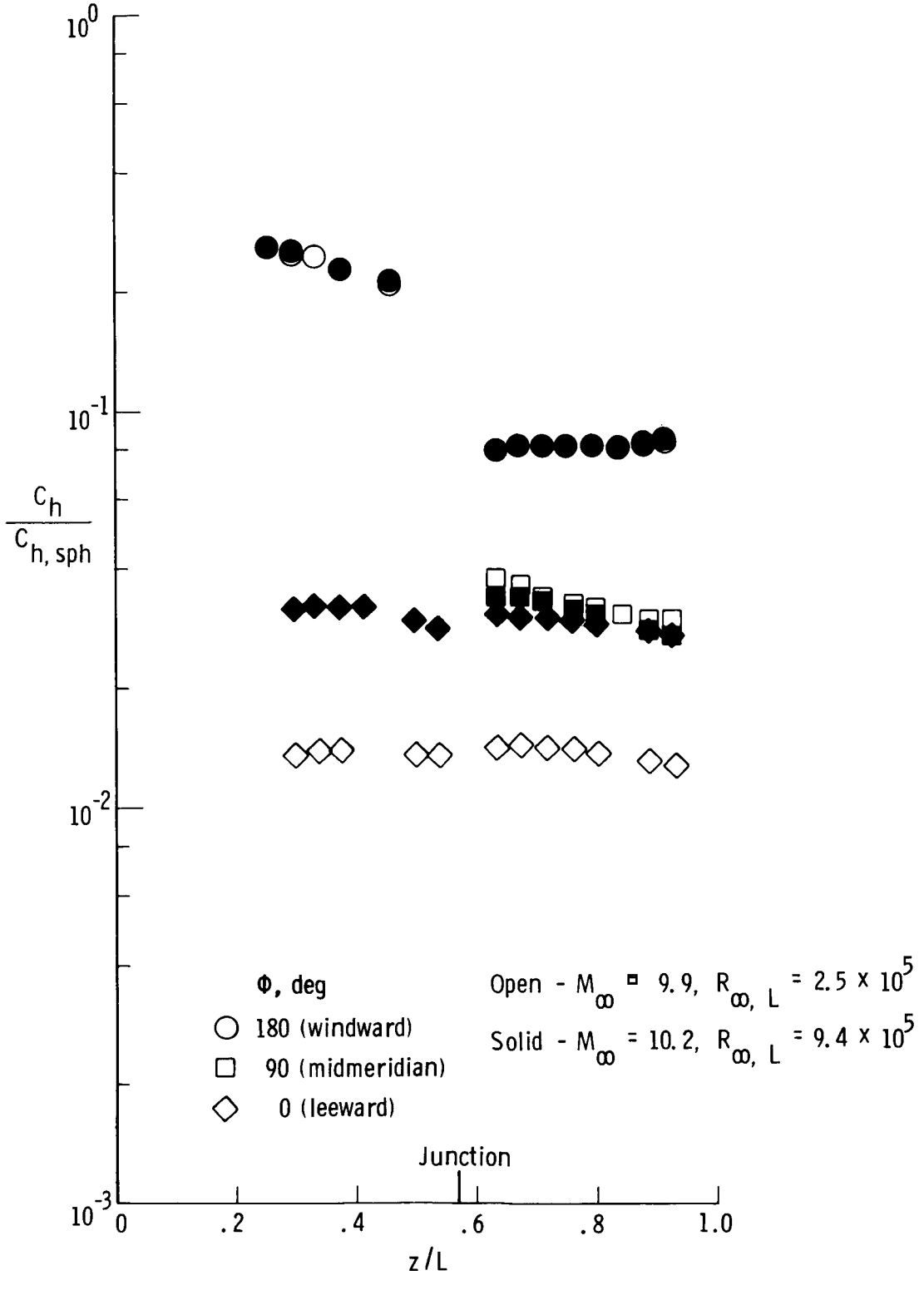

(e) $\alpha = 16°$.

Figure 13. Continued.

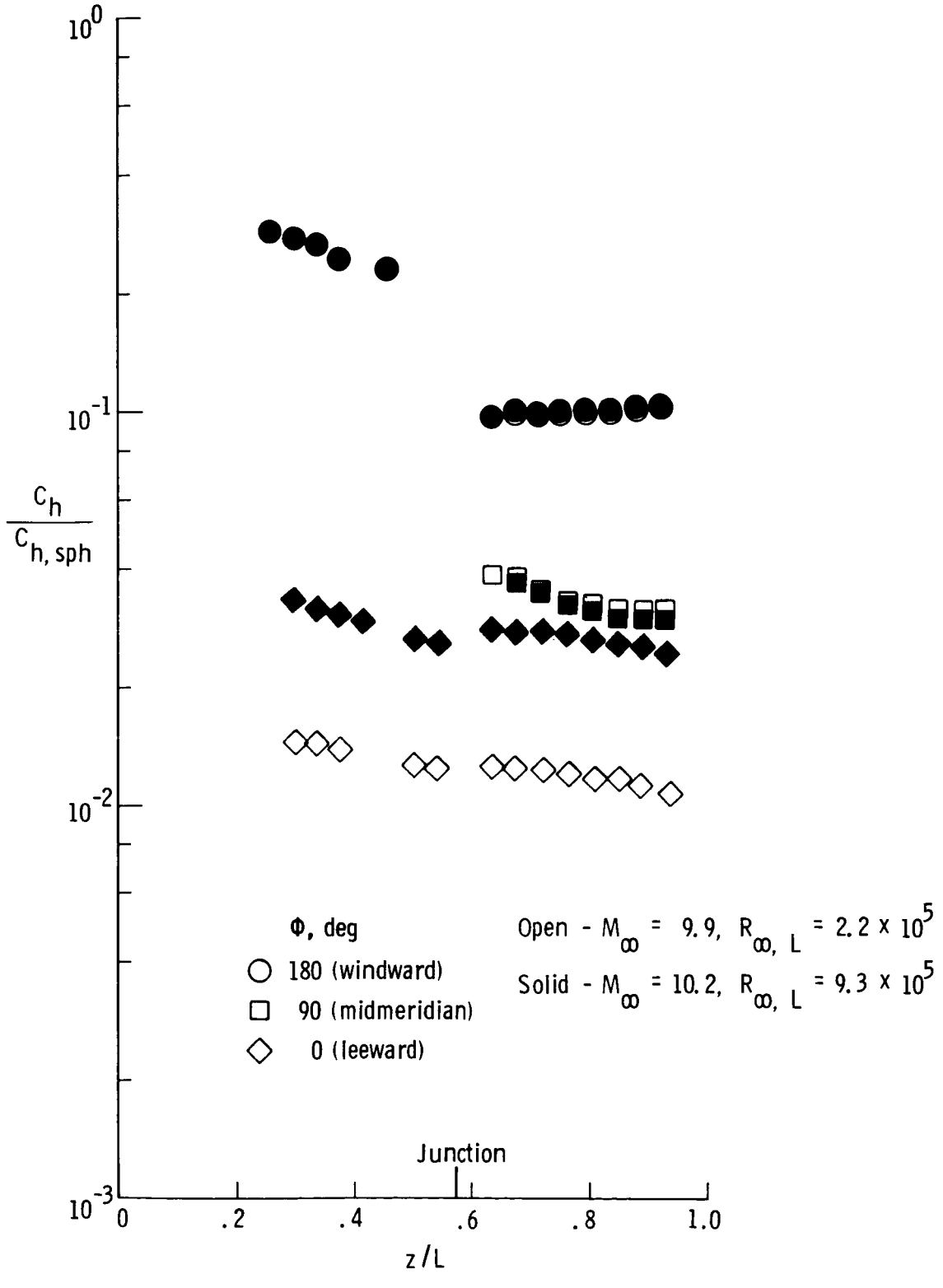

(f) $\alpha = 20°$.

Figure 13. Concluded.

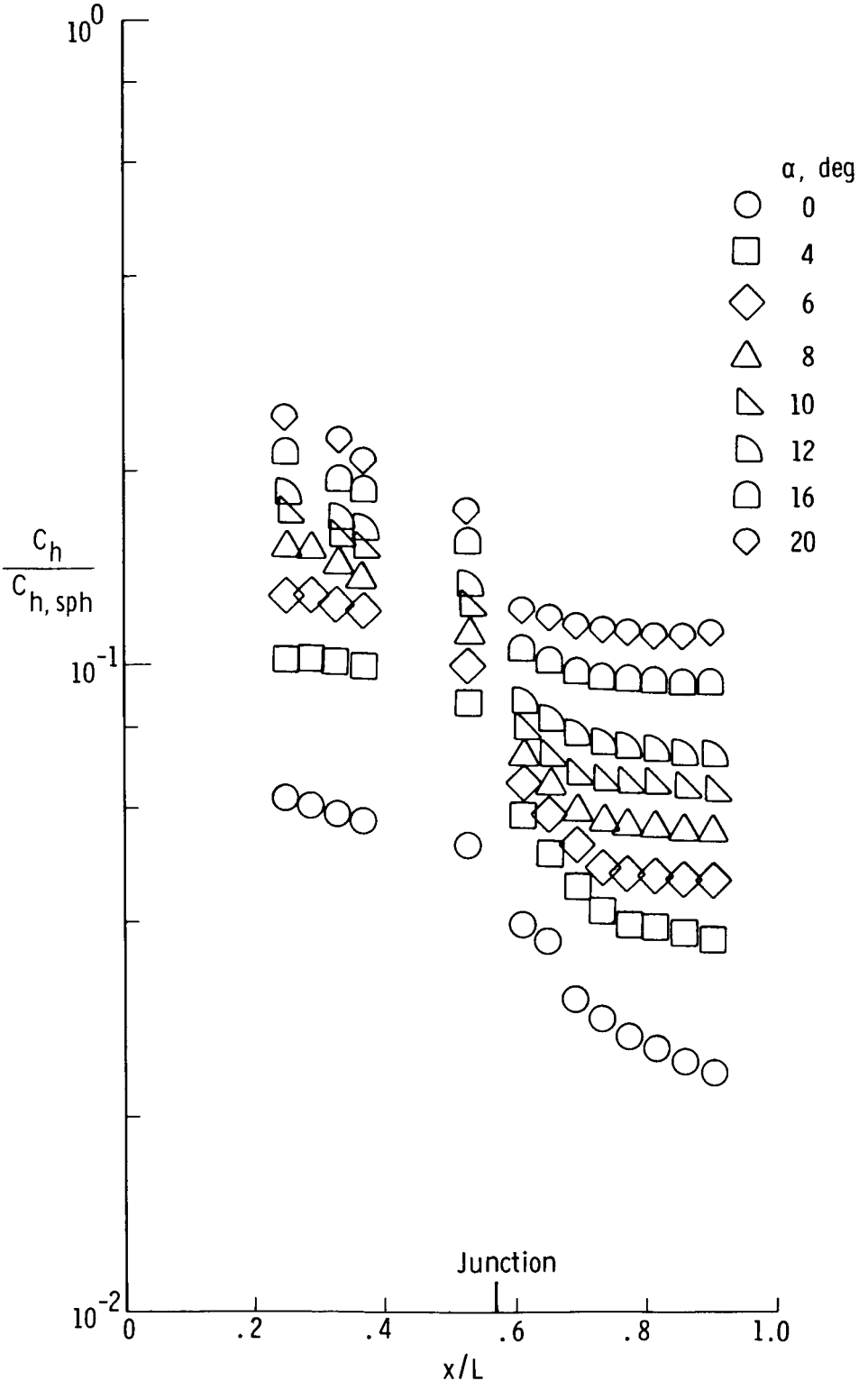

(a) Straight biconic.

Figure 14. Effect of angle of attack on windward heating distribution for both straight and bent-nose biconics. $R_{\infty,L} \approx 2.2 \times 10^5$.

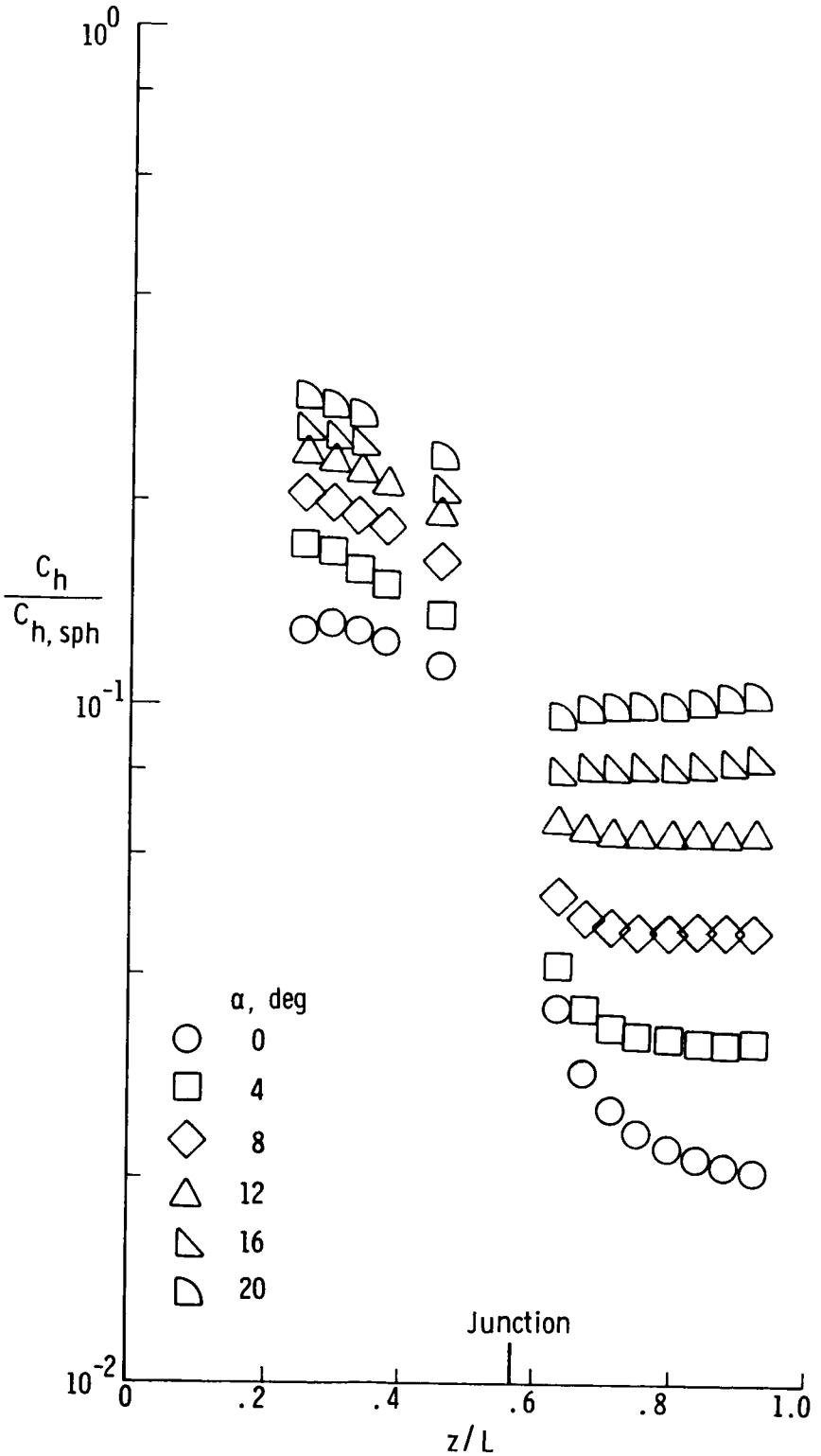

(b) Bent-nose biconic.

Figure 14. Concluded.

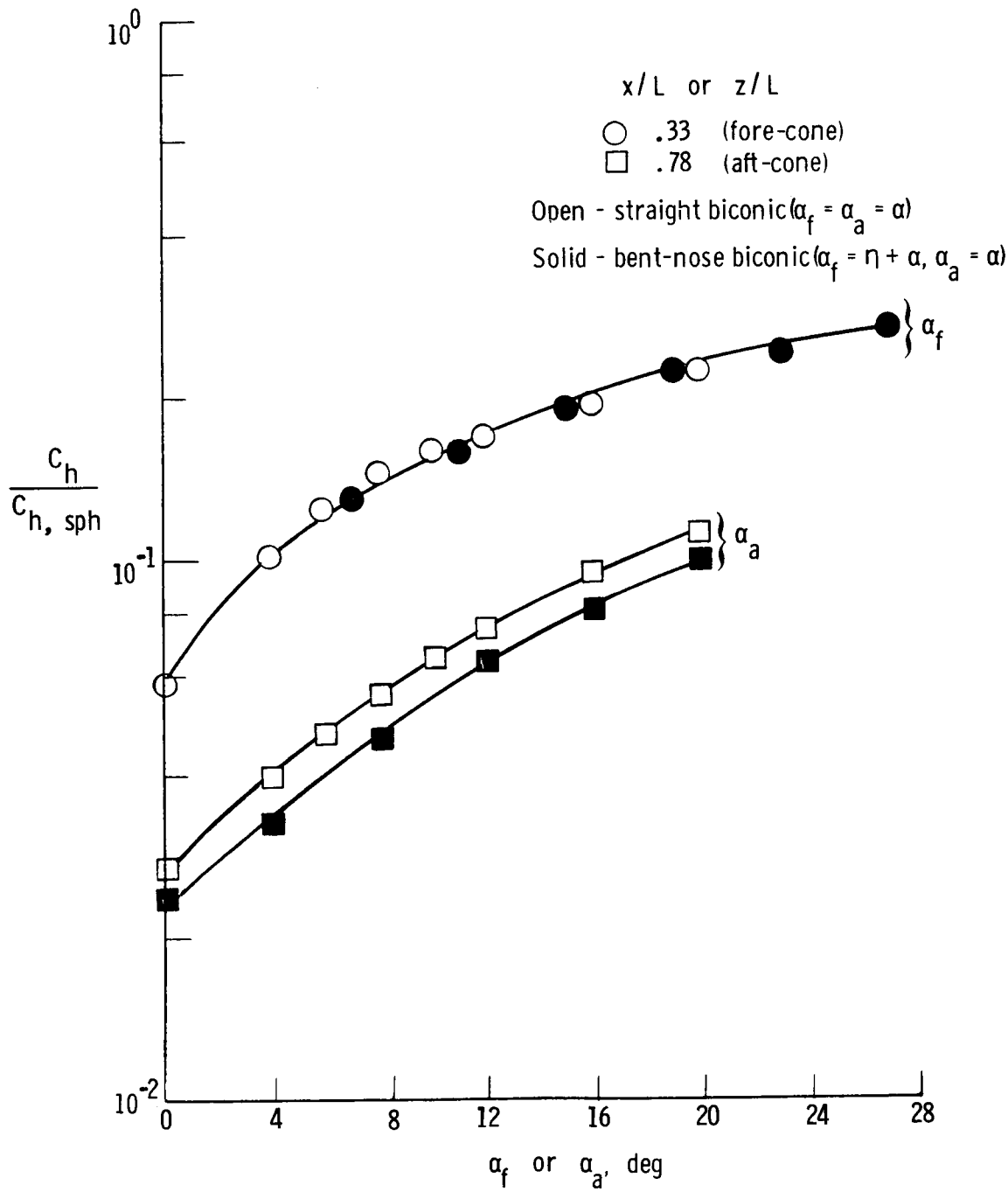

Figure 15. Variation of windward fore-cone and aft-cone heating with angle of attack for both biconics. $R_{\infty,L} \approx 2.2 \times 10^5$.

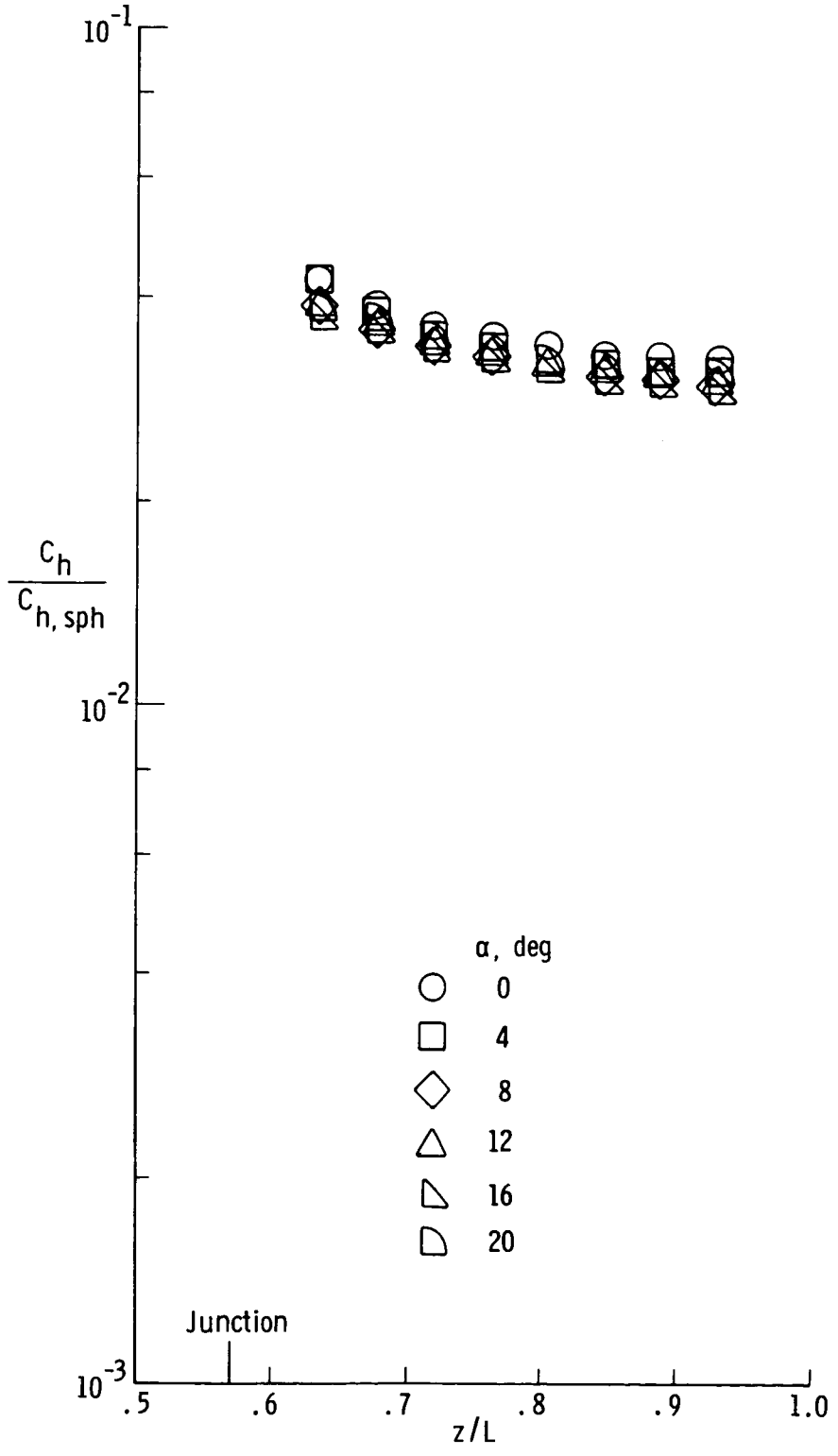

(a) Bent-nose biconic.

Figure 16. Effect of angle of attack on heating along midmeridian ray of aft-cone. $R_{\infty,L} \approx 2.2 \times 10^5$.

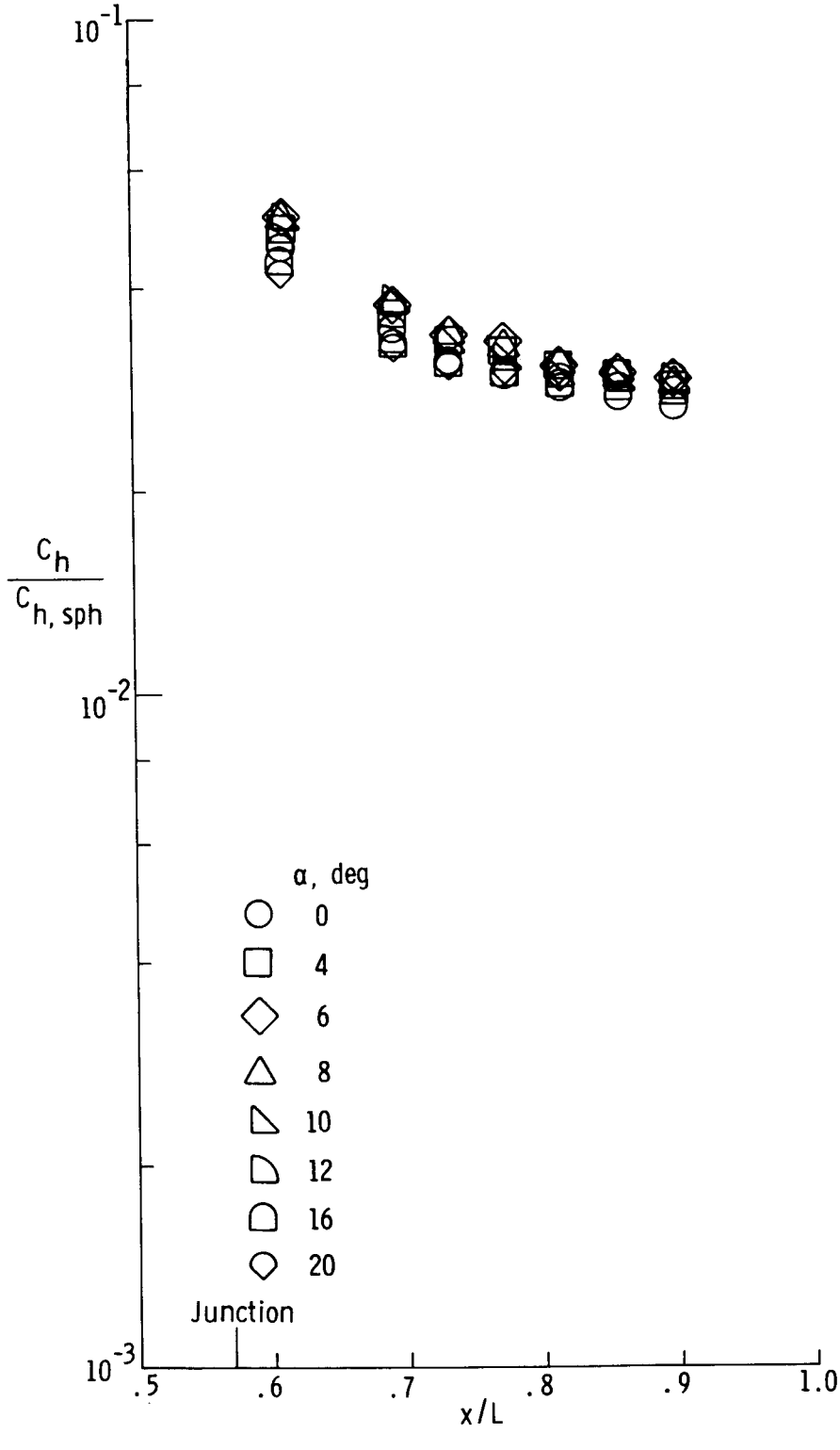

(b) Straight biconic.

Figure 16. Concluded.

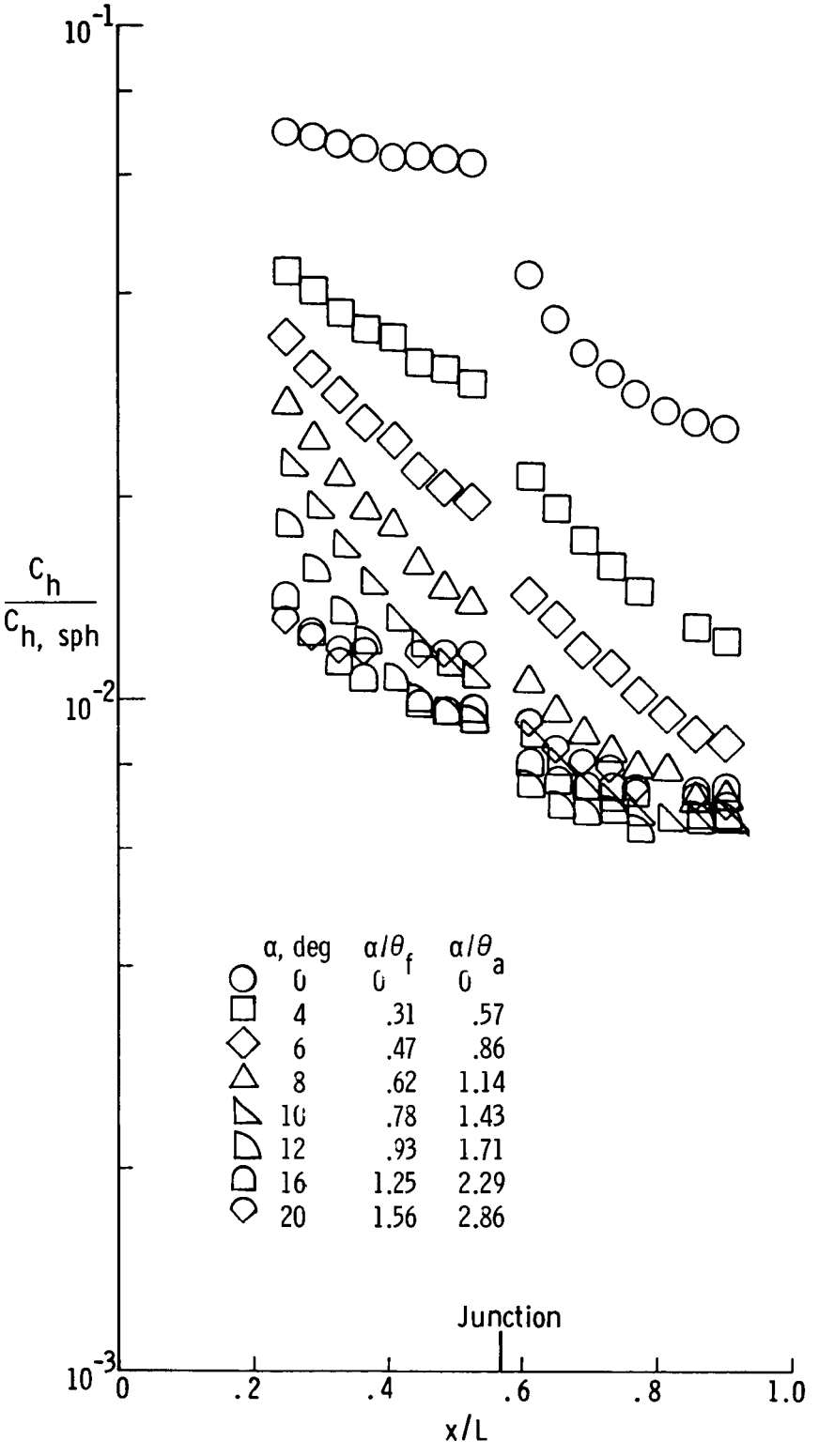

(a) Straight biconic; $R_{\infty,L} \approx 2.2 \times 10^5$.

Figure 17. Effect of angle of attack on leeward heating distribution for both biconics.

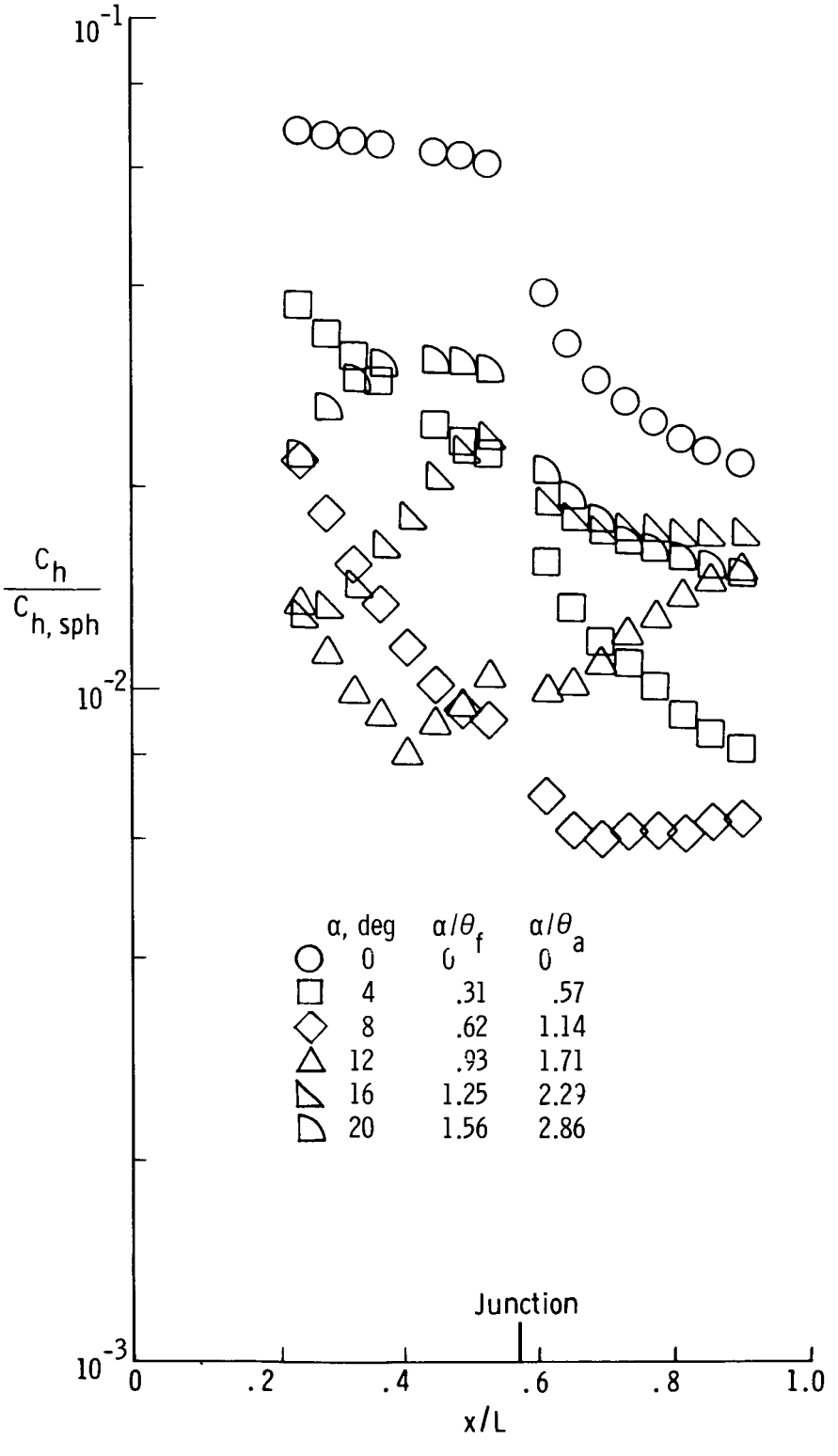

(b) Straight biconic; $R_{\infty,L} \approx 9.3 \times 10^5$.

Figure 17. Continued.

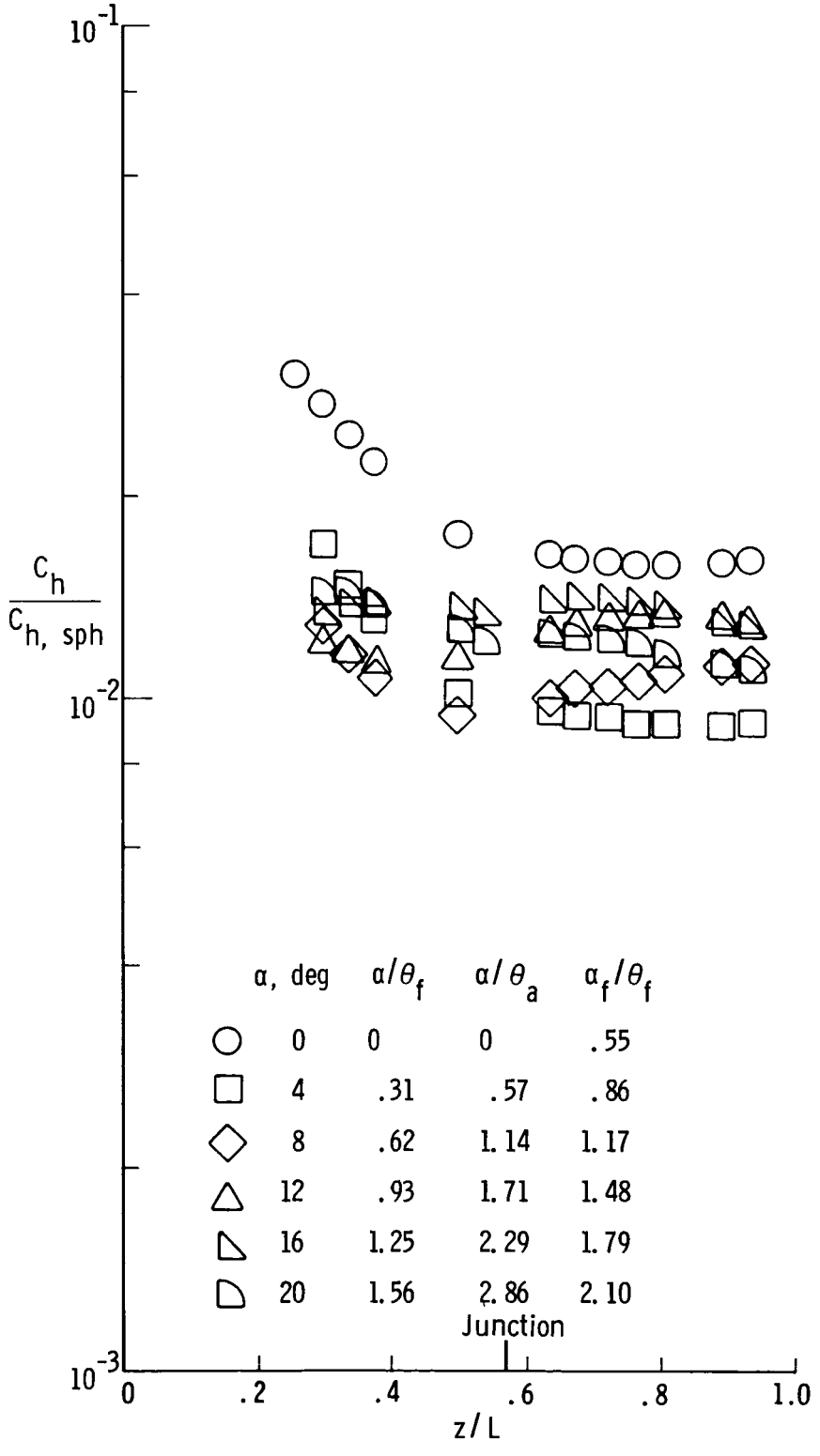

(c) Bent-nose biconic; $R_{\infty,L} \approx 2.2 \times 10^5$.

Figure 17. Continued.

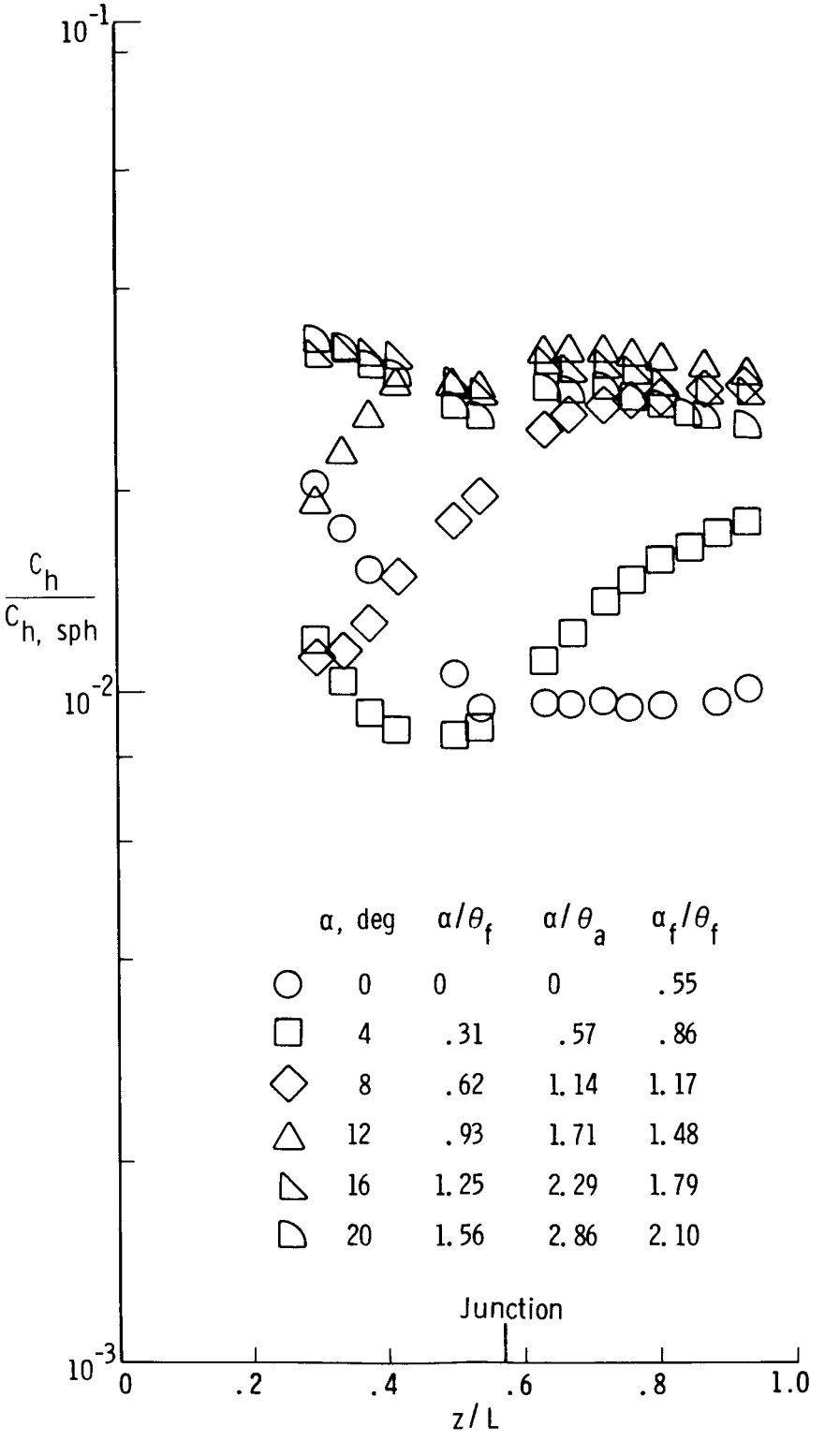

(d) Bent-nose biconic; $R_{\infty,L} \approx 9.3 \times 10^5$.

Figure 17. Concluded.

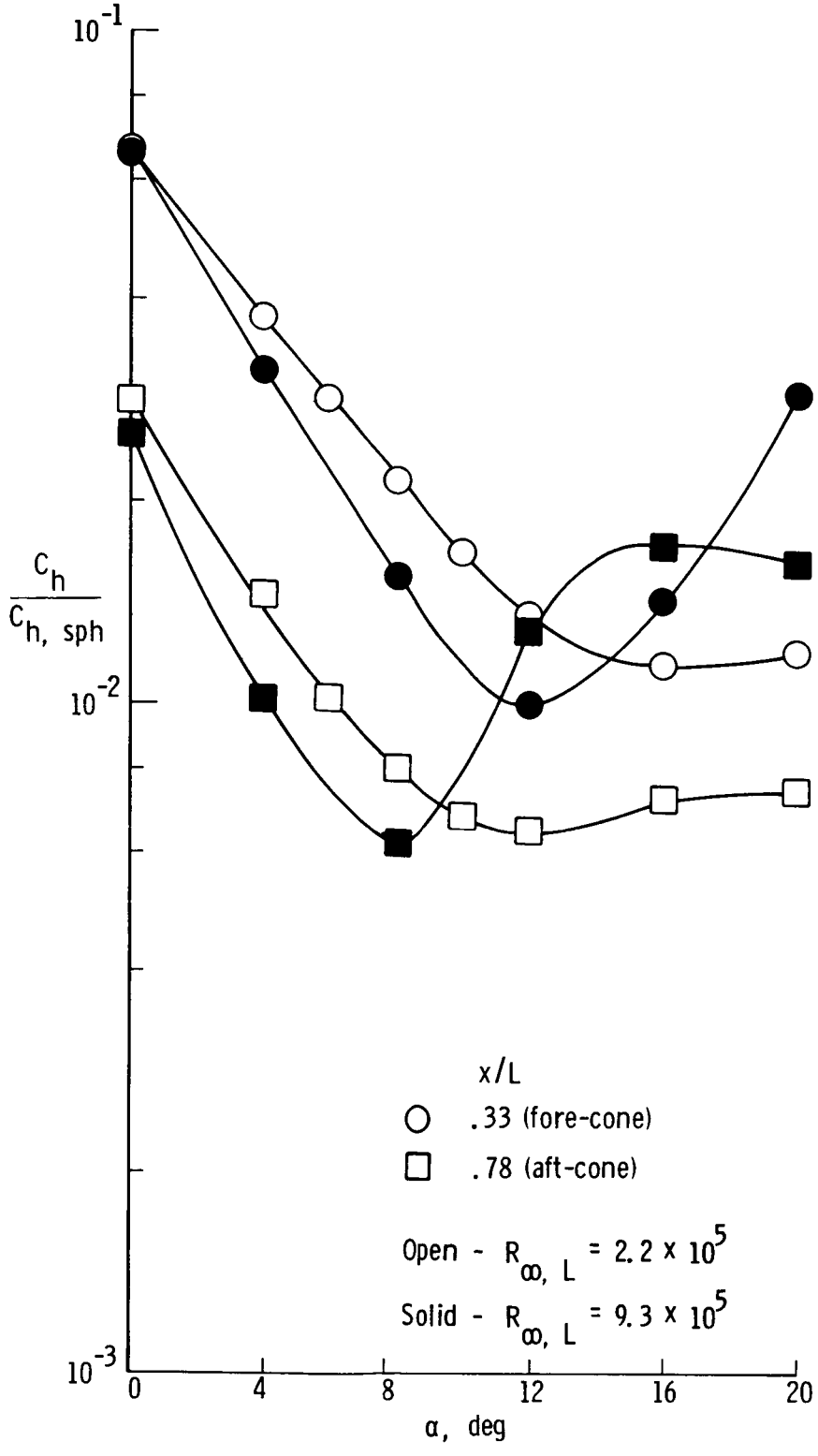

(a) Straight biconic.

Figure 18. Effect of angle of attack on leeward heating.

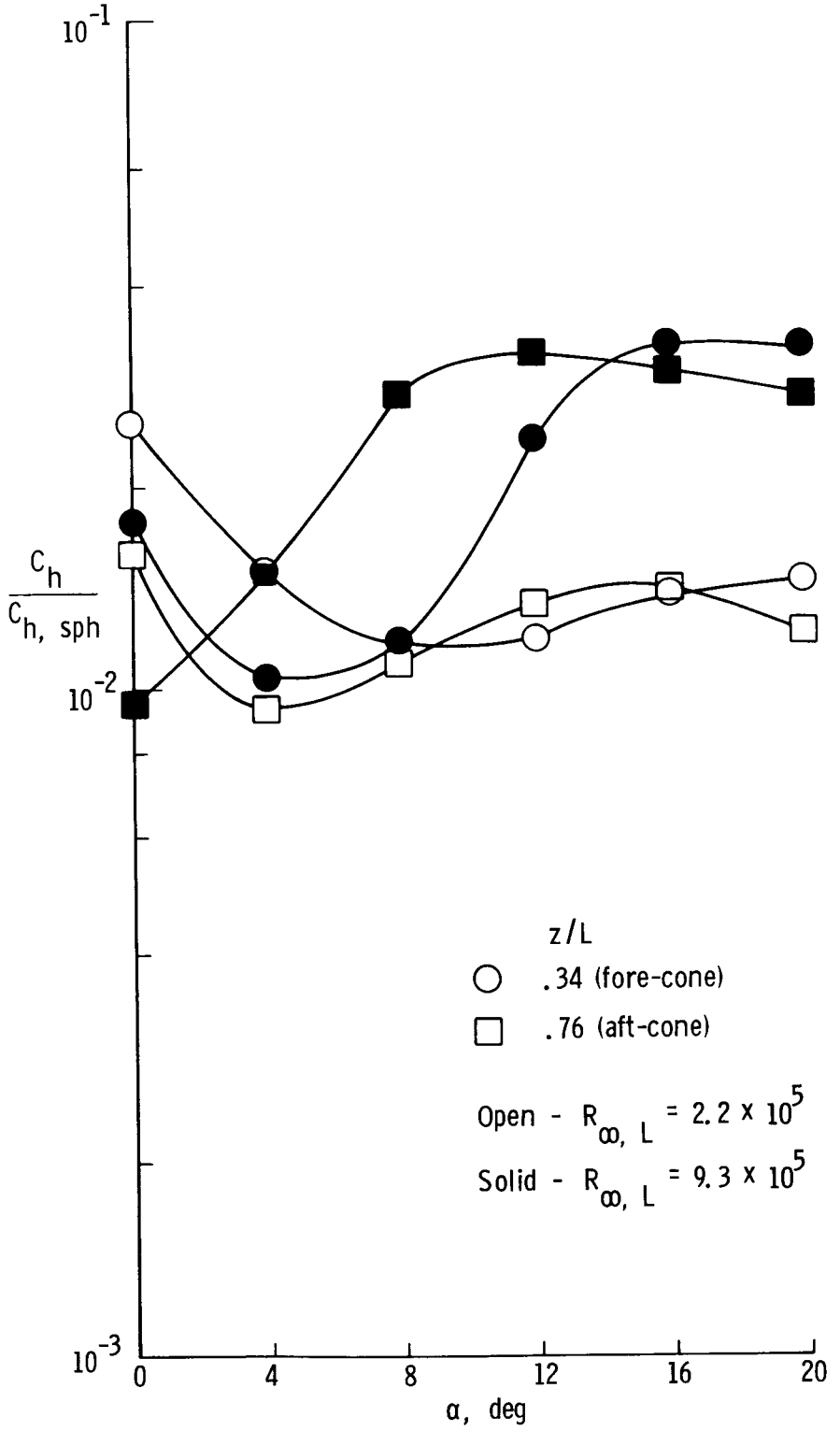

(b) Bent-nose biconic.

Figure 18. Continued.

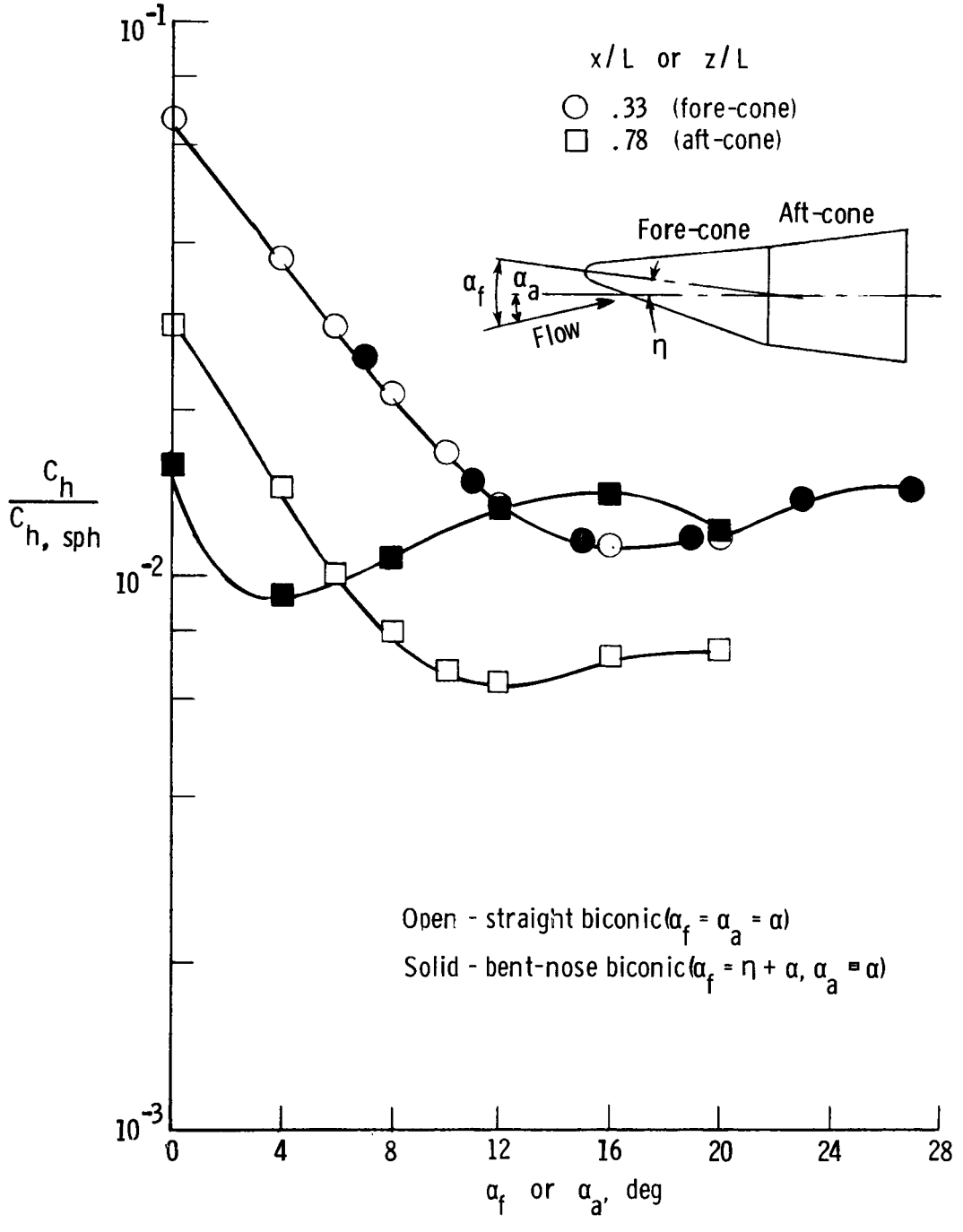

(c) Both biconics, $R_{\infty,L} \approx 2.2 \times 10^5$.

Figure 18. Concluded.

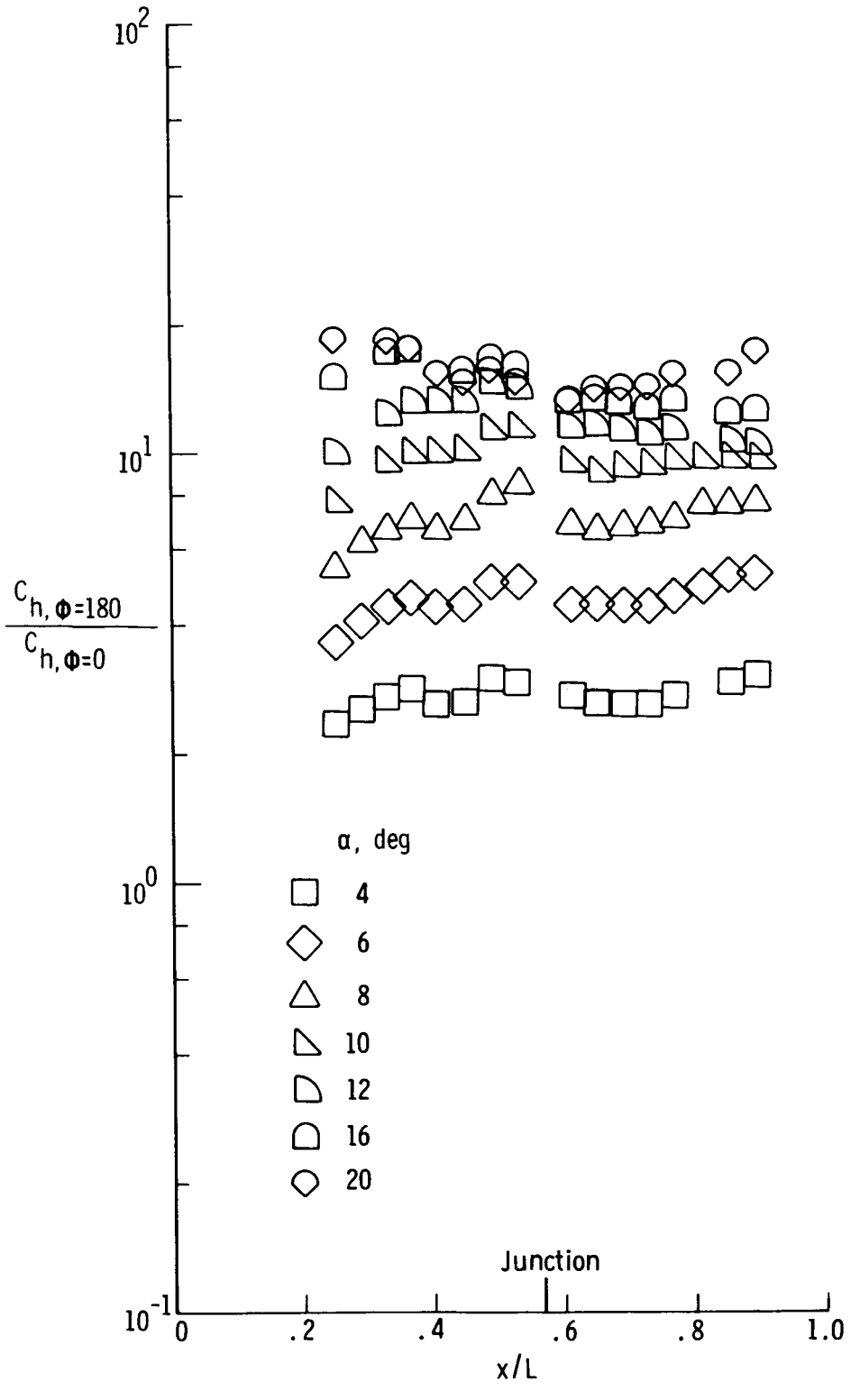

(a) Straight biconic, $R_{\infty,L} \approx 2.2 \times 10^5$.

Figure 19. Ratio of windward heating to leeward heating for both biconics.

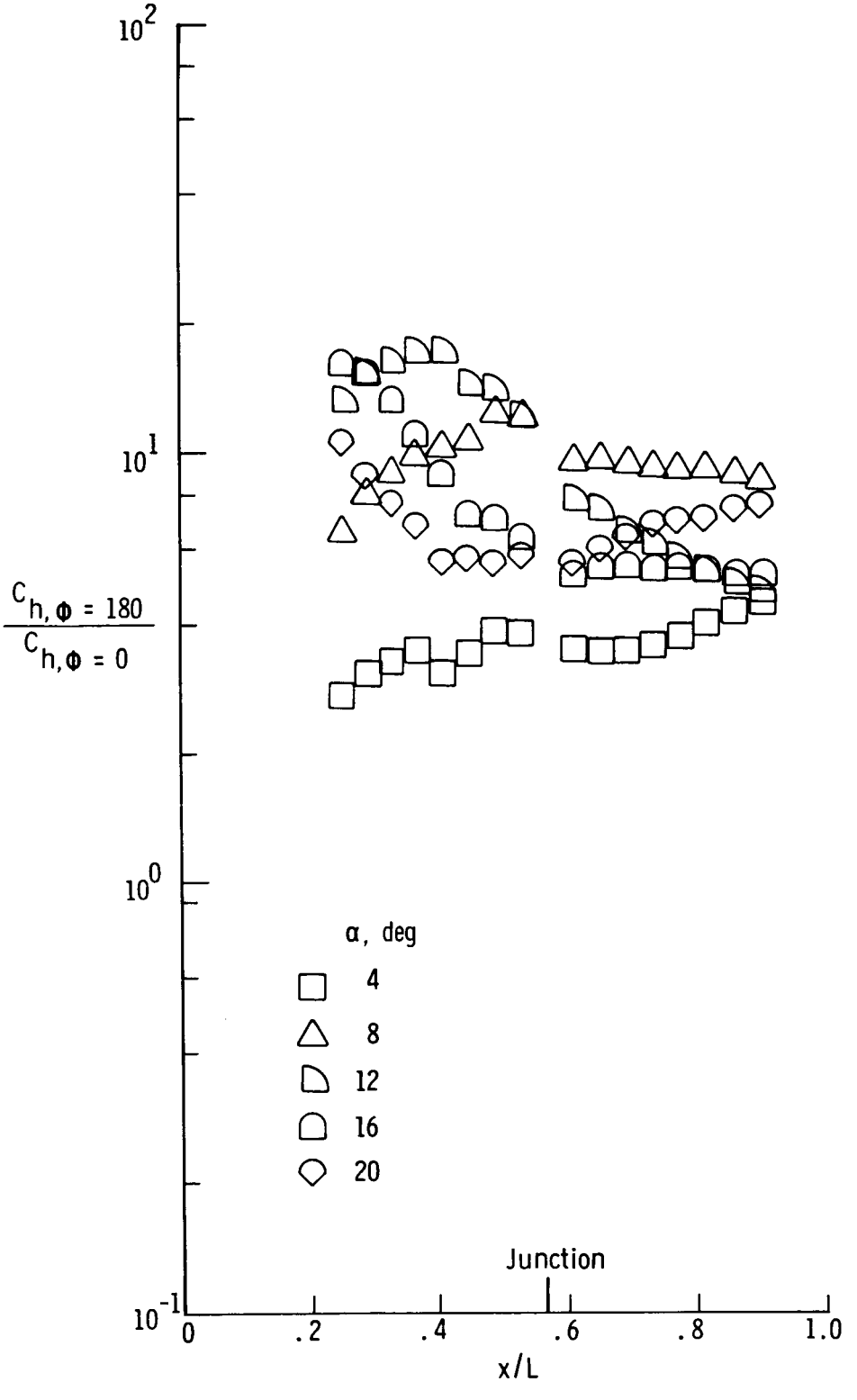

(b) Straight biconic, $R_{\infty,L} \approx 9.3 \times 10^5$.

Figure 19. Continued.

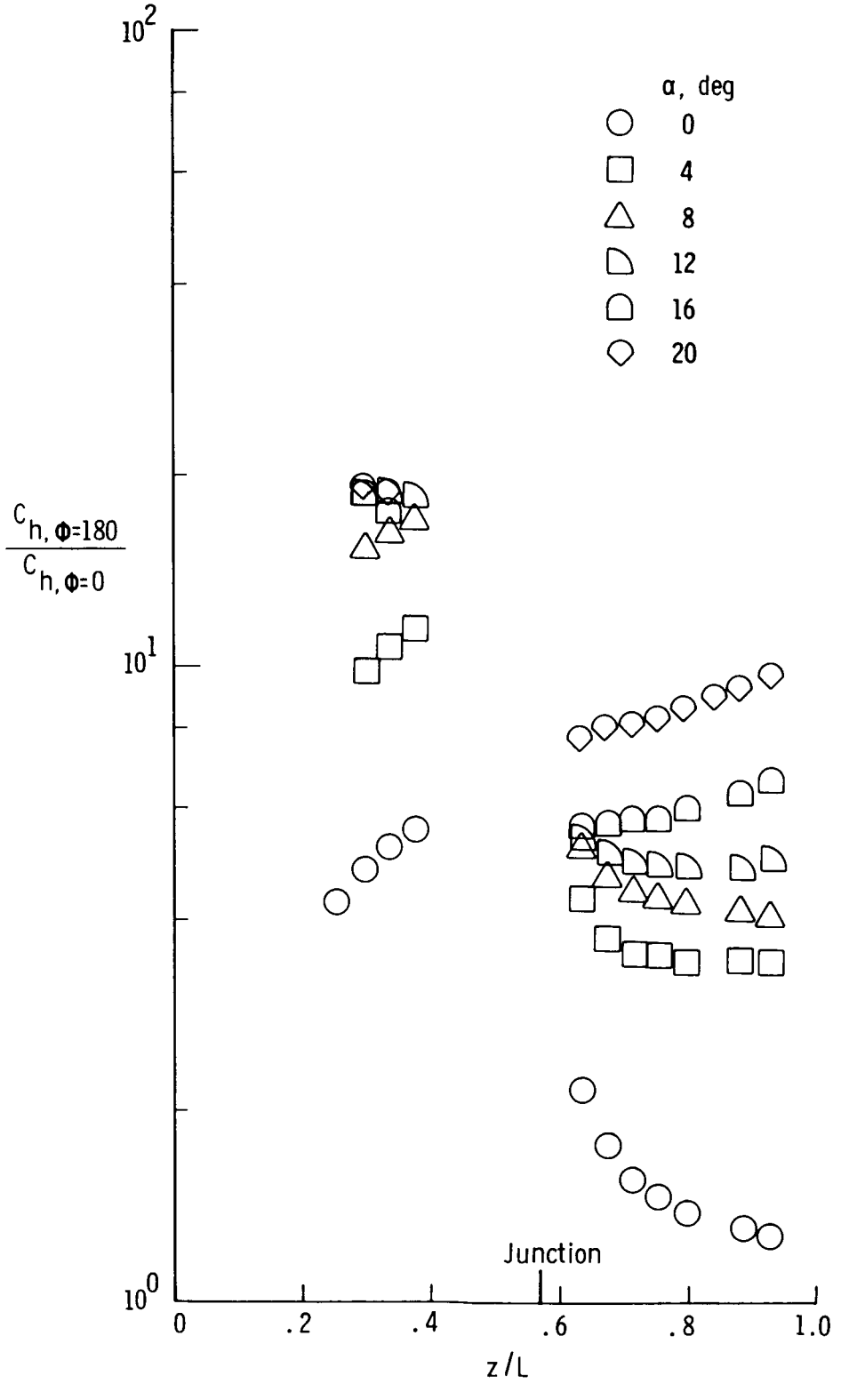

(c) Bent-nose biconic, $R_{\infty,L} \approx 2.2 \times 10^5$.

Figure 19. Continued.

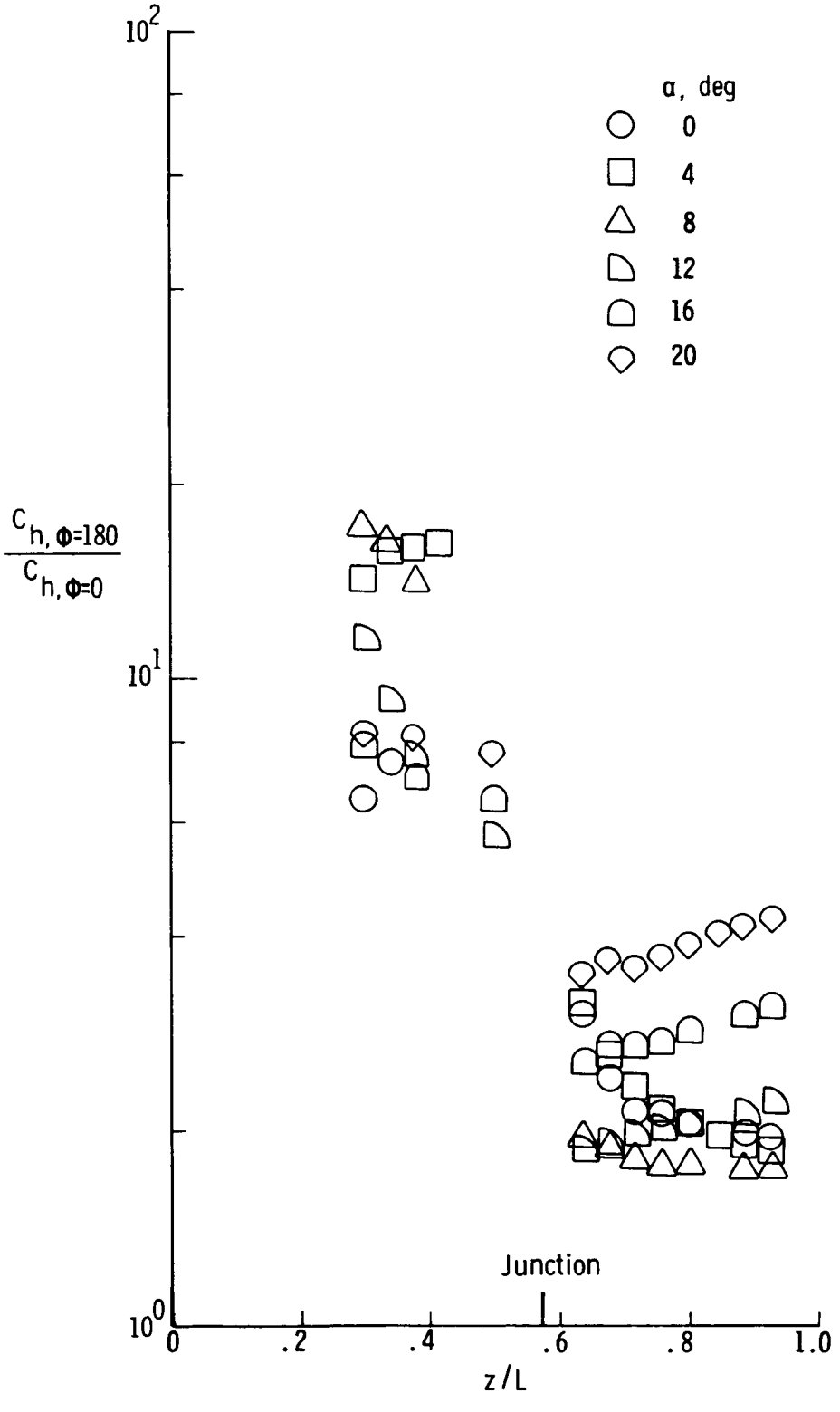

(d) Bent-nose biconic, $R_{\infty,L} \approx 9.3 \times 10^5$.

Figure 19. Concluded.

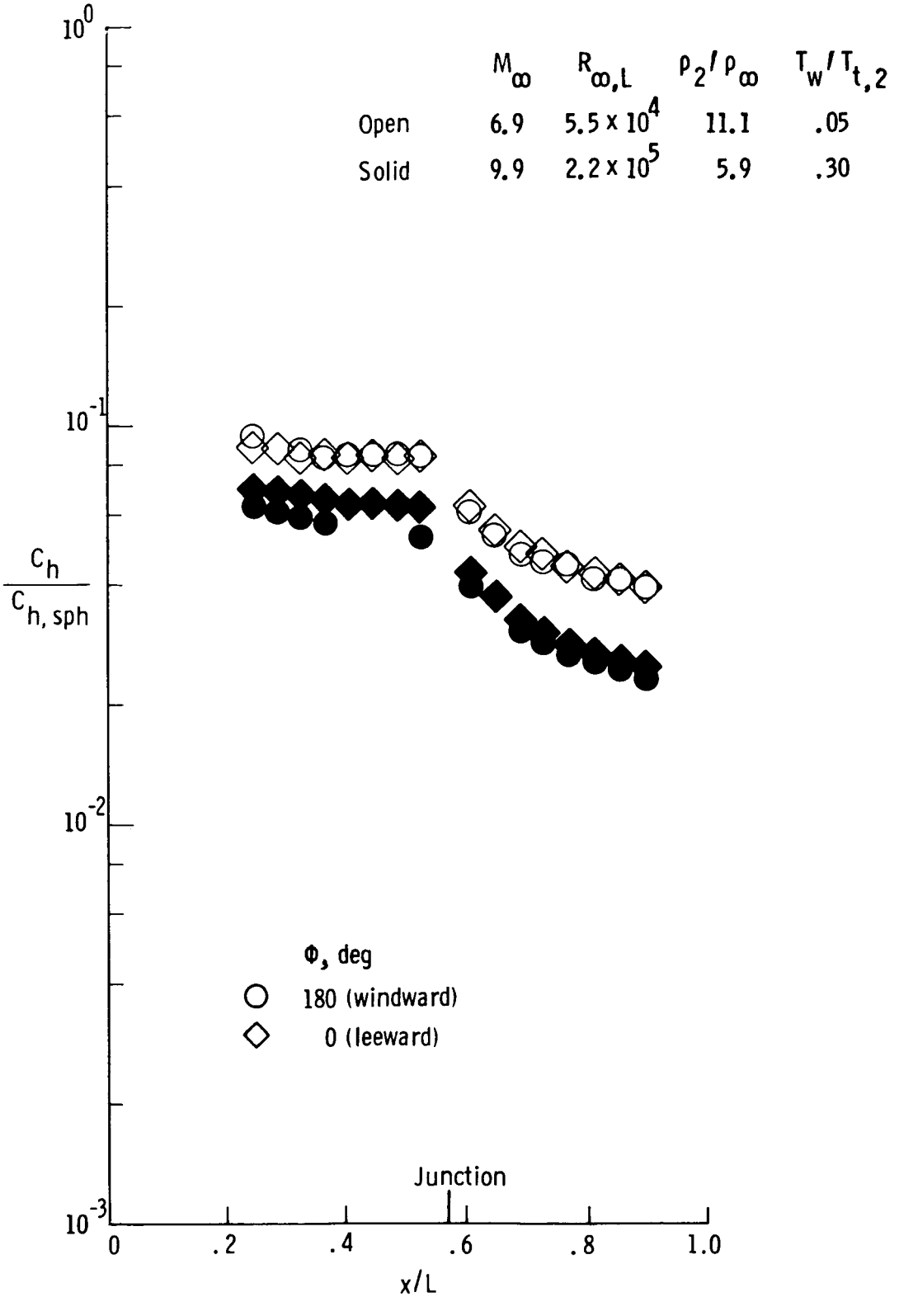

(a) $\alpha = 0°$.

Figure 20. Comparison of present heating of straight biconic in Mach 10 tunnel with that obtained with same model in expansion tube.

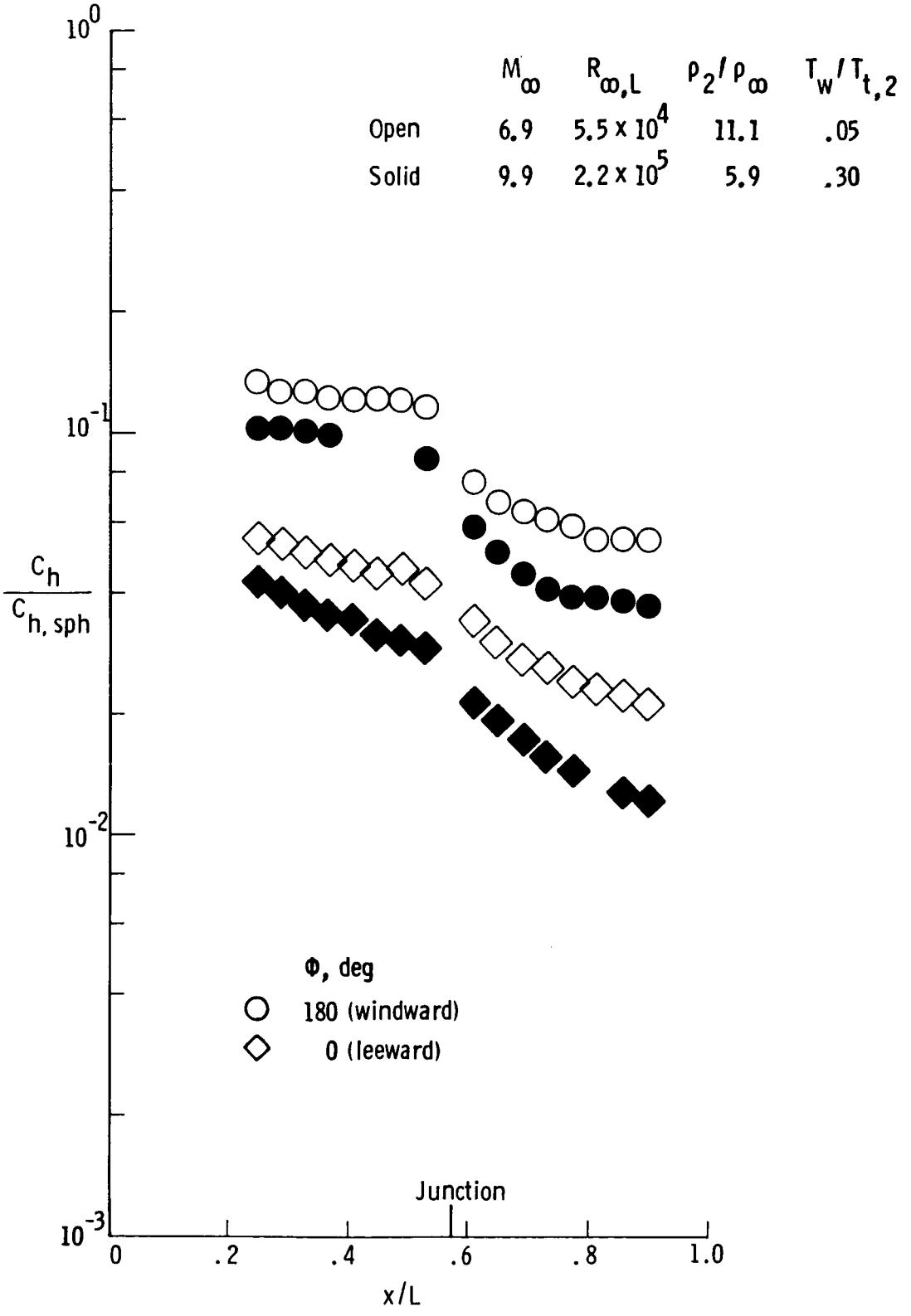

(b) $\alpha = 4°$.

Figure 20. Continued.

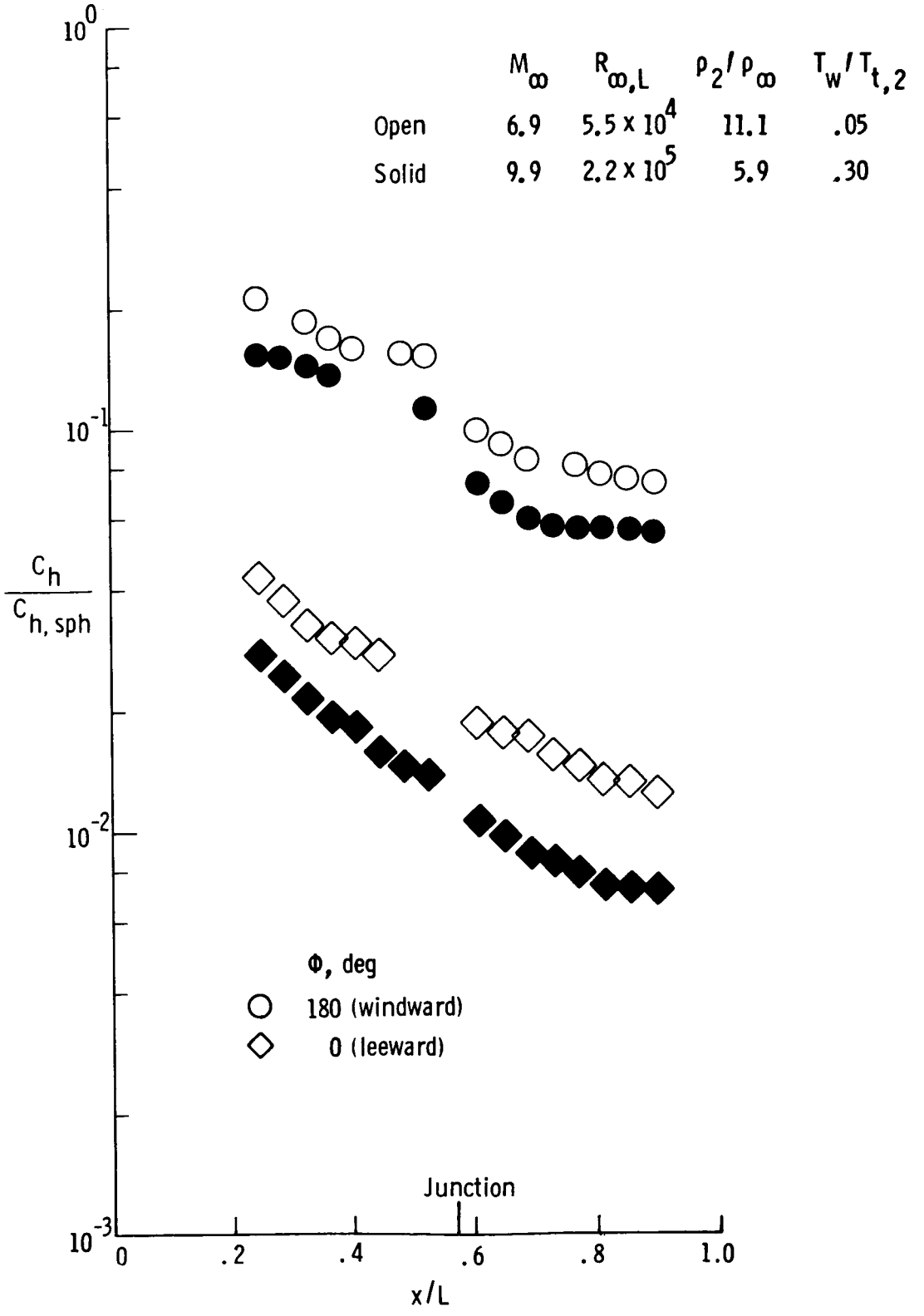

(c) $\alpha = 8°$.

Figure 20. Continued.

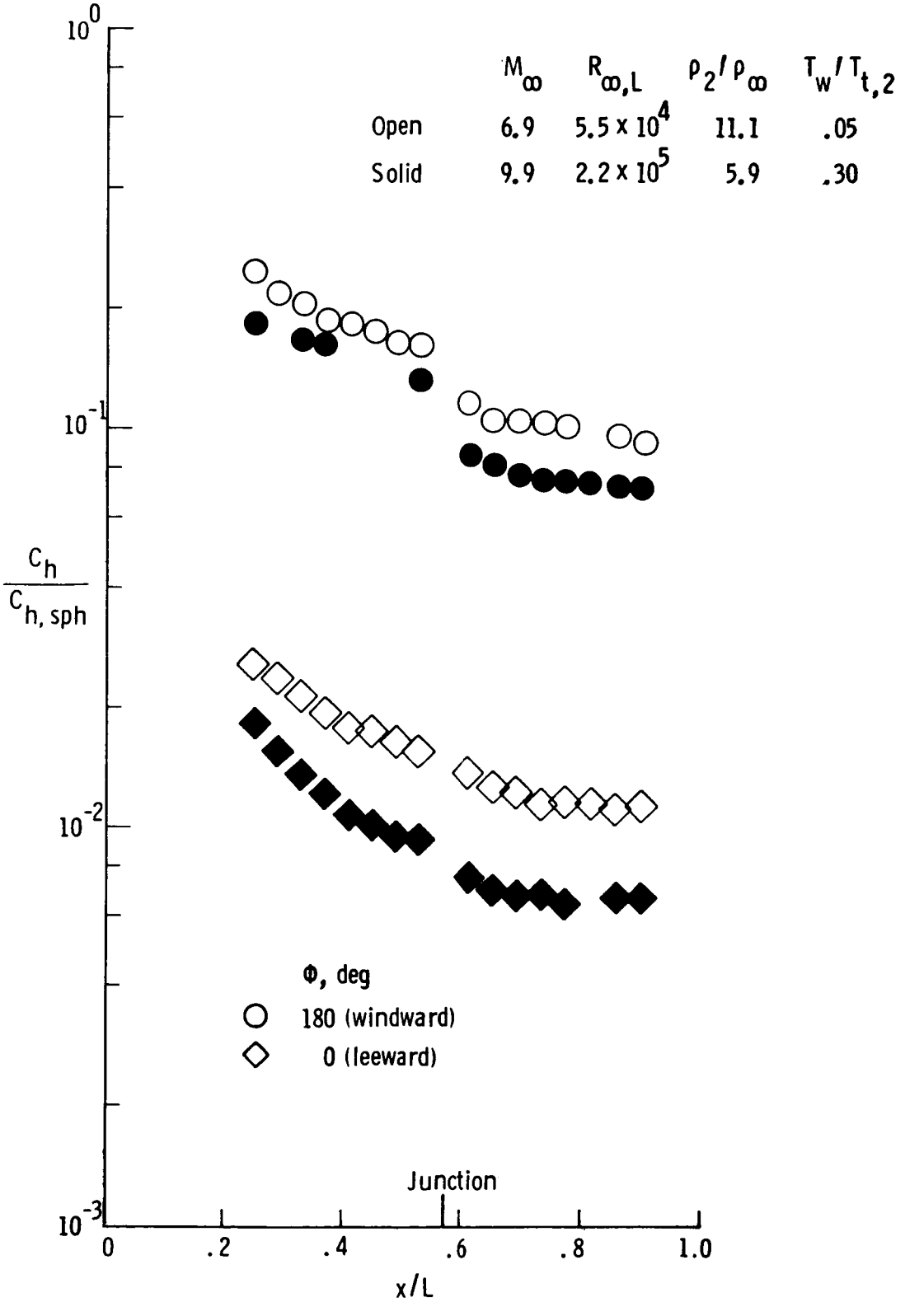

(d) $\alpha = 12°$.

Figure 20. Continued.

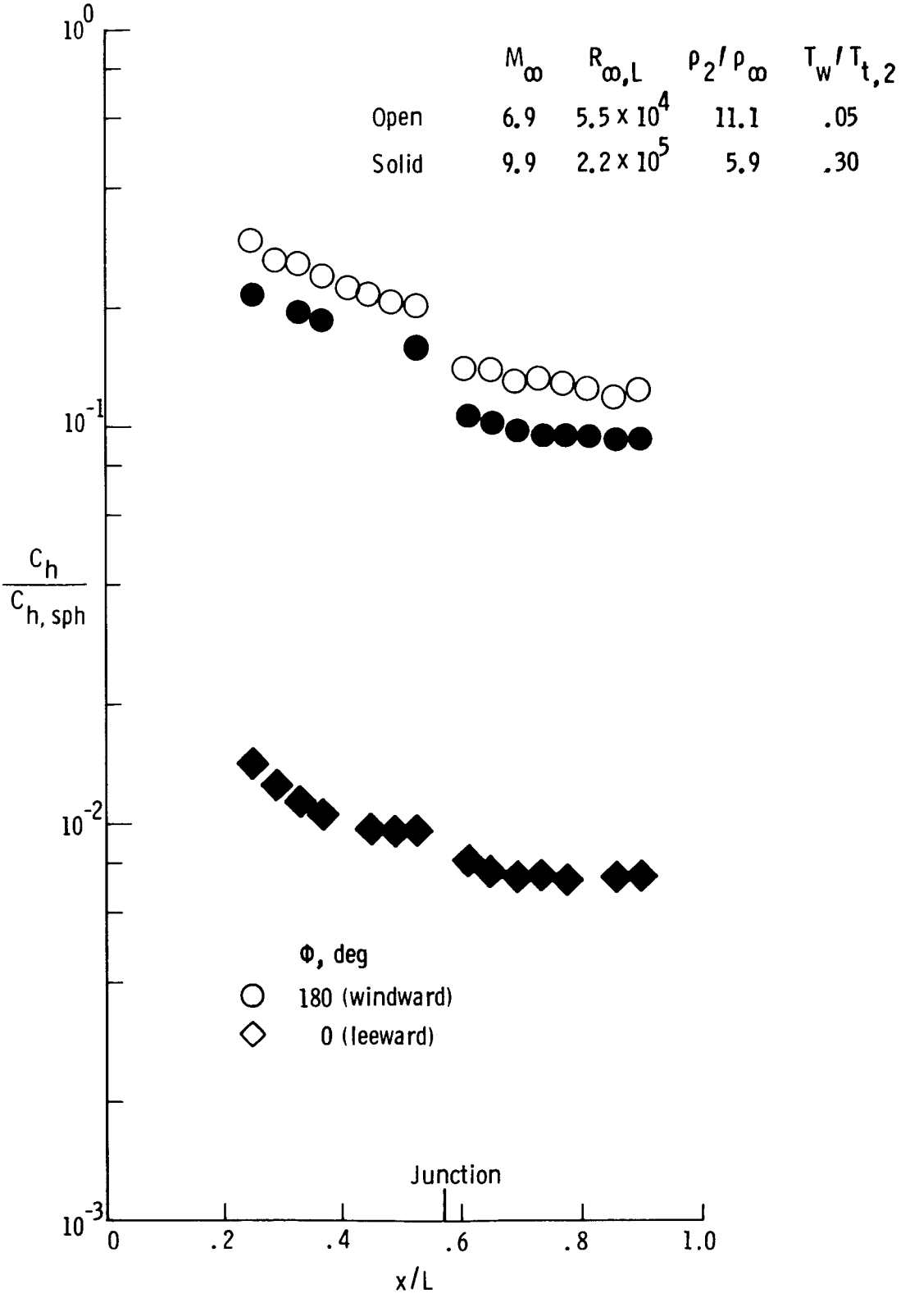

(e) $\alpha = 16°$.

Figure 20. Continued.

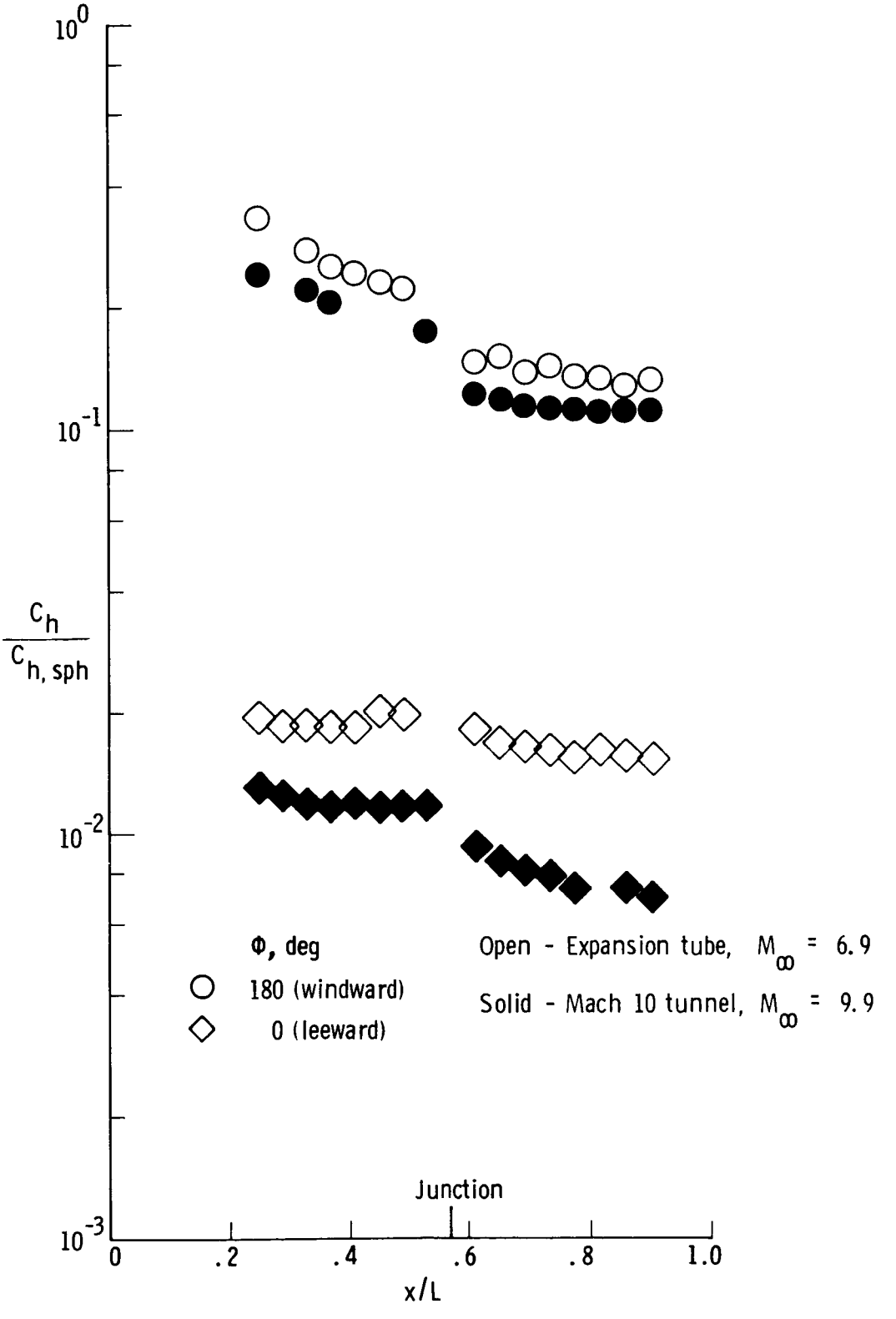

(f) $\alpha = 20°$.

Figure 20. Concluded.

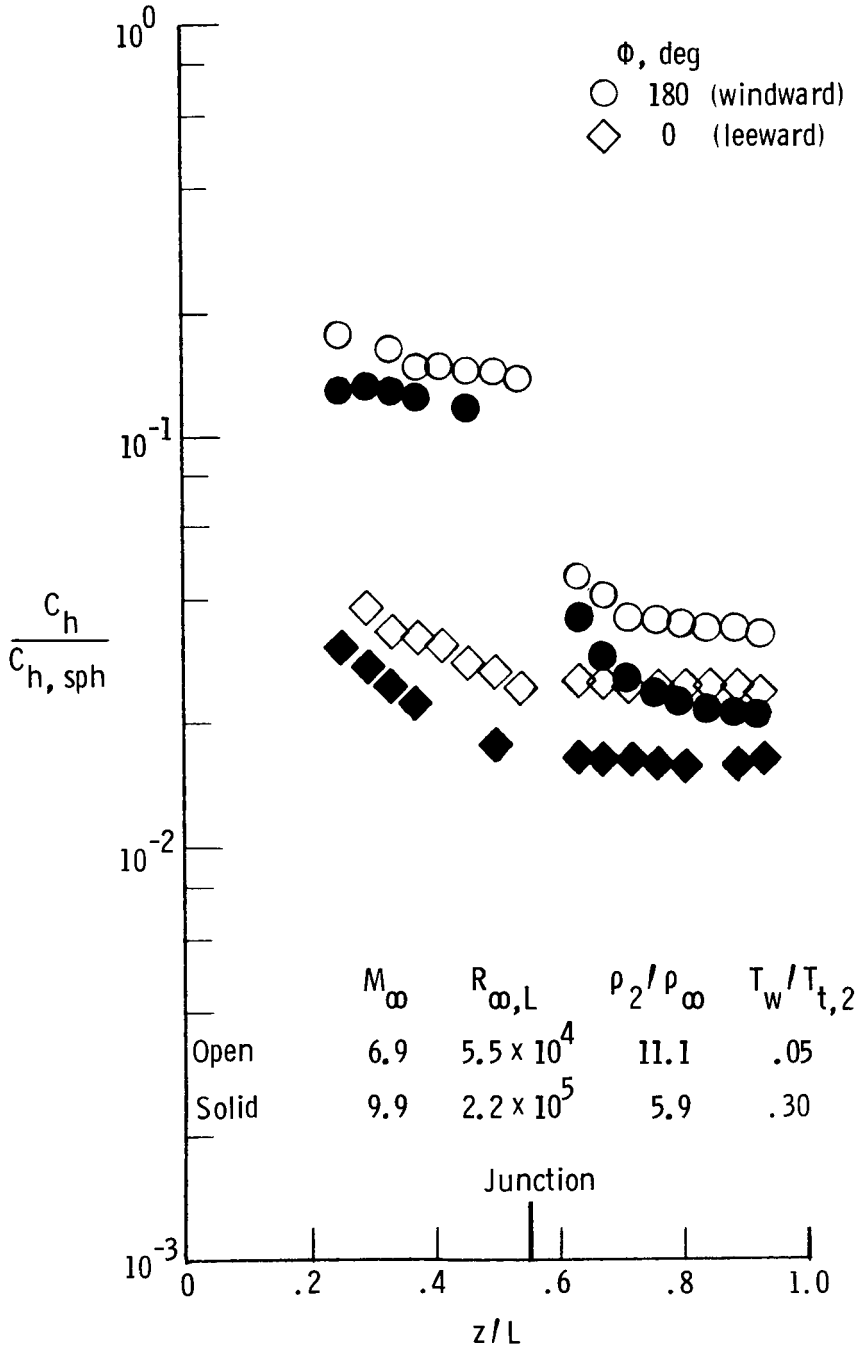

(a) $\alpha = 0°$.

Figure 21. Comparison of present heating of bent-nose biconic in Mach 10 tunnel with that obtained with same model in expansion tube.

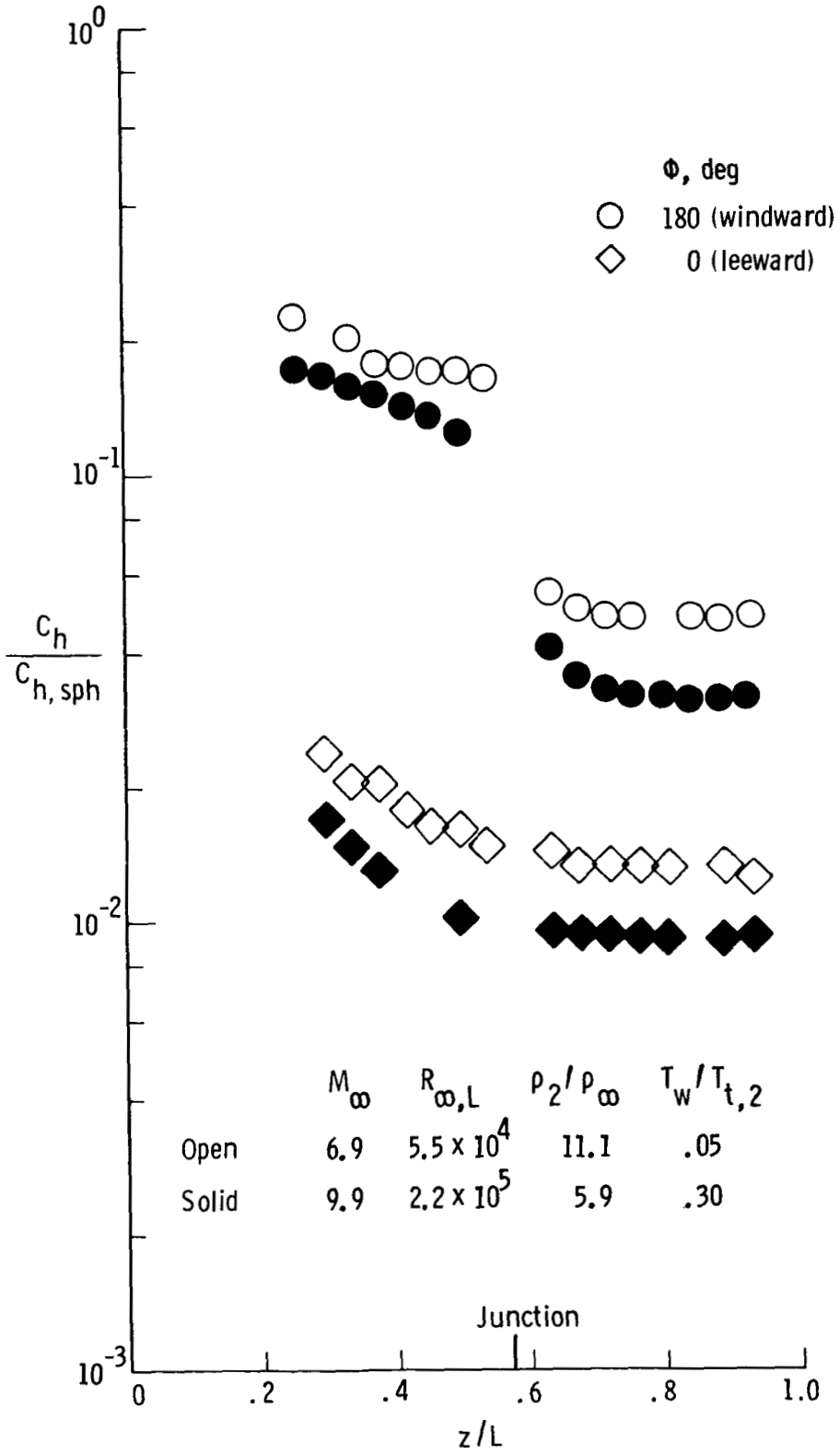

(b) $\alpha = 4°$.

Figure 21. Continued.

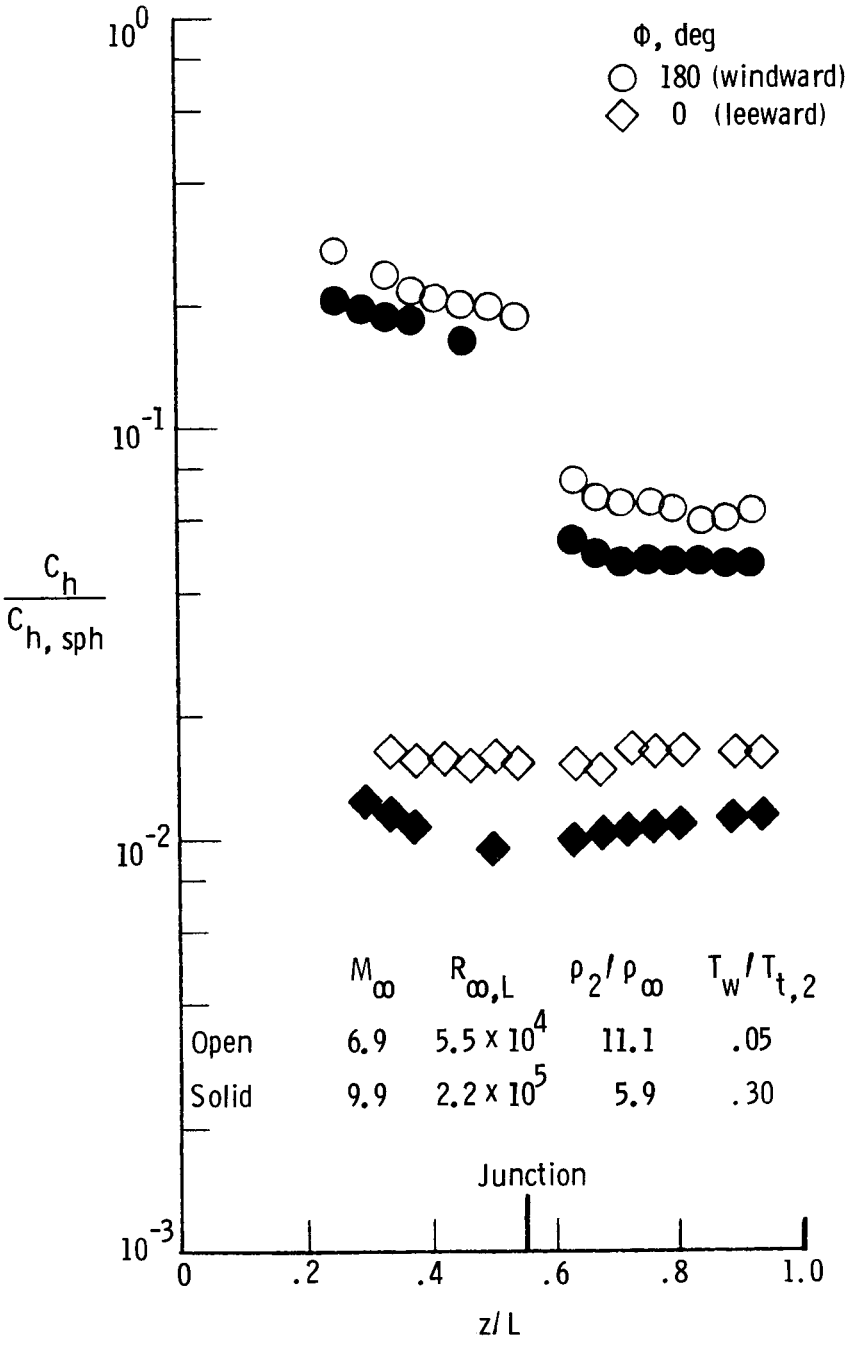

(c) $\alpha = 8°$.

Figure 21. Continued.

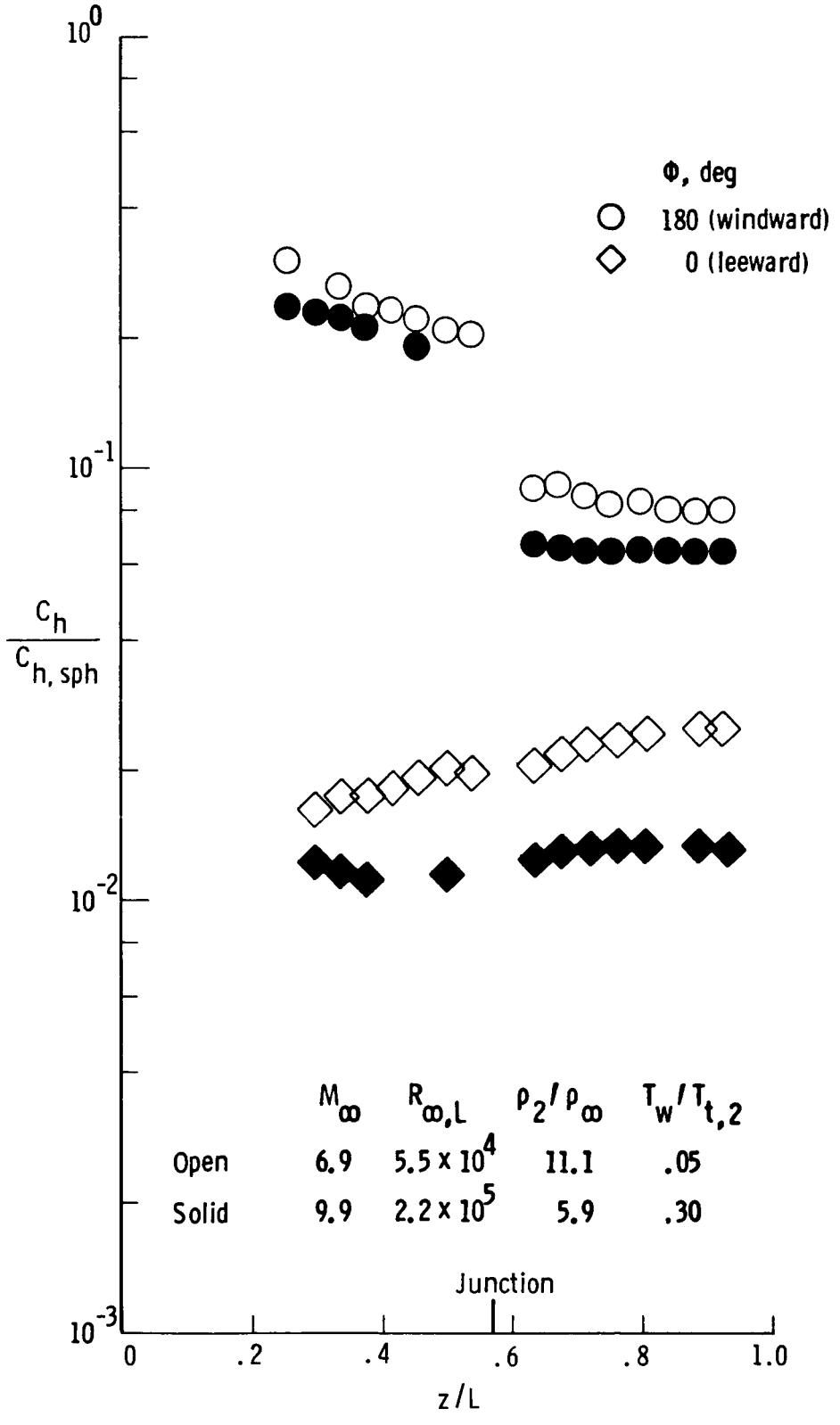

(d) $\alpha = 12°$.

Figure 21. Continued.

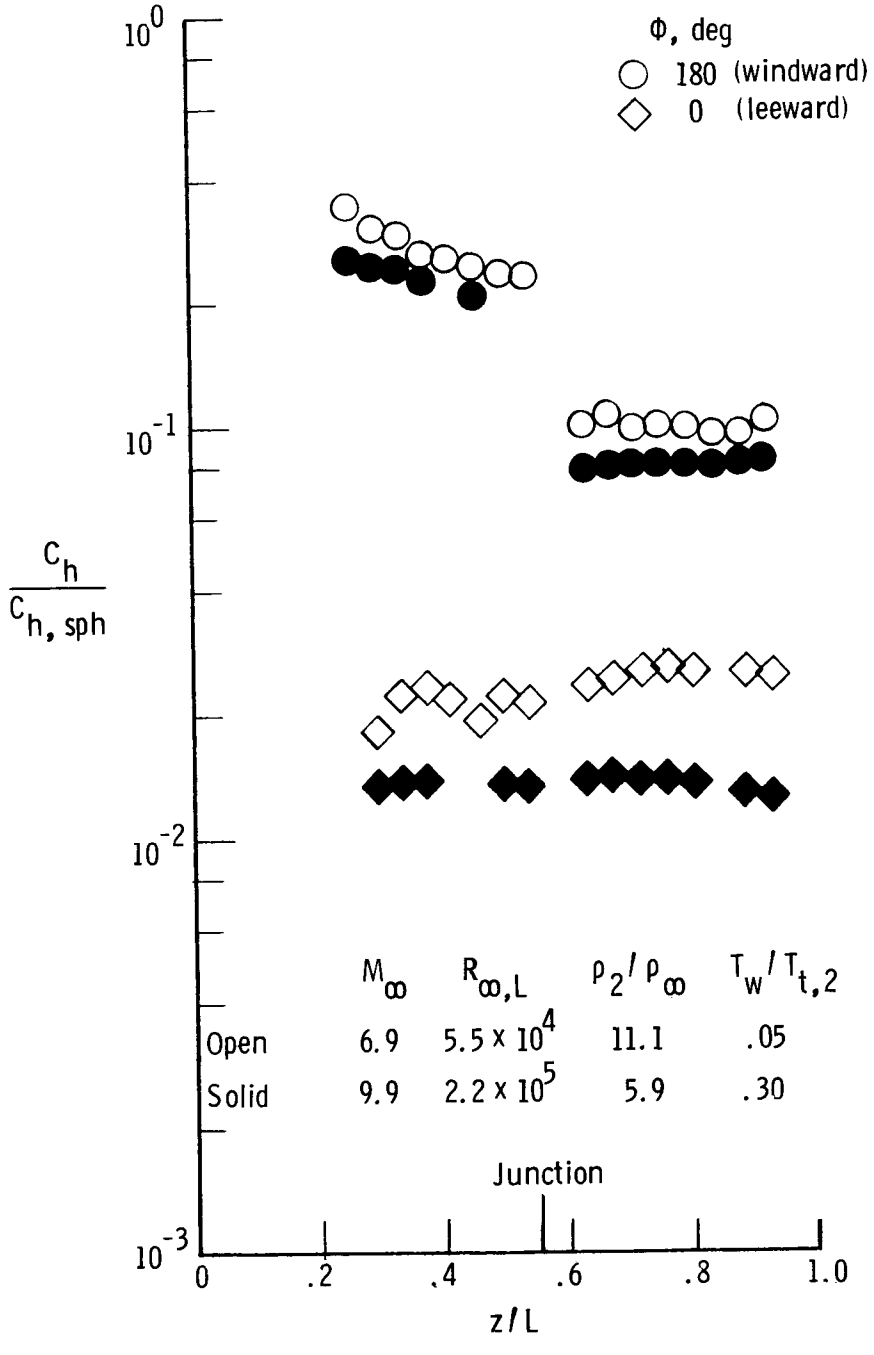

(e) $\alpha = 16°$.

Figure 21. Continued.

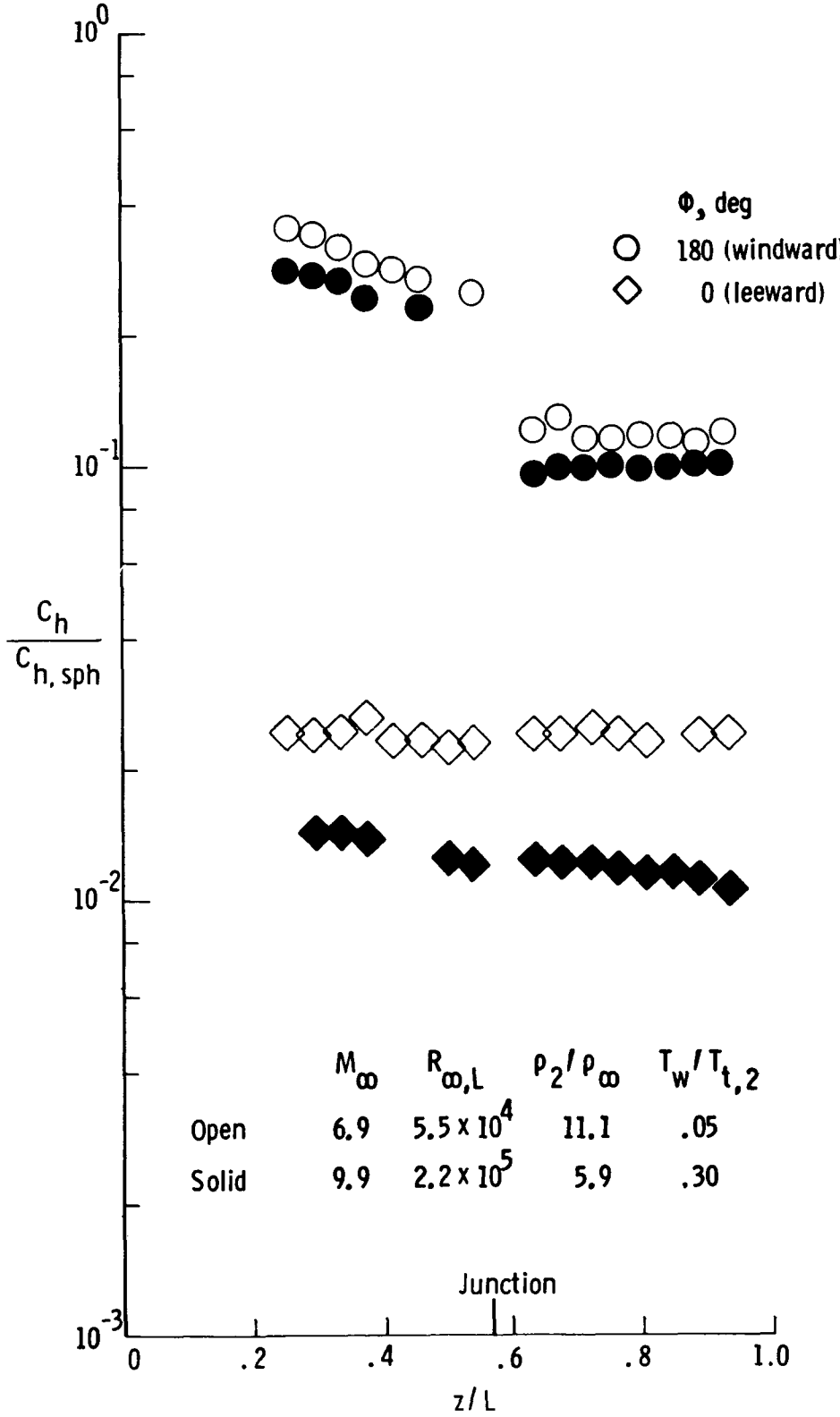

(f) $\alpha = 20°$.

Figure 21. Concluded.

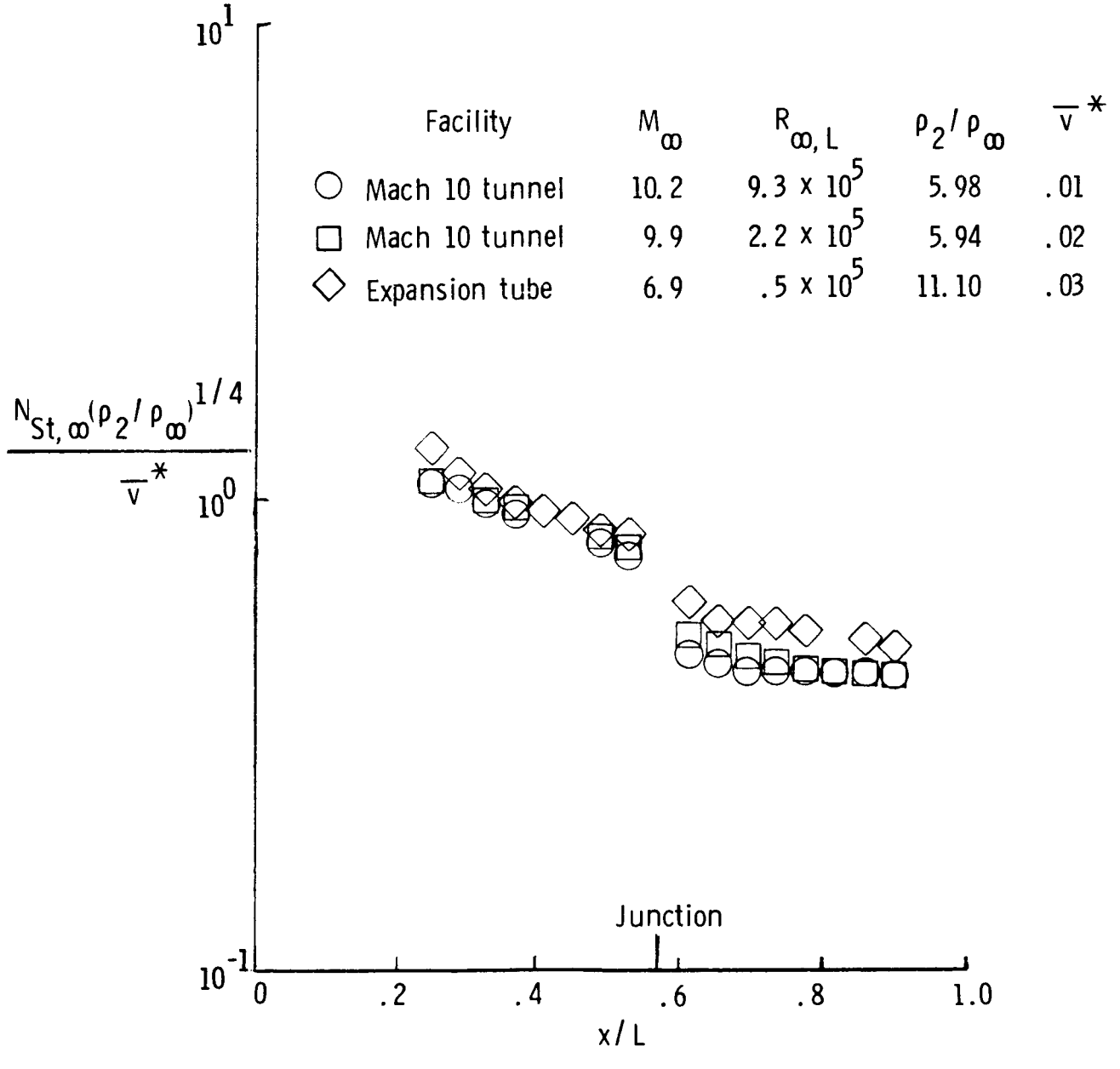

(a) $\alpha = 12°$.

Figure 22. Comparison of ideal-air and real-air windward heating on straight biconic.

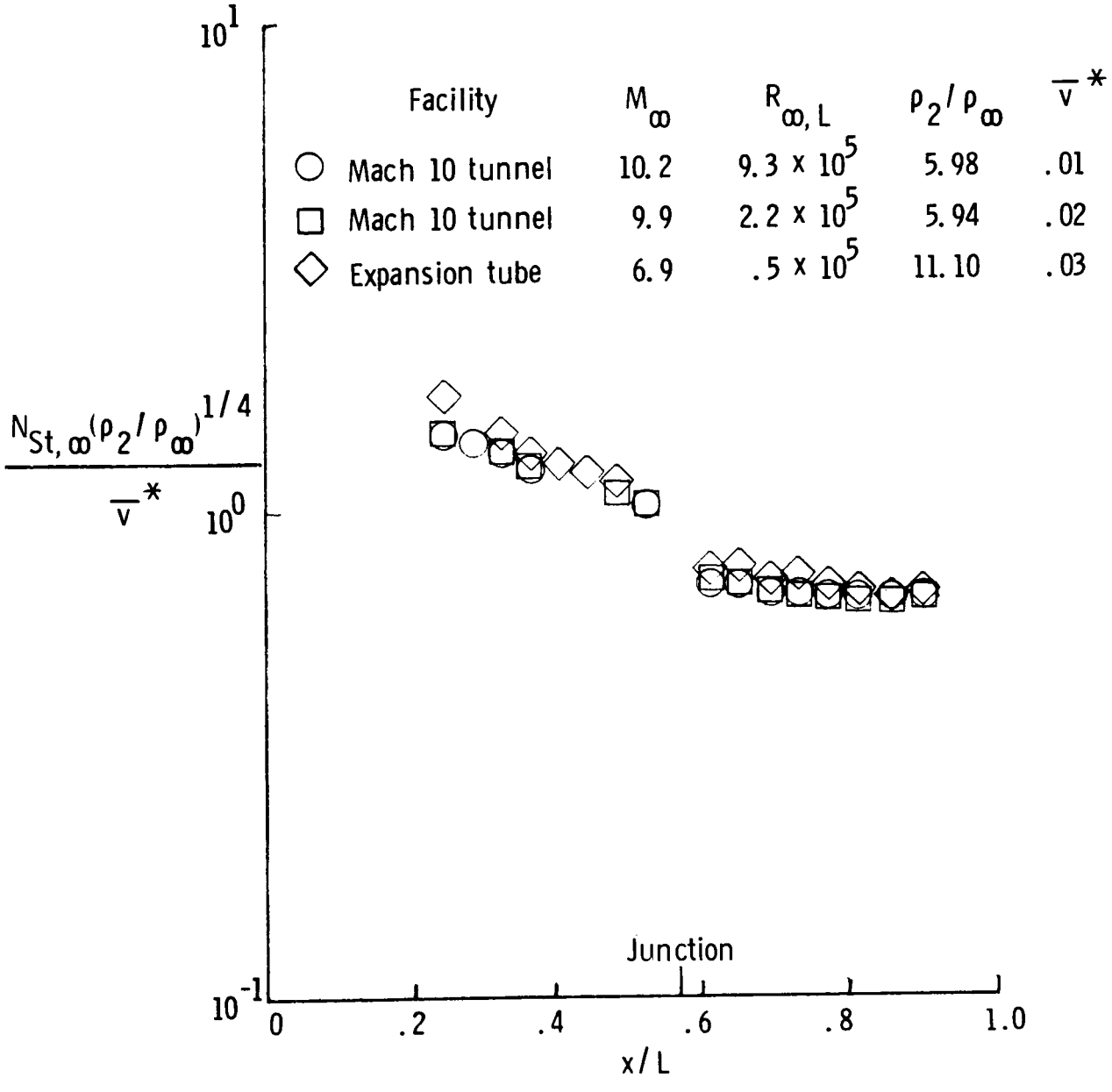

(b) $\alpha = 20°$.

Figure 22. Concluded.

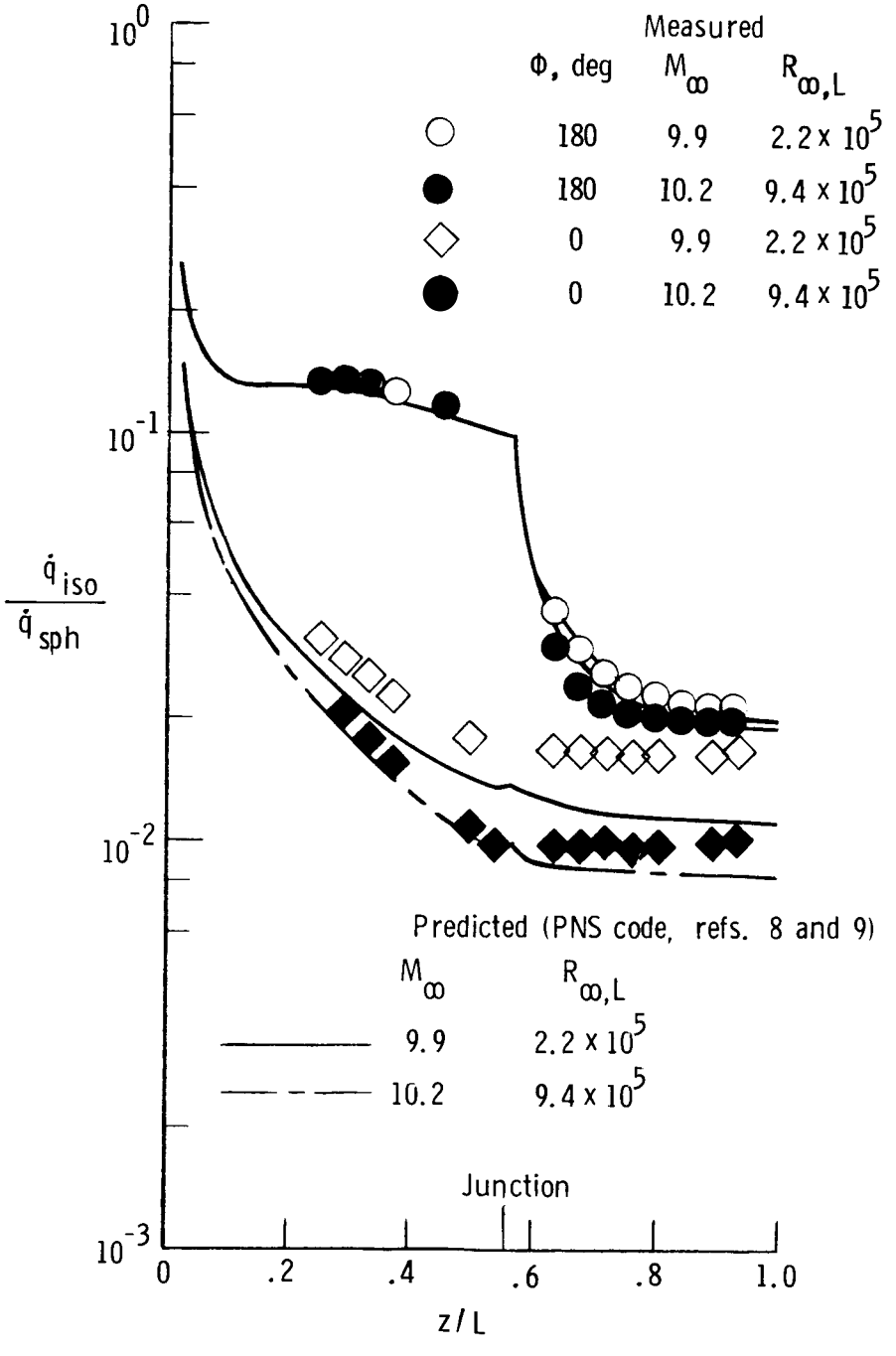

(a) $\alpha = 0°$.

Figure 23. Comparison of measured and predicted heating for bent-nose biconic.

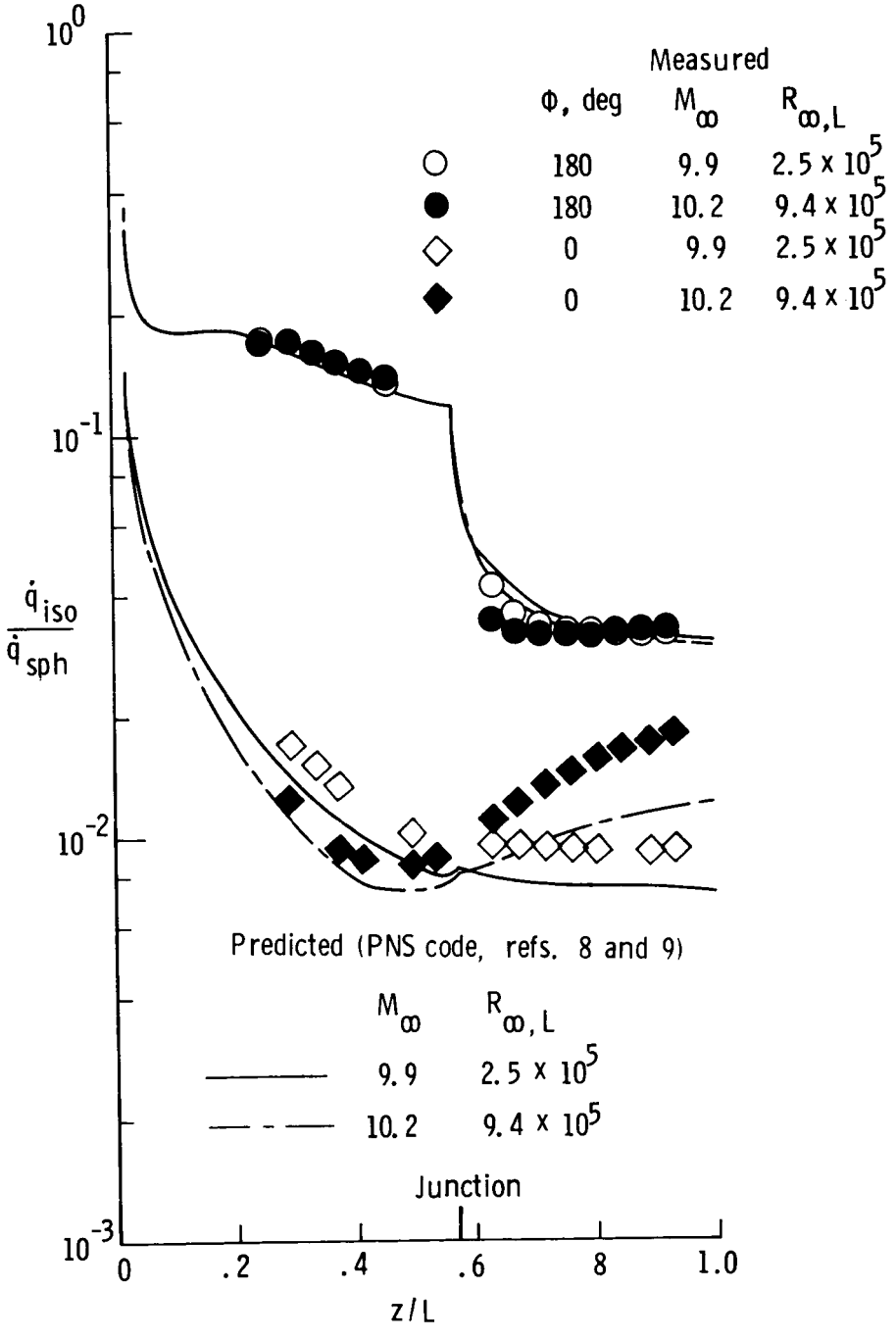

(b) $\alpha = 4°$.

Figure 23. Continued.

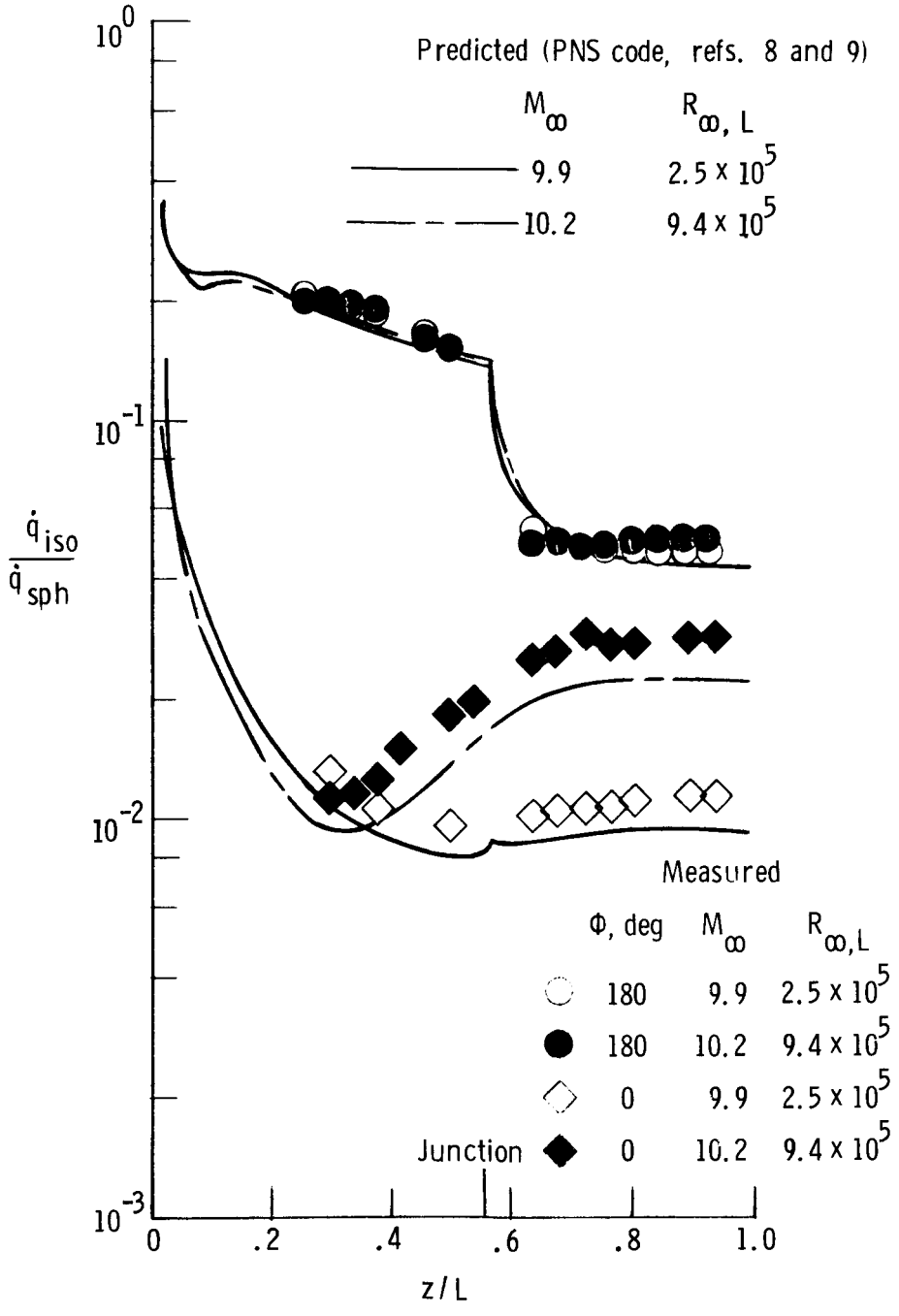

(c) $\alpha = 8°$.

Figure 23. Continued.

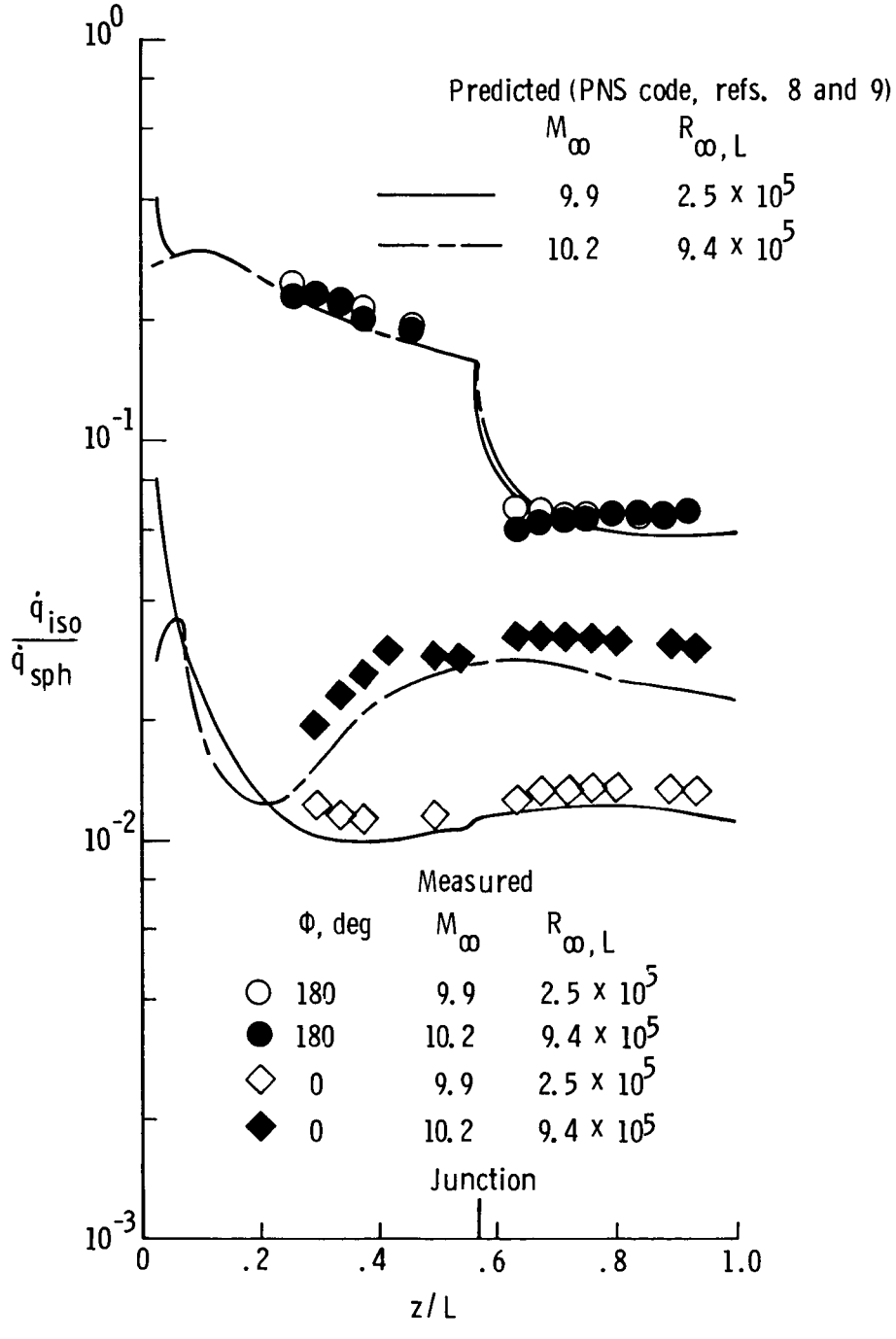

(d) $\alpha = 12°$.

Figure 23. Continued.

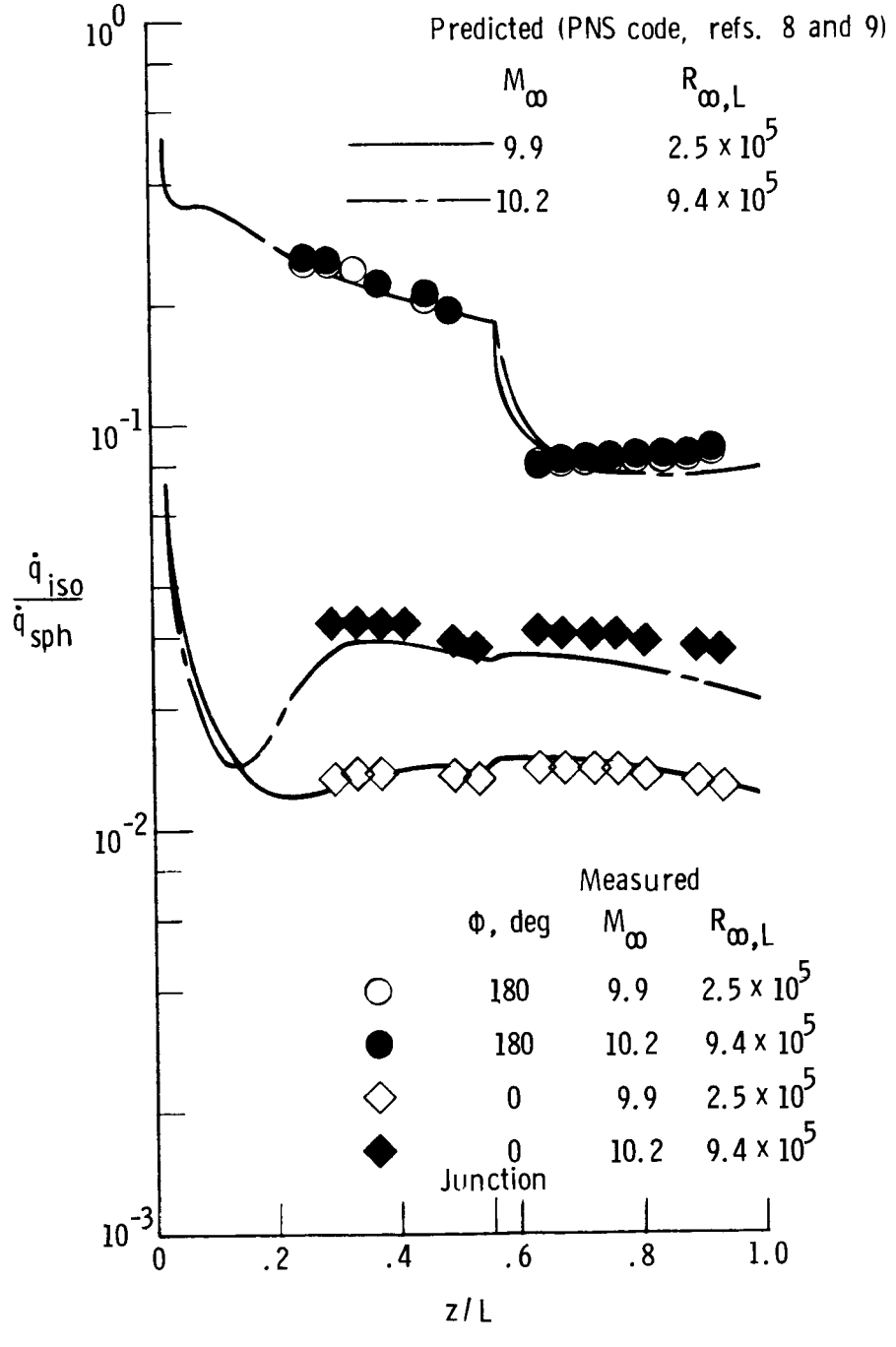

(e) $\alpha = 16°$.

Figure 23. Continued.

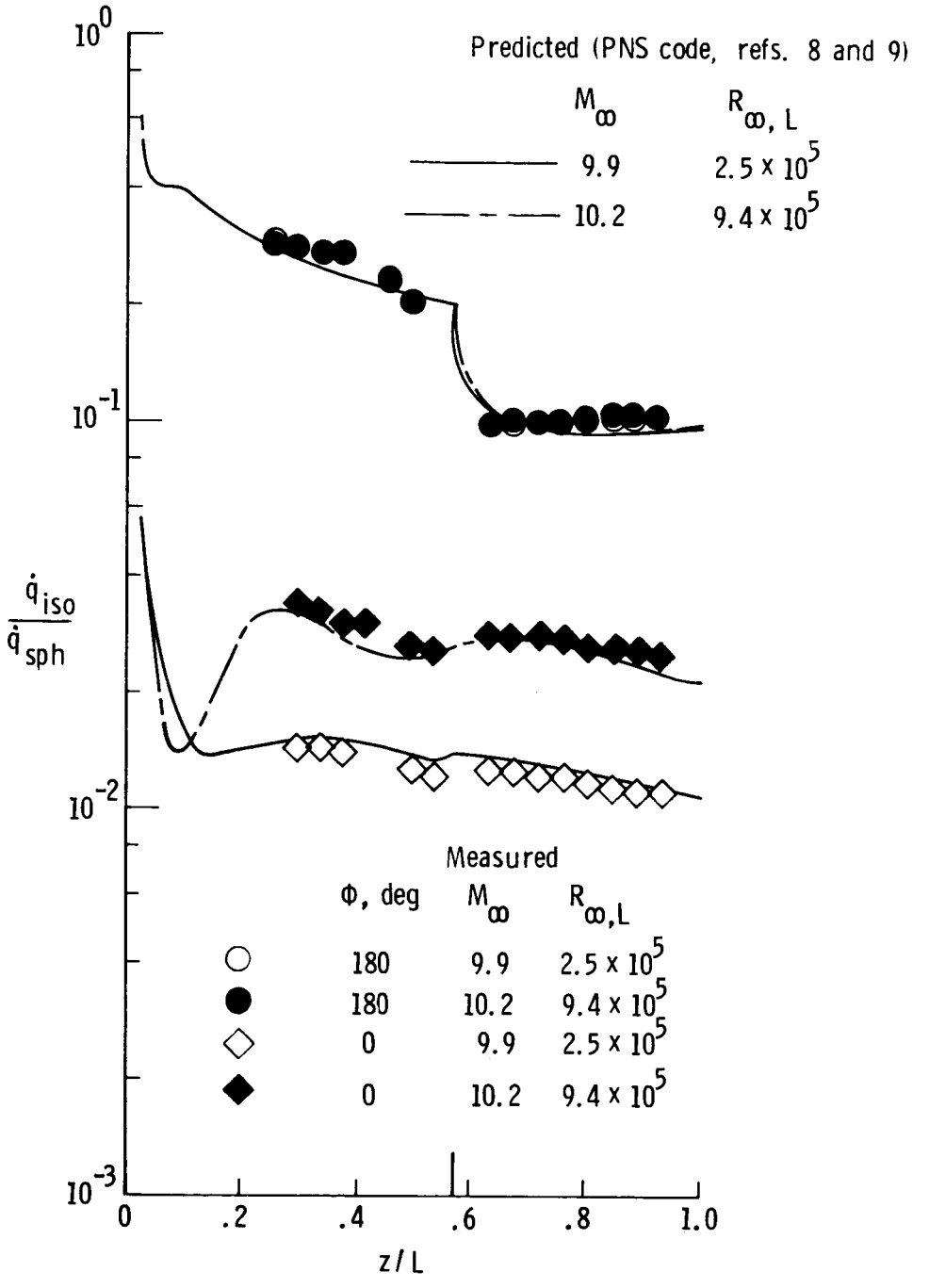

(f) $\alpha = 20°$.

Figure 23. Concluded.

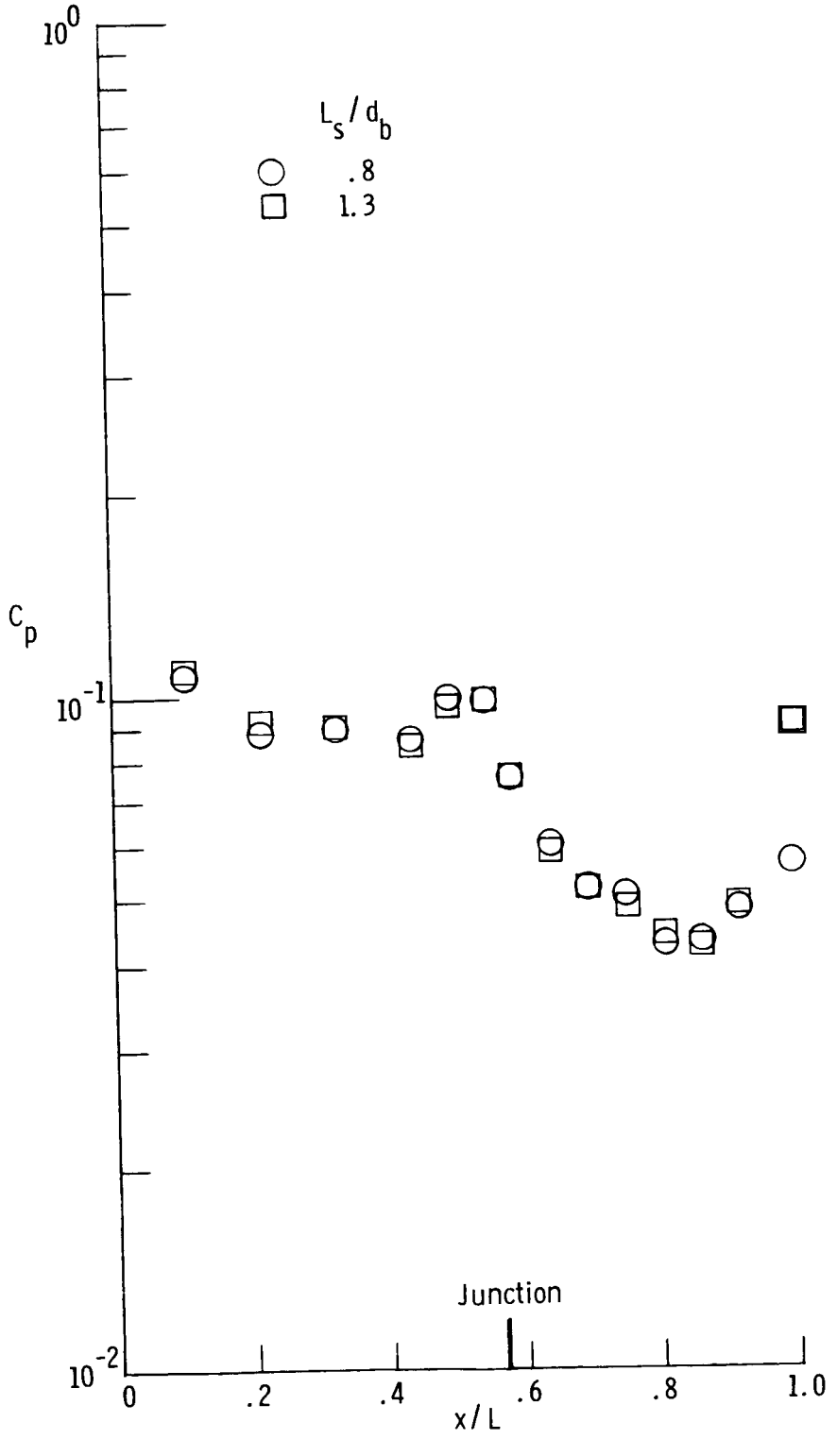

Figure 24. Effect of sting length on longitudinal pressure distribution for straight biconic at $\alpha = 0°$. $M_\infty = 9.9$; $R_{\infty,L} \approx 0.3 \times 10^6$; $d_b = 7.62$ cm.

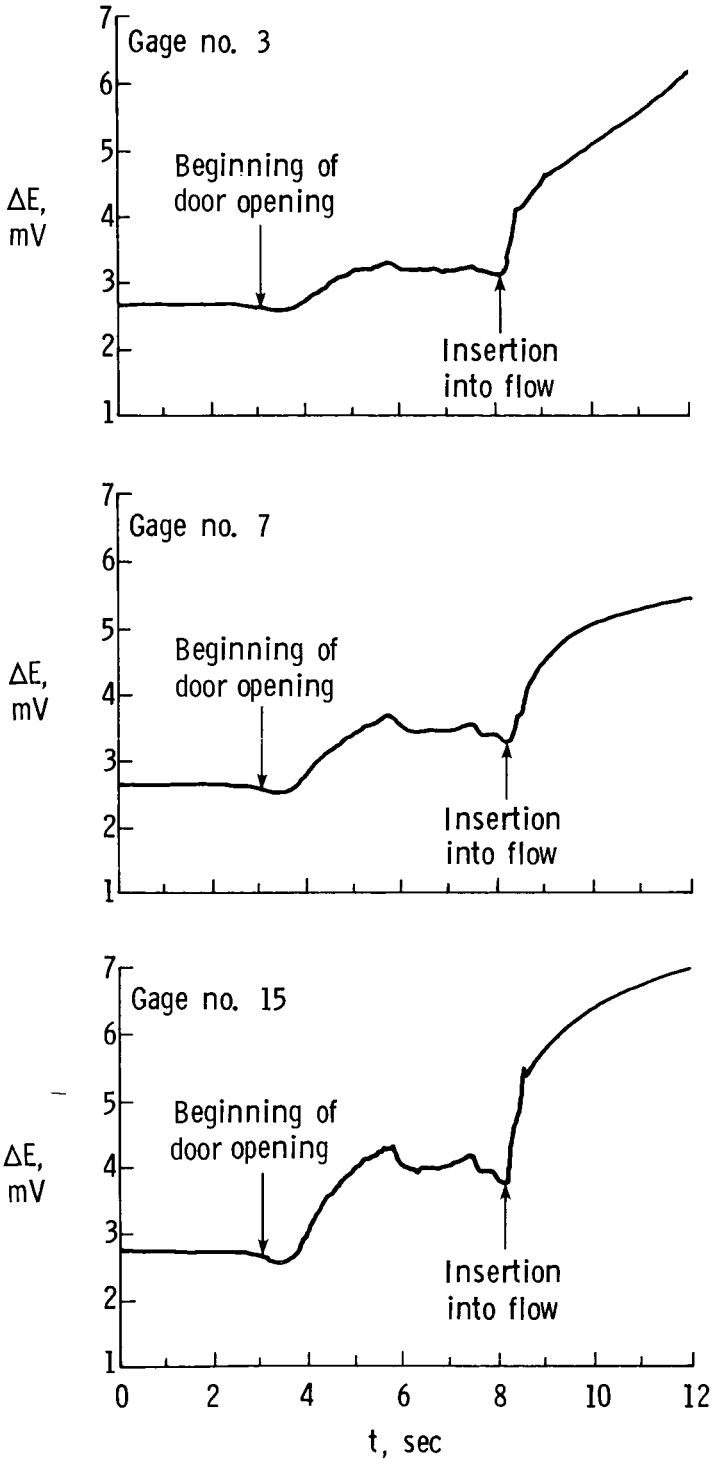

Figure 25. Effect of door opening on output of thin-film gages on leeward centerline of orbiter model in Mach 10 tunnel.

1. Report No.	2. Government Accession No.	3. Recipient's Catalog No.
NASA TP-2334		

4. Title and Subtitle	5. Report Date
EXPERIMENTAL AND PREDICTED HEATING DISTRIBUTIONS FOR BICONICS AT INCIDENCE IN AIR AT MACH 10	November 1984
	6. Performing Organization Code: 506-51-13-01
7. Author(s): Charles G. Miller III	8. Performing Organization Report No.: L-15785
9. Performing Organization Name and Address: NASA Langley Research Center, Hampton, VA 23665	10. Work Unit No.
	11. Contract or Grant No.
12. Sponsoring Agency Name and Address: National Aeronautics and Space Administration, Washington, DC 20546	13. Type of Report and Period Covered: Technical Paper
	14. Sponsoring Agency Code

15. Supplementary Notes

16. Abstract

Heating distributions were measured on a 1.9-percent-scale model of a generic aeroassisted vehicle proposed for missions to a number of planets and for use as a moderate lift-drag ratio Earth orbital transfer vehicle. This vehicle is a spherically blunted, 12.84°/7° biconic with the fore-cone bent upward 7° to provide self-trim capability. A straight biconic with the same nose radius and the same half-angles was also tested. The free-stream Reynolds numbers based on model length were equal to about 2×10^5 or 9×10^5. The angle of attack, referenced to the aft-cone, was varied from 0° to 20°. Heating distributions predicted with a "parabolized" Navier-Stokes (PNS) code are compared with the measurements for the present Reynolds numbers and range of angles of attack. Leeward heating was greatly affected by Reynolds number, with the heating increasing with decreasing Reynolds number for attached flow (low incidence). The opposite was true for separated flow, which occurred when the fore-cone angle of attack exceeded 0.8 times the fore-cone half-angle. Windward heating distributions were predicted to within 10 percent with the PNS code. Leeward heating distributions were predicted qualitatively for both Reynolds numbers, but quantitative agreement was poorer than on the windward side.

17. Key Words (Suggested by Authors(s))
Heat transfer
Biconic
Hypersonic
Thin-film gage

18. Distribution Statement
Unclassified - Unlimited

Subject Category 34

19. Security Classif.(of this report)	20. Security Classif.(of this page)	21. No. of Pages	22. Price
Unclassified	Unclassified	116	A06

For sale by the National Technical Information Service, Springfield, Virginia 22161

NASA-Langley, 1984